ABSTRACT

Title of Thesis: STABILITY AND CONTROL MODELING OF TILTROTOR AIRCRAFT

Kristi Marie Kleinhesselink
Master of Science, 2007

Thesis Directed By: Dr. Roberto Celi, Professor
Department of Aerospace Engineering

This thesis develops a simple open-source model of a tiltrotor using the basic equations of motion. The model focused on stability and control aspects of the XV-15 aircraft using simple linear analysis and, in general, did not add in correction or scaling factors to obtain a better match with flight data. Subsequent analysis performed included a trim and time history solution. A linearized state space model was also developed and analyzed using state space matrices, Bode plots, and eigenvalue analysis. The results were validated against generic tiltrotor simulation model results and compared to flight test where available.

The model resulted in was able to show inherent tiltrotor characteristics, however, further model refinements are needed. Helicopter and airplane mode flight data was used for comparisons. In order to make a true assessment of how well a simple model can approximate a tiltrotor, comparison with conversion mode flight data is required.

STABILITY AND CONTROL MODELING OF TILTROTOR AIRCRAFT

By

Kristi Marie Kleinhesselink

Thesis submitted to the Faculty of the Graduate School of the
University of Maryland, College Park, in partial fulfillment
of the requirements for the degree of
Master of Science
2007

Advisory Committee:
Dr. Roberto Celi, Chair
Dr. I. Chopra
Dr. J. Gordon Leishman

Table of Contents

List of Tables

List of Figures

Acronyms

Acronym	Description
AOA	Angle of attack
APLN	Airplane
CG	Center of gravity
CONV	Conversion
GTRS	Generic Tilt-Rotor Simulation
NAC	Nacelle angle
NASA	National Aeronautics and Space Administration
RPM	Revolutions per minute
SCAS	Stability and control augmentation system
VTOL	Vertical take-off and landing

Symbols

Text Symbol	Description
A	Reference area
A	State/stability matrix
A_R	Aspect ratio
B	Control matrix
C_D	Drag coefficient
C_{D0}	Profile drag coefficient
C_{d0}	Profile drag coefficient
C_{di}	Induced drag coefficient
C_L	Lift coefficient
C_{L0}	Lift coefficient at zero angle of attack
$C_{l\alpha}$	Lift curve slope
C_M	Pitching moment coefficient
C_{M0}	Moment coefficient at zero angle of attack
$C_{M\alpha}$	Moment coefficient vs. angle of attack
C_T	Proprotor thrust coefficient
D	Drag force
E	Interim y-dot matrix
E	Oswald's efficiency factor
F	Interim y matrix
F	Force
G	Interim control matrix
H	H-force
I_b	Blade mass moment of inertial
I_N	Nacelle incidence angle
I_{xx}	x-axis (roll) moment of inertia
I_{xy}	x-y plane moment of inertia
I_{xz}	x-z plane moment of inertia
I_{yy}	y-axis (pitch) moment of inertia
I_{yz}	y-z plane moment of inertia
I_{zz}	z-axis (yaw) moment of inertia
L	Total rolling moment
L	Lift
M	Moment
M	Mach number
M	Total pitching moment
M_A	Aerodynamic rotor moment
M_I	Inertial rotor moment
N	Total yawing moment
N_b	Number of blades
N_R	Proprotor angular velocity
R	Blade radius
R_H	Distance from hub to point ‘P’ on the blade

R_N	Distance from CG to nacelle
R_p	Distance from the nacelle to point 'P' on the blade
R_{TOT}	Distance from CG to point 'P' on blade
T	Proprotor thrust
T	Transformation matrix
U_P	Perpendicular velocity component
U_R	Radial velocity component
U_T	Tangential velocity component
U_x	Velocity in the x-direction
U_y	Velocity in the y-direction
U_z	Velocity in the z-direction
V	Forward flight velocity in body axes
V_{FF}	Forward flight velocity
V_{tip}	Blade tip speed
X	Force along the x-body axis
W	Aircraft gross weight
Y	Force along the y-body axis
Y	Sideforce
Z	Force along the z-body axis
a	Lift curve slope
a_{Pz}	Acceleration of point 'P' in the z-direction
b	Wingspan
c	Proprotor blade chord, wing chord
c_d	Drag coefficient
c_l	Lift coefficient
f	Flat plate drag of the fuselage
e	Hinge offset distance
g	Gravitational acceleration
i	Unit vector in x-direction
i	Incidence angle
j	Unit vector in y-direction
$l_{()}$	Fore/aft distance from CG to center of pressure of the ( )
$lz_{()}$	Vertical distance from CG to center of pressure of the ( )
k	Unit vector in z-direction
k	constant in C_D
k_β	Flapping spring constant
m	Section mass per unit length
m_{ac}	Aircraft mass
n	Number of blade modes ex: cos(nψ)
n_y	Side load factor
p	Body axis roll rate
$\dot{p}$	Pitch acceleration
q	Dynamic pressure
q	Body axis pitch rate
$\dot{q}$	Roll acceleration

r	Body axis yaw rate
r	Blade radial station
$\dot{r}$	Yaw acceleration
r_p	Distance from proprotor hub to point 'P' on the blade
t	Time
u	Body x-axis velocity
u	Control vector
u_0	Trim state
$\dot{u}$	Acceleration in x-direction
v	Body y-axis velocity
v_i	Induced inflow at the proprotor disk
$\dot{v}$	Acceleration in y-direction
w	Body z-axis velocity
$\dot{w}$	Acceleration in z-direction
x	Non-dimensional blade radial station
x	State vector
$x_{( )}$	Longitudinal distance from the reference datum along the reference axis
y	State vector
$\dot{y}$	Time derivative of the state vector
$y_{( )}$	Lateral distance from the reference datum along the reference axis
$z_{( )}$	Vertical location of ( ) with respect to reference datum
α	Angle of attack
α_w	Wing angle of attack
α_{0L}	Zero lift angle of attack
β	Sideslip angle
β	Flapping angle
β_M	Mast angle
$\dot{\beta}_M$	Rate of change of mast angle
$\ddot{\beta}_M$	Acceleration of mast angle
β_p	Proprotor pre-cone angle
β_0	Coning angle
β_{1c}	Longitudinal tip path plane tilt
β_{1s}	Lateral tip path plane tilt
β_{2c}	Longitudinal tip path plane tilt (2/rev)
β_{2s}	Lateral tip path plane tilt (1/rev)
$\overset{*}{\beta}$	Flapping rate with respect to azimuth
$\overset{**}{\beta}$	Flapping acceleration with respect to azimuth
$\dot{\beta}$	Flapping rate
$\ddot{\beta}$	Flapping acceleration
λ	Flight path angle
λ	Lock number
δ_{ail}	Aileron deflection
$\delta C_{D,\,\delta flap}/\delta_{flap}$	Change in drag coefficient of the wing due to flap deflection

$\delta C_{L,H}/\delta_{elev}$	Change in horizontal tail lift coefficient due to elevator deflection
$\delta C_{L,\ \delta flap}/\delta_{flap}$	Change in lift coefficient of the wing due to flap deflection
δ_{coll}	Collective input
δ_{elev}	Elevator deflection
δ_{flap}	Flap deflection
δ_{lat}	Lateral stick input
δ_{long}	Longitudinal stick input
δ_{ped}	Pedal deflection
δ_{rud}	Rudder deflection
ε	Order of magnitude index
ε	Wing downwash angle
ζ	Damping ratio
θ	Euler angle – pitch attitude with respect to CG
θ_{blade}	Blade angle
θ_{tw}	Blade twist angle
θ_0	Collective pitch
θ_{1c}	Lateral cyclic pitch
θ_{1s}	Longitudinal cyclic pitch
λ	Non-dimensional proprotor inflow
μ	Non-dimensional velocity, advance ratio
ρ	Air density
φ	Euler angle – roll attitude with respect to CG
$\dot{\varphi}$	Euler roll rate
ψ	Euler angle – yaw attitude with respect to CG
ψ	Blade azimuth index
$\dot{\psi}$	Euler yaw rate
Ω	Proprotor angular velocity
$\dot{\Omega}$	Proprotor angular acceleration
ω	Angular velocity
ω_n	Natural frequency

SUBSCRIPTS/SUPERSCRIPTS

A	Aerodynamic
B	Body axes
F	Fuselage
G	Gravity axes
HT	Horizontal tail
I	Inertial
*MR*1	Main proprotor #1 (Right)
*MR*2	Main proprotor #2 (Left)
NAC	Nacelle-fixed coordinate
NR	Blade coordinate system (not-rotating)
ROT	Blade-fixed coordinate (rotating)
TOT	Total
VT	Vertical tail (#1 or #2)
blade	Proprotor blade
cg	Center of Gravity
elev	Elevator
f	Fuselage
fuse	Fuselage
ht	Horizontal tail
i	In x-direction
j	In y-direction
k	In z-direction
shaft	Proprotor shaft
spring	Spring
vt	Vertical tail
w	Wing
wing	Wing
*	d( ) / dψ
·	d( ) / dt
'	Blade-flapped coordinate

1. Introduction

1.1 Problem Statement

Most of the research and published work related to tiltrotors stems from issues or problems encountered during aircraft development. For example, there are numerous reports and papers discussing the XV-15 aeroelastic issues and the subsequent efforts to solve the problems. More recently, based on a series of events in the V-22 Osprey program, documentation has been published regarding vortex ring state (Reference 1 and 2), shipboard compatibility, formation flight (Reference 3), Short Take-Off and Landings (Reference 4), general flying qualities test results (Reference 5), etc. There exists, however, little publicly domain literature on tiltrotor aeromechanics versus airplane and helicopter aeromechanics. Therefore, the released documentation on simple modeling of tiltrotor aircraft and handling qualities analysis using these models has even less availability.

Documentation that describes the basics of the tiltrotor using the basic Euler equations, flapping equations of motions, and basic helicopter and airplane theory is difficult to find. Some general information on the stability and control of tiltrotors can be found in the Generic Tiltrotor Simulation (GTRS) documentation of the XV-15 modeling as documented by Sam Ferguson of Systems Technology, Inc. (Reference 6 and 7), and of the Bell 301 modeling as documented in Reference 8. While some of the basic equations were used in the GTRS model, they tend to get lost in the complexity of the system. In

order to achieve better flight correlation, the GTRS uses table lookups and correction factors, instead simple physical equations to model the aircraft.

Some modeling of the stability and control characteristics of a tiltrotor was performed by Gary Klein and is documented in Reference 9. This analysis, however, focused on modifying existing design codes to model a tiltrotor in airplane mode and in helicopter mode only.

Recently, the European Union took the initiative on tiltrotor research in an effort to develop technologies that would help to alleviate the congestion at European airports by using short-range transportation systems. One of the civilian tiltrotor research projects was entitled Rotorcraft Handling, Interactions and Load Predictions or RHILP (Reference 10). The main areas to be addressed in this project were handling qualities criteria, aerodynamic interactions, and transient structural loads. Tiltrotor modeling and simulation development was performed via commercial software, FLIGHTLAB and HOST (Reference 11), with the models based on open source XV-15 data. The development of the models, however, was not open source. These models were then used for tiltrotor research including the development of handling qualities criteria for civil tiltrotors, (References 12 and 13), loads calculation, low speed and hover tiltrotor characteristics (Reference 14).

The purpose of this thesis was to develop a simple open-source model of a tiltrotor for airplane mode, conversion mode, and helicopter mode flight using the basic equations of

motion. The model developed for this project focused on the stability and control aspects of a tiltrotor aircraft from the perspective of a simple linear analysis without regard for the complex aerodynamics, structural couplings, downwash interactions, etc. that in reality depict an actual tiltrotor. In general, it also did not attempt to add in any correction or scaling factors to obtain a better match with flight data.

The goal was to develop a simple model for use in tiltrotor analysis rather than dealing with a complex model that is normally used in tiltrotor analysis. By using a simple model, the basic aerodynamics and dependencies can be more easily recognized, without having to deal with the scaling factors, approximations, and 'fix-it' tables normally associated with tiltrotor models. An assessment of the ability of the simple model to predict tiltrotor characteristics was also performed.

1.2 XV-15 Tiltrotor

1.2.1 Tiltrotor History

Tiltrotor aircraft are hybrid aircraft that attempt to combine the hover capability of a helicopter with the speed and range of an airplane. The most well-known tiltrotors are the XV-15 and the V-22 Osprey, even though development of the tiltrotor concept began earlier in the 20th century with the Bell Helicopter XV-3 and the Transcendental Aircraft Corporation Model 1-G and Model 2. The XV-15 was jointly developed by the US Army, NASA, and the US Navy as a tiltrotor technology demonstrator. The XV-15 predecessor, the XV-3, had serious stability issues that threatened the program. The XV-15 resulted from research into the XV- 3 issues, new technologies, new test techniques,

and basic technological advancement. The XV-15 was another concept demonstrator for the tiltrotor design. (Reference 15)

Based on the results of the XV-15 testing, the V-22 program was stood up. The V-22 was the follow on operational aircraft developed jointly by Bell-Boeing for the US Marine Corps, US Air Force Special Operations Command, and the US Navy. (The US Army was originally involved in the program; however, they later withdrew participation and funding.) (Reference 15)

1.2.2 General Aircraft Description

The aircraft used for this analysis is the XV-15 research aircraft (Figure 1). The XV-15 is a dual tandem proprotor tiltrotor aircraft with a high wing, center fuselage, and counter-rotating proprotors. The empennage consists of an H-tail. The proprotors are located laterally each side of fuselage centerline. Each proprotor has a diameter of 25 ft and a distance of 57 ft 2 in from the outermost tip of the left proprotor to the outermost tip of the right proprotor. The wing has full span flaps and the ailerons that are actually flaperons that provide roll control via differential deflection. In a hover, the wing flaps and flaperons are deflected full down to reduce the wing download. The aircraft is powered by two T-53-L-13B engines, housed in wing-tip mounted nacelles under each proprotor. The engines were re-designated LTC1K-4K after they were modified for starting and operating vertically (Reference 15). The nacelle rotates from 90˚ mast angle (β_M) in airplane mode to 0˚ β_M in hover. The nacelles could actually be rotated aft past

vertical to –5° β_M, which enhanced rearward flight capability. The basic aircraft characteristics and parameters used for this model can be found in Appendix A.

The tiltrotor is said to be in "helicopter mode" when the nacelles are vertical with respect to the wing (0° β_M), thereby positioning the proprotors as a helicopter proprotor. The aircraft is said to be in "airplane mode" when the nacelles are parallel to the wing (90° β_M), thereby positioning the proprotors as an airplane propeller. Hence the rotors/propellers are called proprotors. The flight regime where the nacelles are between helicopter and airplane mode is called "conversion mode".

Tiltrotor aircraft convert/transition from helicopter mode to airplane mode by rotating the nacelles and proprotors so they point forward and function as propellers. As such, most analyses of these aircraft have focused on the primary phases of flight: vertical take-off and landing (VTOL) mode for takeoff and landing and airplane mode (APLN) for cruise flight. The flight regime where the proprotors are not in a position to act as a pure helicopter or a pure airplane is called conversion mode (CONV). This regime was originally seen as simply a transitional flight phase. However, through further development, the potential benefits of operating the aircraft in conversion mode has become of greater interest.

As will be seen in the following discussions, by design, a tiltrotor is a compromise.

Figure 1: XV-15 Aircraft (Reference 15)

1.2.3 Proprotor

Each proprotor system is composed of a 3-bladed, stiff in-plane proprotor mounted on a gimbaled hub. The gimbaled hub allows for proprotor pitch changes to move the entire proprotor system rather than causing each blade to flap individually as in an articulated hinged proprotor. For this analysis, the proprotor system was treated as an articulated system. The hinge offset is zero.

1.2.4 Proprotor Blades

The blade twist for proprotors blades is a compromise between the optimum twist for helicopter mode and that optimum for airplane mode. The designers were essentially trading hover performance and speed. The resulting blade was a highly twisted proprotor blade.

Typical helicopter blade twists are on the order of 10˚. Typical propeller blade twists are much greater (around 60º or more at the root). The tiltrotor blades have a root blade twist

magnitude of –40˚ for the XV-15 and –47˚ for the V-22. The blade twists for the tiltrotor are neither optimal for a helicopter nor an airplane. Instead, the proprotor twists are a compromise between having the ability to hover and having the ability to fly at high speeds in airplane mode. Hence, while tiltrotor aircraft are capable of hovering and flying at high speeds in airplane mode, they are not the best at either. Tiltrotors are adequate helicopters and adequate airplanes, but their strength comes from their versatility to do both and fly in the configurations in between.

For the purpose of this analysis, the twist of the proprotor blade was approximated as linear to simplify the analysis (Figure 2).

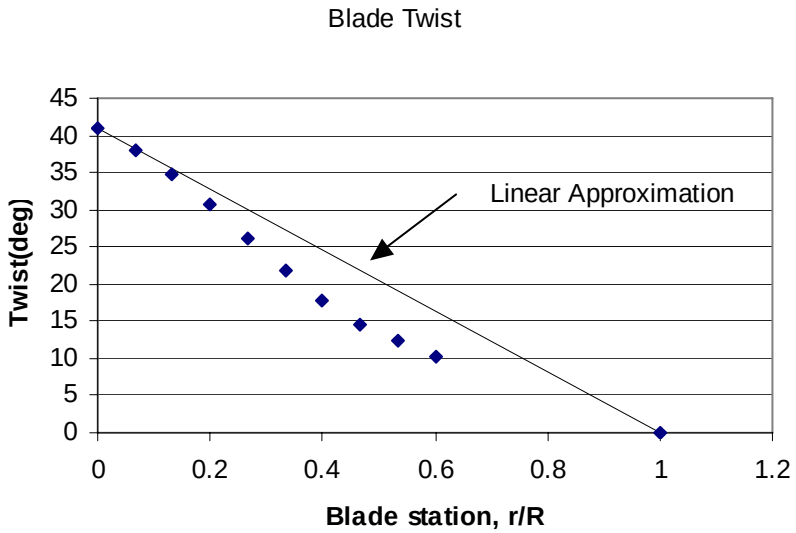

Figure 2: XV-15 Blade Twist

1.2.5 Control Strategy

As the tiltrotor is a hybrid aircraft, it uses both helicopter and airplane control strategies to control the aircraft. In helicopter mode, the tiltrotor uses conventional helicopter control strategies: collective pitch with lateral and longitudinal cyclic pitch to change the

tip path plane tilt. Since the proprotors are counter-rotating, the need for a tail rotor as an anti-torque device is eliminated. In airplane mode, the tiltrotor uses conventional airplane mode control strategies via rudders, ailerons, and an elevator.

While in conversion mode, tiltrotors use a combination of the classic helicopter and airplane control strategies. As the nacelles are rotated forward from helicopter towards airplane mode, the amount of control required from the proprotors decreases as the dynamic pressure increases and the airplane mode control surfaces become more effective. Once the nacelles are positioned for airplane mode, the proprotor contribution to lift has essentially been phased out and essentially only the thrust effects remain. The airplane control surfaces are always active, even though they don't have much effect at low airspeeds.

In addition to the classis control strategies, tiltrotors also implement some more unique control methodologies. In helicopter mode and higher nacelle conversion mode, roll is articulated via differential collective pitch on the proprotors. For example, for a left turn, the collective pitch is increased on the right proprotor to increase thrust and the collective pitch is decreased on the left proprotor to decrease thrust. The thrust imbalance combined with the large moment arm of the proprotors results in a roll.

As stated previously, tiltrotors do not have tail rotors for directional control. Directional control is attained via differential longitudinal cyclic. For a left yaw, the right proprotor is tilted forward and the left proprotor is tilted aft. The resulting moment creates a yaw.

The XV-15 also has a rotor governor which is used to automatically maintain the pilot selected RPM via automatic collective pitch inputs at the rotor. These inputs are in addition to the pilot generated collective control inputs.

1.2.6 Control Inceptors

Another challenge for tiltrotor designers was what type of control inceptors to incorporate. Since the tiltrotor was required to take off and land like a helicopter, many designers felt it was best to use the helicopter control inceptors: a cyclic stick, collective stick, and pedals. However, the tiltrotor would spend a lot of time in cruise as an airplane, which led many designers to believe that airplane control inceptors would be best: a yoke or stick, throttle, and pedals. The main debate centered on the collective stick or throttle. For a helicopter, the collective stick is used to control vertical motion. By pulling up on the collective stick, the aircraft would go up and by pushing down on the collective stick, the aircraft would go down. For an airplane, the throttle controlled forward velocity. Pushing the throttle forward causes the airplane to go faster and pulling back on the throttle would cause the aircraft to slow down.

For tiltrotors, this is an issue because of the desire to have a single controller function as a helicopter collective stick and an airplane throttle. To increase vertical speed in helicopter mode using helicopter control inceptors, the pilot would pull up on the collective stick. This motion resulted in an increase in speed. As the nacelles are rotated forward, pulling up on the collective stick would still increase speed, however, the direction of the speed increase would change due to the nacelle rotation re-orienting the thrust vector from the proprotor. Once the nacelles were on the downstop and the

tiltrotor was in airplane mode, pulling up on the collective would still increase speed, but this time it would result in an increase in forward velocity. Here in lies the problem.

The physical motion of pulling up on a collective stick is the same as that motion required to slow down an aircraft, not cause an aircraft to increase speed. If a conventional aircraft throttle was used, a similar problem would occur in that in airplane mode, pushing forward on the throttle would cause an increase in speed. In helicopter mode, pushing forward on the 'throttle' would cause an increase in vertical speed. This physical motion is again counterintuitive in helicopter mode as the arm extension required to push the throttle forward to increase speed, would, for a collective, cause a descent instead.

The designers of the XV-15 decided to use the helicopter-type control inceptors. A center cyclic stick was used for pitch and roll control. Pedals were used for yaw control. And a collective-like power lever was used to control vertical motion in hover and airspeed in forward flight. While transitioning from helicopter mode to conversion mode to airplane mode, the controls transition between airplane mode and helicopter mode functions.

1.2.7 Engine Placement

Both the XV-15 and V-22 have their engines located in the nacelles at the end of the wings. This results in the roll moment of inertia (about the x axis), I_{xx}, being much greater then the pitch moment of inertia, I_{yy}. Usually, helicopters and airplanes have a much larger I_{yy} than I_{xx}. The large I_{xx} results in a large roll inertial which causes an

increased delta-thrust to start a roll and an increased delta-thrust to stop the roll once it had been established. This large roll inertia can also cause other lateral control issues. As shown in Table 1 below, for the XV-15 and V-22, the ratio of I_{xx} to I_{zz} is approximately 80% while the ratio of I_{yy} to I_{zz} is approximately 30%. For helicopters and airplanes, the ratios are on the order of 30% and 70% respectively.

Table 1: Moment of Inertia Comparison

	I_{xx}	I_{yy}	I_{zz}	I_{xx}/I_{zz} (%)	I_{yy}/I_{zz} (%)
XV-15[1]	52,795	21,360	66,335	79.6	32.2
C-172 [2]	948	1,346	1,967	48.2	68.4
C-5 [2]	19,100,000	31,300,000	47,000,000	40.6	66.6
Puma [3]	9,638	33,240	25,889	37.2	128.4
B-747 [2]	18,200,000	33,100,000	49,700,000	36.6	66.6
BO-105 [3]	1,433	4,973	4,099	35.0	121.3
Lynx [3]	2,767	13,904.5	12,208.8	22.7	113.9
F-16C [2]	6,702	59,143	63,137	10.6	93.7

(1) Reference 7
(2) Reference 16
(3) Reference 17

1.2.8 Operating Envelope

The airspeed limits for each nacelle angle between helicopter mode and airplane mode is dictated by the conversion corridor. The overall maximum airspeed of the XV-15 is 170 kts in conversion mode; however, at higher nacelle angles, the maximum airspeed decreases. The lower boundary of the conversion corridor is defined by the wing loading limits: wing stall. The upper boundary of the conversion corridor is defined by the blade

loading limits: blade stall and compressibility effects. The conversion corridor is shown in Figure 3.

1.2.9 Changing Rotation Velocity

Tiltrotors change proprotor rotational velocity as they change configuration. The proprotor speed for helicopter and conversion modes is 589 RPM. The proprotor speed for airplane mode is 517 RPM. The proprotor RPM at 90º β_M can be either 517 RPM or 589 RPM. The aircraft is only considered to be in airplane mode once the RPM change has occurred. The change in proprotor RPM is to reduce tip speed in airplane mode, which reduces the tip Mach number, thereby allowing for a greater maximum forward airspeed prior to tip compressibility effects.

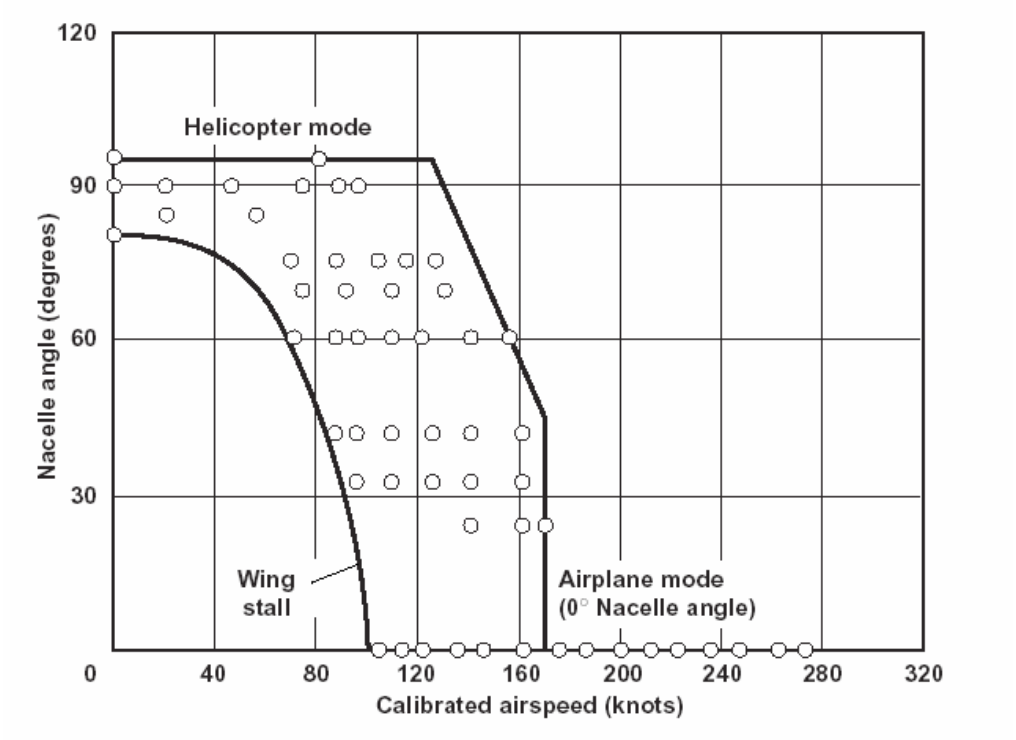

Figure 3: XV-15 Conversion Corridor (Reference 15)

1.2.10 Center of Gravity Shift with Nacelle Movement

An additional facet of tiltrotors is that as the nacelles are rotated forward from helicopter to airplane mode, the aircraft center of gravity (CG) moves and the moments of inertia change. The XV-15 CG envelopes for airplane mode and helicopter mode are shown in Figure 4. For simplicity's sake, tiltrotor CGs are usually discussed with respect to the helicopter mode CG so the nacelle effect is eliminated. The changes in moments of inertia due to nacelle movement are shown in Figure 5 with the corresponding equations shown below.

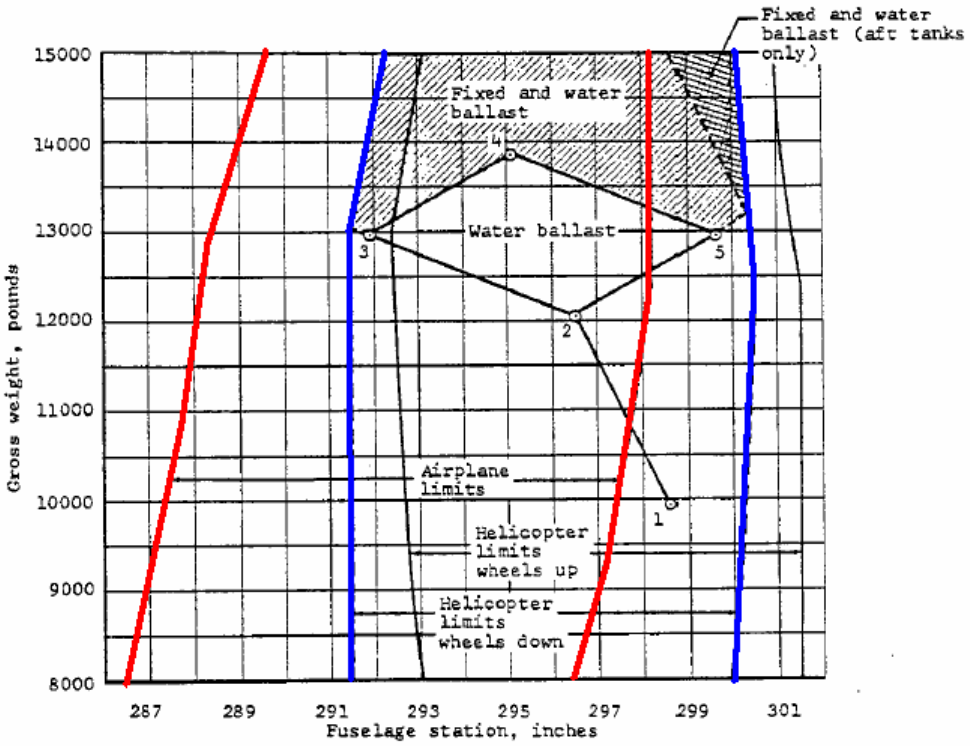

Figure 4: XV-15 Longitudinal Center of Gravity Envelope (Reference 7)

$$I_{xx} = I_{xx0} - KI1\beta_M$$
$$I_{yy} = I_{yy0} - KI2\beta_M$$
$$I_{zz} = I_{zz0} + KI3\beta_M$$
$$I_{xz} = I_{xz0} - KI4\beta_M$$

where

I_{xx0}, I_{yy0}, I_{zz0}, and I_{xz0} are the helicopter mode values for I_{xx}, I_{yy}, I_{zz}, I_{xz}, respectively

β_M is the mast angle in degrees

$KI1$, $KI2$, $KI3$, $KI4$ are the inertia coefficients in slug-ft^2/degree

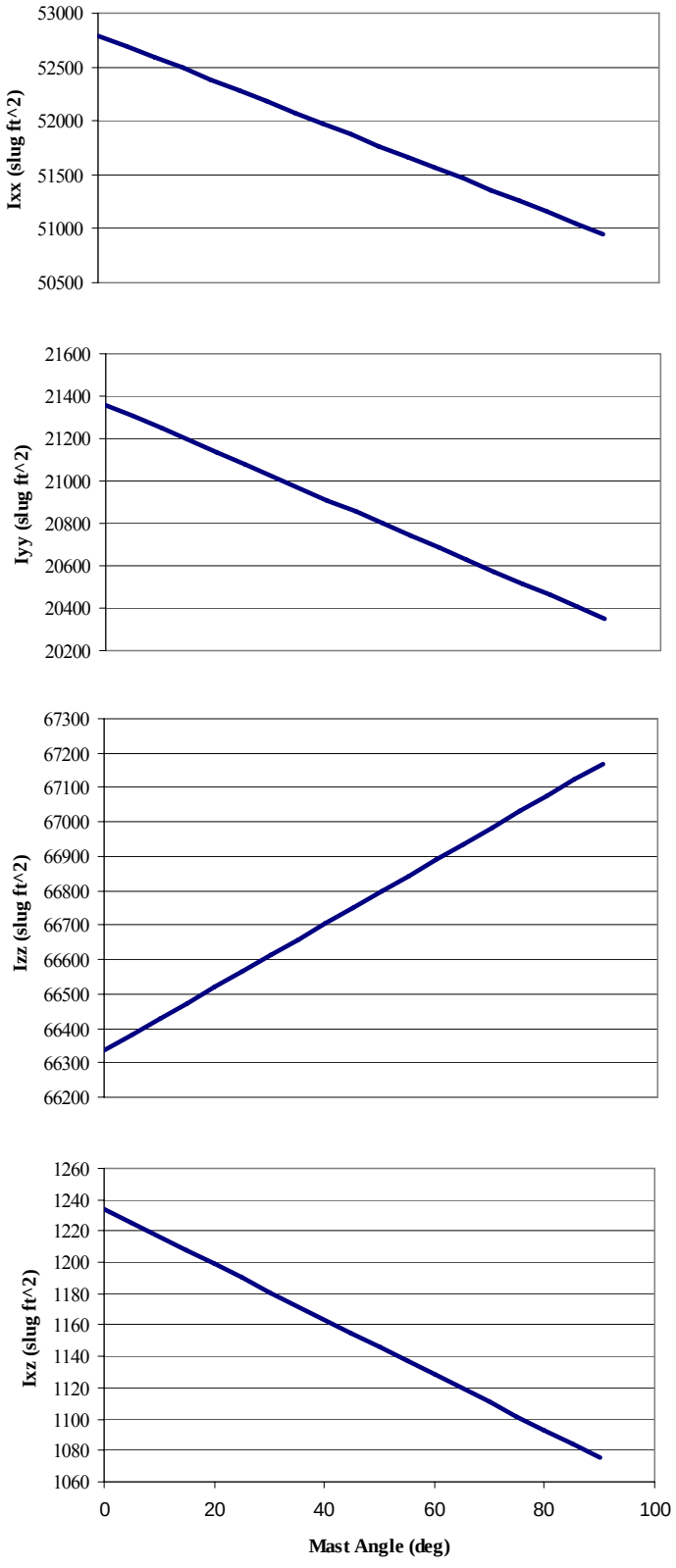

Figure 5: Moment of Inertia Change with Nacelle Movement

2. Governing Equations / Math model

The basic methodology used for this model was that the tiltrotor is a hybrid aircraft. First, development started with airframe equations. Then, proprotor equations were developed. To get conversion mode equations, the transition information needed to be incorporated. Essentially the airplane and helicopter mode equations were determined and then a trade-off was made between wing-borne flight and proprotor-borne flight to transition between the two states as nacelle changed.

2.1 Model Scope

Model complexity is always a balance between model applications, complexity, validation capabilities, understanding of the engineering of the issues, model flexibility, and, of course, cost. An assessment of the minimum model complexity required for piloted simulation for handling qualities applications was performed by Heffley and Mnich and is presented in Reference 18. While this discussion focused on real-time piloted models, the list of desired features can be used as a starting point for development of this tiltrotor model. The list focused on those areas and equations that directly affect the areas to be looked at from a handling qualities perspective and also covers those features that would be observed or needed by the pilot.

The following is the summarized list of desired features:

1. All rigid-body degrees of freedom.

2. Hover and forward flight dynamic modes
3. First-order flapping dynamics for the rotor (coupled or uncoupled).
4. Main rotor induced velocity computations (A first order approximation using momentum theory is sufficient.)
5. Potential for rotor RPM variation (Per Heffley and Mnich, assuming constant RPM is satisfactory for most applications.)

Desired features not included in this model are as follows:

1. Realistic power requirements over the flight envelope
2. Rearward and sideward flight without computational singularities
3. Dihedral effect
4. Correct transition from hover to forward flight
5. Correct power-off glide for minimum rate of descent and maximum glide.

Realistic power requirements are mainly required for assessing issues with tail rotor aircraft. Dihedral effect, correct transition from hover to forward flight, and correct power-off glide are especially important for piloted simulations and are not explicitly covered here. For this model, the trigonometric form of the angle of attack and sideslip equations were used, therefore allowing for singularities.

The above features were used as a starting point for the helicopter mode model. Additional restrictions to scope were made in keeping with the simple model concept. Therefore, the development of the rotor equations followed the development outlined in

Reference 19 which also limited the rotor to an articulated flapping rotor with no lead-lag degree of freedom. Simple modifications to this development for tiltrotor specific factors such as rotor blade twist, flapping spring, and hinge offset were, however, included. The airplane mode model was developed using the standard airplane equations for lift and drag.

For simplicity, the proprotor analysis developed here is only shown for the right hand rotor (*MR*1). Extraction of the second rotor's equations (*MR*2) can be found in section 2.6.

2.2 Trim Routine

The basic equations governing flight are that, for trim:

$\sum$Forces = 0

$\sum$Moments = 0

Each component's contributions to the forces and moments should be taken into consideration. The components of interest are the fuselage, wing, horizontal tail, two vertical tails, and the two proprotors. The nacelle effects are not included in this analysis.

Therefore, for example, the force in the *x* direction is:

$$X = X_{fuse} + X_{wing} + X_{HT} + X_{VT1} + X_{VT2} + X_{MR1} + X_{MR2}$$

These forces and moments are used in conjunction with the nonlinear, rigid body equations of motion, known as the Euler equations. The Euler equations, shown below, are a set of three force equations, three moment equations, and three kinematic equations, one for each body axis.

$$X = m(\dot{u} + qw - rv) + m_{ac} g \sin\theta$$

$$Y = m(\dot{v} + ru - pw) - m_{ac} g \sin\varphi \cos\theta$$

$$Z = m(\dot{w} + pv - qu) - m_{ac} g \cos\varphi \cos\theta$$

$$L = I_{xx}\dot{p} - (I_{yy} - I_{zz})qr + I_{yz}(r^2 - q^2) - I_{xz}(pq + \dot{r}) + I_{xy}(pr - \dot{q})$$

$$M = I_{yy}\dot{q} - (I_{zz} - I_{xx})pr + I_{xz}(p^2 - r^2) - I_{xy}(qr + \dot{p}) + I_{yz}(pq - \dot{r})$$

$$N = I_{zz}\dot{r} - (I_{xx} - I_{yy})pq + I_{xy}(q^2 - p^2) - I_{yz}(pr + \dot{q}) + I_{xz}(qr - \dot{p})$$

$$p = \dot{\varphi} - \dot{\psi}\sin\theta$$

$$q = \dot{\theta}\cos\varphi + \dot{\psi}\sin\varphi\cos\theta$$

$$r = \dot{\psi}\cos\varphi\cos\theta - \dot{\theta}\sin\varphi$$

For simplicity, the assumption can be reasonably made that the *x*-*y* plane is a plane of symmetry; therefore I_{xy} and I_{yz} are small and can be neglected.

Note: p, q, r, u, v, w are defined with respect to the body axis system.
Additional discussions on the trim equations and trim solution will follow the discussions on the individual component force and moment development.

2.3 Axes Systems

First the reference axes need to be defined. The axes systems are: the gravity axis system, the body axis system, the nacelle axis system, the non-rotating hub axis system, the rotating hub axis system, and the prime axis system. In order to transfer forces, moments, and motions between coordinate systems, the coordinate transfer matrices were developed. The matrices are shown below as each axis system is introduced. The relative reference locations of the axes systems are shown in Figure 6.

2.3.1 Gravity Axis System

The gravity coordinate system is defined with respect to the aircraft and the Earth. The *z*-axis always points vertically down towards the center of the Earth. The *x*-axis points North, the *y*-axis points East. The gravity coordinate system is centered at the aircraft CG. For simplicity, only the gravity-to-body axes transformation is included here.

$$\begin{Bmatrix} i \\ j \\ k \end{Bmatrix}_B = \begin{bmatrix} \\ T_{G\to B} \\ \\ \end{bmatrix} \begin{Bmatrix} i \\ j \\ k \end{Bmatrix}_G$$

$$T_{G\to B} = \begin{bmatrix} \cos\theta\cos\psi & \cos\theta\sin\psi & -\sin\theta \\ \sin\varphi\sin\theta\cos\psi - \cos\varphi\sin\psi & \sin\varphi\sin\theta\sin\psi + \cos\varphi\cos\psi & \sin\varphi\cos\theta \\ \cos\varphi\sin\theta\cos\psi + \sin\varphi\sin\psi & \cos\varphi\sin\theta\sin\psi - \sin\varphi\cos\psi & \cos\varphi\cos\theta \end{bmatrix}$$

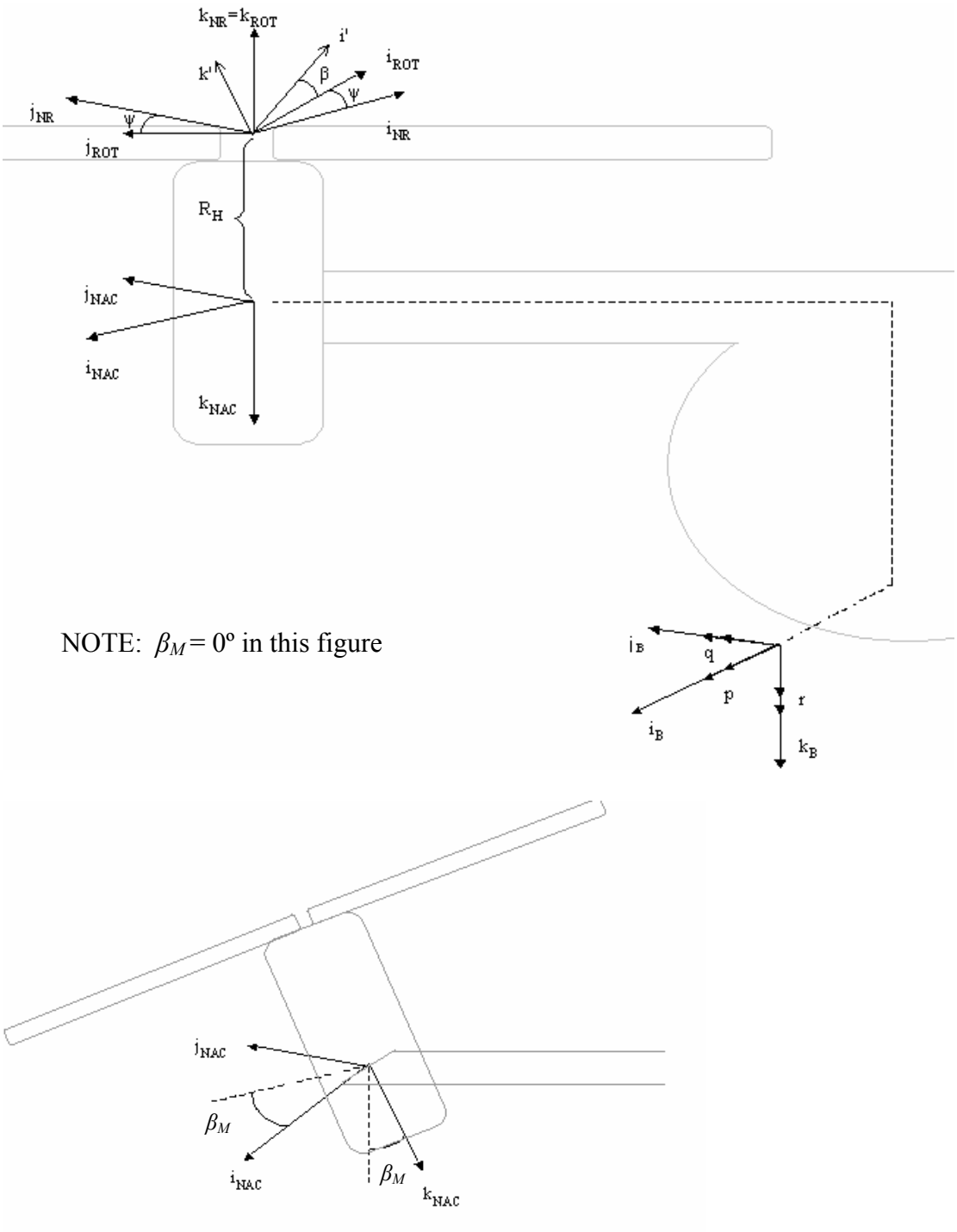

NOTE: $\beta_M = 0^\circ$ in this figure

Figure 6: Reference Axis Systems

2.3.2 Body Axis System

The body axis system is the conventional National Advisory Committee on Aeronautics orthogonal aircraft axis system. The *x*-axis runs along the longitudinal axis directed out the nose of the aircraft, the *y*-axis is directed out the right wing, and the *z*-axis is perpendicular to the *x* and *y* axes, directed downward. The body axis system is centered at the aircraft CG, fixed to the aircraft and rotates with it.

$$\begin{Bmatrix} \mathrm{i} \\ \mathrm{j} \\ \mathrm{k} \end{Bmatrix}_{\mathrm{NAC}} = \begin{bmatrix} \cos\beta_{\mathrm{M}} & 0 & \sin\beta_{\mathrm{M}} \\ 0 & 1 & 0 \\ -\sin\beta_{\mathrm{M}} & 0 & \cos\beta_{\mathrm{M}} \end{bmatrix} \begin{Bmatrix} \mathrm{i} \\ \mathrm{j} \\ \mathrm{k} \end{Bmatrix}_{\mathrm{B}}$$

$$\begin{Bmatrix} i \\ j \\ k \end{Bmatrix}_{NR} = \begin{bmatrix} -\cos\beta_M & 0 & -\sin\beta_M \\ 0 & 1 & 0 \\ \sin\beta_M & 0 & -\cos\beta_M \end{bmatrix} \begin{Bmatrix} i \\ j \\ k \end{Bmatrix}_B$$

$$\begin{Bmatrix} i \\ j \\ k \end{Bmatrix}_{ROT} = \begin{bmatrix} -\cos\psi\ \cos\beta_M & \sin\psi & -\cos\psi\ \sin\psi \\ \sin\psi\ \cos\beta_M & \cos\psi & \sin\psi\ \sin\beta_M \\ \sin\beta_M & 0 & -\cos\beta_M \end{bmatrix} \begin{Bmatrix} i \\ j \\ k \end{Bmatrix}_B$$

$$\begin{Bmatrix} i' \\ j' \\ k' \end{Bmatrix} = \begin{bmatrix} T_{B\to'} \end{bmatrix} \begin{Bmatrix} i \\ j \\ k \end{Bmatrix}_B$$

$$T_{B\to'} = \begin{bmatrix} -\cos\beta\ \cos\psi\ \cos\beta_M + \sin\beta\ \sin\beta_M & \sin\psi\ \cos\beta & -\cos\beta\ \cos\psi\ \sin\beta_M - \sin\beta\ \cos\beta_M \\ \sin\psi\ \cos\beta_M & \cos\psi & \sin\psi\ \sin\beta_M \\ \cos\psi\ \sin\beta\ \cos\beta_M + \cos\beta\ \sin\beta_M & -\sin\psi\ \sin\beta & \cos\psi\ \sin\beta\ \sin\beta_M - \cos\beta\ \cos\beta_M \end{bmatrix}$$

2.3.3 Nacelle Axis System

The nacelle axis system is defined originally with the nacelle at 0º β_M in helicopter mode. In this configuration, the *x*-axis runs parallel to the aircraft body axis, the *y*-axis runs out the right wing, and the *z*-axis is perpendicular to the x and *y* axes directed downward. The nacelle axis system is centered on the nacelle axis of rotation. The nacelle axis system is fixed to the nacelle and therefore rotates with the nacelle about the *y*-axis (axis of rotation).

$$\begin{Bmatrix} i \\ j \\ k \end{Bmatrix}_B = \begin{bmatrix} \cos\beta_M & 0 & -\sin\beta_M \\ 0 & 1 & 0 \\ \sin\beta_M & 0 & \cos\beta_M \end{bmatrix} \begin{Bmatrix} i \\ j \\ k \end{Bmatrix}_{NAC}$$

$$\begin{Bmatrix} i \\ j \\ k \end{Bmatrix}_{NR} = \begin{bmatrix} -1 & 0 & 0 \\ 0 & 1 & 0 \\ 0 & 0 & -1 \end{bmatrix} \begin{Bmatrix} i \\ j \\ k \end{Bmatrix}_{NAC}$$

$$\begin{Bmatrix} i \\ j \\ k \end{Bmatrix}_{ROT} = \begin{bmatrix} -\cos\psi & \sin\psi & 0 \\ \sin\psi & \cos\psi & 0 \\ 0 & 0 & -1 \end{bmatrix} \begin{Bmatrix} i \\ j \\ k \end{Bmatrix}_{NAC}$$

$$\begin{Bmatrix} i' \\ j' \\ k' \end{Bmatrix} = \begin{bmatrix} -\cos\beta\ \cos\psi & \sin\psi\ \cos\beta & -\sin\beta \\ \sin\psi & \cos\psi & 0 \\ \sin\beta\ \cos\psi & -\sin\beta\ \sin\psi & -\cos\beta \end{bmatrix} \begin{Bmatrix} i \\ j \\ k \end{Bmatrix}_{NAC}$$

2.3.4 Non-rotating Hub Axis System

The non-rotating hub axis system is centered at the proprotor hub on 'top' of the nacelle. When in helicopter mode, the *x*-axis is parallel to the aircraft body axis, however it is directed aft. The *y*-axis is parallel to the y-body axis, in the same direction. The *z*-axis is perpendicular to the *x* and *y* axes directed upward. The non-rotating hub axis system is fixed to the hub, therefore when the nacelle rotates, this axis system moves with it.

$$\begin{Bmatrix} i \\ j \\ k \end{Bmatrix}_B = \begin{bmatrix} -\cos\beta_M & 0 & \sin\beta_M \\ 0 & 1 & 0 \\ -\sin\beta_M & 0 & -\cos\beta_M \end{bmatrix} \begin{Bmatrix} i \\ j \\ k \end{Bmatrix}_{NR}$$

$$\begin{Bmatrix} i \\ j \\ k \end{Bmatrix}_{NAC} = \begin{bmatrix} -1 & 0 & 0 \\ 0 & 1 & 0 \\ 0 & 0 & -1 \end{bmatrix} \begin{Bmatrix} i \\ j \\ k \end{Bmatrix}_{NR}$$

$$\begin{Bmatrix} i \\ j \\ k \end{Bmatrix}_{ROT} = \begin{bmatrix} \cos\psi & \sin\psi & 0 \\ -\sin\psi & \cos\psi & 0 \\ 0 & 0 & 1 \end{bmatrix} \begin{Bmatrix} i \\ j \\ k \end{Bmatrix}_{NR}$$

$$\begin{Bmatrix} i' \\ j' \\ k' \end{Bmatrix} = \begin{bmatrix} \cos\beta\ \cos\psi & \cos\beta\ \sin\psi & \sin\beta \\ -\sin\psi & \cos\psi & 0 \\ -\sin\beta\ \cos\psi & -\sin\beta\ \sin\psi & \cos\beta \end{bmatrix} \begin{Bmatrix} i \\ j \\ k \end{Bmatrix}_{NR}$$

2.3.5 Rotating Hub Axis System

The rotating hub axis system is centered at the proprotor hub on top of the nacelle. The coordinate system rotates with the blade and, since its origin is hub-fixed, it moves with the nacelle. The system is defined at the point when the proprotor blade passes over the tail of the aircraft. At this point, the *x*-axis runs parallel to the aircraft body axis, however it is directed aft. The *y*-axis runs parallel to the *y*-body axis and in the same direction. The *z*-axis is perpendicular to the *x* and *y* axes and is directed upward.

$$\begin{Bmatrix} i \\ j \\ k \end{Bmatrix}_B = \begin{bmatrix} -\cos\psi & \cos\beta_M & \cos\beta_M \sin\psi & \sin\beta_M \\ \sin\psi & & \cos\psi & 0 \\ -\sin\beta_M & \cos\psi & \sin\beta_M \sin\psi & -\cos\beta_M \end{bmatrix} \begin{Bmatrix} i \\ j \\ k \end{Bmatrix}_{ROT}$$

$$\begin{Bmatrix} i \\ j \\ k \end{Bmatrix}_{NAC} = \begin{bmatrix} -\cos\psi & \sin\psi & 0 \\ \sin\psi & \cos\psi & 0 \\ 0 & 0 & -1 \end{bmatrix} \begin{Bmatrix} i \\ j \\ k \end{Bmatrix}_{ROT}$$

$$\begin{Bmatrix} i \\ j \\ k \end{Bmatrix}_{NR} = \begin{bmatrix} \cos\psi & -\sin\psi & 0 \\ \sin\psi & \cos\psi & 0 \\ 0 & 0 & 1 \end{bmatrix} \begin{Bmatrix} i \\ j \\ k \end{Bmatrix}_{ROT}$$

$$\begin{Bmatrix} i' \\ j' \\ k' \end{Bmatrix} = \begin{bmatrix} \cos\beta & 0 & \sin\beta \\ 0 & 1 & 0 \\ -\sin\beta & 0 & \cos\beta \end{bmatrix} \begin{Bmatrix} i \\ j \\ k \end{Bmatrix}_{ROT}$$

2.3.6 Prime Blade Axis System

The prime blade axis system is centered at the blade hinge point (located at the proprotor hub for zero hinge offset, located at the hinge for blades with hinge offset). The *x*-axis runs parallel to the blade, directed out the blade. In an un-flapped condition, the *z*-axis is directed downward and the *y*-axis is then perpendicular to the *x* and *z*-axes directed in the opposite direction of rotation. The primed blade axis system flaps with the blade.

$$\begin{Bmatrix} i \\ j \\ k \end{Bmatrix}_B = \begin{bmatrix} -\cos\psi\ \cos\beta_M\ \cos\beta + \sin\beta_M\ \sin\beta & \cos\beta_M\ \sin\psi & \cos\beta_M\ \cos\psi\ \sin\beta + \sin\beta_M\ \cos\beta \\ \cos\beta\ \sin\psi & \cos\psi & -\sin\beta \sin\psi \\ -\sin\beta_M\ \cos\psi\ \cos\beta - \cos\beta_M\ \sin\beta & \sin\beta_M\ \sin\psi & \sin\beta_M\ \cos\psi\ \sin\beta - \cos\beta_M\ \cos\beta \end{bmatrix} \begin{Bmatrix} i' \\ j' \\ k' \end{Bmatrix}$$

$$\begin{Bmatrix} i \\ j \\ k \end{Bmatrix}_{NAC} = \begin{bmatrix} -\cos\psi\ \cos\beta & \sin\psi & \sin\beta\ \cos\psi \\ \sin\psi\ \cos\beta & \cos\psi & -\sin\beta\ \sin\psi \\ -\sin\beta & 0 & -\cos\beta \end{bmatrix} \begin{Bmatrix} i' \\ j' \\ k' \end{Bmatrix}$$

$$\begin{Bmatrix} i \\ j \\ k \end{Bmatrix}_{NR} = \begin{bmatrix} \cos\beta\ \cos\psi & -\sin\psi & -\cos\psi\ \sin\beta \\ \cos\beta\ \sin\psi & \cos\psi & -\sin\psi\ \sin\beta \\ \sin\beta & 0 & \cos\beta \end{bmatrix} \begin{Bmatrix} i' \\ j' \\ k' \end{Bmatrix}$$

$$\begin{Bmatrix} i \\ j \\ k \end{Bmatrix}_{ROT} = \begin{bmatrix} \cos\beta & 0 & -\sin\beta \\ 0 & 1 & 0 \\ \sin\beta & 0 & \cos\beta \end{bmatrix} \begin{Bmatrix} i' \\ j' \\ k' \end{Bmatrix}$$

2.4 Airframe Forces and Moments

2.4.1 General

The trim equations for the aircraft depend on the forces and moments of each component. The proprotor contributions are discussed in section 2.5. The methodology used to calculate the airframe forces and moments is to determine the lift and drag of each component, and then, using the relative position on the aircraft, determine the associated body axis forces and moments. By definition:

1. Dynamic pressure: $q = \frac{1}{2}\rho V^2$
2. Lift: $Lift = \frac{1}{2}\rho V^2 A C_L$
3. Drag: $Drag = \frac{1}{2}\rho V^2 A C_D$

The forces and moments from the airframe were gathered from Reference 20 and 21. The airframe components used for this analysis were the wing, fuselage, horizontal tail, and vertical tails. For the purposes of this analysis, the lift and drag from the nacelles were ignored. The following main assumptions were used in the development of these equations:

Airframe assumptions:

1. $C_L = \frac{Lift}{qA}$ and $C_D = \frac{Drag}{qA}$
2. C_L is linear therefore $C_L = C_{L\alpha}\,\alpha$.
3. C_M is linear therefore $C_M = C_{M\alpha}\,\alpha + C_{M0}$.

4. Drag Coefficient: $C_D = C_{D0} + k\,C_L^2$
5. Wing has a constant airfoil section
6. Proprotor effects on the airflow over the wing and other aircraft components are negligible. [Note: this assumption is not strictly valid for a tiltrotor; it was made as a simplifying assumption.]
7. The small angle assumption was made for the angle of attack and sideslip angles.

See Figure 7 for a pictorial view of the forces and moments acting on the aircraft in airplane mode flight.

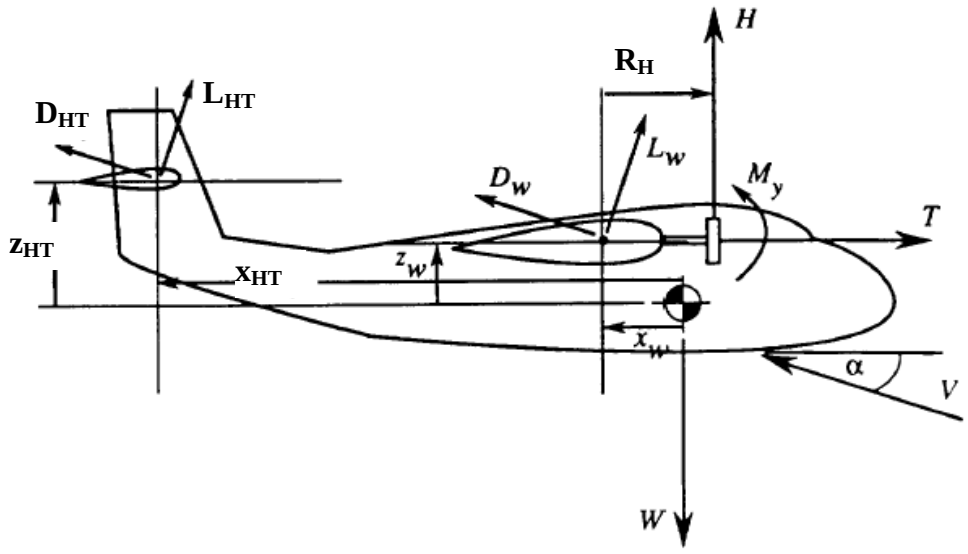

Figure 7: Forces and Moments Acting on the Aircraft (Reference 22)

2.4.2 Wing

The velocities at the wing are a sum of the freestream velocity and the velocity due to angular rates. For the purposes of this analysis, the velocities due to angular rates over

each wing were assumed to be equivalent to a constant velocity profile equal in magnitude to the velocity $b/3$ from the wing root (angular velocity at 2/3 distance from wing root to wing tip ($b/2$) = $b/3$). Therefore, the velocities at the wing are

$$V_{wing,R} = \begin{bmatrix} u - \frac{rb_w}{3} \\ v \\ w + \frac{pb_w}{3} \end{bmatrix}$$

$$V_{wing,L} = \begin{bmatrix} u + \frac{rb_w}{3} \\ v \\ w - \frac{pb_w}{3} \end{bmatrix}$$

$$V_{wing,TOT} = \sqrt{u_{wing}^2 + w_{wing}^2}$$

The equations for lift and drag developed for the wing are as follows:

$$Lift_{wing,L} = \frac{1}{2}\rho V^2 \frac{A_{wing}}{2}\left[a_w(\alpha_w - \alpha_{oL}) + \frac{\partial C_{l,flap}}{\partial \delta_{flap}}\delta_{flap} - \frac{\partial C_{l,ail}}{\partial \delta_{ail}}\delta_{ail}\right]$$

$$Lift_{wing,R} = \frac{1}{2}\rho V^2 \frac{A_{wing}}{2}\left[a_w(\alpha_w - \alpha_{oL}) + \frac{\partial C_{l,flap}}{\partial \delta_{flap}}\delta_{flap} + \frac{\partial C_{l,ail}}{\partial \delta_{ail}}\delta_{ail}\right]$$

$$Drag_{wing,L} = q_{wing}\frac{A_{wing}}{2}C_{D,wingL}$$

$$Drag_{wing,R} = q_{wing}\frac{A_{wing}}{2}C_{D,wingR}$$

where:

$$\alpha_{wing} = \tan^{-1}\left(\frac{w_{wing}}{u_{wing}}\right)$$

$$k_{wing} = \frac{1}{\pi E_{wing} A_{R,wing}}$$

$$C_{D,wing} = C_{D0,wing} + k_{wing}C_{L,wing}^2 + \frac{dC_{D,flap}}{\delta_{flap}}\delta_{flap} + \frac{dC_{D,flap}}{d\alpha}\delta\alpha$$

Which gives the following contribution to the forces and moments:

$$X_{wing} = Lift_{wing} \sin\alpha_w - Drag_{wing} \cos\alpha_w$$

$$Y_{wing} = 0$$

$$Z_{wing} = -Lift_{wing} \cos\alpha_w - Drag_{wing} \sin\alpha_w$$

$$L_{wing,L} = Y_{wing} z_w - Z_{wing} \frac{b_w}{3}$$

$$L_{wing,R} = Y_{wing} z_w + Z_{wing} \frac{b_w}{3}$$

$$M_{wing,L} = Z_{wing} l_w - X_{wing} z_w$$

$$M_{wing,R} = Z_{wing} l_w - X_{wing} z_w$$

$$N_{wing,L} = X_{wing} \frac{b_w}{3} - Y_{wing} l_w$$

$$N_{wing,R} = -X_{wing} \frac{b_w}{3} - Y_{wing} l_w$$

Positive flap deflection is defined as trailing edge down. Positive aileron deflection is defined as trailing edge down on the right wing.

2.4.3 Fuselage

The equations for lift and drag developed for the fuselage are as follows:

$$Lift_{fuse} = q_{fuse} A_{wing} \left| a_f \left(\alpha_f - \alpha_{0L,f} \right) \right|$$

$$Drag_{fuse} = q_{fuse} C_{D,fuse}$$

where:

$$q_f = \frac{1}{2} \rho \left(u^2 + v^2 + w^2 \right)$$

$\alpha_f = \alpha_F - i_w$, and

$$C_{D,fuse} = C_{D0,fuse} + k_{fuse} C_{L,fuse}^2 = f$$

Which gives the following contribution to the forces and moments:

$$X_{fuse} = Lift_{fuse} \sin\alpha_f - Drag_{fuse} \cos\alpha_f$$

$$Y_{fuse} = 0 \text{ (approximation, see Reference 21)}$$

$$Z_{fuse} = -Lift_{fuse} \cos\alpha_f - Drag_{fuse} \sin\alpha_f$$

$$L_{fuse} = 0 \text{ (negligible, see Reference 21)}$$

$$M_{fuse} = q_{fuse} A_{wing} c\left(C_{M,of} + C_{M\alpha f} \alpha_f\right) - \ell_f Lift_{fuse}$$

$$N_{fuse} = f\beta_F \ell_f$$

2.4.4 Horizontal Tail

The velocities at the horizontal tail are a sum of the freestream velocity and the velocity due to angular rates. Therefore, the velocities at the horizontal tail are

$$V_{HT} = \begin{bmatrix} u - qh_{HT} \\ v - rl_{HT} + ph_{HT} \\ w + ql_{HT} \end{bmatrix}$$

$$V_{HT,TOT} = \sqrt{u_{HT}^2 + w_{HT}^2}$$

The equations for lift and drag developed for the horizontal tail are as follows:

$$Lift_{HT} = q_{HT} A_{HT} \left[a_{HT} \alpha_{HT} + \frac{\partial C_{l,H}}{\partial \delta_e} \delta_e \right]$$

$$Drag_{HT} = q_{HT} A_{HT} C_{D,HT}$$

where:

$$q_{HT} = \frac{1}{2}\rho V_{HT,TOT}^2$$

$$\alpha_{HT} = \tan^{-1}\left(\frac{w_{HT}}{u_{HT}}\right) + i_{HT} - \varepsilon$$

$$\varepsilon = \varepsilon_0 + \frac{\partial\varepsilon}{\partial\alpha}\left(\alpha_F - \alpha_{0l,HT} + \frac{\partial C_{l,flap}}{\partial\delta_{flap}}\frac{\delta_{flap}}{a_w}\right)$$

$$k_{HT} = \frac{1}{\pi E_{HT} A_{R,HT}}$$

$$C_{D,HT} = C_{D0,HT} + k_{HT} C_{L,HT}{}^2$$

Which gives the following contribution to the forces and moments:

$$X_{HT} = Lift_{HT}\sin\alpha_{HT} - Drag_{HT}\cos\alpha_{HT}$$

$$Y_{HT} = 0$$

$$Z_{HT} = -Lift_{HT}\cos\alpha_{HT} - Drag_{HT}\sin\alpha_{HT}$$

$$L_{HT} = 0$$

$$M_{HT} = M_{0,HT} + \ell_{HT} Z_{HT} - Z_{HT} h_{HT}$$

$$N_{HT} = 0$$

Positive elevator deflection is defined at trailing edge down.

2.4.5 Vertical Tail

The velocities at the vertical tails are a sum of the freestream velocity and the velocity due to angular rates. Therefore, the velocities at the vertical tails are

$$V_{VT,1} = \begin{bmatrix} u - ql_{z,VT} - rl_{y,VT} \\ v - rl_{x,VT} + pl_{z,VT} \\ w + ql_{x,VT} + pl_{y,VT} \end{bmatrix}$$

$$V_{VT,2} = \begin{bmatrix} u - ql_{z,VT} + rl_{y,VT} \\ v - rl_{x,VT} + pl_{z,VT} \\ w + ql_{x,VT} - pl_{y,VT} \end{bmatrix}$$

$$V_{VT,TOT} = \sqrt{u_{VT}^2 + v_{VT}^2 + w_{VT}^2}$$

The equations for lift and drag developed for the each vertical tail are as follows:

$$Lift_{VT} = q_{VT} A_{VT} \left[a_{VT} \alpha_{VT} + \frac{\partial C_{l,rud}}{\partial \delta_r} \delta_r \right]$$

$$Drag_{VT} = q_{VT} A_{VT} C_{D,VT}$$

where

$$q_{VT} = \frac{1}{2} \rho V_{VT,TOT}^2$$

$$\alpha_{VT} = \tan^{-1}\left(\frac{v_{VT}}{\sqrt{u_{VT}^2 + v_{VT}^2}} \right)$$

$$k_{VT} = \frac{1}{\pi E_{VT} A_{R,VT}}$$

$$C_{D,VT} = C_{D0,VT} + k_{VT} C_{L,VT}{}^2$$

As the XV-15 has two vertical tails, the force and moment equations needed to be duplicated for two tails, each with a different lateral offset from centerline. The contribution to the forces and moments from each vertical tail is as follows:

Vertical Tail #1 (right):

$$X_{VT1} = Lift_{VT1} \sin\alpha_{VT1} - Drag_{VT1} \cos\alpha_{VT1}$$

$$Y_{VT1} = -Lift_{VT1} \cos\alpha_{VT1} - Drag_{VT1} \sin\alpha_{VT1}$$

$$Z_{VT1} = 0$$

$$L_{VT1} = Y_{VT1}\ell_{z,VT1} + Z_{VT1}\ell_{y,VT1}$$

$$M_{VT1} = Z_{VT1}\ell_{x,VT1} - X_{VT1}\ell_{z,VT1}$$

$$N_{VT1} = -Y_{VT1}\ell_{x,VT1} - X_{VT1}\ell_{y,VT1}$$

Vertical Tail #2 (left):

$$X_{VT2} = Lift_{VT2} \sin\alpha_{VT2} - Drag_{VT} \cos\alpha_{VT2}$$

$$Y_{VT2} = -Lift_{VT2} \cos\alpha_{VT2} - Drag_{VT2} \sin\alpha_{VT2}$$

$$Z_{VT2} = 0$$

$$L_{VT2} = Y_{VT2}\ell_{z,VT2} - Z_{VT2}\ell_{y,VT2}$$

$$M_{VT2} = Z_{VT2}\ell_{x,VT2} - X_{VT2}\ell_{z,VT2}$$

$$N_{VT2} = -Y_{VT2}\ell_{x,VT2} + X_{VT2}\ell_{y,VT2}$$

Positive rudder deflection is defined as trailing edge right as viewed from above.

2.5 Proprotor Forces and Moments

2.5.1 General

The trim equations for the proprotor depend on the forces and moments of the proprotors. The methodology used to calculate proprotor forces and moments is to determine the aerodynamic and inertial forces on the blades, sum the forces and moments for all the blades around the azimuth, and then transform the forces and moments into body forces

and moments using the relative position of the proprotors on the aircraft. The following development is for the right rotor (*MR*1).

The forces and moments from the proprotors were determined based on the technique outlined in Reference 19. The following main assumptions were used in the development of these equations:

Helicopter/proprotor assumptions:

1. Aircraft and proprotor blades are rigid bodies
2. Climb angles, pitch attitudes, and angles of bank are small.
3. All derivatives and partial derivatives (first order Taylor Series approximations) are linear.
4. Lift curve slope and blade drag coefficient for the proprotor blades are an average over the entire span of the blade and is not a function of the local blade parameters around the azimuth.
5. Inflow through proprotor system is uniform.
6. The aircraft operates out of ground effect.
7. The two proprotors behave like two counter-rotating helicopter rotor heads.
8. The right proprotor rotates counterclockwise as viewed from the top and the left proprotor rotates clockwise.
9. The airframe is out of proprotor wake influence.

2.5.2 Flapping Equation of Motion

The flapping equation of motion was determined for a pitching, rolling, and yawing articulated hub with a hinge offset (*e*) and a flapping spring. The forces acting on the blade are inertial (due to blade rotation) and aerodynamic. The sum of blade forces must equal zero and the sum of the moments at the hinge must equal zero.

When viewing the proprotor, the following forces and moments are acting on the blades:

1. Inertial force at the hinge due centrifugal forces
2. Aerodynamic lift and drag forces
3. Moment due to inertial forces because of the hinge offset
4. Moment due to the aerodynamic lift and drag
5. Moment due to the flapping spring

While these forces and moments are easiest calculated in the prime, rotating, and non-rotating coordinate systems, they must be transferred to the body system for final trim calculations.

Inertial Forces and Moments

In order to determine the inertial forces, we begin by looking at generic point P on the blade (Figure 8).

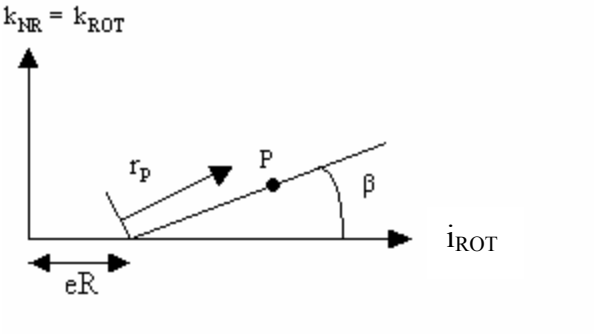

Figure 8: Position of Point 'P' on the Blade

The position vector, R_{TOT}, from the aircraft CG to the point P on the blade, as shown in Figure 9, when converted into the rotating axis system is as follows:

$$R_{TOT,ROT} = \begin{bmatrix} -R_{Ni}\cos\psi\cos\beta_M + R_{Nj}\sin\psi - R_{Nk}\cos\psi\sin\beta_M + eR + r_p\cos\beta \\ R_{Ni}\sin\psi\cos\beta_M + R_{Nj}\cos\psi + R_{Nk}\sin\psi\sin\beta_M \\ R_{Ni}\sin\beta_M - R_{Nk}\cos\beta_M + r_p\sin\beta + R_H \end{bmatrix}_{ROT}$$

Since point P is rotating at the angular velocity, Ω, as well as experiencing the pitch, roll and yaw (p, q, r) in the body axes, the velocity of point P in the rotating system is determined generically by:

$$\frac{d(\ )}{dt} = \frac{\partial(\ )}{\partial t} + \omega \times (\ )$$

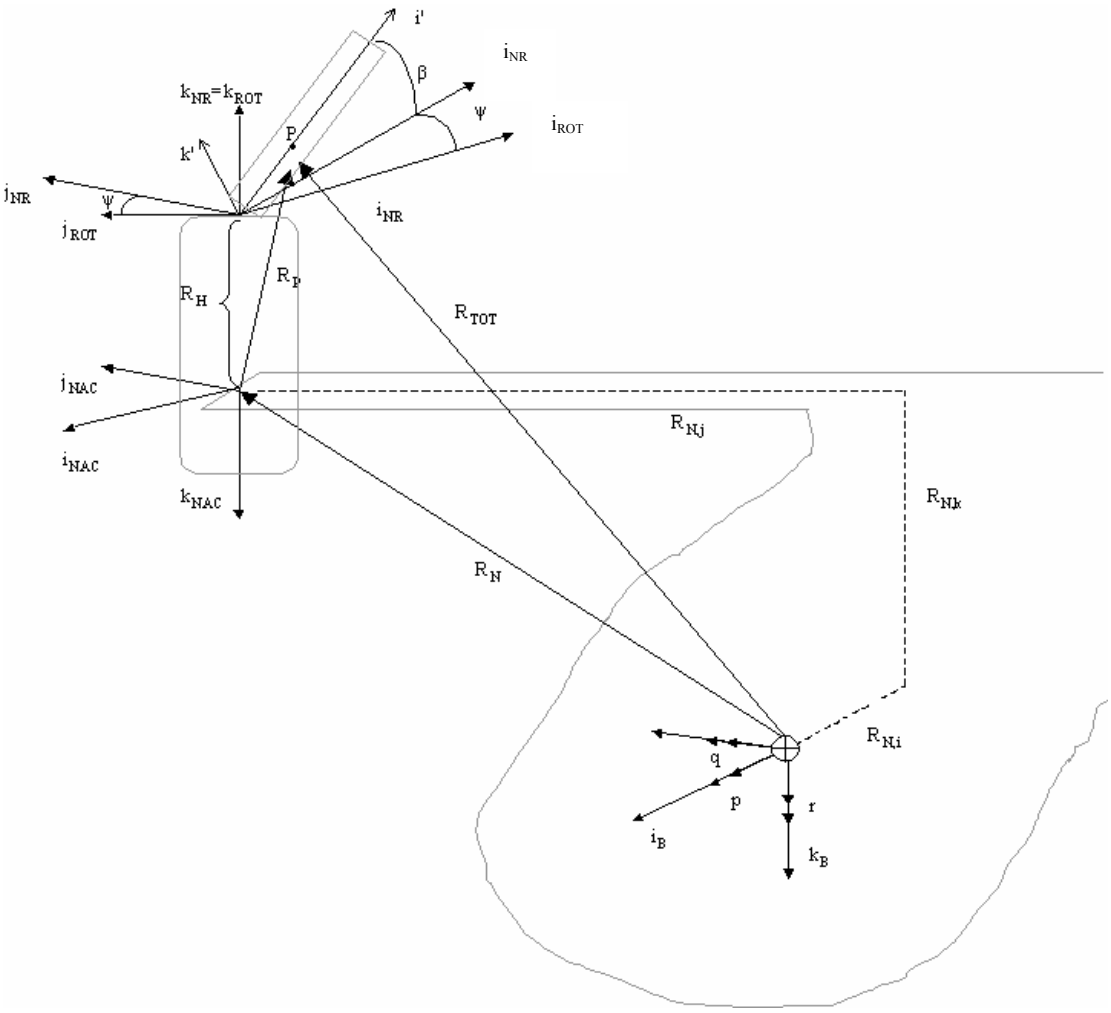

Figure 9: Position of Point 'P' with respect to the Aircraft CG

where the derivative with respect to time is the total velocity, the partial derivative with respect to time is the velocity in the rotating system, and ω is the angular velocity of the rotating system with respect to the fixed system (in this case, the body system).

$$V_{TOT,ROT}=\frac{d\left(R_{TOT,ROT}\right)}{dt}=\frac{\partial\left(R_{TOT,ROT}\right)}{\partial t}+\omega\times\left(R_{TOT,ROT}\right) \quad \text{where}$$

$$\omega = \begin{bmatrix} p \\ q \\ r \end{bmatrix}_B + \begin{bmatrix} 0 \\ 0 \\ \Omega \end{bmatrix}_{ROT} = \begin{bmatrix} -p\cos\psi\cos\beta_M + q\sin\psi - r\cos\psi\sin\beta_M \\ p\sin\psi\cos\beta_M + q\cos\psi + r\sin\psi\sin\beta_M \\ p\sin\beta_M - r\cos\beta_M + \Omega \end{bmatrix}_{ROT}$$

Therefore the total velocity of point P in the rotating axis system is:

$$V_{TOT,ROT} = \begin{bmatrix} V_{x,ROT} \\ V_{y,ROT} \\ V_{z,ROT} \end{bmatrix}$$

where

$$\begin{aligned} V_{x,ROT} &= R_{Ni}\Omega\sin\psi\cos\beta_M + R_{Ni}\dot{\beta}_M\cos\psi\sin\beta_M + R_{Nj}\Omega\cos\psi + R_{Nk}\Omega\sin\psi\sin\beta_M \\ &+ \left(p\sin\psi\cos\beta_M + q\cos\psi + r\sin\psi\sin\beta_M\right)\left(R_{Ni}\sin\beta_M - R_{Nk}\cos\beta_M + r_p\sin\beta + R_H\right) \\ &- \left(p\sin\beta_M - r\cos\beta_M + \Omega\right)\left(R_{Ni}\sin\psi\cos\beta_M + R_{Nj}\cos\psi + R_{Nk}\sin\psi\sin\beta_M\right) \\ &- R_{Nk}\dot{\beta}_M\cos\psi\cos\beta_M - r_p\sin\beta\dot{\beta} \end{aligned}$$

$$\begin{aligned} V_{y,ROT} &= R_{Ni}\Omega\cos\psi\cos\beta_M - R_{Ni}\dot{\beta}_M\sin\psi\sin\beta_M - R_{Nj}\Omega\sin\psi + R_{Nk}\Omega\cos\psi\sin\beta_M \\ &- \left(-p\cos\psi\cos\beta_M + q\sin\psi - r\cos\psi\sin\beta_M\right)\left(R_{Ni}\sin\beta_M - R_{Nk}\cos\beta_M + r_p\sin\beta + R_H\right) \\ &+ \left(p\sin\beta_M - r\cos\beta_M + \Omega\right)\left(-R_{Ni}\cos\psi\cos\beta_M + R_{Nj}\sin\psi - R_{Nk}\cos\psi\sin\beta_M + eR + r_p\cos\beta\right) \\ &+ R_{Nk}\dot{\beta}_M\sin\psi\cos\beta_M \end{aligned}$$

$$\begin{aligned} V_{z,ROT} &= R_{Ni}\dot{\beta}_M\cos\beta_M + R_{Nk}\dot{\beta}_M\sin\beta_M + r_p\cos\beta\dot{\beta} \\ &+ \left(-p\cos\psi\cos\beta_M + q\sin\psi - r\cos\psi\sin\beta_M\right)\left(R_{Ni}\sin\psi\cos\beta_M + R_{Nj}\cos\psi + R_{Nk}\sin\psi\sin\beta_M\right) \\ &- \left(p\sin\psi\cos\beta_M + q\cos\psi + r\sin\psi\sin\beta_M\right)\left(-R_{Ni}\cos\psi\cos\beta_M + R_{Nj}\sin\psi - R_{Nk}\cos\psi\sin\beta_M + eR + r_p\cos\beta\right) \end{aligned}$$

The acceleration of point P was determined similarly, where ( ) is now $V_{TOT,ROT}$.

In order to determine the inertia forces on the blade, the acceleration of point P needs to be converted the prime coordinate system. The flapping moment about the hinge due to inertia of the blade is defined as:

$$M_I = -\int_0^{1\text{-}e} ma'_{Pz} r_p \, dr$$

where

m is the distributed mass of the blade

$a_{pz}^{'}$ is acceleration of point P in the z direction as calculated above, converted from the rotating to the prime coordinate system

The following simplifying assumptions were made:

1. There are no dynamic nacelle movements therefore $\dot{\beta}_M = \ddot{\beta}_M = 0$
2. Proprotor angular velocity is constant therefore $\dot{\Omega} = \ddot{\Omega} = 0$

The analysis was also modified to include:

1. The non-dimensional blade coordinate 'x' where $x=r_pR$
2. The blade flapping inertia '$I_{b,e}$' where $I_{\mathrm{b,e}} = R^3 \int_0^{1-e} mx^2 dx = \frac{1}{3} mR^3 (1-e)^3$. The reference blade flapping inertia for blades without hinge offset has an integrand calculated from root (0) to tip (R) which gives $I_b = R^3 \int_0^R mx^2 dx = \frac{1}{3} mR^3$

   The mass distribution of the blade is assumed constant, so the integral of m from root (or offset) to tip is the total mass of the blade.
3. The blade Lock number where $\gamma = \rho\, a\, c\, R^4 / I_b$
4. The derivative with respect to blade azimuth position, $\partial/\partial\psi$ where $\partial/\partial t = \Omega\partial/\partial\psi$. The notation for the derivative with respect to blade azimuth position is a '*' instead of a dot over the quantity.

Another simplification method used is the concept of an ordering scheme. An ordering scheme allows for simplification of the equations by assigning a relative magnitude to each variable and then neglecting the small order of magnitude terms. The order of magnitudes used are O(1), O(ε), O(ε^2), O(ε^3), etc. Where 'ε' represents a quantity of approximately 0.1-0.2. For terms that have an order of O(ε^2) or smaller, the relative magnitude is 1% (0.1^2) to 4% (0.2^2) when compared to a term with the order of magnitude of 1 (O(1)). Small order of magnitude terms relative to the other terms in the equation can be neglected in this manner. (Reference 19)

The following orders of magnitude were applied to the terms used in these equations:

O(1): R_{Ni}, R_{Nj}, R_{Nk}, $\partial / \partial t$, $\partial / \partial \psi$,R_H,V, R, m, r_p, β_M, μ, x, ψ, cos, sin, θ_0, θ_{1s}, θ_{1c}, θ_{tw}

O(ε): p, q, r, e, β, α_F, β_F, λ

The ordering scheme was mechanized using a multivariate Taylor series expansion. Because the order of magnitude of β, α_F, β_F is O(ε), the Taylor series expansion essentially applies the small angle approximation where $\cos(\beta) \approx 1$ and $\sin(\beta) \approx \beta$.

Applying the above simplifications, non-dimensional variable substitutions, and ordering scheme results in the following equation for M_I:

$$M_I = -I_b\Omega^2\left(-\frac{\overset{*}{q}}{\Omega}\cos\psi + 2\frac{q}{\Omega}\sin\psi - \frac{\overset{*}{p}}{\Omega}\sin\psi\cos\beta_M + \beta - \frac{\overset{*}{r}}{\Omega}\sin\psi\sin\beta_M + \overset{**}{\beta} \right.$$
$$\left. - 2\frac{p}{\Omega}\cos\psi\cos\beta_M - 2\frac{r}{\Omega}\cos\psi\sin\beta_M \right)$$

$$-\frac{3}{2}I_b\Omega^2\left(-\frac{\overset{*}{p}}{\Omega}\frac{R_{Nj}}{R}\cos\beta_M + \frac{\overset{*}{q}}{\Omega}\frac{R_{Ni}}{R}\cos\beta_M + \frac{\overset{*}{q}}{\Omega}\frac{R_{Nk}}{R}\sin\beta_M - \frac{\overset{*}{r}}{\Omega}\frac{R_{Nj}}{R}\sin\beta_M \right)$$

Aerodynamic Forces and Moment

Due to the blade motion and aircraft movement through the air, there is an additional aerodynamic moment of the blade outboard of the hinge about the hinge (due to the hinge offset). The velocity seen by the blade is a combination of the blade rotation and aircraft movement.

The aircraft relative velocities (u, v, and w) are defined with respect to the body axes and can be defined in terms of α and β of the fuselage where

$u = V\cos\alpha_F\cos\beta_F$
$v = V\sin\beta_F$
$w = V\sin\alpha_F\cos\beta_F$

These body velocities are then transformed from the body frame into the rotating frame and added to the induced velocity.

$$\begin{bmatrix} -u \\ -v \\ -w \end{bmatrix}_B + \begin{bmatrix} 0 \\ 0 \\ -v_i \end{bmatrix}_{ROT} = V_{uvw,vi}$$

where

$$V_{uvw,vi} = \begin{bmatrix} V\cos\alpha_F\cos\beta_F\cos\psi\cos\beta_M - V\sin\beta_F\sin\psi + V\sin\alpha_F\cos\beta_F\cos\psi\sin\beta_M \\ -V\cos\alpha_F\cos\beta_F\sin\psi\cos\beta_M - V\sin\beta_F\cos\psi - V\sin\alpha_F\cos\beta_F\sin\psi\sin\beta_M \\ -V\cos\alpha_F\cos\beta_F\sin\beta_M + V\sin\alpha_F\cos\beta_F\cos\beta_M - v_i \end{bmatrix}_{ROT}$$

In addition, since the proprotors are located at a distance offset from the CG, there is also a velocity component due to the angular velocity of the aircraft. This linear velocity is equal to the cross product of the angular rates and position vector of the rotor rub with respect to the CG.

Linear velocity = $\begin{bmatrix} -p \\ -q \\ -r \end{bmatrix}_B \times \begin{bmatrix} R_{Ni} + R_H\sin(\beta_M) \\ R_{Nj} \\ R_{Nk} - R_H\cos(\beta_M) \end{bmatrix}_B$ where both vectors must be transformed to the non-rotating axis prior to taking the cross product. The total is then transformed to the rotating frame.

Linear velocity in the non- rotating coordinate system equals:

$$V_{Lin,NR} = \begin{bmatrix} V_1 \\ V_2 \\ V_3 \end{bmatrix}_{NR} = \begin{bmatrix} -\left(\left(\left(-qR_{Nk} + qR_H\cos(\beta_M) + R_{Nj}r\right)\cos(\beta_M) + \left(qR_{Ni} + qR_H\sin(\beta_M) - R_{Nj}p\right)\sin(\beta_M)\right)\right) \\ -\left(-pR_{Nk} + pR_H\cos(\beta_M) + rR_{Ni} + rR_H\sin(\beta_M)\right) \\ -\left(\left(qR_{Ni} + qR_H\sin(\beta_M) - R_{Nj}p\right)\cos(\beta_M) + \left(-R_{Nj}r + qR_{Nk} - qR_H\cos(\beta_M)\right)\sin(\beta_M)\right) \end{bmatrix}$$

This is then converted to the rotating coordinate system as follows:

$$V_{Lin,ROT} = \begin{bmatrix} V_1 \\ V_2 \\ V_3 \end{bmatrix}_{ROT} = \begin{bmatrix} V_{1,NR}\cos(\psi) + V_{2,NR}\sin(\psi) \\ -V_{1,NR}\sin(\psi) + V_{2,NR}\cos(\psi) \\ V_{3,NR} \end{bmatrix}$$

Therefore the total velocity at the rotor is $V_{FF,ROT} = V_{Lin,ROT} + V_{uvw,vi}$

By definition, the flow velocity in the k_{ROT} direction is equal to the proprotor inflow. At this point, the non-dimensional quantity inflow ratio, λ, which is the total velocity perpendicular to the disk non-dimensionalized by the proprotor tip speed, ΩR, will be introduced.

$$\lambda = \frac{\text{Velocity} \perp \text{rotor disk}}{\Omega R}$$

Due to the sign convention, the total velocity is actually in the negative k_{ROT} direction, and therefore equals $-\lambda\Omega R$.

The velocity of a point on the blade due to the blade rotation (V_{TOT_ROT}) was previously determined during the derivation of the inertial forces. The total velocity seen by a point on the blade, V_{ROT}, is $V_{ROT} = V_{FF,ROT} - V_{TOT,ROT}$ where V_{ROT} can also be written:

$$V_{ROT} = \begin{bmatrix} V_X \\ V_Y \\ V_Z \end{bmatrix}_{ROT} = \begin{bmatrix} U_x \\ U_y \\ U_z \end{bmatrix}_{ROT}$$

As shown in Figure 10 (from Reference 19), the velocity at point P in the prime axes system:

U_R i' $-U_T$ j' $-U_P$ k'

When we transfer this to the primed coordinate system we get:

$$V' = \begin{bmatrix} V_X \\ V_Y \\ V_Z \end{bmatrix}' = \begin{bmatrix} U_R \\ -U_T \\ -U_P \end{bmatrix}'$$

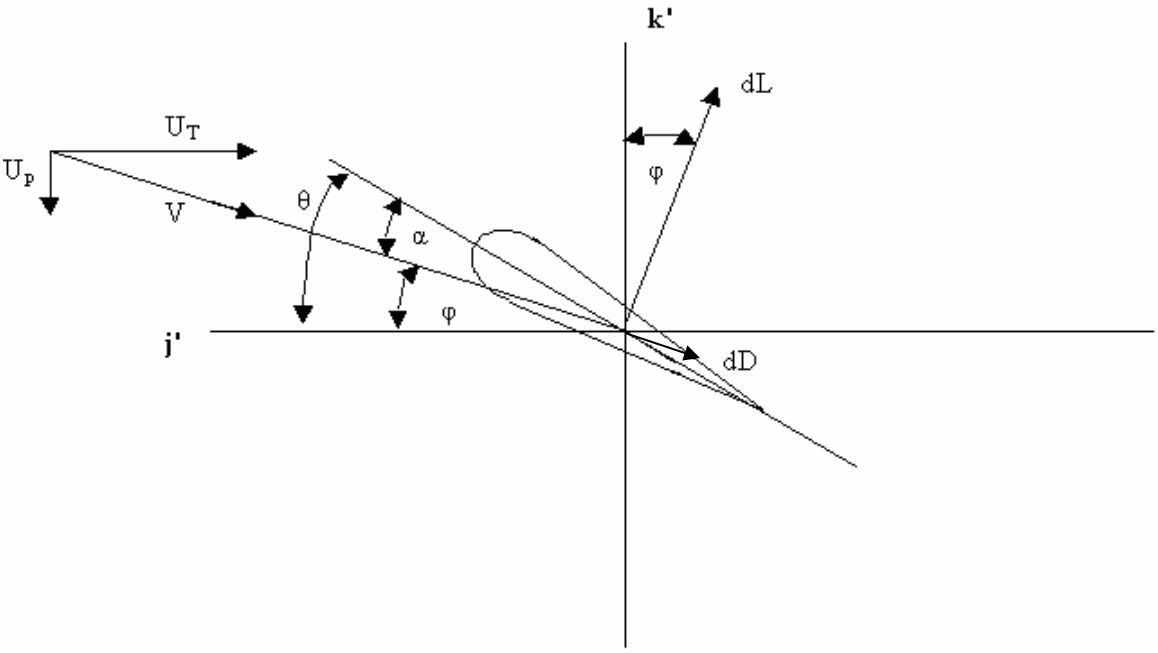

Figure 10: Blade Aerodynamics (Reference 19)

If we assume that the profile drag coefficient is an average value over the blade span and is not a function of local angle of attack and blade Mach number around the azimuth, the lift and drag forces on the blade are:

$$dL = \frac{1}{2}\rho V^2 c_l c dr$$

$$dD = \frac{1}{2}\rho V^2 c_d c dr$$

where

$$c_l = c_{l\alpha}\alpha_{blade} = a\alpha_{blade}$$

$$\alpha_{blade} = \theta_{blade} - \varphi = \theta_{blade} - \tan^{-1}\left(\frac{U_P}{U_T}\right)$$

$$\theta_{blade} = \theta_0 + \theta_{1c}\cos\psi + \theta_{1s}\sin\psi + \theta_{twist}\frac{r}{R} + \theta_{twist,0}$$

Applying the ordering scheme,

$$\alpha_{blade} = \theta_{blade} - \left(\frac{U_P}{U_T}\right)$$

$$V^2 = U_T^2 + U_P^2 = O(1)^2 + O(\varepsilon)^2 \approx U_T^2$$

This reduces the equations to:

$$dL = \frac{1}{2}\rho ac\left(\theta_{blade}U_T^2 - U_P U_T\right)dr$$

$$dD = \frac{1}{2}\rho U_T^2 c_d c dr$$

The flapping moment about the hinge due to aerodynamic forces on the blade is defined as:

$$M_A = \int_0^{1\text{-e}} r_p dL$$

The following simplifying assumptions were made:

1. There are no dynamic nacelle movements therefore $\dot{\beta}_M = \ddot{\beta}_M = 0$
2. Proprotor angular velocity is constant therefore $\dot{\Omega} = \ddot{\Omega} = 0$

The analysis was modified to include:

1. The non-dimensional blade coordinate 'x' where $x=r_p/R$
2. The blade flapping inertia '$I_{b,e}$' where $I_{b,e} = R^3 \int_0^{1-e} mx^2 dx = \frac{1}{3} mR^3 (1-e)^3$. The reference blade flapping inertia for blades without hinge offset has an integrand calculated from root (0) to tip (R) which gives $I_b = R^3 \int_0^R mx^2 dx = \frac{1}{3} mR^3$. The mass distribution of the blade is assumed constant, so the integral of m from root (or offset) to tip is the total mass of the blade.
3. The ordering scheme was applied to the analysis. When the ordering scheme is applied to the blade flapping inertia, the blade flapping inertia with hinge offset reduces to the blade flapping inertia without hinge offset.

Due to the size of the full M_A equation, it will not be included here.

Hub Spring Moment

Due to the presence of a hub spring, an additional reaction due to flapping is present. The moment at the hinge due to the hub spring is:

$M_{spring} = K_\beta (\beta - \beta_P)$ where β_p is the precone angle.

$$M_{spring,NR} = \begin{bmatrix} L_{spring} \\ M_{spring} \\ N_{spring} \end{bmatrix} = \begin{bmatrix} -M_{spring} \sin\psi \\ -M_{spring} \cos\psi \\ 0 \end{bmatrix}_{NR}$$

When the steady average is taken around the proprotor revolution by substituting in the Fourier series approximation for the flapping angle, integrating around the azimuth, assuming there is no precone angle, and multiplying by the number of blades and dividing by 2π, the resulting moment is:

$$M_{spring} = \begin{bmatrix} -\frac{1}{2} N_b K_\beta \beta_{1s} \\ -\frac{1}{2} N_b K_\beta \beta_{1c} \\ 0 \end{bmatrix}_{NR} = \begin{bmatrix} \frac{1}{2} N_b K_\beta \beta_{1s} \cos\beta_M \\ -\frac{1}{2} N_b K_\beta \beta_{1c} \\ \frac{1}{2} N_b K_\beta \beta_{1s} \sin\beta_M \end{bmatrix}_B$$

Flapping Equation of Motion

To determine the flapping equation of motion, the sum of the moments about the hinge was set equal to zero.

$\Sigma M = M_A + M_I + M_{spring} = 0$

The flapping equation of motion for a single blade is also too large to be included here.

Flapping Angles

From the flapping we can extract the individual flapping components for each blade. Assuming a periodic flapping solution as a Fourier series, we get

$$\beta = \beta_0 + \beta_{1s} \sin\psi + \beta_{1c} \cos\psi + \beta_{2s} \sin(2\psi) + \beta_{2c} \cos(2\psi) + ...$$

If we truncate the series and only include first order terms we get the following:

$$\beta = \beta_0 + \beta_{1s}\sin\psi + \beta_{1c}\cos\psi$$
$$\overset{*}{\beta} = \beta_{1s}\cos\psi - \beta_{1c}\sin\psi$$
$$\overset{**}{\beta} = -\beta_{1s}\sin\psi - \beta_{1c}\cos\psi$$

When we substitute these values for $\beta, \overset{*}{\beta}$, and $\overset{**}{\beta}$ into the flapping equation of motion, we change the equation from a differential equation to an algebraic equation. The unknowns are now β_0, β_{1s}, and β_{1c}. From this we can solve the equations for each of the unknowns. The equation for β_0 is comprised of only the constant terms. If we set $\sin(n\psi)=0$ and $\cos(n\psi)=0$ for all values of n, we get an equation for β_0. The equation for β_{1s} is found by setting all the $\sin(n\psi)=0$ for all values of n and setting the higher order $\cos(n\psi)$ terms equal to zero. The equation for β_{1c} is found by setting all the $\cos(n\psi)=0$ for all values of n and setting the higher order $\sin(n\psi)$ terms equal to zero.

2.5.3 Proprotor Forces

Blade Aerodynamic and Inertial Forces

In order to determine the proprotor contribution to the Euler equations, the proprotor lift and drag aerodynamic forces must be converted to body forces. The forces in the prime coordinate system are:

$$dX' = 0$$

$$dY' = dL\sin\varphi + dD\cos\varphi$$

$$dZ' = dL\cos\varphi - dD\sin\varphi$$

Using the non-dimensional blade coordinate 'x' where $x=r_p/R$ and applying the ordering scheme prior to integrating across the blade (where $dD << dL$) gives:

$$X' = \int_0^{1-e} dX'$$

$$Y' = \int_0^{1-e} dY' = \int_0^{1-e} dL\frac{U_P}{U_T} + dD = \int_0^{1-e}\left(\frac{1}{2}\rho ac\left(\theta_{blade}U_P U_T - U_P^2\right) + \frac{1}{2}\rho c_d c U_T^2\right)dr$$

$$Z' = \int_0^{1-e} dZ' = \int_0^{1-e} dL = \int_0^{1-e}\frac{1}{2}\rho ac\left(\theta_{blade}U_T^2 - U_P U_T\right)dr$$

The integrated forces are then converted to the body coordinate system.

$$\begin{bmatrix} X \\ Y \\ Z \end{bmatrix}_B = \begin{bmatrix} -\cos\beta\cos\psi\cos\beta_M + \sin\beta\sin\beta_M & \sin\psi\cos\beta_M & \sin\beta\cos\psi\cos\beta_M + \cos\beta\sin\beta_M \\ \cos\beta\sin\psi & \cos\psi & -\sin\beta\sin\psi \\ -\cos\beta\cos\psi\sin\beta_M - \sin\beta\cos\beta_M & \sin\psi\sin\beta_M & \sin\beta\cos\psi\sin\beta_M - \cos\beta\cos\beta_M \end{bmatrix}\begin{bmatrix} X' \\ Y' \\ Z' \end{bmatrix}$$

Previously, the forces from the main proprotor were only for one blade. Now we need to get the total forces and moments for all three blades combined. The assumption is made that all three blades are identical and therefore the steady state motion of all the blades is the same. In that case, the force and moment calculations can be derived for one blade and applied to the rest of the blades by simply adjusting the blade azimuth angle. Since the XV-15 has three blades, the three azimuth angles used will be ψ_1=0 radians, ψ_2= 2/3 π radians, and ψ_3= 4/3 π radians. The resulting forces and moments are:

$$F_{MR,B} = F_{MR,B}\Big|_{\psi=0} + F_{MR,B}\Big|_{\psi=\frac{2\pi}{3}} + F_{MR,B}\Big|_{\psi=\frac{4\pi}{3}}$$

The inertial forces were not included in the above discussion, as once the blade forces are summed, the resultant contribution due to the inertial forces is zero.

To find the trim value, we apply the ordering scheme and then substitute in the Fourier series approximation used earlier for $\beta, \overset{*}{\beta}, \text{and } \overset{**}{\beta}$. Since the steady state proprotor trim forces and moments are needed for trim, all periodic terms are set equal to zero because they are averaged/summed over the proprotor revolution.

Proprotor Thrust

The integrated *Z*' force is also known as the rotor thrust contribution from that blade. Because the blades are assumed identical, the total rotor thrust is simply equal to 3 times the *Z*' force.

The non-dimensional thrust coefficient is defined as follows:

$$C_T = \frac{Thrust}{\rho A_{disk} \Omega^2 R^2}$$

2.5.4 Proprotor Moments

Moment due to Inertial and Aerodynamic Blade Forces

By definition, a moment is the cross product of the direction vector and the force vector. In this case, the moment about the CG due to the proprotor forces is:

$$M_{MR,B} = r_{CG \to Hub} \times F_{MR,B} = L_{MR}\mathbf{i} + M_{MR}\mathbf{j} + N_{MR}\mathbf{k}$$

The moments due to the rotor forces are as follows:

$$\begin{bmatrix} L \\ M \\ N \end{bmatrix}_{MR,B} = \begin{bmatrix} R_{Nj} Z_{MR,B} - \left(- R_H \cos\beta_M + R_{Nk}\right) Y_{MR,B} \\ \left(- R_H \cos\beta_M + R_{Nk}\right) X_{MR,B} - \left(R_H \sin\beta_M + R_{Ni}\right) Z_{MR,B} \\ \left(R_H \sin\beta_M + R_{Ni}\right) Y_{MR,B} - R_{Nj} X_{MR,B} \end{bmatrix}_B$$

2.6 Control Inceptors

A simplified relationship between the pilot controls and the response at the rotor and control surfaces was implemented for this model. Due to the assumption that rotor RPM was constant, there was no need for the rotor governor that is required for the actual aircraft and is included in the GTRS model. The Stability and Control Augmentation System (SCAS) was not modeled for this project; hence, the results are essentially for a SCAS off XV-15.

The pilot controls can be tied to the control surfaces as follows:

$\delta_{elev}=(\delta_{long}-\delta_{long,\ neutral})(\ \delta_{elev}/\delta_{long})$

$\delta_{ail}=-(\delta_{lat}-\delta_{lat,\ neutral})(\ \delta_{ail}/\delta_{lat})$

$\delta_{rud}=(\delta_{ped}-\delta_{ped,\ neutral})(\ \delta_{rud}/\delta_{ped})$

Per GTRS, the pilot controls can be tied to the rotor via the swashplate by:

$\theta_0=-\delta\theta_0/\delta_{coll}\ \delta_{coll}+\theta_{0LL}\pm(\delta_{lat}-\delta_{lat,\ neutral})\ \delta\theta_0/\delta_{lat}+\theta_{rotor\ governor}$ + SCAS

$\theta_{1s}=(\delta_{long}-\delta_{long,\ neutral})\ \delta\theta_{1s}/\delta_{long}\pm(\delta_{ped}-\delta_{ped,\ neutral})\ \delta\theta_{1s}/\delta_{ped}+1.5^{\circ}(1-\cos\beta_M)$ + SCAS

$\theta_{1c}=0$ (Lateral cyclic is not used in the basic XV-15 control system)

While the equations are valid, because there is no need for a rotor governor in this model and there is no SCAS, the θ_0 equation as implemented in the aircraft resulted in zero inches of pilot collective control required for airplane mode trim and a constant θ_0 at the rotor of 21.5 degrees (θ_{0LL}). (As stated in the aircraft description, the collective controller is phased out in airplane mode and the rotor governor takes over as the collective

controller.) In reality, zero inches of trim collective is not correct, therefore the pilot collective control was removed from the model and the model was trimmed at the swashplate using θ_0 rather than δ_{coll}. The other pilot controls (δ_{long}, δ_{lat}, and δ_{ped}) were, however, used for the analysis.

The above equations were simplified via the removal of the SCAS and rotor governor to be as follows:

$$\theta_{0,1} = \theta_{00} - (\delta_{lat}-\delta_{lat,\ neutral})\ \delta\theta_0/\delta_{lat}$$

$$\theta_{0,2} = \theta_{00} + (\delta_{lat}-\delta_{lat,\ neutral})\ \delta\theta_0/\delta_{lat}$$

$$\theta_{1s,1} = -(\delta_{long}-\delta_{long,\ neutral})\ \delta\theta_{1s}/\delta_{long} + (\delta_{ped}-\delta_{ped,\ neutral})\ \delta\theta_{1s}/\delta_{ped} - 1.5\pi(1-\cos(\beta_M))/180$$

$$\theta_{1s,2} = -(\delta_{long}-\delta_{long,\ neutral})\ \delta\theta_{1s}/\delta_{long} - (\delta_{ped}-\delta_{ped,\ neutral})\ \delta\theta_{1s}/\delta_{ped} - 1.5\pi(1-\cos(\beta_M))/180$$

$\theta_{1c1}=\theta_{1c2}=0$ (Lateral cyclic is not used in the basic XV-15 control system)

The control travel for the pilot cockpit control inceptors are

Controller	Total Control Travel (100%), in.	Neutral Control Position (50%), in.
Longitudinal Stick	9.6	4.8
Lateral Stick	9.6	4.8
Pedal	5	2.5
Collective	10	--

2.7 Solution Setup

2.7.1 Trim

As previously discussed, the basic equations of motion are the Euler equations. If I_{xy} and I_{yz} are considered negligible, the Euler equations become:

$$X = m_{ac}\left(\dot{u} + qw - rv\right) + mg\sin\theta$$

$$Y = m_{ac}\left(\dot{v} + ru - pw\right) - mg\sin\varphi\cos\theta$$

$$Z = m_{ac}\left(\dot{w} + pv - qu\right) - mg\cos\varphi\cos\theta$$

$$L = I_{xx}\dot{p} - \left(I_{yy} - I_{zz}\right)qr - I_{xz}\left(pq - \dot{r}\right)$$

$$M = I_{yy}\dot{q} - \left(I_{zz} - I_{xx}\right)pr + I_{xz}\left(p^2 - r^2\right)$$

$$N = I_{zz}\dot{r} - \left(I_{xx} - I_{yy}\right)pq + I_{xz}\left(qr - \dot{p}\right)$$

$$p = \dot{\varphi} - \dot{\psi}\sin\theta$$

$$q = \dot{\theta}\cos\varphi + \dot{\psi}\sin\varphi\cos\theta$$

$$r = \dot{\psi}\cos\varphi\cos\theta - \dot{\theta}\sin\varphi$$

where X, Y, Z, L, M and N are composed of the forces and moment from each aircraft component and m_{ac} is the mass of the aircraft. For example:

$$X = X_{fuse} + X_{wing} + X_{HT} + X_{VT} + X_{MR1} + X_{MR2}$$

In order to de-couple the kinematic equations, the kinematic equations are re-arranged as equations for $\dot{\phi}, \dot{\theta}, \text{and } \dot{\psi}$:

$$\dot{\varphi} = p + \frac{q\sin\theta\sin\phi}{\cos\theta} + \frac{r\sin\theta\cos\phi}{\cos\theta}$$

$$\dot{\theta} = q\cos\varphi - r\sin\varphi$$

$$\dot{\psi} = \frac{q\sin\varphi}{\cos\theta} + \frac{r\cos\phi}{\cos\theta}$$

To extract the trim equations, the steady-state components of the Euler equations had to be developed. The Euler equations were linearized using the small perturbation technique. The following substitutions and assumptions were made:

1. Small perturbations were taken around a trimmed steady state value for the linear and angular velocities and the body angles. For example, substitute in $u=u_0+\Delta u$, where u_0 is the trim value and Δu is the small perturbation from trim.
2. Forces were divided by the aircraft mass in order to remove the weight component from the force equations.
3. An ordering scheme was applied to the equations, which resulted in the small perturbation assumption for the angles and products of angular and linear velocity perturbations.
4. Set perturbations equal to zero to get trim equations.

The above substitutions and assumptions result in the following trim equations:

$$\frac{X}{m_{ac}} = qw - rv + g\sin\theta$$

$$\frac{Y}{m_{ac}} = ru - pw - g\sin\varphi\cos\theta$$

$$\frac{Z}{m_{ac}} = pv - qu - g\cos\varphi\cos\theta$$

$$L = -\left(I_{yy} - I_{zz}\right)qr - I_{xz}pq$$

$$M = -\left(I_{zz} - I_{xx}\right)pr + I_{xz}\left(p^2 - r^2\right)$$

$$N = -\left(I_{xx} - I_{yy}\right)pq + I_{xz}qr$$

$$\dot{\varphi} = p + \frac{q\sin\theta\sin\phi}{\cos\theta} + \frac{r\sin\theta\cos\phi}{\cos\theta}$$

$$\dot{\theta} = q\cos\varphi - r\sin\varphi$$

$$\dot{\psi} = \frac{q\sin\varphi}{\cos\theta} + \frac{r\cos\phi}{\cos\theta}$$

The unknowns in the above equations are: u, v, w, p, q, r, $\theta, \phi, \dot{\phi}, \dot{\theta},$ and $\dot{\psi}$. Additional unknowns hidden in the X, Y, Z, L, M, and N terms are:

θ_0, $\beta_{01}, \beta_{1s1}, \beta_{1c1,}$ $\beta_{02}, \beta_{1s2}, \beta_{1c2,}$ $\delta_{lat}, \delta_{long}, \delta_{ped}$ λ_1 and λ_2.

By substituting the relationships for u, v, and w as a function of α_F and β_F into the trim equations, the number of unknowns are reduced and the equations become a function of α_F and β_F rather than u, v, and w.

By definition, $\alpha_F = \tan^{-1}\left(\frac{w}{u}\right)$ and $\beta_F = \sin^{-1}\left(\frac{v}{V}\right)$, which gives;

$$u = V\cos\alpha_F \cos\beta_F$$

$$v = V\sin\beta_F$$

$$w = V\sin\alpha_F \cos\beta_F$$

Since the problem is looking for a steady trim solution, the system can be further constrained by the assumption that $\dot{\phi} = \dot{\theta} = 0$. This is true in a steady banked turn due to the influence of the weight vector. For a steady banked turn, the weight vector stays constant in the body axes system. If $\dot{\phi} \neq \dot{\theta} \neq 0$, then the weight vector in the body axes system is constantly changing. Straight and level flight is essentially a special case of a steady turn with a turn radius approaching infinity. With this constraint, the kinematic equations become a function of $\dot{\psi}, \theta, \text{and } \varphi$, which further reduces the number of unknowns. V and $\dot{\psi}$ are now input parameters.

The unknowns in the above equations are now: p, q, r, θ, ϕ, α_F, and β_F, and the additional unknowns hidden in the X, Y, Z, L, M, and N equations,

θ_0, $\beta_{01}, \beta_{1s1}, \beta_{1c1,}$ $\beta_{02}, \beta_{1s2}, \beta_{1c2,}$ $\delta_{lat}, \delta_{long}, \delta_{ped}$ λ_1 and λ_2.

This results in 19 unknowns and therefore requires 19 equations to solve. There are already 9 equations from the force, moment, and kinematic equations.

Equations 1-9:

$$\frac{X}{m_{ac}} = V\dot{\psi}\sin\phi\sin\theta\sin\alpha_F\cos\beta_F - V\dot{\psi}\cos\phi\cos\theta\sin\beta_F + g\sin\theta$$

$$\frac{Y}{m_{ac}} = V\dot{\psi}\cos\phi\cos\theta\cos\alpha_F\cos\beta_F + V\dot{\psi}\sin\theta\sin\alpha_F\cos\beta_F - g\sin\phi\cos\theta$$

$$\frac{Z}{m_{ac}} = -V\dot{\psi}\sin\theta\sin\beta_F - V\dot{\psi}\sin\phi\sin\theta\cos\alpha_F\cos\beta_F - g\cos\phi\cos\theta$$

$$L = -\left(I_{yy} - I_{zz}\right)\dot{\psi}^2\sin\phi\cos\phi\cos^2\theta + I_{xz}\dot{\psi}^2\sin\phi\sin\theta\cos\theta$$

$$M = \left(I_{zz} - I_{xx}\right)\dot{\psi}^2\cos\phi\cos\theta\sin\theta + I_{xz}\left(\dot{\psi}^2\sin^2\theta - \dot{\psi}^2\cos^2\phi\cos^2\theta\right)$$

$$N = \left(I_{xx} - I_{yy}\right)\dot{\psi}^2\sin\phi\sin\theta\cos\theta - I_{xz}\dot{\psi}^2\sin\phi\cos\phi\cos^2\theta$$

$$p = -\dot{\psi}\sin\theta$$

$$q = \dot{\psi}\sin\phi\cos\theta$$

$$r = \dot{\psi}\cos\phi\cos\theta$$

Equation 10: Coordinated Turn

In order to be steady, the turn must be coordinated. Hence, the side load factor, n_y, must be equal to 0. By definition, $n_y = Y/(m_{ac}g)$. From the Y-force equilibrium equation:

$$n_y = \frac{Y}{m_{ac}g} = \frac{1}{g}(ru - pw) - \sin\varphi\cos\theta = 0$$

The requirement for n_y=0 can be satisfied by either setting Y=0 or by setting the right hand side of the equation equal to 0.

When the substitutions are made for p, q, r, u, v, and w, the equation becomes:

$$-\sin\phi\cos\theta + \frac{V\dot{\psi}}{g}\left(\cos\alpha_F\cos\phi\cos\theta + \sin\alpha_F\sin\theta\right)\cos\beta_F = 0$$

Equation 11: Flight Path Angle

A relationship for the flight path angle can be derived by equating two expressions for the vertical component of velocity. The vertical component of velocity is $V\sin(-\gamma)$

The vertical component of velocity is also $-u\sin\theta + v\sin\phi\cos\theta + w\cos\phi\cos\theta$,

which can be re-written as:

$$-V\cos\alpha_F\cos\beta_F\sin\theta + V\sin\beta_F\sin\phi\cos\theta + V\sin\alpha_F\cos\beta_F\cos\phi\cos\theta$$

Therefore:

$$\sin\gamma = \cos\alpha_F\cos\beta_F\sin\theta - \sin\beta_F\sin\phi\cos\theta - \sin\alpha_F\cos\beta_F\cos\phi\cos\theta$$

Equation 12 and 13: Rotor Inflow

By definition, the rotor inflow is the total velocity perpendicular to the rotor. This was previously defined as the component of $V_{Lin,ROT}$ in the k_{ROT} direction multiplied by ΩR.

$$\lambda\Omega R = (V\sin(\alpha_F)\cos(\beta_F) + qR_{Ni} - R_{Nj}p)\cos(\beta_M) + (qR_{Nk} - V\cos(\alpha_F)\cos(\beta_F) - R_{Nj}r)\sin(\beta_F) - v_i$$

Therefore,

$$\lambda = -\frac{\left((V\sin(\alpha_F)\cos(\beta_F) + qR_{Ni} - R_{Nj}p)\cos(\beta_M) + (qR_{Nk} - V\cos(\alpha_F)\cos(\beta_F) - R_{Nj}r)\sin(\beta_F)\right)}{\Omega R} + \frac{v_i}{\Omega R}$$

where

$$\frac{v_i}{\Omega R} = \frac{C_T}{2\sqrt{\left(\mu^2 + \lambda^2\right)}}$$

The inflow needs to be calculated iteratively for each proprotor.

The advance ratio, μ, in the above equation is defined as the non-dimensional in-plane velocity. When $V_{FF,ROT}$ is converted back to the non-rotating coordinate system, the total in plane velocity is a combination of the components in the i_{NR} and j_{NR} directions. If we let $U_{FF,NR}$ be the component in the i_{NR} direction and $V_{FF,NR}$ be the component in the j_{NR} direction, we get the following:

$$\mu = \frac{\sqrt{\left(U_{FF,NR}^2 + V_{FF,NR}^2\right)}}{\Omega R}$$

Equation 14-19:

Equations for β_0, β_{1s}, and β_{1c} for each proprotor from the expressions derived in section 2.5.

Using the above equations, the trim solution can be determined for a given free stream velocity, flight path angle, and turn rate. Additional parameters that need to be defined are mast angle, gross weight, CG location, pressure altitude, rotor RPM, and flap setting.

Main Rotor Trim

As tiltrotors have two proprotors, equations are needed for both proprotors. For the XV-15, the right hand proprotor (*MR*1) rotates counter-clockwise, as viewed from above, while the left hand proprotor (*MR*2) rotates clockwise. The difference between the inflow, flapping equations, advance ratio, and forces and moments for the proprotors is simply a matter of different signs.

The flapping angle is defined as $\beta_0+\beta_{1s}\sin(\psi)+\beta_{1c}\cos(\psi)$. Since the second main rotor is rotating in the opposite direction, ψ_2 is $-\psi_1$. Therefore, the flapping for the second rotor will be in the form as follows: $\beta_{02}+\beta_{1s2}\sin(\psi_2)+\beta_{1c2}\cos(\psi_2)$ which is the same as $\beta_{02}-\beta_{1s2}\sin(\psi_1)+\beta_{1c2}\cos(\psi_1)$. Since the sign of β_{1s} is opposite between the two rotors, the rotors both have positive flapping inward towards the aircraft centerline. Therefore, if the same flapping equation is used to define the rotor response, the resulting rotor response will be equal values of β_0, β_{1s}, and β_{1c}, however, they will be in different directions due to sign convention.

Since the proprotors rotate in opposite directions, the rotating coordinate systems will differ in direction. The system is defined at the point when the proprotor blade passes over the tail of the aircraft. At this point, the *x*-axis runs parallel to the aircraft body axis, and for both rotors is directed aft. For right rotor, the *y*-axis runs parallel to the *y*-body axis and in the positive y_B direction; however, for the left rotor, the *y*-axis runs parallel to the *y*-body axis but in the negative y_B direction. The *z*-axis is perpendicular to the *x* and *y* axes and is directed upward for the right rotor and directed downward for the left rotor.

The following are the coordinate transformations to get to and from the left rotor's rotating coordinate system.

Left rotor (*MR*2):

$$\begin{Bmatrix} i \\ j \\ k \end{Bmatrix}_{NR} = \begin{bmatrix} \cos\psi & -\sin\psi & 0 \\ -\sin\psi & -\cos\psi & 0 \\ 0 & 0 & -1 \end{bmatrix} \begin{Bmatrix} i \\ j \\ k \end{Bmatrix}_{ROT}$$

$$\begin{Bmatrix} i' \\ j' \\ k' \end{Bmatrix} = \begin{bmatrix} \cos\beta & 0 & -\sin\beta \\ 0 & -1 & 0 \\ -\sin\beta & 0 & -\cos\beta \end{bmatrix} \begin{Bmatrix} i \\ j \\ k \end{Bmatrix}_{ROT}$$

The forces in the rotating direction are as follows due to the above sign convention:

$$\begin{bmatrix} X_R \\ Y_R \\ Z_R \end{bmatrix}_{MR1} = \begin{bmatrix} X_R \\ Y_R \\ -Z_R \end{bmatrix}_{MR2}$$

When these forces are transformed into the non-rotating coordinate system, we get the following:

$$\begin{bmatrix} X \\ Y \\ Z \end{bmatrix}_{NR,MR1} = \begin{bmatrix} \cos(\psi) & -\sin(\psi) & 0 \\ \sin(\psi) & \cos(\psi) & 0 \\ 0 & 0 & 1 \end{bmatrix} \begin{bmatrix} X \\ Y \\ Z \end{bmatrix}_{ROT,MR1} = \begin{bmatrix} X_R\cos(\psi) - Y_R\sin(\psi) \\ X_R\sin(\psi) + Y_R\cos(\psi) \\ Z_R \end{bmatrix}_{NR,MR1}$$

$$\begin{bmatrix} X \\ Y \\ Z \end{bmatrix}_{NR,MR2} = \begin{bmatrix} \cos(\psi) & -\sin(\psi) & 0 \\ -\sin(\psi) & -\cos(\psi) & 0 \\ 0 & 0 & -1 \end{bmatrix} \begin{bmatrix} X \\ Y \\ -Z \end{bmatrix}_{ROT,MR2} = \begin{bmatrix} X_R\cos(\psi) - Y_R\sin(\psi) \\ -X_R\sin(\psi) + -Y_R\cos(\psi) \\ Z_R \end{bmatrix}_{NR,MR2}$$

As is shown, the *Y*-force generated by the left rotor is in the opposite direction of the *Y*-force from the right rotor. Since the rotors have opposite lateral offsets from centerline, the sign on the roll rate, yaw rate, lateral linear velocity, and sideslip angle are also negative. For example, a positive roll rate will result in a down-going right hand rotor and an up-going left hand rotor. Therefore the right hand rotor is in a descent while the left hand rotor is in a climb of equal magnitude. The same logic applies for v (and therefore, β_F) and r.

In summary, the equations developed for the right rotor can be applied to get the values for the left rotor by letting $p_{MR2}=-p_{MR1}$, $r_{MR2}=-r_{MR1}$, $v_{MR2}=-v_{MR1}$, and $\beta_{F,MR2}=-\beta_{F,MR1}$. When transforming the forces from the non-rotating coordinate system to the body coordinate system, the lateral offset value, R_{Nj}, must also be modified.

2.7.2 Time-Marching Solution

Time Marching Model Development

In order to get a time marching solution, a time-varying model had to be developed. Matlab's fully implicit ordinary differential equation solver, ode15i, was then used to run the solution. The base equations for this model were the original Euler equations and the flapping equation of motion. The initial conditions for the time marching solution are the trim solution states and rate of change of the states. In order to get a time marching solution, the equations used for the trim solution had to be modified by removing the

steady state rotor assumption. The flapping equations, thrust, and rotor force and moment equations were now a function of azimuth angle again. The full Euler equations which include $\dot{u}, \dot{v}, \dot{w}, \dot{p}, \dot{q},$ and $\dot{r}$ were also used.

The p and r equations were solved simultaneously for $\dot{p}$ and $\dot{r}$ in order to de-couple the equations, which resulted in the following:

$$\dot{p} = \frac{LI_{zz} + I_{xz}N - I_{xz}^2 qr + I_{xz}pqI_{xx} - I_{xz}pqI_{yy} + I_{xz}pqI_{zz} + qrI_{yy}I_{zz} - qrI_{zz}^2}{I_{zz}I_{xx} - I_{xz}^2}$$

$$\dot{r} = \frac{NI_{xx} + I_{xz}L + I_{xz}^2 pq + I_{xz}qrI_{yy} - I_{xz}qrI_{zz} - I_{xz}qrI_{xx} + pqI_{xx}^2 - pqI_{xx}I_{yy}}{I_{zz}I_{xx} - I_{xz}^2}$$

2.7.3 Linearized Model

Stability and Control Derivatives

Creation of the symbolic perturbation equations for the linearized model was discussed during the development of the trim equations earlier in this section and is covered in depth in Reference 19 and Reference 23. Therefore, the discussion here focuses on the methodology used to create the model numerically.

When the forces and moments are expanded via a Taylor series expansion about a trimmed state, the resulting change in total aircraft perturbation is divided among the states, thereby allocating the total change to the components (states). If we assume that the perturbations are small, then the products of the perturbations can be neglected and the resulting equations are linear. The remaining partial derivatives are called stability

derivatives if they are a partial derivative with respect to a state variable or control derivatives if they are a partial derivative with respect to a control variable.

The partial derivatives are commonly re-written as a new variable that has a main variable and a subscript variable. The main variable is the force or moment variable and the subscript variable is the perturbed state or control.

$$[\ ]_{(\ )} = \frac{\partial[\ ]}{\partial(\ )}$$

Therefore, for example: $X_u = \frac{\partial X}{\partial u}$ which means the change in the X force due to the perturbation in 'u'.

The total change in X force is then

$$X = X_u u + X_v v + X_w w + X_p p + X_q q + X_r r + X_\varphi \varphi + X_\theta \theta + X_\psi \psi + X_{\theta 01}\theta_{01} + X_{\theta 1s1}\theta_{1s1} + X_{\theta 1c1}\theta_{1c1}$$
$$+ X_{\theta 02}\theta_{02} + X_{\theta 1s2}\theta_{1s2} + X_{\theta 1c2}\theta_{1c2}$$

where $X = \Delta X$

The stability and control derivatives are also usually normalized. The force derivates are divided by the aircraft mass, the moment derivatives are divided by the appropriate inertia. The above symbology is usually not changed to reflect this normalization, therefore, for example, X_u actually means X_u/m when defined as a stability derivative.

Note: because the rolling moment and yawing moment equations are coupled, 'Primed' derivatives are usually introduced. 'Primed' derivatives include the inertial coupling into

the derivative. Examples of 'primed' derivatives are as follows:

$$\frac{I_{xz}}{I_{xz}-I_{xz}^2}L_u+\frac{I_zI_{xz}}{I_{xz}-I_{xz}^2}N_u=L_u^{'}$$
$$\frac{I_{xz}}{I_{xz}-I_{xz}^2}N_u+\frac{I_xI_{xz}}{I_{xz}-I_{xz}^2}L_u=N_u^{'}$$

Numeric Model Development

The numeric values for the stability and control derivatives were developed using the time marching solution equations. A state space model was developed by individually perturbing each state, state derivative, and control to get the resultant change in *X*, *Y*, *Z*, *L*, *M*, and *N* due to the perturbation. The resulting changes in forces and moments for the state derivative perturbations are found in matrix *E*, matrix *F* for the states, and matrix *G* for the controls.

state vector, $y = [u, v, w, p, q, r, \varphi, \theta, \psi]$

derivative of state vector = $\dot{y} = \left[\dot{u}, \dot{v}, \dot{w}, \dot{p}, \dot{q}, \dot{r}, \dot{\varphi}, \dot{\theta}, \dot{\psi}\right]$

control vector = $u = [\theta_{01}, \theta_{1s1}, \theta_{1c1}, \theta_{02}, \theta_{1s2}, \theta_{1c2}, \delta_{elev}, \delta_{ail}, \delta_{rud}]$

however, for the purposes of this evaluation, the control vector was determined at the pilot controls, so $u = [\theta_0, \delta_{long}, \delta_{lat}, \delta_{ped}]$

In order to numerically calculate the *E*, *F*, and *G* matrices, the linearized equations of motion were numerically perturbed about a trim value, one state or control at a time. Then the trim value was subtracted from the perturbed value in order to get the delta due to the perturbation. This was done for each state, state derivative, and control, for each force, moment, and kinematic equation.

This resulted in: $[E]\dot{y} = [F]y + [G]u$

Since the equations are time varying, the above matrices needed to be evaluated for multiple equidistant times steps around the rotor azimuth and then averaged to get the time invariant matrices.

The ’ and *B* matrices normally used for derivative development were extracted as follows:

$$[E]\dot{y} + [F]y + [G]u = 0$$

$$[E]\dot{y} = -[F]y + -[G]u$$

$$\dot{y} = -[E]^{-1}[F]y - [E]^{-1}[G]u$$

$$\dot{y} = [A]y + [B]u \quad \text{therefore}$$

$$[\mathrm{A}] = -[E]^{-1}[F]$$

$$[B] = -[E]^{-1}[G]$$

where

A = 9 x 9 matrix with columns equating to the state being perturbed and the rows being the force or moment effect

B = 9 x 4 matrix with columns equating to the controls being perturbed and the rows being the force or moment effect.

Units:

Force/linear velocity = 1/sec

Force / angular rate = ft/(sec rad)

Moment/linear velocity =rad/(ft sec)

Moment/angular rate = 1/sec

Force / control = [ft/(sec^2 inch)] (except L'_w and N'_w = 1/sec)

The derivatives calculated above are actually slightly different than the before discussed 'stability derivatives' since they include both the aerodynamic and inertial effects.

3. Results

3.1 Trim Results

The trim results from the math model are discussed below. These results were compared to the trim solutions from GTRS. The following items should be noted prior to the discussion:

1. The center of gravity shown is the actual center of gravity for that nacelle setting. It is not the helicopter-referenced center of gravity.
2. The GTRS values were transferred from Reference 6. The total airframe and rotor forces and moments in GTRS include items such as the engine pylons, jet thrust, and proprotor hub spinner in their force and moment calculations; therefore, the values shown here as the GTRS total force and moments are not just sums of the values shown.
3. Due to the math model implementation method, the θ_0 from the math model does not include the 40º of initial rotor twist at the root in the θ_0 output. (In the math model, this is accounted for in a separate term.) For comparison purposes, the θ_0 values shown here as math model output were modified to include the initial rotor twist of 40º to show a one-to-one comparison with the GTRS output.

Table 2 shows the mast angle and speed for the various trim cases that were run. Tabular output for the trim cases, including component forces and moments and overall aircraft parameters can be found in Appendix C.

Table 2: Trim Cases

	β_M (deg)				
	0º	15º	30º	60º	90º
V (kts)	0.01 20 40 60 80 100	40 60 80 100 120	80 100 120 140	100 120 140 160	140 160 180 200 220 240 260 280

All trims were run at 13,000 lbs gross weight and a flight path angle and turn rate equal to 0 º/s. Center of gravity and flap deflection changed with mast angle. The aircraft trimmed in all cases with β_F, p, q, r, $\dot{p}$, $\dot{q}$, $\dot{r}$, θ_{1c}, δ_{ail}, and roll angle essentially equal to zero. Lateral stick and pedal remained centered.

In general, the trims were consistent with what was expected. Some parameters of interest are shown in Figure 11. APLN517 corresponds to airplane mode data at 517 RPM, VTOL is the helicopter mode data, CONVXX is the XXº β_M conversion mode data. All nacelle angles showed positive speed stability as shown by increasing forward stick and decreasing pitch attitude with increasing airspeed. For conversion and airplane modes, the data shows increasing collective pitch requirement with increasing forward speed. The helicopter mode data shows a standard helicopter power required trend.

One item of note that is characteristic of a tiltrotor, is that, as the nacelles are rotated forward to gain airspeed, the longitudinal stick will actually migrate **aft**. This results in apparent negative speed stability while converting (aft stick requirement for increasing airspeed). This is shown in Figures 12 and 13.

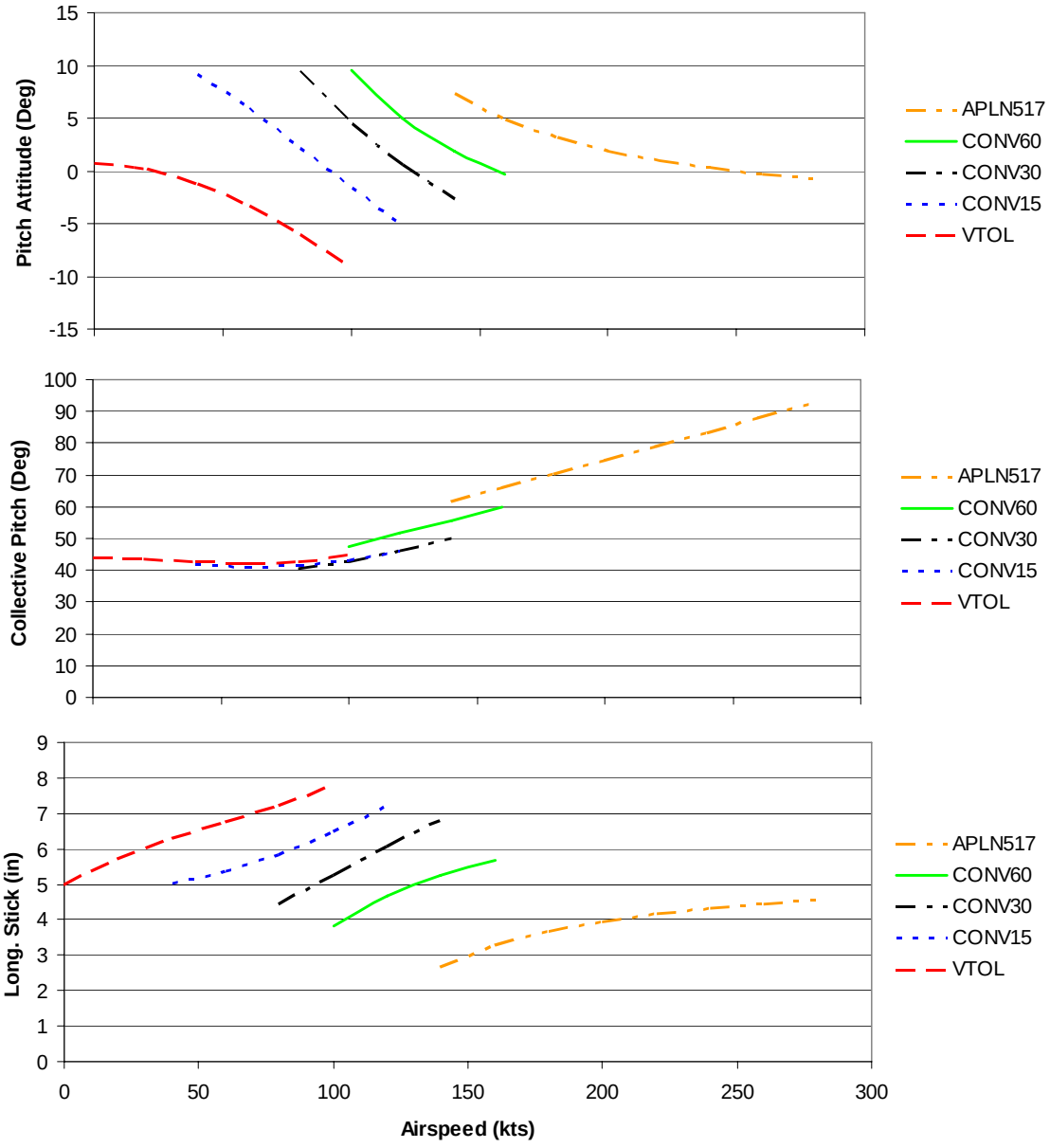

Figure 11: Math Model Results with respect to Airspeed

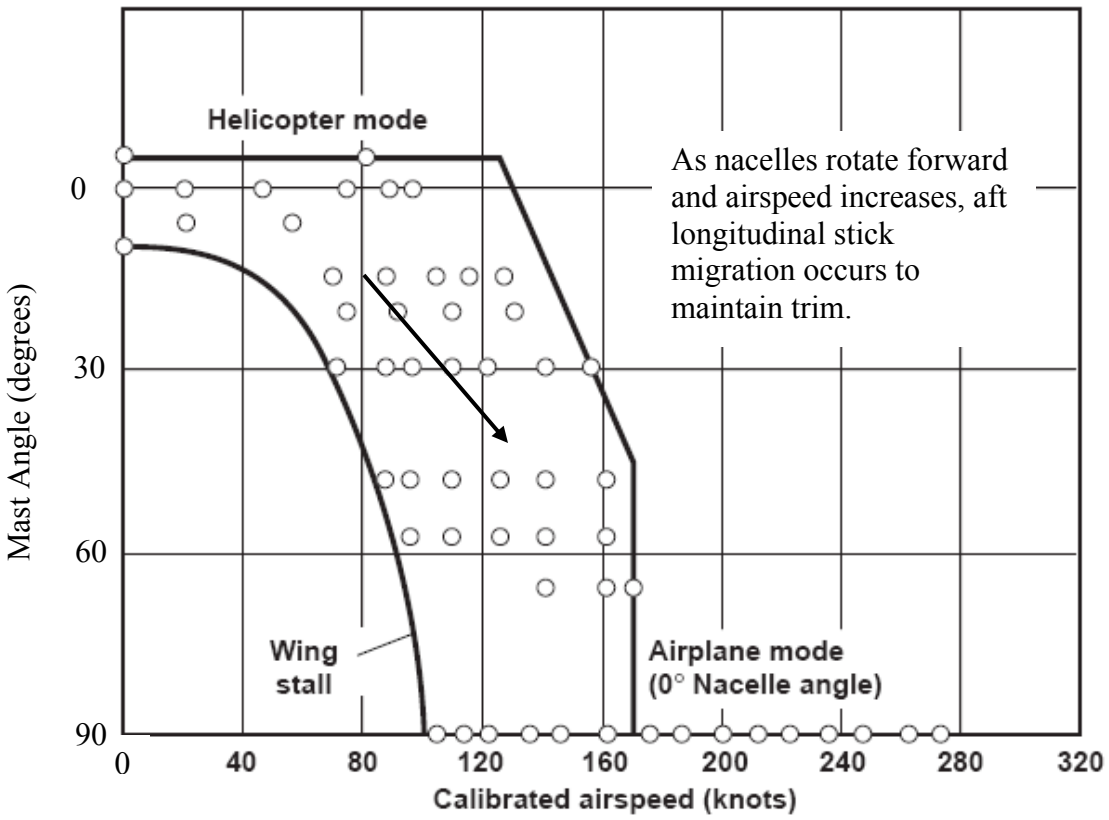

Figure 12: Sample Conversion Path

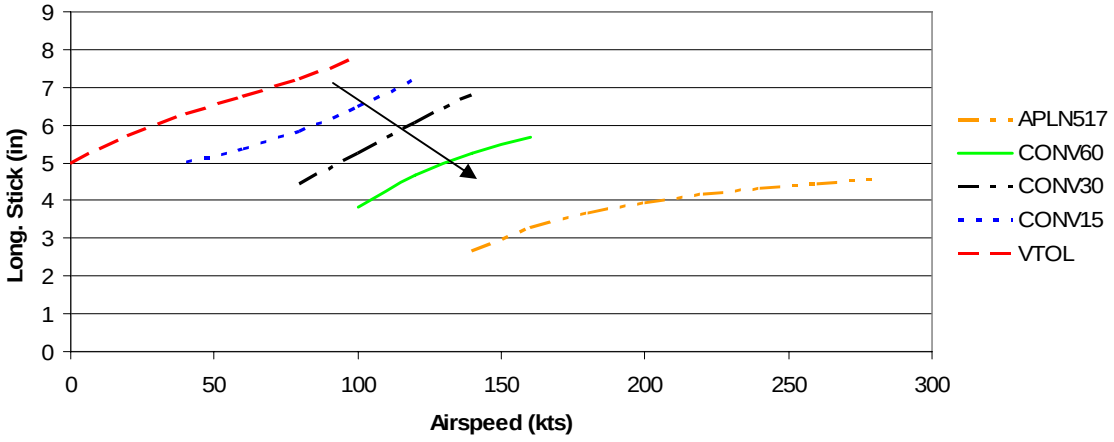

Figure 13: Aft Longitudinal Stick Migration with Sample Conversion Path

Flight test data was available for helicopter and airplane mode trims. A comparison of the math model to this data is shown in Figure 14 for helicopter mode trims and Figure 15 for airplane mode trims. The math model data plotted was trimmed at 13,000 lbs with a longitudinal CG of 301.2 inches in helicopter mode and 298.2 inches in airplane mode. For both helicopter and airplane modes, the model, GTRS, and aircraft show positive apparent speed stability (increasing forward longitudinal stick with increasing airspeed).

In helicopter mode, the math model trims at approximately 15% more forward longitudinal stick (1.4 in.) and approximately 1–2 degrees more nose down pitch attitude than flight and GTRS. The math model data for longitudinal stick position at 60 kts is at 72%. The math model longitudinal stick data for 80 kts is outside the plotted area and is at 82% stick deflection. The increased forward longitudinal stick requirement indicates that there is a difference in the amount of rotor thrust and tip path plane tilt required to trim the model.

In airplane mode, the math model trims at the same pitch attitude, but requires approximately 16% (1.5 in.) less longitudinal stick and 6º less elevator deflection. The decreased math model stick requirement indicates that there is either an aerodynamic effect (AOA change) at the horizontal tail that is not being modeled or the elevator effectiveness is incorrect as modeled. Note that one of the simplifying assumptions was that there was no rotor wake interaction modeled. Since the offset is essentially constant, that indicates that the elevator effectiveness value is also a contributing factor. The

elevator effectiveness value defined in Reference 7 was not changed for this model in keeping with the 'simple' model concept.

As there was little trimmed flight test data available for comparison, GTRS data was mainly used for comparison. GTRS has been previously validated against flight test data. That validation is documented in GTRS Validation report, Reference 6. Comparison plots and tabular data for GTRS and the math model developed for this project are included in Appendix C.

An assessment was made between the trim characteristics of the math model vs GTRS. The overall differences are summarized below.

In general, the math model requires less trim elevator deflection. This is increasingly more evident as the elevator becomes increasingly effective (greater mast angles). However, the elevator (and longitudinal stick) have the same characteristic curve and trending with airspeed as GTRS. As discussed in the airplane mode trim flight comparison, the difference in trim elevator deflection implies aerodynamic interactions at the empennage not being modeled in the math model or a difference in elevator effectiveness. For 15º β_M, the elevator deflection required from the math model is linear, but the GTRS elevator requirement is more curved. This also implies that there is an aerodynamic interaction at the tail that is not being modeled in the math model.

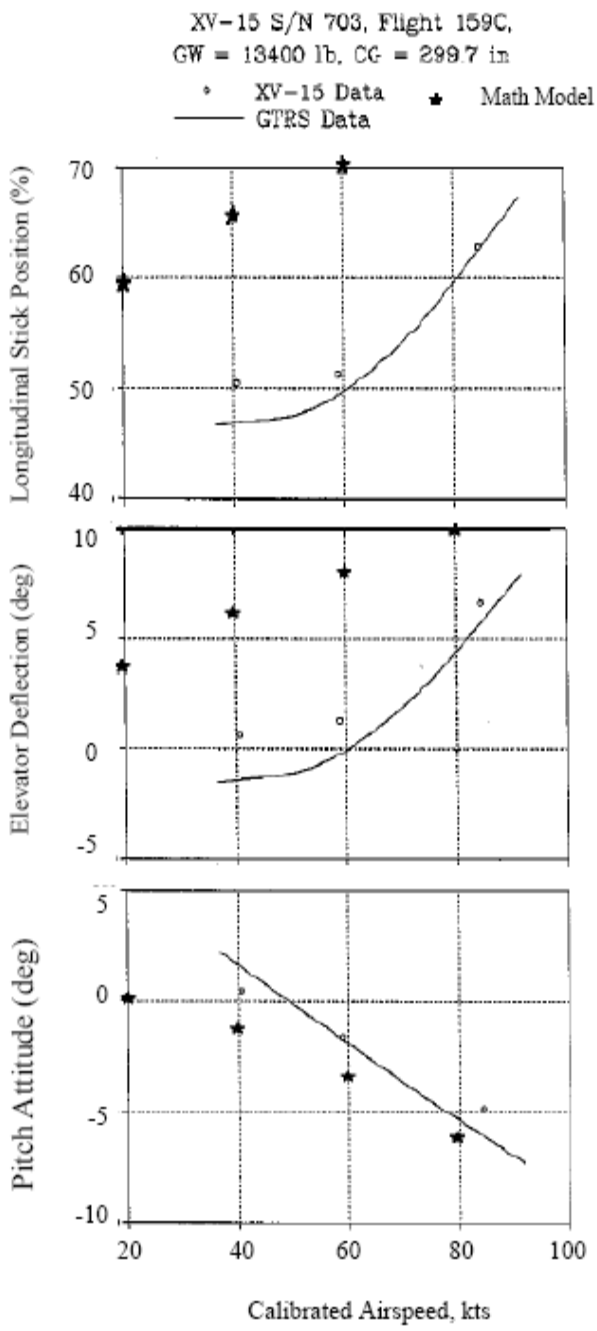

Figure 14: Math Model Comparison to Flight Test Data in Helicopter Mode

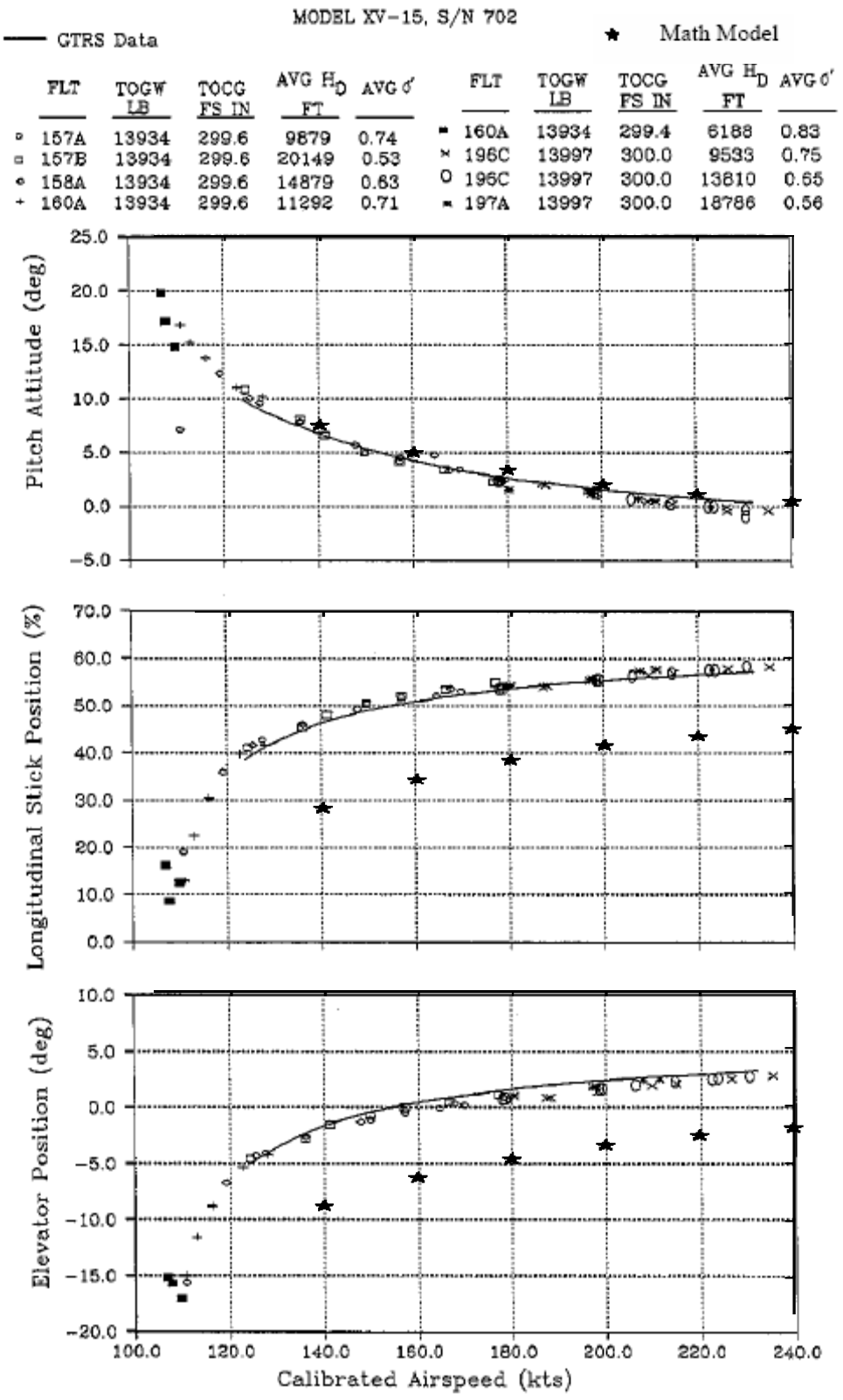

Figure 15: Math Model Comparison to Flight Test Data in Airplane Mode

The *Y*-force predicted by the math model has large differences from that predicted by GTRS. For 15º β_M, GTRS shows significantly more *Y*-force at the lower trim airspeeds than that required by the math model. For 30º β_M, the GTRS proprotor *Y*-force changes sign of *Y*-force as airspeed increases which is not predicted by the math model. For 60º β_M, the math model trims with much less *Y*-force than GTRS and in airplane mode, the proprotor *Y*-force is actually opposite in sign between the math model and GTRS. For helicopter mode, the *Y*-force from GTRS shows more *Y*-force required for trim than the math model requires. The differences in *Y*-force are due to GTRS modeling a gimbaled rotor and the math model containing an articulated rotor model.

In airplane mode, the math model requires more θ_0 than GTRS, which is exacerbated as *V* increases. As previously discussed, the GTRS includes a mode of the rotor governor functionality, while the math model does not model the rotor governor. Hence, in GTRS, the increase in collective results in a change in the rotor governor input and in the math model, this increased in collective pitch is manifested in an increase in θ_0. This is also seen in rotor coning in that GTRS shows an essentially constant β_0 where the math model shows β_0 increasing with velocity.

In helicopter mode for velocities less than 40 kts, the math model requires less rotor thrust than GTRS (see Appendix C for plots). The reason for this can be seen when looking at the forces and moments. For hover, there is a +*Z* force on the wing (wing download) that is not seen in the simplified math model. This download can also be seen in the 20 kt case. Wing download due to wake interaction on the vertical projected area

of the wing was not modeled in this math model. The simplified model, however, does essentially match GTRS for the free stream component. For velocities greater than 40 kts, the simplified model requires slightly more thrust than GTRS.

In general, the flapping angles did not match well. The flapping angles had the same order of magnitude, and the same general trends existed. However, for example, in airplane mode the math model shows very flat lateral and longitudinal flapping curves while GTRS shows them almost linearly increasing To determine the validity of the steady state flapping values, the math model developed for this project was compared to a simple helicopter flapping rotor, both with zero longitudinal CG offset between the rotor hub and the CG. The results are shown in Table 3.

Table 3: Math Model Flapping vs. Idealized Hover Flapping

	Hover		20 kts		40 kts	
	Math Model	Helicopter Equation	Math Model	Helicopter Equation	Math Model	Helicopter Equation
β_0	2.35º	2.35º	2.40º	2.32º	2.24º	2.24º
β_{1s}	10^{-6}º	10^{-4}º	–0.14º	–0.16º	–0.27º	–0.27º
β_{1c}	10^{-5}º	10^{-5}º	0.274º	0.211º	0.18º	0.18º

Based on the above results, the math model results were assumed reasonable and the correlation between GTRS and the math model was determined to be sufficient for the continuing with further model development. The differences in flapping angles can be attributed to articulated vs gimbaled rotor modeling.

3.2 Time Marching Results

A time marching analysis was performed to determine the model response to pilot inputs from the trim solution. Flight test data time histories for pilot step inputs were available in helicopter and airplane mode from Reference 6. In helicopter mode, data was available for longitudinal and directional step inputs. In airplane mode, data was available for a longitudinal step input, lateral step input, and directional step input.

The time history code used the time varying solution for the rotor forces and moments and the blade flapping equation. Due to the slight differences in rotor forces and moments calculated using the steady state equations and the time varying equations, even though the trim solution resulted in essentially zero rates and accelerations, the time marching solution shows small rates and accelerations in airplane mode and an appreciable pitch rate in helicopter mode. These rates and accelerations affected the time history solutions in that the aircraft response is not just due to pilot inputs. The residual pitch rate and pitch attitude were approximated with polynomial equations which were then used to subtract out the trim pitch rate and attitude for the longitudinal stick inputs in order to only show the effects due to the pilot input.

The time history results for the helicopter mode and airplane mode trim cases with no additional pilot inputs are shown in Figure 16 and Figure 17. As can be seen, the force differences due to the incorporation of the time varying equations resulted in a pitch rate and a vertical climb, while the angular velocities for the trim solution were essentially zero. The yaw rate and roll rate changes were negligible.

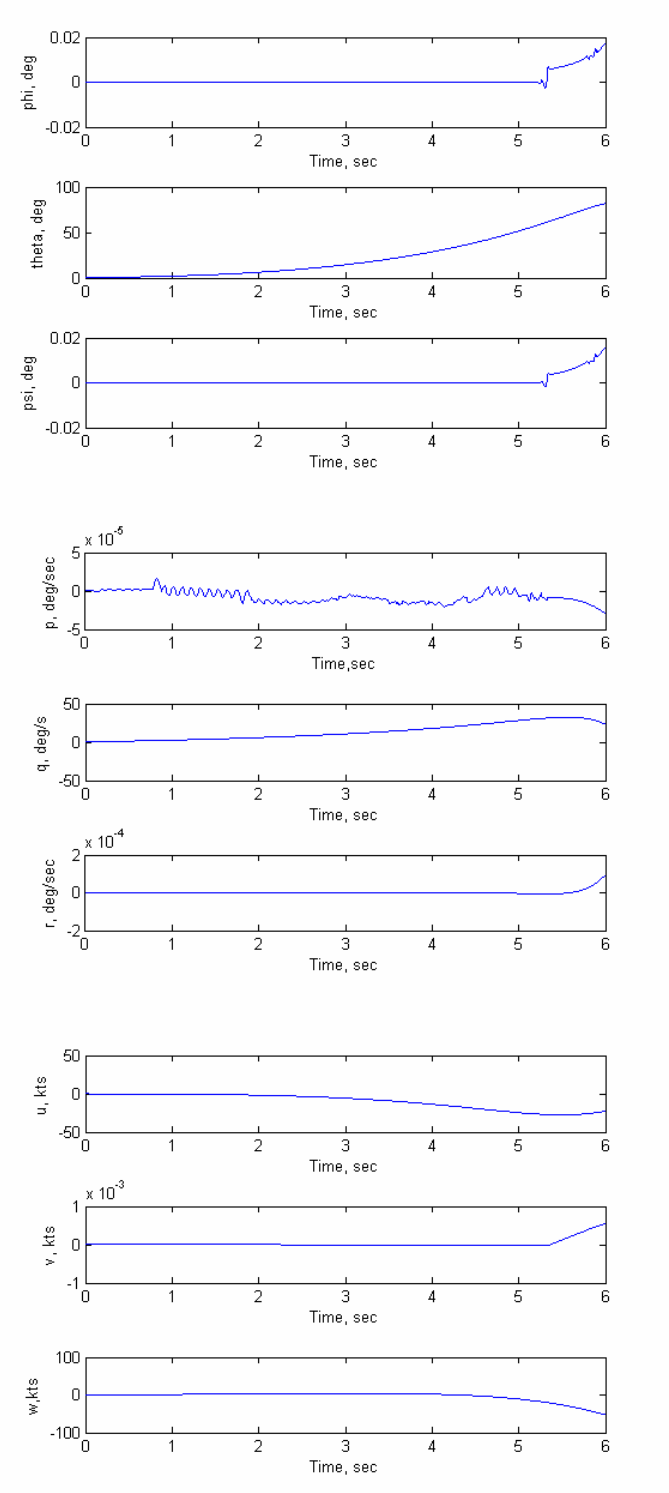

Figure 16: Helicopter Mode Trim Time History with Time Varying Equations

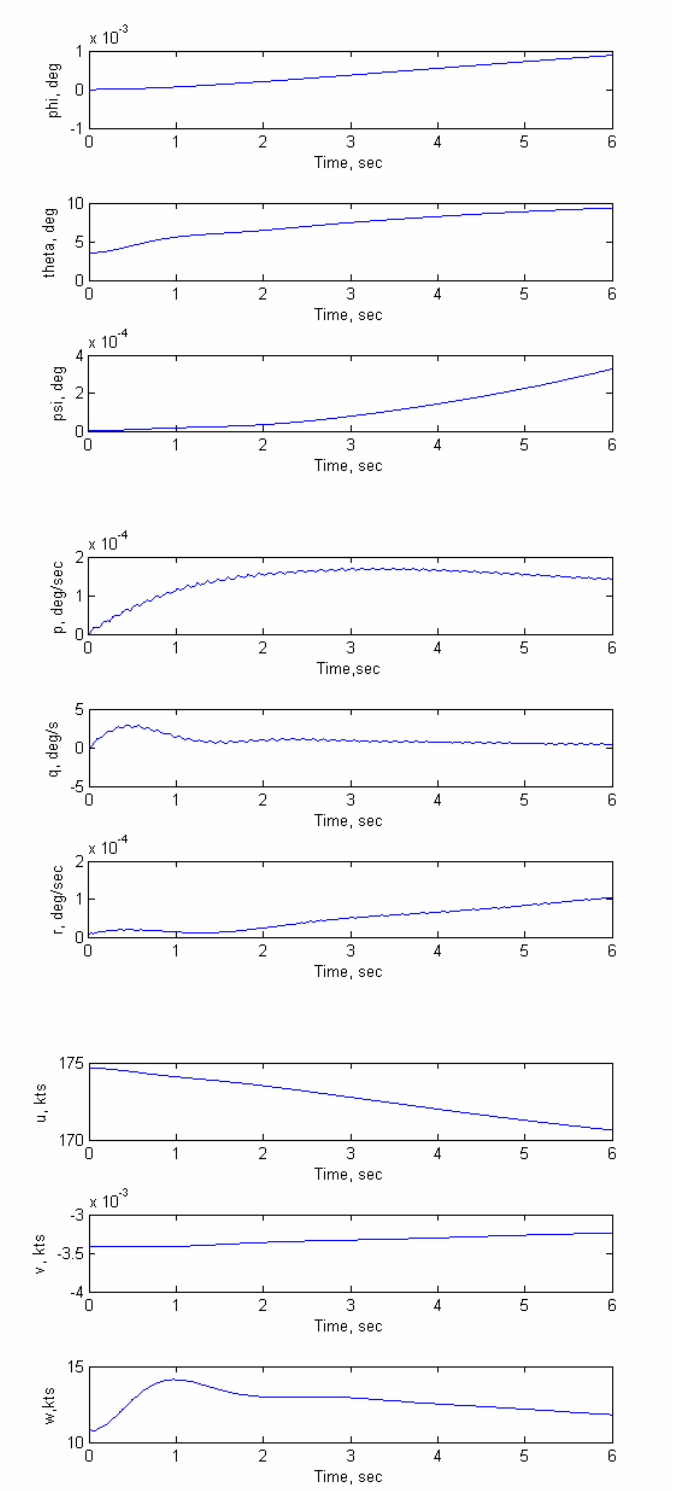

Figure 17: Airplane Mode Trim Time History with Time Varying Equations

Figure 18 shows the helicopter mode time history due to a pilot longitudinal step input. The math model has a slower initial pitch rate that appears to lag the flight data by approximately 0.5 sec. The math model peak pitch rate is also less than that seen in flight. Hence, the pitch attitude attained by the math model is also less than the flight peak pitch attitude. The 'trim' residual pitch rate also affects the math model in that once the pitch attitude is greater than approximately 15º (time greater than approximately 6.5sec), the small angle approximation becomes invalid therefore making the solution more and more inaccurate as the pitch attitude increases. This 'trim' residual pitch rate in the helicopter mode time history solution needs to be addressed prior to further time domain analysis.

Figure 19 shows the helicopter mode time history due to a pilot directional step input. The pedal input resulted in a yaw rate in the correct direction but at a magnitude approximately half that seen in flight and GTRS. Note that the residual trim yaw rate was very small therefore this is unlikely to be a large source of error. Yaw angle grows as expected and increases steeply. One item of note is that for time greater than approximately 3.5 seconds, the pitch attitude is greater than 15º and for time greater than 6 seconds, the yaw angle is greater than 15º, which make the small angle approximation invalid. This high pitch attitude will also be a large source of error even for the off-axis responses like yaw attitude.

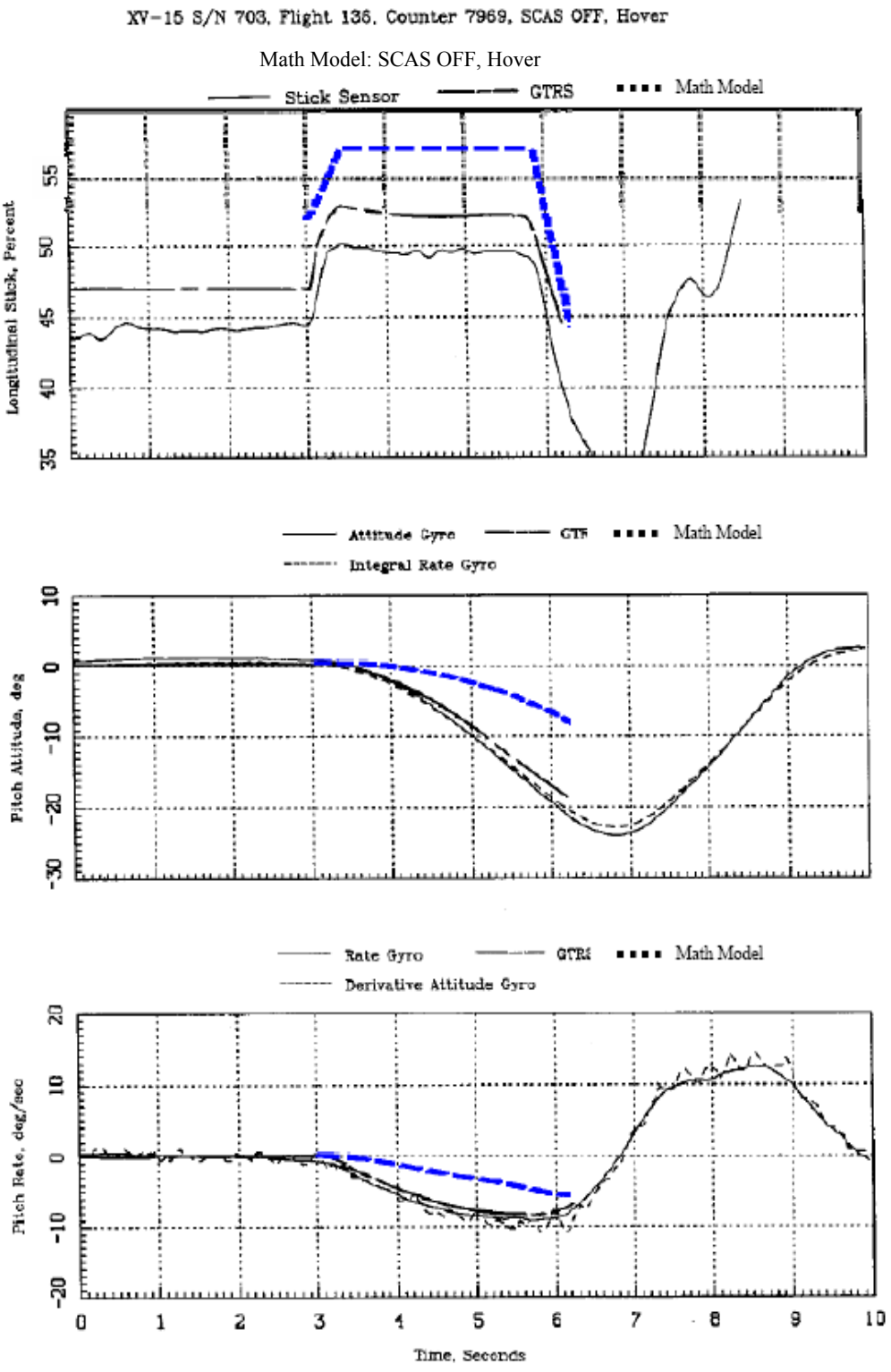

Figure 18: Helicopter Mode Longitudinal Step Input

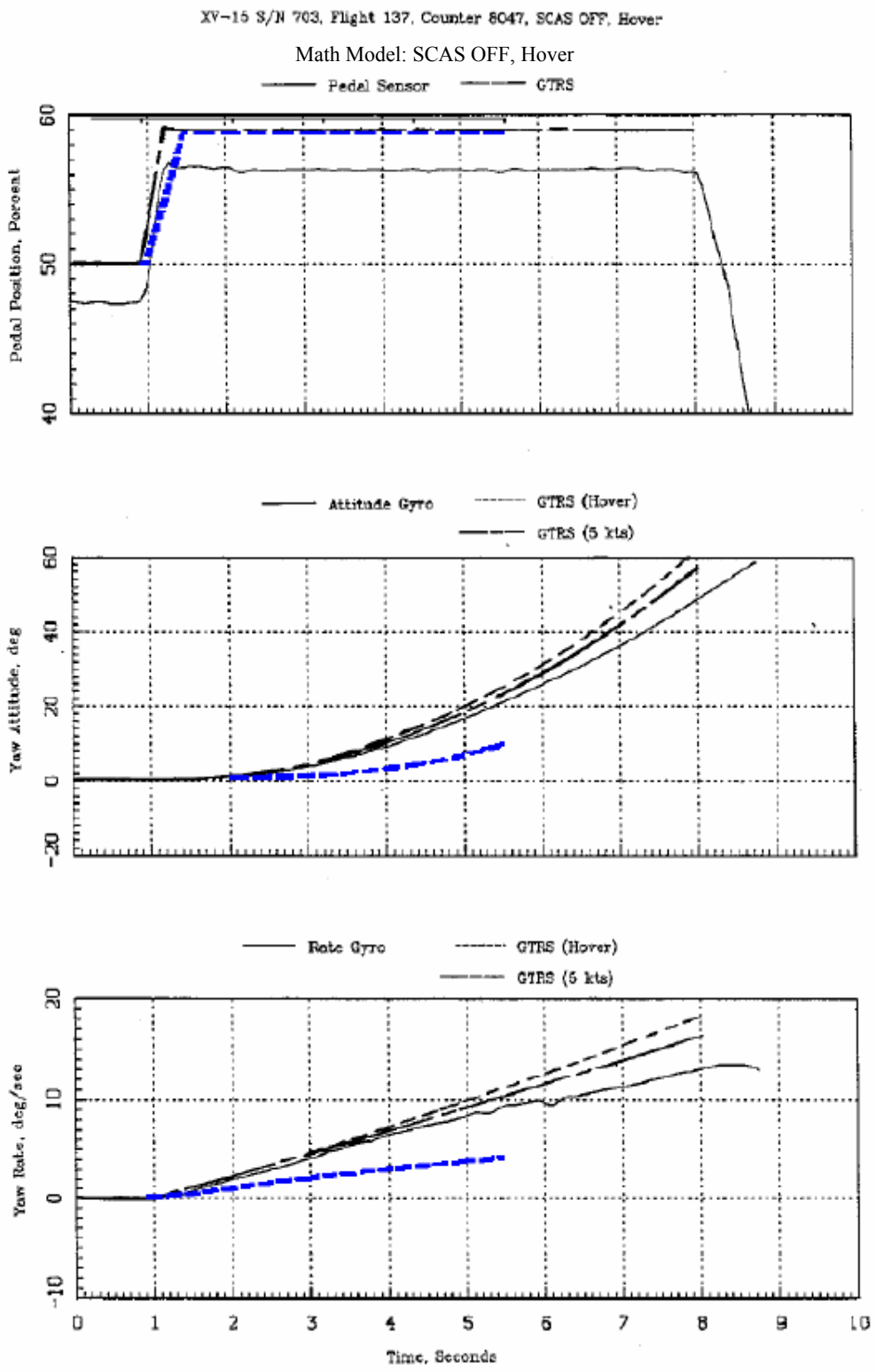

Figure 19: Helicopter Mode Pedal Step Input

The airplane mode longitudinal step input into the math model, shown in Figure 20, results in much better correlation than the helicopter mode trims. The pitch attitude matches well in slope, but is smaller in magnitude. While the math model has an initial pitch rate response with a slightly smaller frequency and magnitude, it damps out to approximately the same value as the flight test data. The math model has a peak to peak time period of approximately 1 sec. while the flight data shows a slightly longer peak to peak time. Note that the aircraft is already pitching up prior to the stick input due to the trim residual however that has been subtracted out of the results shown. The pitch attitude exceeds 15º for time greater than approximately 5.5 seconds.

The airplane mode lateral step input, shown in Figure 21, has a much slower roll acceleration/initial rate response than the flight test data. However, while the flight test data showed the roll rate leveling off to a constant 10 deg/s, the math model shows the roll rate leveling off at about 4–5 deg/s. One item of note is that beyond a time of approximately 4.5 seconds, the pitch attitude exceeds 15º and beyond approximately 5.5 seconds the yaw attitude exceeds 15º; therefore the small angle assumption is no longer valid for the off axis response and can contaminate the on-axis response. Since the roll rate attained is smaller than the flight test roll rate, the math model also attains a lower peak roll attitude.

Due to the extremely large difference in aileron control effectiveness between flight and the math model, the math model aileron control effectiveness was multiplied by a factor of three which resulted in a much better match as shown in Figure 22. While this is in

fact a ‘correction factor’ applied to the model, the lateral results would be greatly affected if this fix was not made.

The airplane mode directional input, shown in Figure 23, shows a larger initial yaw rate due to the pedal input which starts the aircraft yawing right. The same oscillatory characteristic can also be seen in the yaw rate for the subsequent few seconds. The math model has a larger magnitude and smaller period. The steady state yaw rate due to the pedal input is zero for the math model while it is approximately 4º/s for the flight data. This results in a smaller steady yaw angle response.

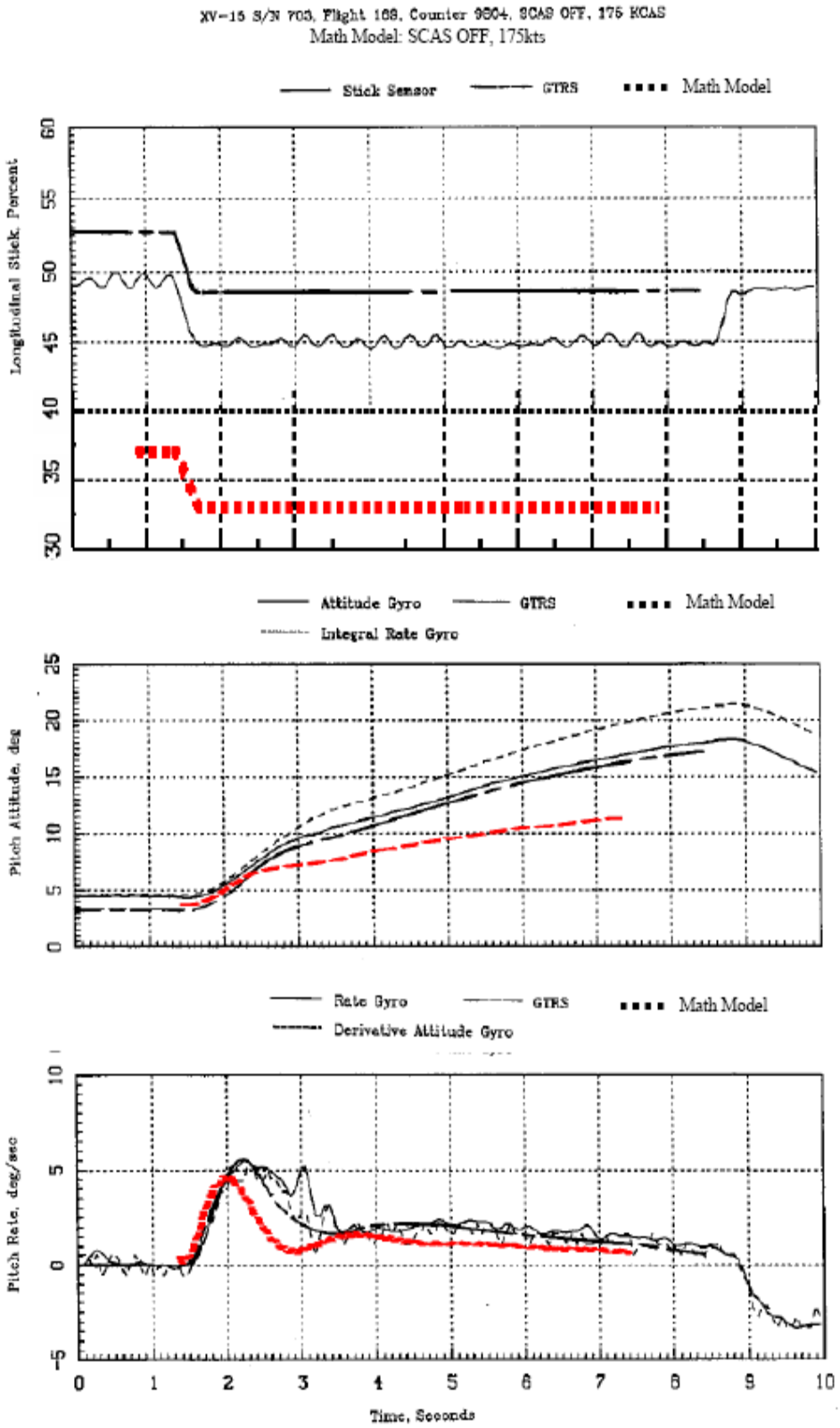

Figure 20: Airplane Mode Longitudinal Step Input Time History

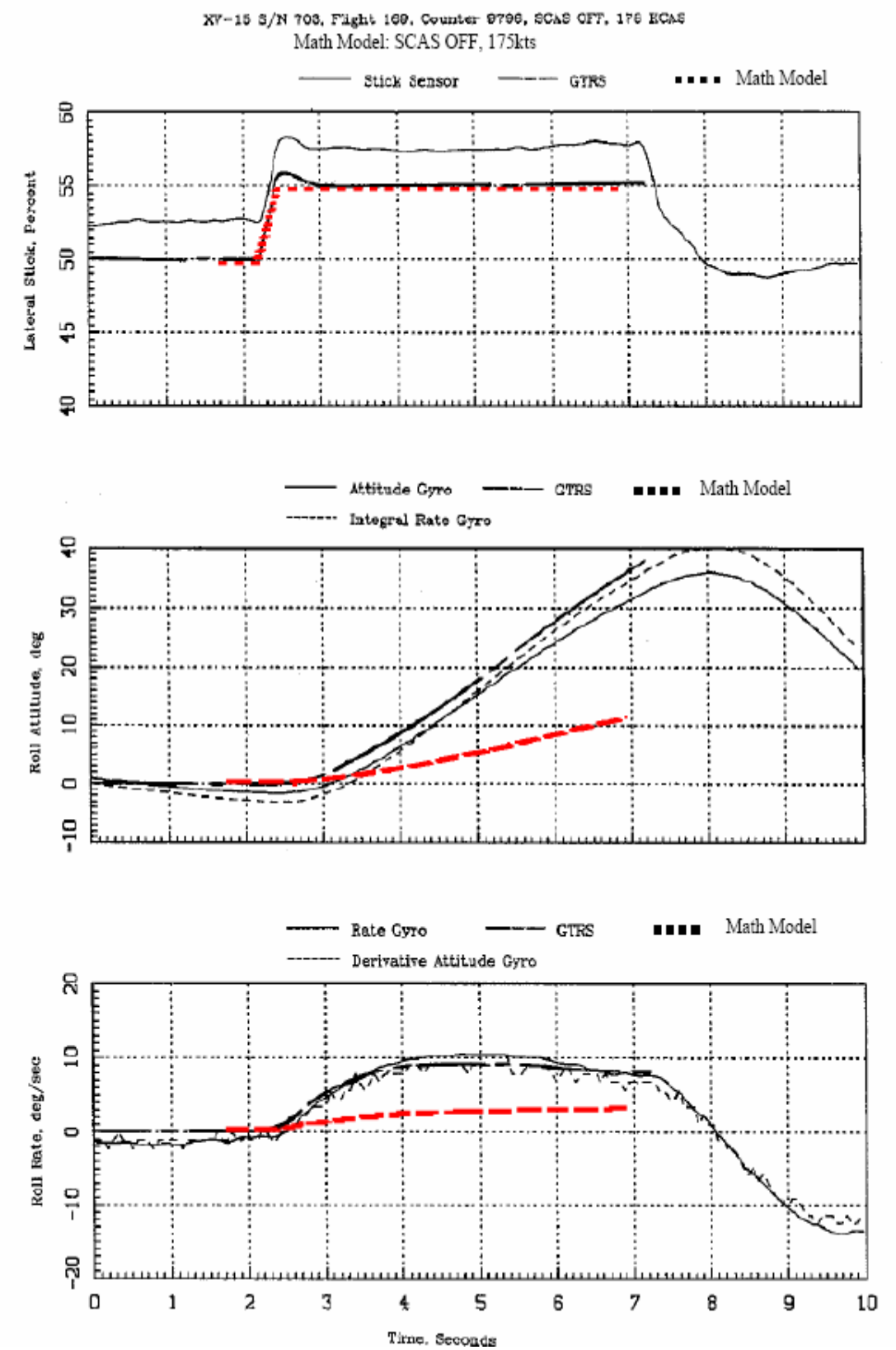

Figure 21: Airplane Mode Lateral Step Input Time History

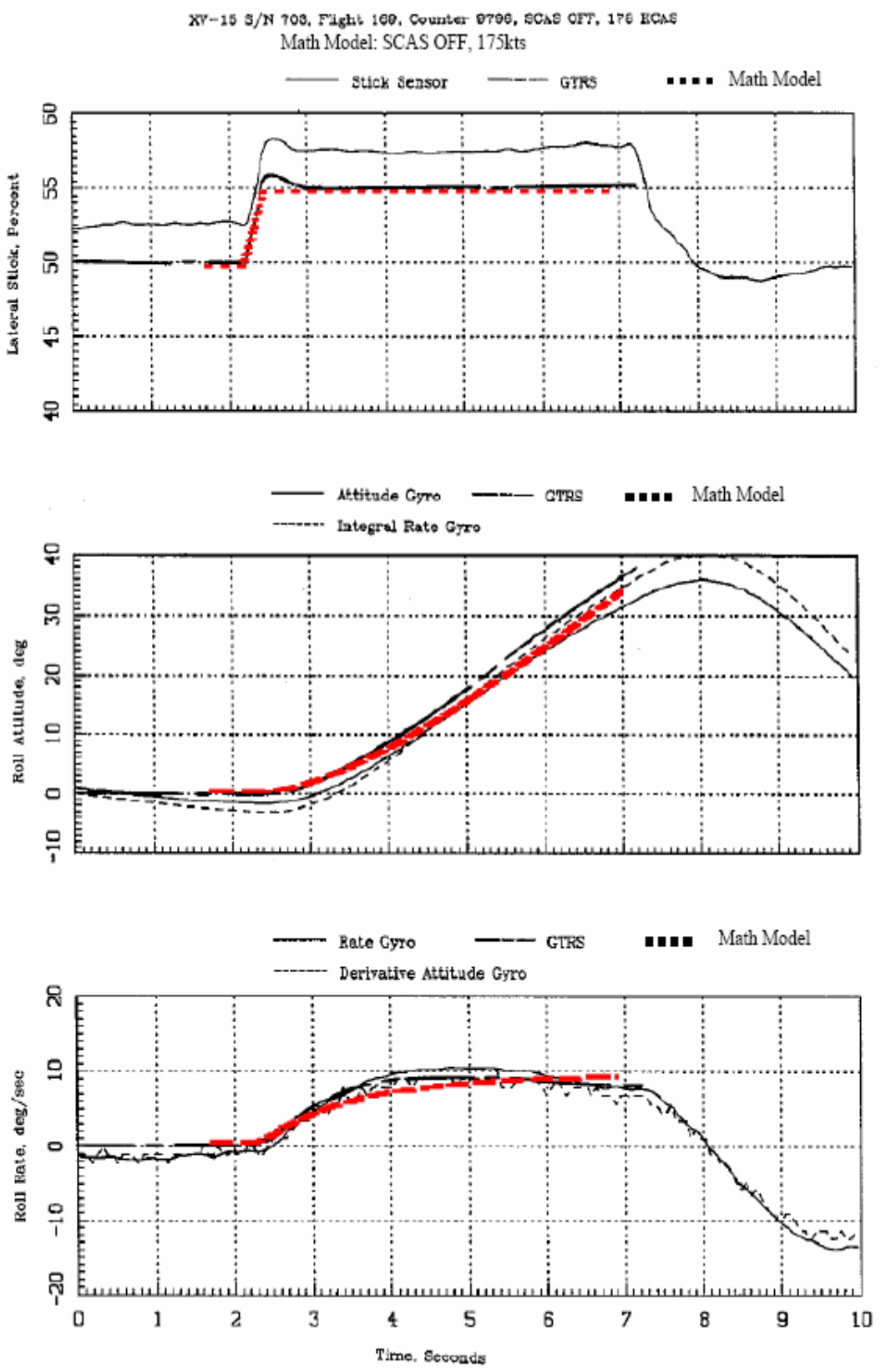

Figure 22: Airplane Mode Lateral Step Input Time History (Modified Aileron)

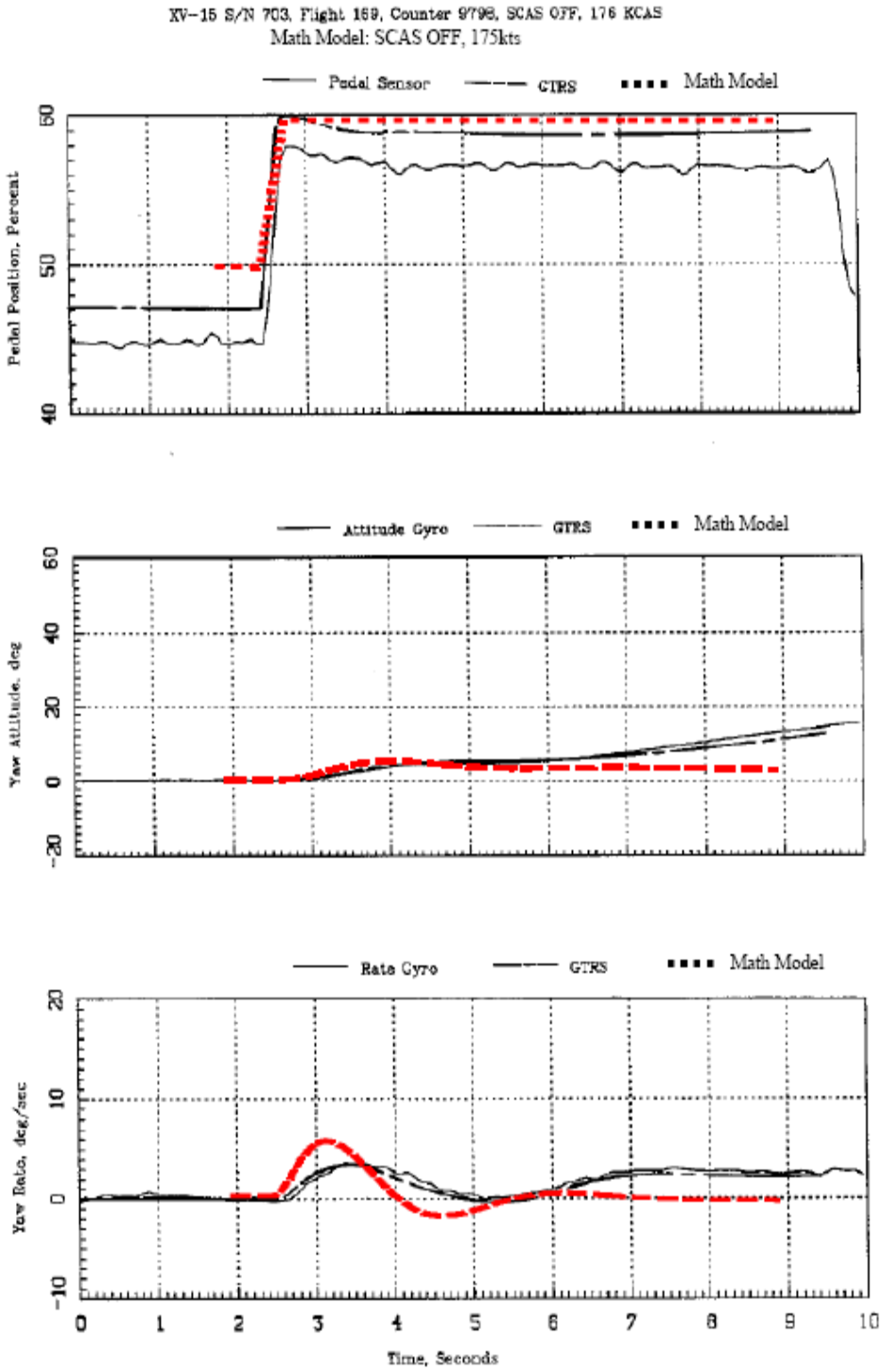

Figure 23: Airplane Mode Directional Step Input Time History

3.3 Linearized System

As previously discussed, the *A* and *B* matrices were extracted from the model in order to extract the math model dynamics. The time varying solution for the rotor forces and moments and blade flapping were also used for the linearized model extraction. As previously discussed in the time marching solution section, incorporation of these time varying equations resulted in changes from trim. In order to remove the effect on the overall force and moment equations, the total forces and moments were also re-baselined in the linearized model extraction code so the only effect from the perturbation of the state or control was the effect due to the perturbation of the state or control.

Below are the *A* and *B* matrices extracted from the math model, compared to the GTRS matrices (Reference 9). For the *B* matrices, the GTRS matrix uses collective, where as the math model is perturbed using θ_0. The math model shows some minor cross couplings that are not evident in GTRS as can be seen by non-zero values for Z_p, r_φ, and $Y_{\theta 0}$ (airplane mode only).

The matrices compare very well in airplane mode. The main difference between the math model coefficients and the GTRS coefficients is that L_r, $X_{\theta 0}$ ($X_{\delta coll}$), and $Z_{\delta long}$ have different signs. L_r is positive for the math model and negative for GTRS, which means that the math model rolls into a heading change while GTRS rolls away from a heading change. $X_{\theta 0}$ ($X_{\delta coll}$) have different signs and the magnitude of $X_{\theta 0}$ in the math model is much larger in magnitude than $X_{\delta coll}$ in GTRS. This is due to gearing ratios as well as the inclusion of the governor in GTRS. $Z_{\delta long}$ is positive for GTRS and negative for the math

model. The negative sign on $Z_{\delta long}$ from the math model conceptually makes sense in that for a positive δ_{long} (forward stick), the elevator becomes more trailing edge down therefore creating more lift on the horizontal tail, which results in a negative *Z*-force.

In airplane mode, the math model $X_{\delta lat}$ has a magnitude of zero while GTRS has a non-zero value for $X_{\delta lat}$. In the math model, lateral stick inputs in airplane mode only result in aileron deflection as the differential collective pitch at the rotors is phased out in airplane mode. No radial velocity, wake effects due to aileron deflection, or fuselage effects due to aileron deflection are modeled.

There are also differences that exist in the magnitude of some of the derivatives. For example, N_v, N_p, N_r, and L_r have approximately twice the magnitude of the GTRS values. L_v is approximately half the magnitude found in GTRS. $N_{\delta lat}$ and $L_{\delta lat}$ are approximately 1/3 the magnitude of the GTRS derivatives. If the assumption is made that GTRS more accurately matches flight test, then the magnitude differences imply that there are errors in the math model, primarily in the lateral-directional axes. Using the rationale described in the trim section, if the aileron control effectiveness is increased by a factor of 3, $L_{\delta lat}$ then matches the GTRS data.

The *A* and *B* matrix comparison is worse in helicopter mode. In helicopter mode, the following coefficients have opposite signs: Z_u, Z_w, Z_q, Z_θ, X_w, Y_r, N_v, N_p, $Z_{\theta 0}$, $M_{\theta 0}$, $X_{\delta long}$, $Z_{\delta long}$, $N_{\delta lat}$, $Y_{\delta ped}$, $L_{\delta ped}$.

Z_u: For a positive u, the rotor will flap backwards which tilts the thrust vector further aft thereby implying a net negative Z-force change. The actual sign depends on the final orientation of the thrust vector. The longitudinal flapping condition at trim between GTRS and the math model were not the same; therefore, it is not unexpected that the sign on Z_u is not the same. Z_u is not a very powerful derivative. The magnitude of Z_u from the math model and GTRS are essentially equal.

Z_w: For the case of V=0.01 kts, the math model shows negative heave damping. As V increases, the aircraft becomes more stable in heave and for V>0.5 kts, heave damping has the correct sign. The sign error at the small forward velocities is probably due to the difficulty in trimming at low velocities. The change in Z_w with increasing velocity can be seen in Figure 24.

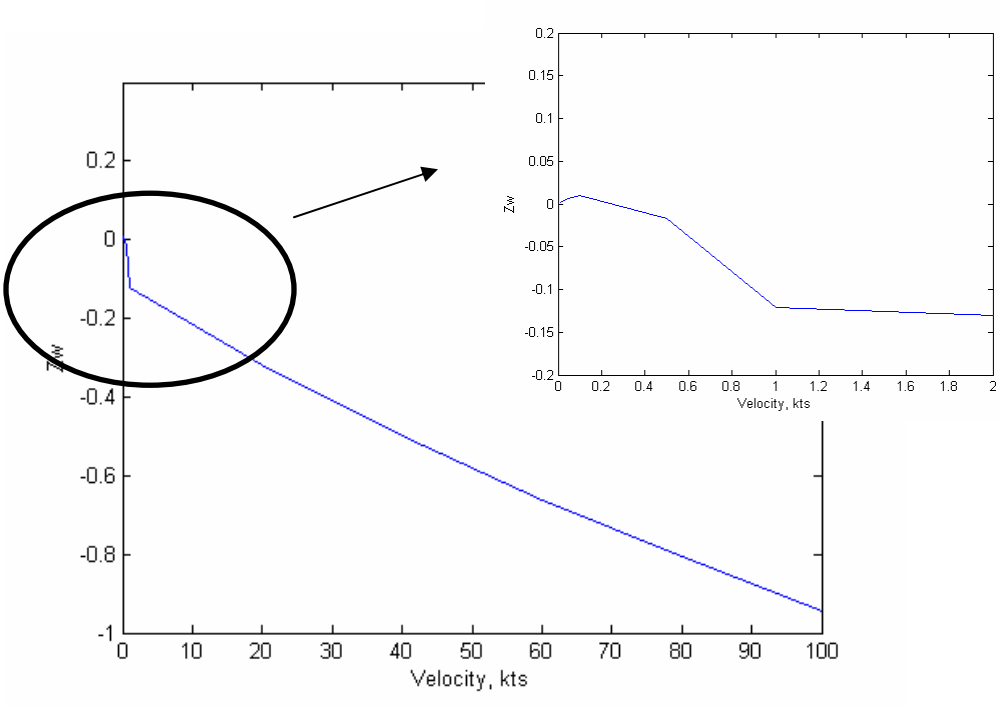

Figure 24: Z_w Change with Velocity

Z_q: For a positive q, the rotor tip path plane will initially lag the shaft orientation. Therefore the thrust vector changes orientation and the net effect should be a positive Z-force change. Therefore the sign on Z_q from the math model appears to be incorrect; however, Z_q is considered a minor stability derivative therefore the sign is not extremely important. The magnitude of Z_q between the math model and GTRS are essentially equal.

Z_θ: The positive sign on Z_θ from the math model conceptually makes sense in that for a positive θ (aircraft instantly attains a new pitch attitude), the angle of attack will also increase, thereby causing thrust to increase, which results in a negative change in Z-force. The magnitude of Z_θ between the math model and GTRS are essentially equal.

The fact that for hover, all the signs on the Z-force derivatives have the opposite sign of GTRS raises a concern that there is a modeling or trim problem in hover.

X_w: The magnitudes for both the math model and GTRS are very small which is expected as a perturbation in w will cause a constant increase in angle of attack over the rotor therefore it will increase rotor thrust, but shouldn't create additional longitudinal or lateral flapping. The net change in drag around the azimuth should be negligible. The sign difference between GTRS and the math model was deemed insignificant.

Y_r: The value of Y_r from the math model is essentially equal and opposite in sign from GTRS. The vertical tails should contribute a positive Y force to damp the yaw rate. The contribution from the rotors depends on the signs of Y_{MR}. Sources of error for this derivative are Y_{MR} and the use of the small angle assumption for the angle off attack at the vertical tails.

$Z_{\theta 0}$: The negative sign on $Z_{\theta 0}$ from the math model conceptually makes sense in that for a positive θ_0 (collective pitch input via collective stick), the coning increases which creates more thrust, which results in a negative Z-force.

$M_{\theta 0}$: The positive sign on $M_{\theta 0}$ from the math model conceptually makes sense in that a positive θ_0 (collective pitch input via collective stick) results in a negative Z-force. Since the Z-force is acting in front of the CG, that results in a positive pitching moment.

$X_{\delta long}$ and $Z_{\delta long}$: The positive signs on $X_{\delta long}$ and $Z_{\delta long}$ from the math model conceptually make sense in that a forward (+) longitudinal stick input results in the rotor disc flapping forward, thereby re-orienting the thrust vector forward and creating an increase in the $+X$ component and a decrease in the upward ($-Z$) component (resultant is a net $+Z$) .

$N_{\delta lat}$, $Y_{\delta ped}$, $L_{\delta ped}$: These derivates are the off-axis response to control inputs and therefore do not have the impact that the on-axis derivatives will have.

N_v: Also called directional or weathercock stability. The preferred sign is positive which will give a restoring yaw moment into the sideward velocity perturbation. The math model shows an unstable N_v. The sign difference in N_v, weathercock stability, is probably due to errors in the calculation of Y_{MR}. The second rotor does not seem to be behaving properly for side velocities.

N_p: The preferred magnitude for N_p is zero for a helicopter. The math model and GTRS magnitudes of N_p are small. Therefore it was deemed negligible that the signs were different.

Differences also exist in the magnitude of some of the derivatives. For example, laterally the math model magnitude of N_v is twice that of GTRS, N_p is 50 times GTRS, L_v is 3 times GTRS, $N_{\delta lat}$ is 1/3 GTRS and $L_{\delta lat}$ is 50% greater. Longitudinally, M_q is twice that of GTRS, M_u is 8 times greater, X_u is 4 times greater, and Z_w is off by two orders of magnitude. Assuming that GTRS more accurately matches flight test, then the magnitude differences imply that there are errors in the math model, primarily in the rotor since the number of gross magnitude differences were less in airplane mode.

Helicopter Mode, 0.01 kts:

A matrix

	u	*v*	*w*	*p*	*q*	*r*	*φ*	*θ*	*ψ*
X	-0.0506	0	0.0008	0	3.7899	0	0	-32.1973	0
Y	0	-0.0355	0	-3.7822	0	0.4317	32.1974	0	0
Z	0.0697	0	0.0022	0.0037	-0.3388	0	0	-0.4132	0
L	0	-0.0017	0	-1.1448	0	0.1055	0	0	0
M	0.0058	0	0	0	-0.4409	0	0	0	0
N	0	-0.0020	0	-0.0030	0	-0.0211	0	0	0
φ	0	0	0	1	0	0.0128	0	0	0
θ	0	0	0	0	1	0	0	0	0
ψ	0	0	0	0	0	1	0	0	0

A matrix (GTRS)

	u	*v*	*w*	*p*	*q*	*r*	*φ*	*θ*	*ψ*
X	-0.0127	0	-0.0027	0	1.3154	0	0	-32.166	0
Y	0	-0.057	0	-1.2538	0	-0.487	32.1662	0	0
Z	-0.0707	0	-0.1984	0	0.3676	0	0	0.4963	0
L	0	-0.005	0	-0.3568	0	0.1159	0	0	0
M	0.0007	0	0	0	-0.2007	0	0	0	0
N	0	0.0012	0	0.1511	0	-0.0286	0	0	0
φ	0	0	0	1	0	0	0	0	0
θ	0	0	0	0	1	0	0	0	0
ψ	0	0	0	0	0	1	0	0	0

B matrix (Math Model)

	*θ*0	*δlong*	*δlat*	*δped*
X	1.8066	2.1794	0	0
Y	0	0	-0.0016	-0.1036
Z	-250.61	0.0239	0	0
L	0	0	0.3364	-0.0033
M	0.2633	-0.2539	0	0
N	0	0	0.0082	0.1615
φ	0	0	0	0
θ	0	0	0	0
ψ	0	0	0	0

B matrix (GTRS)

	δcoll	*δlong*	*δlat*	*δped*
X	1.33	-0.0843	0	0
Y	0	0	-0.0434	0.2446
Z	0.0154	-5.3566	0	0
L	0	0	0.2411	0.0232
M	-0.1887	-0.0029	0	0
N	0	0	-0.0211	0.1006
φ	0	0	0	0
θ	0	0	0	0
ψ	0	0	0	0

Airplane Mode, 200 kts:

A matrix (math model, 200 kts)

	u	*v*	*w*	*p*	*q*	*r*	φ	θ	ψ
X	-0.3893	0	0.0654	0	-9.4549	0.0039	0	-32.1820	0
Y	0	-0.2709	0	10.4945	0	-340.9048	32.1821	0	0
Z	-0.1668	0	-1.3015	-0.0040	339.9659	0	0	-1.0754	0
L	0	-0.0043	0	-0.9309	0	0.1337	0	0	0
M	0.0199	0	-0.0269	0	-2.6295	0	0	0	0
N	0	0.0177	0	-0.4196	0	-1.8442	0	0	0
φ	0	0	0	1	0	0.0334	0	0	0
θ	0	0	0	0	1	0	0	0	0
ψ	0	0	0	0	0	1	0	0	0

A matrix (GTRS)

	u	*v*	*w*	*p*	*q*	*r*	φ	θ	ψ
X	-0.4138	0	0.0729	0	-6.5286	0	0	-32.1621	0
Y	0	-0.3744	0	6.3158	0	-328.3823	32.1621	0	0
Z	-0.1709	0	-1.2073	0	325.1683	0	0	-0.7124	0
L	0	-0.0131	0	-0.8073	0	-0.065	0	0	0
M	0.0215	0	-0.0372	0	-2.1913	0	0	0	0
N	0	0.0096	0	-0.1881	0	-1.0034	0	0	0
φ	0	0	0	1	0	0	0	0	0
θ	0	0	0	0	1	0	0	0	0
ψ	0	0	0	0	0	1	0	0	0

B matrix (Math Model)

	θ_0	δ *long*	δ *lat*	δ *ped*
X	169.8514	0.0976	0	0
Y	-0.0023	0	0	-2.7234
Z	-1.3988	-2.8112	0	0
L	0	0	0.1233	-0.0670
M	-7.1790	-1.223342	0	0
N	0	0	0.0334	0.3696
φ	0	0	0	0
θ	0	0	0	0
ψ	0	0	0	0

B matrix (GTRS)

	δ*coll*	δ*long*	δ*lat*	δ*ped*
X	-0.0656	5.1084	0	0
Y	0	0	0.0041	-2.7109
Z	-3.1791	0.0615	0	0
L	0	0	0.3339	-0.0694
M	-1.4324	-0.2439	0	0
N	0	0	0.0902	0.3816
φ	0	0	0	0
θ	0	0	0	0
ψ	0	0	0	0

Airplane Mode, 200 kts:

A matrix (math model, 200 kts) , modified aileron

	u	*v*	*w*	*p*	*q*	*r*	*φ*	*θ*	*ψ*
X	-0.3893	0	0.0654	0	-9.4549	0.0039	0	-32.1820	0
Y	0	-0.2709	0	10.4945	0	-340.9048	32.1821	0	0
Z	-0.1668	0	-1.3015	-0.0040	339.9659	0	0	-1.0754	0
L	0	-0.0043	0	-0.9309	0	0.1337	0	0	0
M	0.0199	0	-0.0269	0	-2.6295	0	0	0	0
N	0	0.0177	0	-0.4196	0	-1.8442	0	0	0
φ	0	0	0	1	0	0.0334	0	0	0
θ	0	0	0	0	1	0	0	0	0
ψ	0	0	0	0	0	1	0	0	0

A matrix (GTRS)

	u	*v*	*w*	*p*	*q*	*r*	*φ*	*θ*	*ψ*
X	-0.4138	0	0.0729	0	-6.5286	0	0	-32.1621	0
Y	0	-0.3744	0	6.3158	0	-328.3823	32.1621	0	0
Z	-0.1709	0	-1.2073	0	325.1683	0	0	-0.7124	0
L	0	-0.0131	0	-0.8073	0	-0.065	0	0	0
M	0.0215	0	-0.0372	0	-2.1913	0	0	0	0
N	0	0.0096	0	-0.1881	0	-1.0034	0	0	0
φ	0	0	0	1	0	0	0	0	0
θ	0	0	0	0	1	0	0	0	0
ψ	0	0	0	0	0	1	0	0	0

B matrix (Math Model) , modified aileron

	θ_0	*δlong*	*δlat*	*δped*
X	169.8514	0.0976	0	0
Y	-0.0023	0	0	-2.7234
Z	-1.3988	-2.8112	0	0
L	0	0	0.3676	-0.0670
M	-7.1790	-1.223342	0	0
N	0	0	0.0309	0.3696
φ	0	0	0	0
θ	0	0	0	0
ψ	0	0	0	0

B matrix (GTRS)

	δcoll	*δlong*	*δlat*	*δped*
X	-0.0656	5.1084	0	0
Y	0	0	0.0041	-2.7109
Z	-3.1791	0.0615	0	0
L	0	0	0.3339	-0.0694
M	-1.4324	-0.2439	0	0
N	0	0	0.0902	0.3816
φ	0	0	0	0
θ	0	0	0	0
ψ	0	0	0	0

The poles extracted from the linearized model are presented in Figures 25 to 29. The arrows show the direction of increasing airspeed. In general, the math model shows the aircraft getting more stable with increasing speed. The eigenvalues associated with the plots can be found in Appendix D.

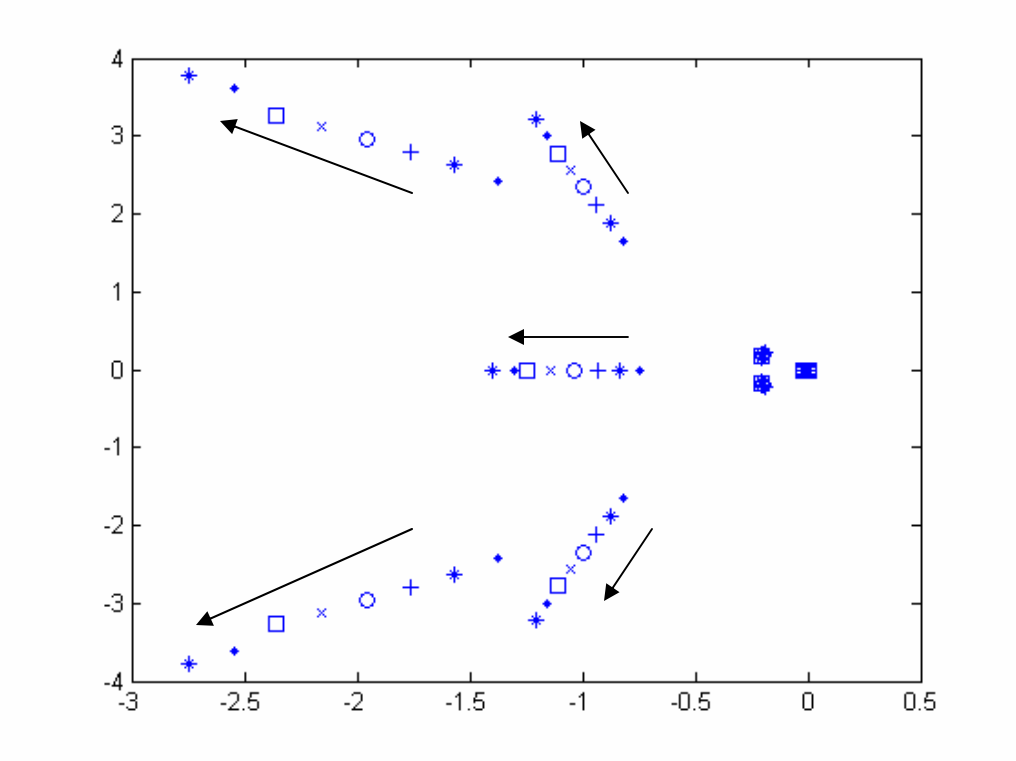

Figure 25: Math Model Airplane Mode Pole Movement

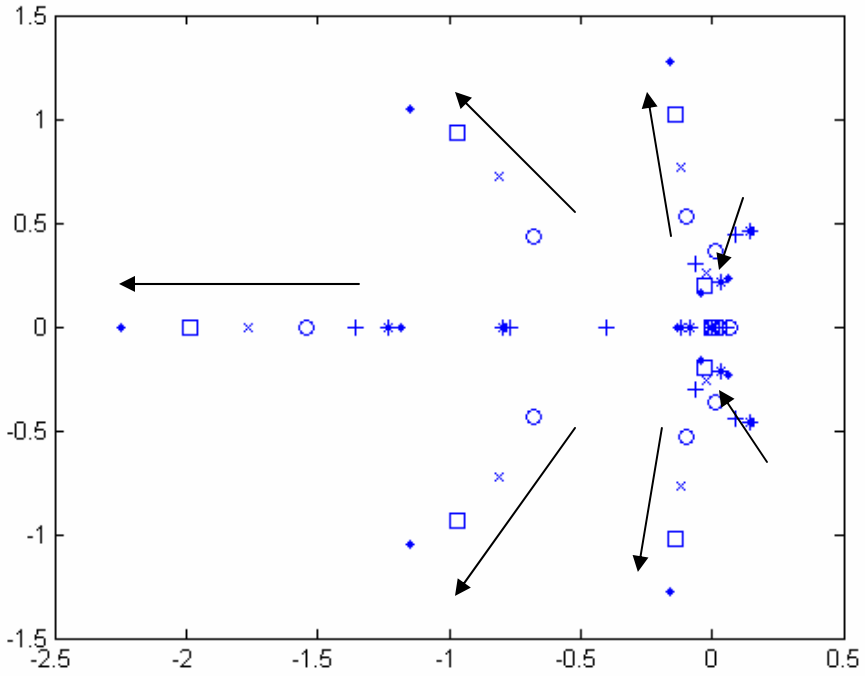

Figure 26: Math Model Helicopter Mode Pole Movement

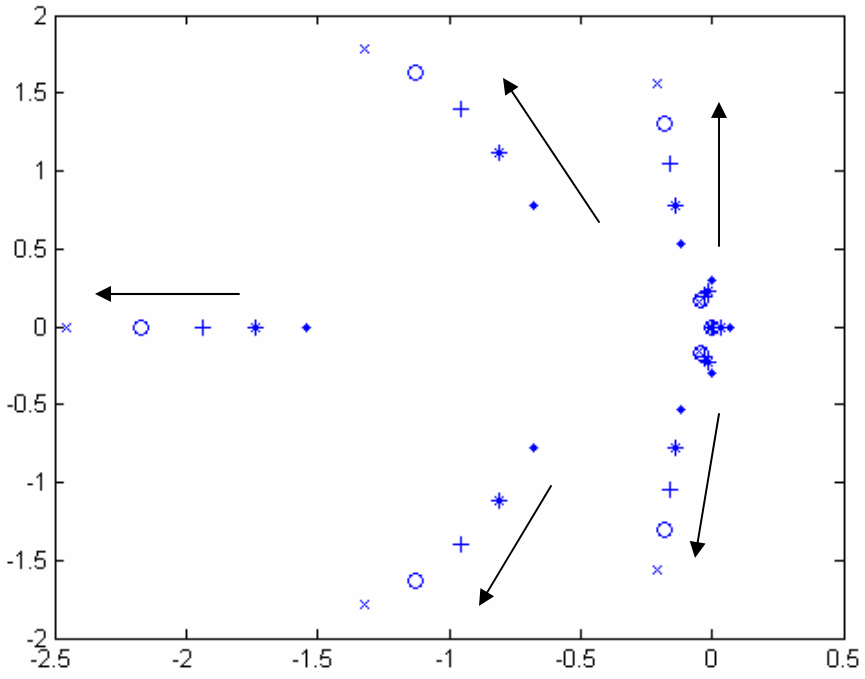

Figure 27: Math Model Conversion Mode, 15ºβ_M, Pole Movement

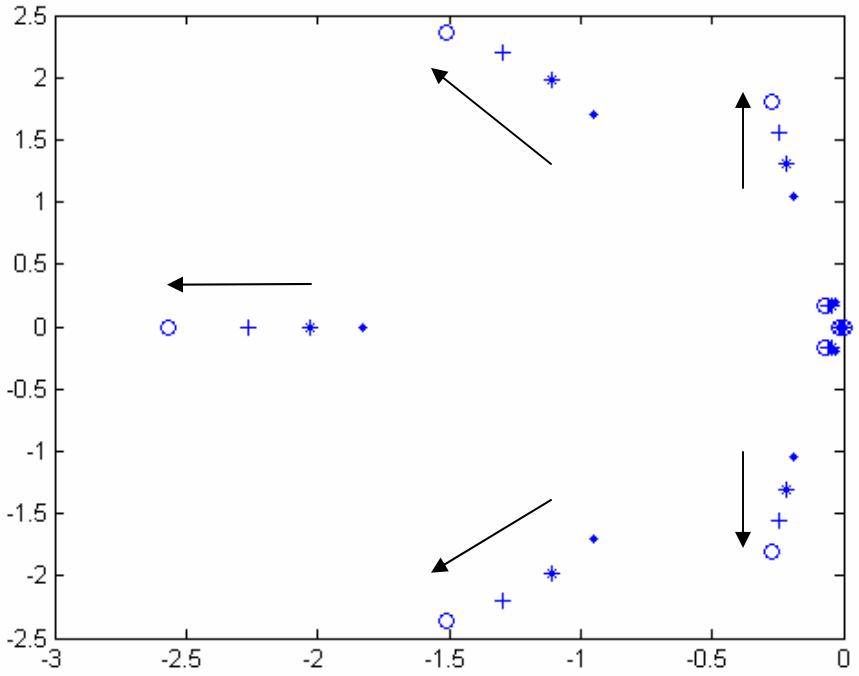

Figure 28: Math Model Conversion Mode, 30ºβ_M, Pole Movement

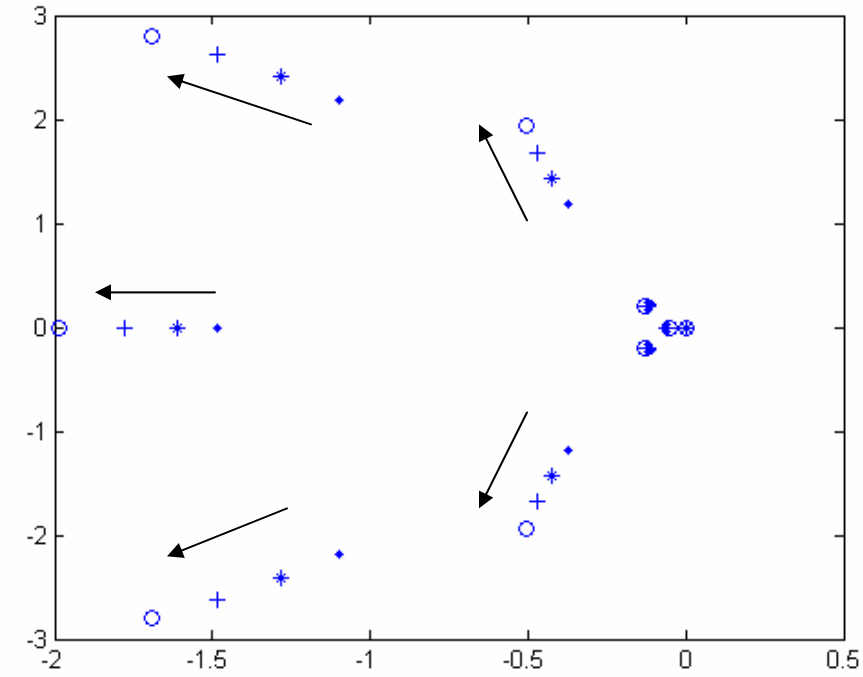

Figure 29: Math Model Conversion Mode, 60ºβ_M, Pole Movement

Flight test data was available from Reference 24 in hover and in airplane mode at 170 kts. Frequency sweeps were performed to extract the aircraft dynamics. Data was also gathered at β_M=60º and β_M=20º however that data was not published and was unavailable for this project. A comparison between the modes from the math model, GTRS (from Reference 9), and flight are shown in Figures 30 to 38.

The comparison for the hover modes is shown in Figure 30, the lateral directional modes are shown in Figure 31, and the longitudinal modes are shown in Figure 32. The characteristic of the pole distribution between the math model, GTRS, and flight are similar. For the lateral-directional oscillatory mode, the math model has 78% of the damping in GTRS and 58% of the damping in flight. The math model oscillatory period is roughly twice that of GTRS and flight. For the real poles, the math model short period mode has a slightly shorter period than GTRS (5.3 sec vs. 8.6 sec); however, the period is essentially the same as the flight test period (5.3 sec vs. 5.1 sec). The long period mode from the math model has a much shorter time period (48 sec) than GTRS which has a time period >1000 sec. A much better comparison is made between the math model and the flight data which has a long period frequency of 61 sec. The real pole at the origin is the heading mode.

For the longitudinal modes, the oscillatory modes have essentially the same damping ratio (math model has 94% the damping of GTRS); however, when compared to flight, the math model has only 66% of the damping. The math model oscillatory period is half that of GTRS (13 sec vs. 25 sec); however the math model frequency is closer to the

flight value (13 sec vs. 11 sec). For the real poles, the math model short period mode has a period that is half that for GTRS and approximately 60% of the flight value. The math model long period mode is unstable compared to the stable mode from GTRS and flight.

Math Model Helicopter Mode Longitudinal Roots (Hover):

Eigenvalue	Damping	Frequency (rad/sec)
0.0033	–1.00	0.0033
–0.7892	1.00	0.7892
0.1483 + 0.4616i	–0.306	0.485
0.1483 – 0.4616i	–0.306	0.485

Math Model Helicopter Mode Lateral Roots (Hover):

Eigenvalue	Damping	Frequency (rad/sec)
0	–1.00	0
0.0579 + 0.2321i	–0.242	0.239
0.0579 – 0.2321i	–0.242	0.239
–0.1312	1.00	0.1312
–1.1861	1.00	1.19

Flight Test Helicopter Mode Longitudinal Roots (Hover):

Eigenvalue	Damping	Frequency (rad/sec)
–0.105	1.00	0.105
–1.32	1.00	1.32
0.2681 + 0.5132i	–0.463	0.579
0.2681 – 0.5132i	–0.463	0.579

Flight Test Helicopter Mode Lateral Roots (Hover):

Eigenvalue	Damping	Frequency (rad/sec)
0	–1.00	0
0.1868 + 0.4061i	–0.418	0.447
0.1868 – 0.4061i	–0.418	0.447
–0.102	1.00	0.102
–1.23	1.00	1.23

GTRS (XV-15) Hover Model Longitudinal Roots:

Eigenvalue	Damping	Freq. (rad/sec)
0.0810 + 0.2352i	-0.3256	0.2487
0.0810 - 0.2352i	-0.3256	0.2487
-0.3733	1.0000	0.3733
-0.2005	1.0000	0.2005

GTRS (XV-15) Hover Model Lateral Roots:

Eigenvalue	Damping	Freq. (rad/sec)
0.1445 + 0.4459i	-0.3083	0.4688
0.1445 - 0.4459i	-0.3083	0.4688
-0.7305	1.0000	0.7305
-0.0008	1.0000	0.0008
0	-1.0000	0

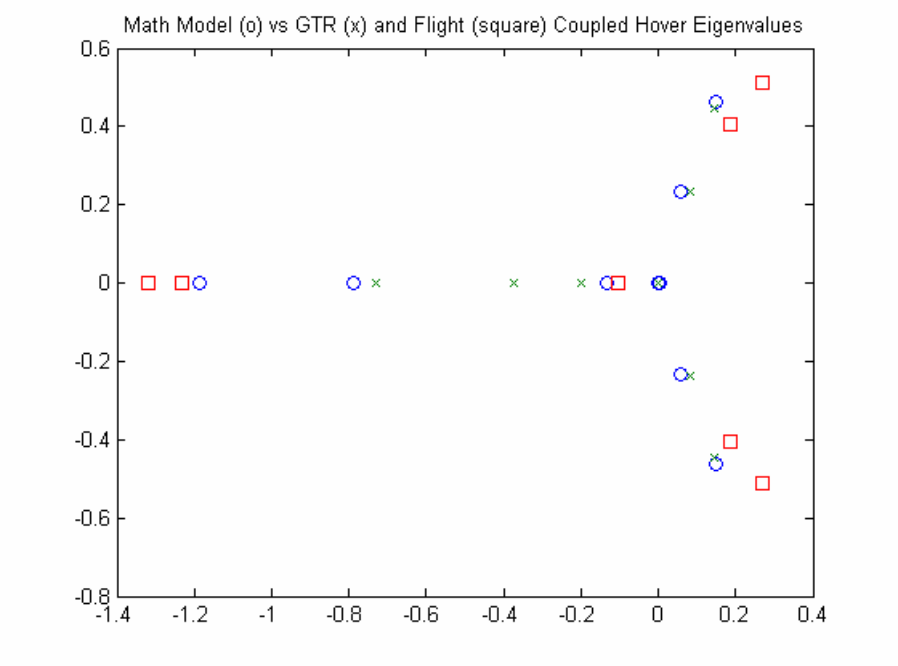

Figure 30: Helicopter Mode Hover Pole Comparison

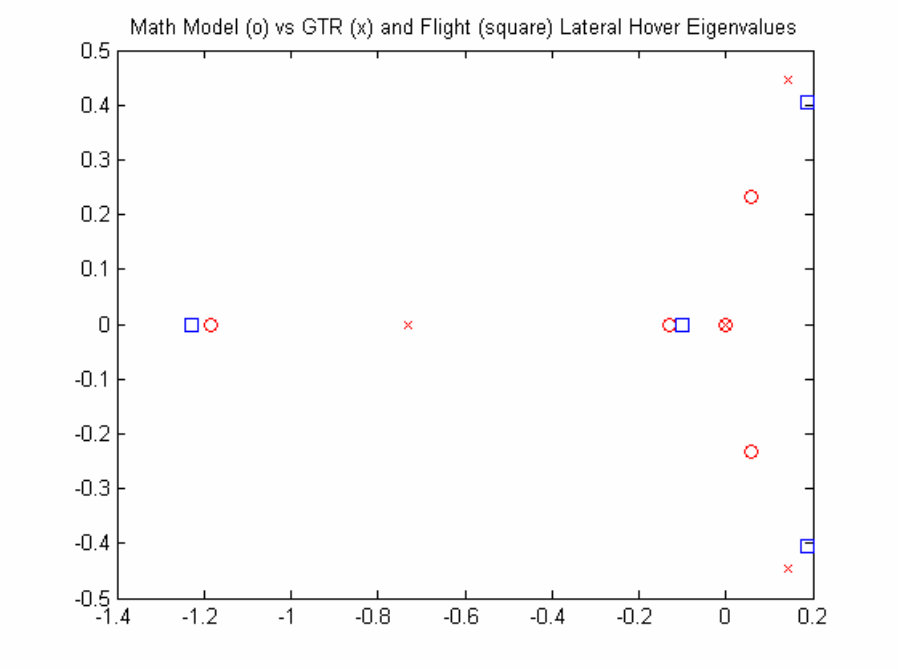

Figure 31: Helicopter Mode Hover Lateral Pole Comparison

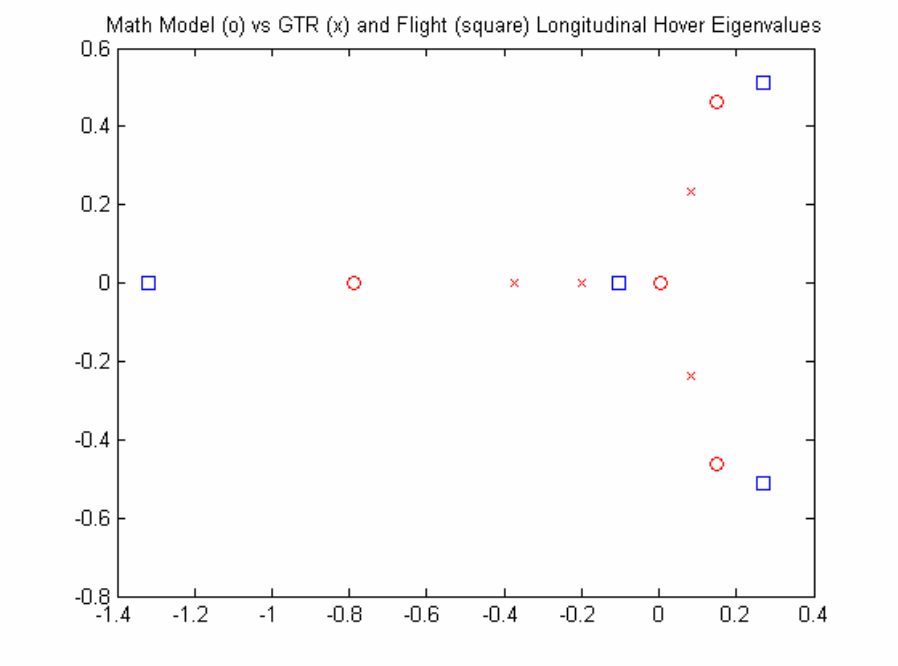

Figure 32: Helicopter Mode Hover Longitudinal Pole Comparison

The airplane mode 200 kts modes are compared to GTRS in Figure 33, the lateral directional modes are shown in Figure 34, and the longitudinal modes are shown in Figure 35. The characteristic of the pole distribution between the math model and GTRS are similar. For the lateral-directional oscillatory mode, the math model has 38% more damping than GTRS. The frequency associated with these oscillatory modes is also 44% different as the math model oscillatory period is 2.5 sec where GTRS period is 3.4 sec. For the real roots, the lateral-directional short period mode is at essentially the same location for the math model and GTRS (5.9 sec vs. 6.1 sec). The math model long period mode has a much longer period than GTRS. The real pole at the origin is the heading mode.

For the longitudinal oscillatory modes, the math model and GTRS are essentially at the same locations in the right hand plane (unstable). One mode has 90% the damping of GTRS and the other mode has 125% the damping of GTRS. The frequencies vary by only 5–7%.

Math Model Airplane Mode Longitudinal Roots (200 kts):

Eigenvalue	Damping	Frequency (rad/sec)
–0.2007 + 0.1898i	0.727	0.276
–0.2007 – 0.1898i	0.727	0.276
–1.9594 + 2.9700i	0.551	3.56
–1.9594 – 2.9700i	0.551	3.56

Math Model Airplane Mode Lateral Roots (200 kts):

Eigenvalue	Damping	Frequency (rad/sec)
0	–1.00	0
–0.0238	1.00	0.0238
–0.9950 + 2.3457i	0.391	2.55
–0.9950 – 2.3457i	0.391	2.55
–1.0323	1.00	1.03

GTRS (XV-15) Airplane Model Longitudinal Roots:

Eigenvalue	Damping	Freq. (rad/sec)
-0.2115 + 0.1576i	0.8018	0.2637
-0.2115 - 0.1576i	0.8018	0.2637
-1.6948 + 3.4555i	0.4403	3.8488
-1.6948 - 3.4555i	0.4403	3.8488

GTRS (XV-15) Airplane Model Lateral Roots:

Eigenvalue	Damping	Freq. (rad/sec)
0	-1.0000	0
-0.1226	1.0000	0.1226
-0.4989 + 1.7702i	0.2712	1.8392
-0.4989 - 1.7702i	0.2712	1.8392
-1.0649	1.0000	1.0649

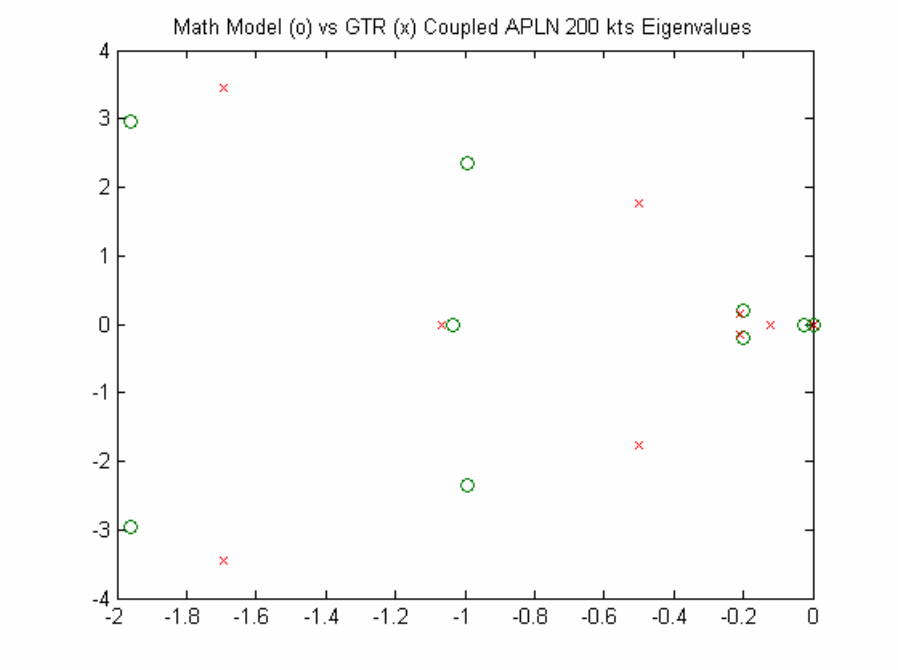

Figure 33: Airplane Mode 200kts Pole Comparison

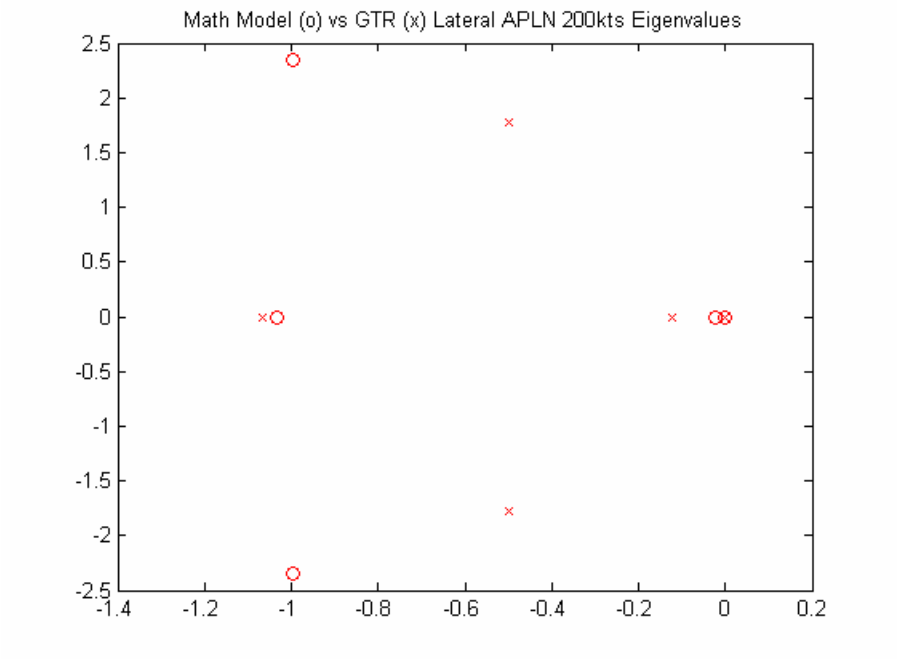

Figure 34: Airplane Mode 200kts Lateral Pole Comparison

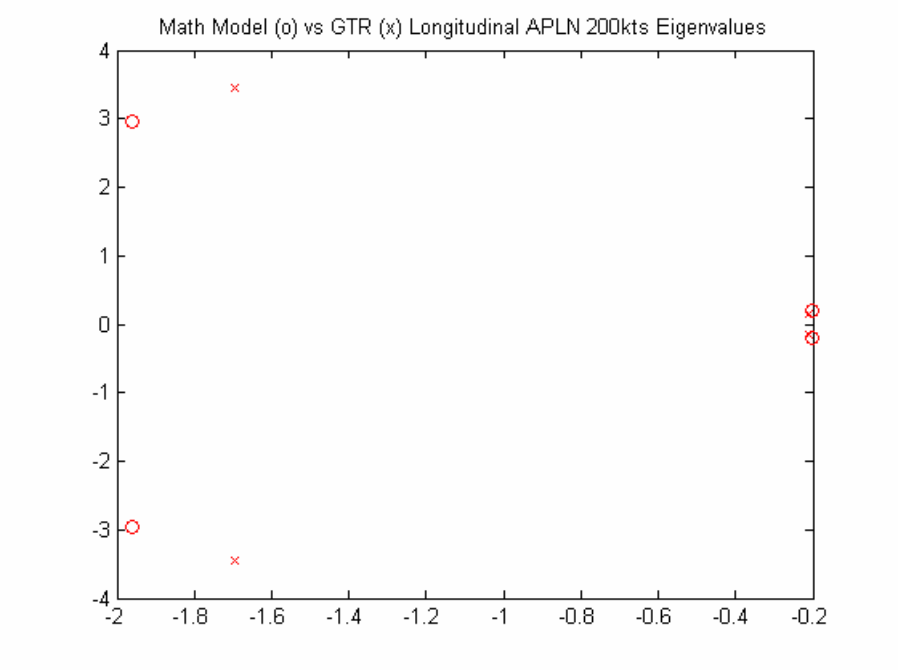

Figure 35: Airplane Mode 200kts Longitudinal Pole Comparison

The airplane mode 170 kts modes are compared to flight in Figure 36, the lateral directional modes are shown in Figure 37, and the longitudinal modes are shown in Figure 38. The characteristic of the pole distribution between the math model and flight are similar. For the lateral-directional oscillatory mode, the math model has 60% more damping than flight. The frequency associated with these oscillatory modes is also 40% different as the math model oscillatory period is 2.9 sec where the flight period is 4 sec. For the real roots, the lateral-directional short period mode has 80% of the flight damping and 25% smaller frequency which gives a math model time period of 7.1 sec and a flight time period of 5.8 sec. The math model long period mode has approximately 2.5 times the period of flight. The short period mode is probably the roll mode and the long period mode is probably the spiral mode. The real pole at the origin is the heading mode.

For the longitudinal oscillatory modes, the flight phugoid dynamics were not presented by Tischler as they are only important at the lowest frequency inputs. For the other oscillatory mode, the math model has essentially the same damping but has a frequency that is 60% greater than the flight value.

Math Model Airplane Mode Longitudinal Roots (170 kts):

Eigenvalue	Damping	Frequency (rad/sec)
–1.6653 + 2.7127i	0.523	3.18
–1.6653 – 2.7127i	0.523	3.18
–0.1946 + 0.2097i	0.680	0.286
–0.1946 – 0.2097i	0.680	0.286

Math Model Airplane Mode Lateral Roots (170 kts):

Eigenvalue	Damping	Frequency (rad/sec)
0	–1.00	0
–0.9076 + 2.0046i	0.412	2.20
–0.9076 + 2.0046i	0.412	2.20
–0.0234	1.00	0.0234
–0.8838	1.00	0.8838

Flight Test Airplane Mode Longitudinal Roots (airplane mode 170kts):

Eigenvalue	Damping	Frequency (rad/sec)
–1.0833 + 1.7062i	0.536	2.021
–1.0833 + 1.7062i	0.536	2.021

Flight Test Airplane Mode Lateral Roots (airplane mode 170kts):

Eigenvalue	Damping	Frequency (rad/sec)
0	–1.00	0
–0.3918 + 1.5306i	.248	1.58
–0.3918 – 1.5306i	.248	1.58
–0.0630	1.00	0.063
–1.09	1.00	1.09

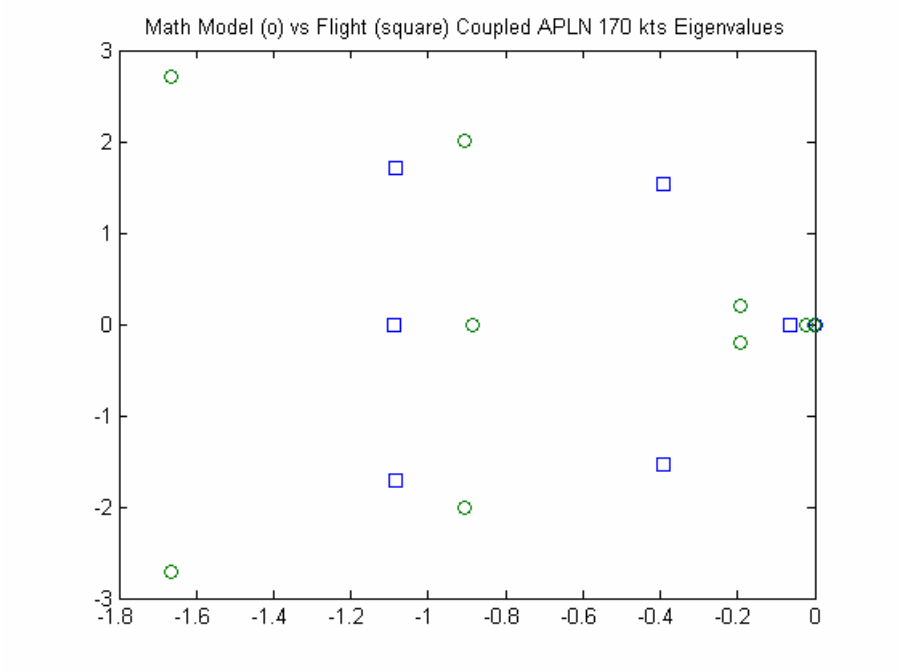

Figure 36: Airplane Mode 170kts Pole Comparison

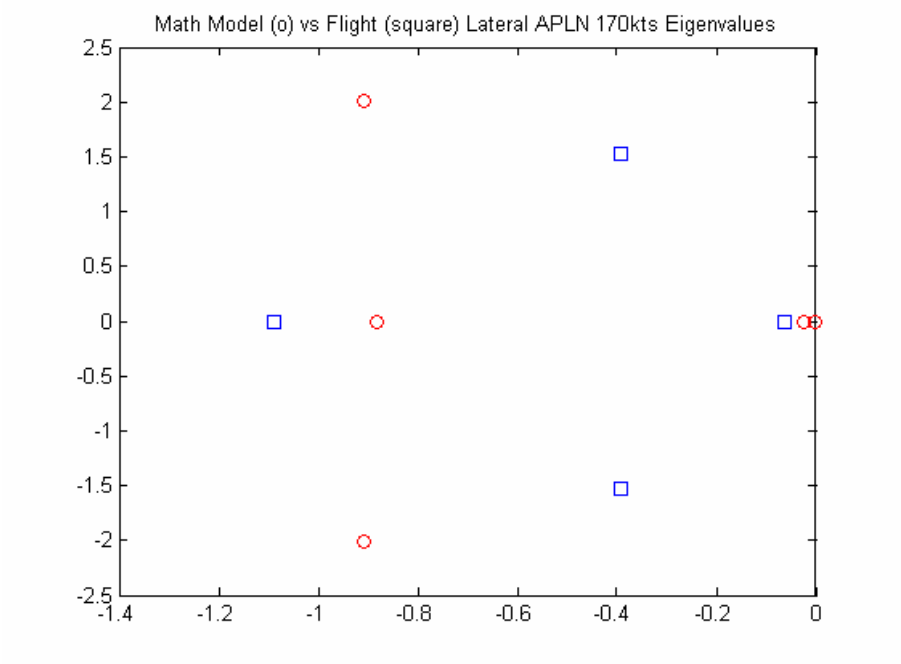

Figure 37: Airplane Mode 170kts Lateral Pole Comparison

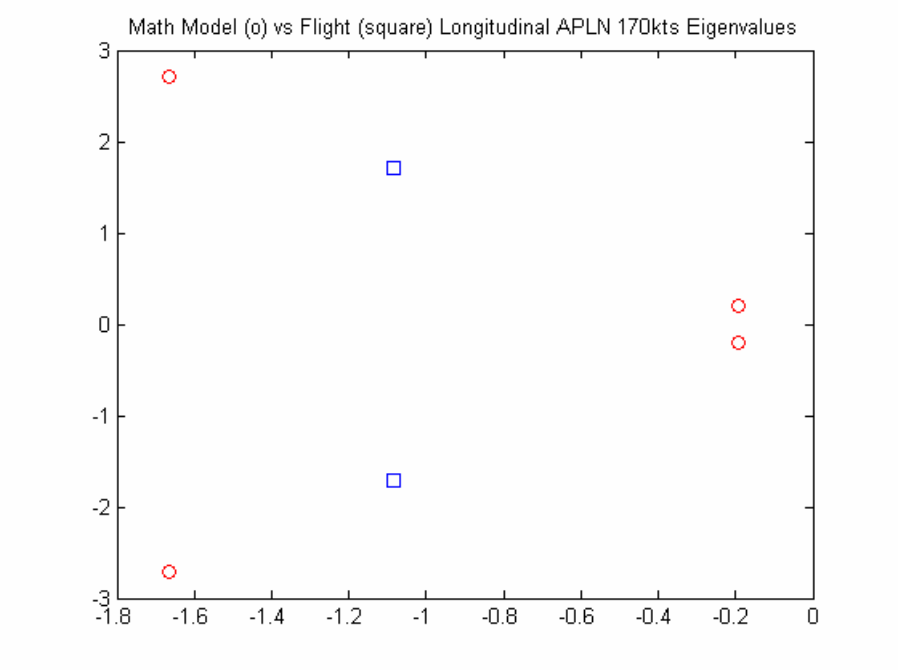

Figure 38: Airplane Mode 170kts Longitudinal Pole Comparison

Bode plot comparisons can be made with flight test data (see Figures 39–45). The flight test data analysis (see Reference 24, 25, and 26) was done in a form that compared the aircraft response to the control surface deflection, rather than the cockpit control deflection. Therefore, the math model data had to be multiplied by the gearing ratio in order to be plotting consistent data. All figures show a positive input/output ratio. For example, the q/δ_{elev} plot is actually showing $q/-\delta_{elev}$ since a positive elevator deflection would give a negative pitch rate. Due to the frequency of pilot inputs, only the range of interest is plotted (approximately 10^{-1} to 10^{1}). The additional data on the plots is Tischler's analysis of the data using simulator frequency sweeps and non-real time simulation. That analysis is detailed in Reference 24 and is not covered here.

The airplane mode p/δ_{ail} (Figure 39) Bode plot matches fairly well over the range of interest. The gain slope change for both curves between approximately 1–2.5 rad/sec is also the location of the lateral-directional oscillatory mode. There is approximately a 10 dB offset in the gain plot which equates to a factor of 3. This delta can also be seen in the lateral input time history data where the peak roll attitude and roll rate from the math model is essentially 1/3 that seen in flight. If GTRS is assumed to match flight, the potential source of this difference can be contributed to $L_{\delta ail}$ differing by approximately a factor of 3. For the lower frequencies, the gain is essentially constant. Beyond the lateral-directional oscillatory frequency the gain falls off at the standard rate of 20 dB/decade which implies a standard 1/s roll rate response for the aircraft.

The math model provides a good approximation of the phase response. For the lower frequencies the math model shows more phase lag while at the higher frequencies the math model shows less phase lag but is approaching –90º. The flight data goes below the –90º phase point. Part of this phase difference at the higher frequencies may be due to the actuator dynamics that exist in the real aircraft. The character of the phase curve indicates that the system is stable.

Again, applying a factor of three to the aileron effectiveness results in much better flight correlation. The Bode plot of the response with for the modified aileron is shown in Figure 40. The magnitude of the aircraft response to an aileron input now matches flight.

The airplane mode q/δ_{elev} plot (Figure 41) also matches fairly well to flight. For the gain plot, the peak gain from the math model at the just over 3 rad/sec is due to the location of the short period mode. The math model peaks at approximately the same gain, but at a higher frequency that the flight data. As is expected, the phase lag for both of the gain

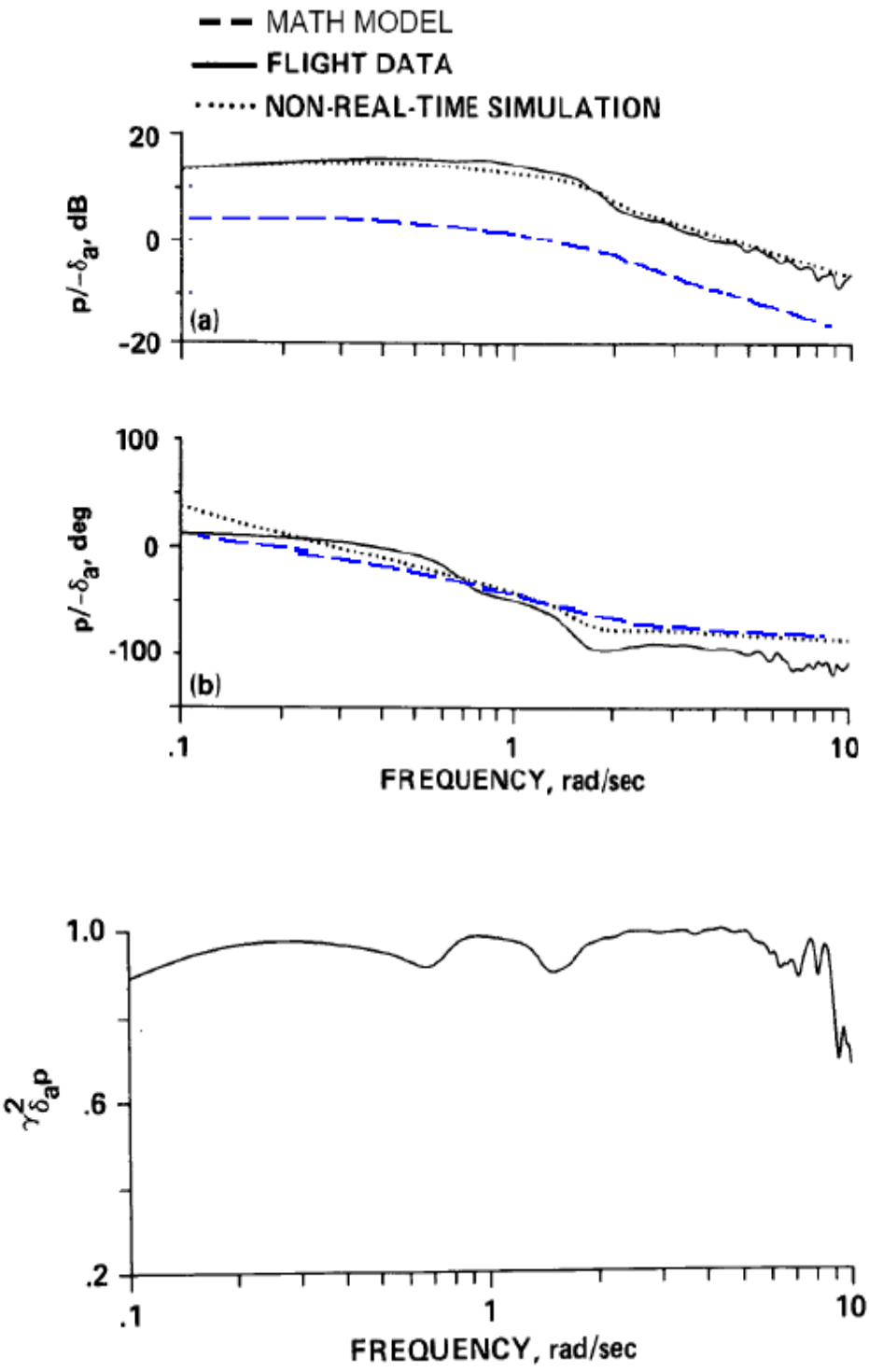

Figure 39: Airplane Mode 170 kts p/δ_{ail} Bode Plot and Coherence Function

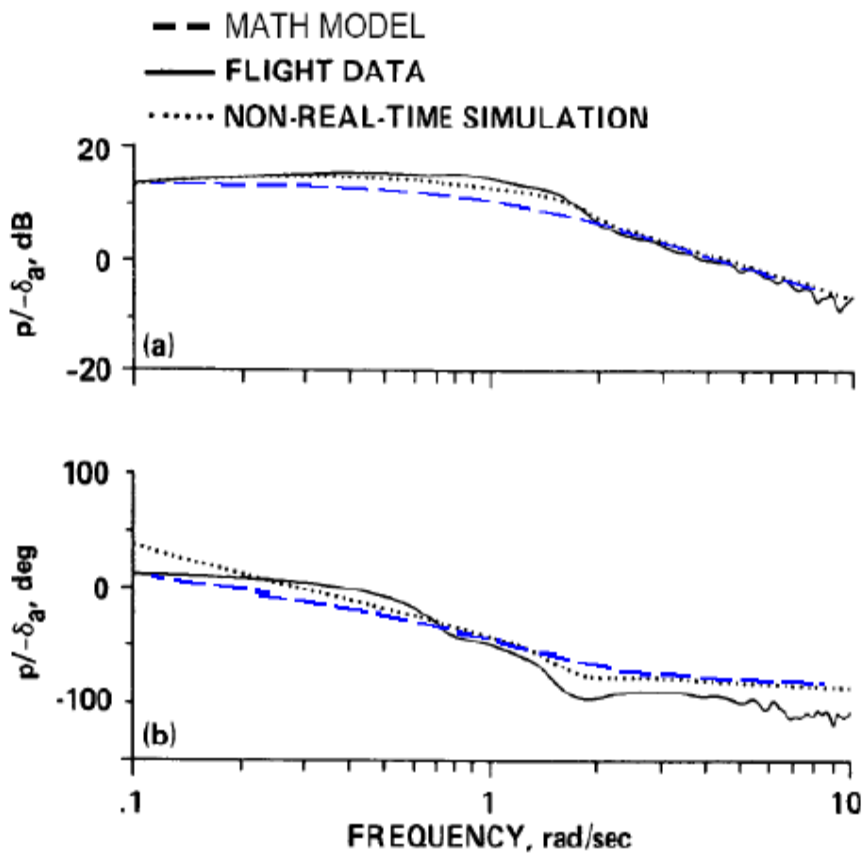

Figure 40: Airplane Mode 170 kts p/δ_{ail} Bode Plot (Modified Aileron)

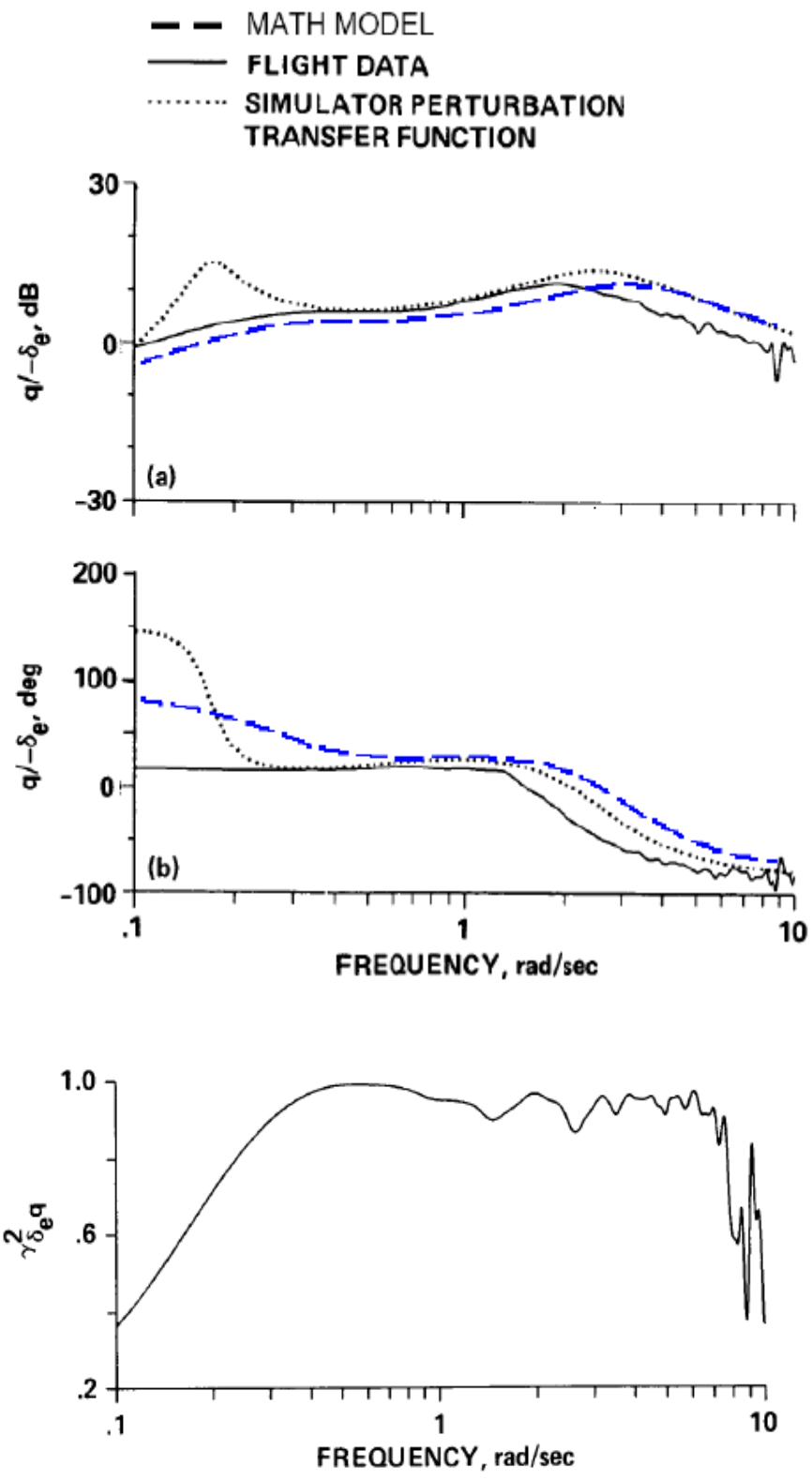

Figure 41: Airplane Mode 170 kts q/δ_{elev} Bode Plot and Coherence Function

peaks in the 1–3 rad/sec area is –45º. The significant shift in the gain and phase at the higher frequencies shows gain and mode location differences. The math model gain for frequencies less than 2 rad/sec appears to have a constant offset from the flight data which indicates that there is a control effectiveness error in the math model that is resulting in less response than the aircraft. The large difference in phase below 0.6 rad/sec is probably due to the locations of the phugoid modes. The +90º phase shift associated with the stable phugoid mode from the math model occurs around the phugoid frequency of 0.286 rad/sec. The flight phugoid mode frequency is much lower and therefore the flight data is already at a constant phase offset by the time the frequency is above 0.1 rad/s.

For helicopter mode, the p/δ_{ail} Bode plot can be seen in Figure 42. The gain plot appears to have fairly good correlation however the phase plot shows larger differences. For the gain plot, the flight and math model curves have the same character; however, the peak response frequencies differ due to the determined frequencies of the lateral oscillatory mode. For the frequencies beyond the lateral oscillatory mode frequency the plot shows the classic –20 dB/decade roll off associated with the 1/s roll rate response of the aircraft. With respect to the phase plot, it can be seen from the positive slope change that the lateral oscillatory mode in both the math model and in flight are unstable. The math model's prediction of the phase below approximately 3 rad/sec differs from the flight data. The math model is off by 50º – 90º in phase at these lower frequencies. Part of the issue appears to be the difference in depicting the frequency of the long period mode.

The flight test data is also showing low coherence below 0.6 rad/sec. Further examination of the poles and zeros for the p/δ_{ail} transfer function shows that there is a pole zero pair that is not quite cancelling at the lower frequencies. Since the flight data was gathered in 'hover' with winds less than 5 kts, the flight Bode plot was also compared to the math model at 1 kt forward velocity (Figure 43). As can be seen in this comparison, the phase comparison is better at the lower frequencies when using the higher velocity, however, the large phase difference between approximately 0.2 – 2 rad/s still exists. This indicated that the phase error is probably just due to the frequency difference of the lateral-directional oscillation poles.

Hover:

$$\frac{p}{\delta_{ail}} \Rightarrow \frac{zeros}{poles} = \frac{(0)(-0.7892)(-0.1103)(0.0033)(0.1483 \pm 0.4616i)(0.0255 \pm 0.0817i)}{(0)(-0.7892)(-0.1312)(0.0033)(-1.1861)(0.1483 \pm 0.4616i)(0.0579 \pm 0.2321i)}$$

$$\frac{zeros}{poles} = \frac{(-0.1103)(0.0255 \pm 0.0817i)}{(-0.1312)(-1.1861)(0.0579 \pm 0.2321i)}$$

Hover		Damping	Freq
Zero	0.0255±0.0817i	–0.3285	0.0776
Pole	0.0579±0.2321i	–0.242	0.239

1 kt:

$$\frac{p}{\delta_{ail}} \Rightarrow \frac{zeros}{poles} = \frac{(0)(-0.7961)(-0.1204)(-0.0999)(0.147 \pm 0.4620i)(0.0186 \pm 0.0570i)}{(0)(-0.7961)(-0.1204)(-0.0823)(-1.2331)(0.147 \pm 0.4620i)(0.0315 \pm 0.2136i)}$$

$$\frac{zeros}{poles} = \frac{(-0.0999)(0.0186 \pm 0.0570i)}{(-0.0823)(-1.2331)(0.0315 \pm 0.2136i)}$$

1 kts		Damping	Freq
Zero	0.0186±0.0570i	–0.01548	0.2137
Pole	0.0315±0.2136i	–0.146	0.2159

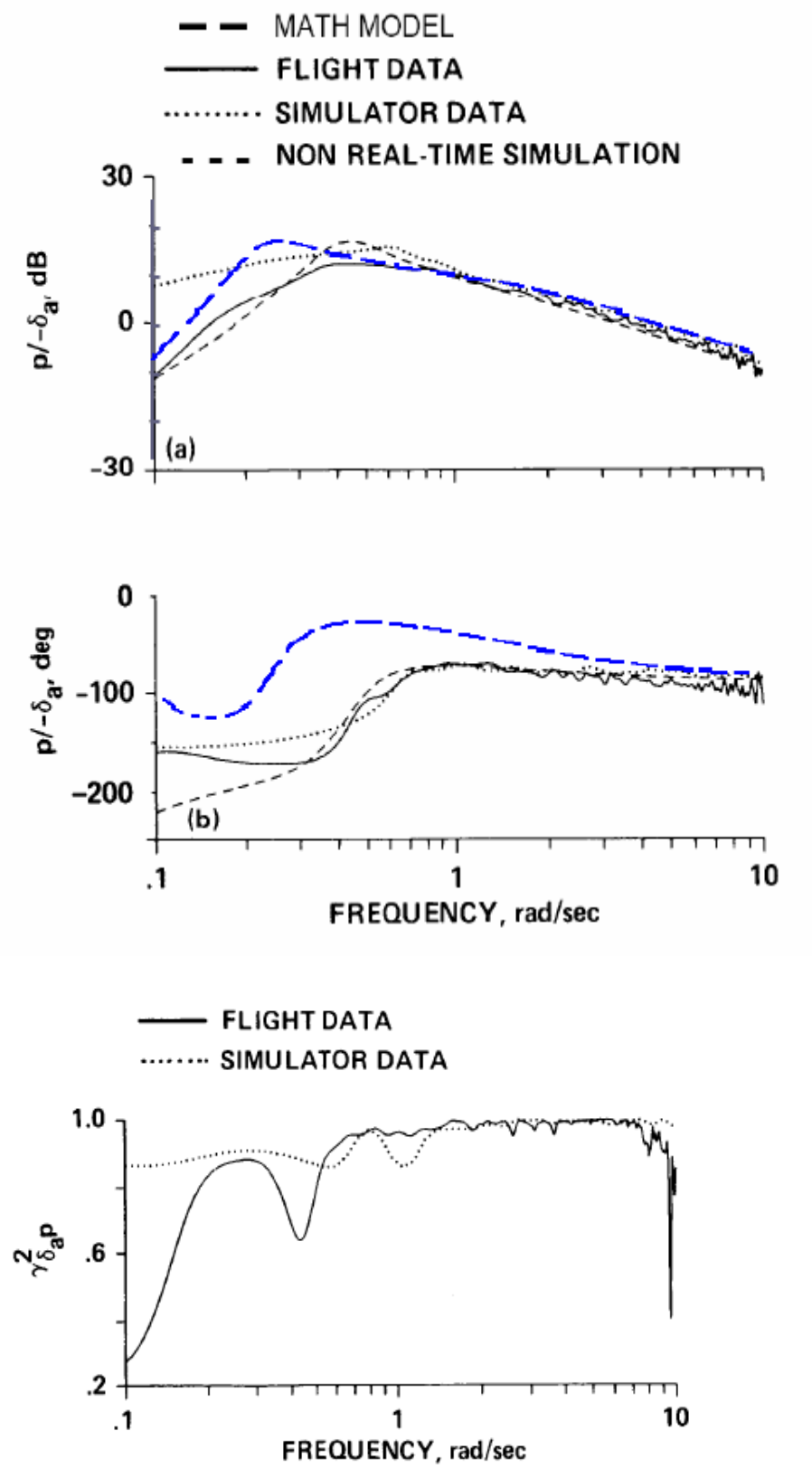

Figure 42: Helicopter Mode Hover p/δ_{ail} Bode Plot and Coherence Function

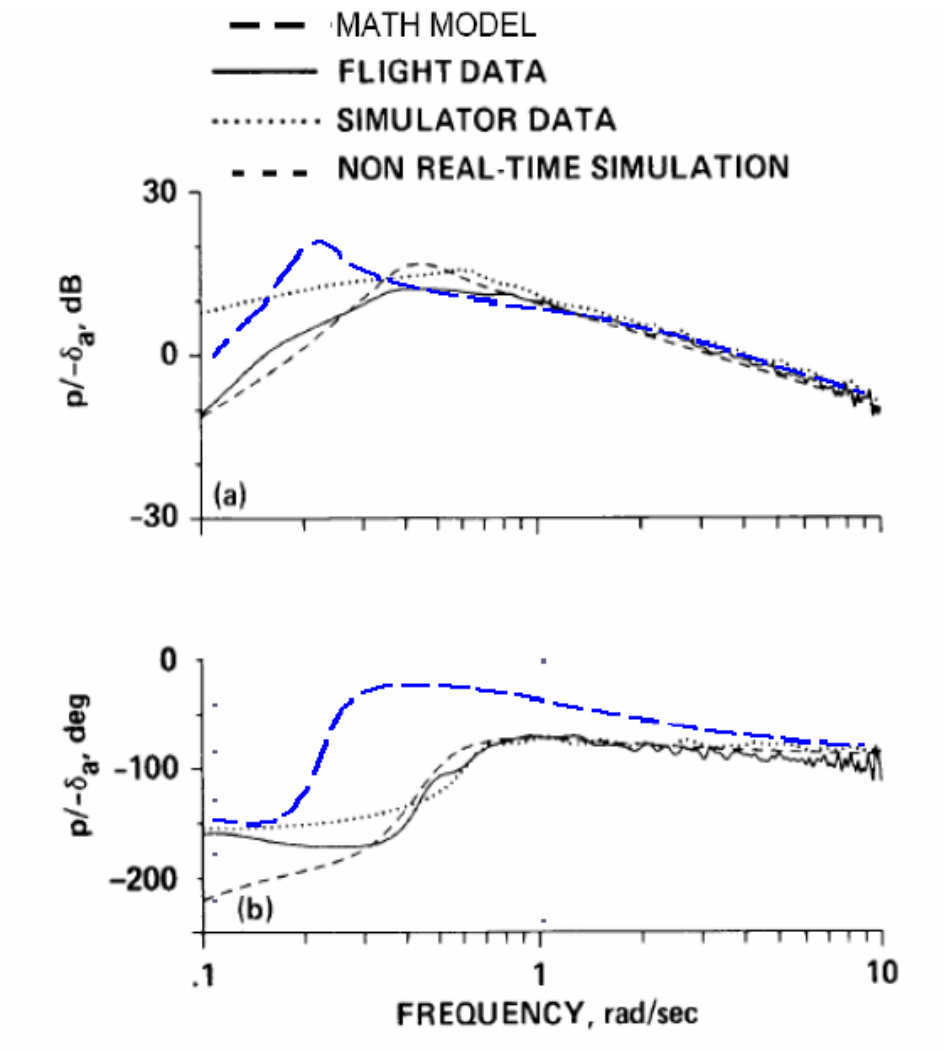

Figure 43: Helicopter Mode 1 kt p/δ_{ail} Bode Plot and Coherence Function

The helicopter mode q/δ_{elev} response can is shown in Figure 44. The gain response again has the same characteristic as the flight data however the peak gain frequencies differ due to the difference in the phugoid frequency. The math model also has a larger response at that peak frequency. For frequencies greater than the phugoid frequency the model and the flight data both have the characteristic –20 dB/decade gain change. During the gain drop-off the math model has an offset of approximately 2–3 dB from the flight test data.

This shows that the math model is about 30% more responsive than the aircraft. Per Reference 24, there was additional ballast placed into the tail for the test flights. This additional weight and change in inertia is not reflected in the math model and could explain why the math model is more responsive.

From the q/δ_{elev} phase plot, it can be seen that the phugoid is unstable due to the decrease in phase offset. For frequencies greater than 1 rad/sec, both the flight test data and math model show the phase offset essentially equaling –90º. However, the flight test phase offset starts getting larger and drifting away from the –90º value. As shown in Reference 24, the coherence of the flight data above 5 rad/s is less than unity which helps explain some of this increase.

The r/δ_{rud} Bode plot for helicopter mode is shown in Figure 45. For frequencies greater than 0.6 rad/sec, the math model prediction of the flight response is good. The difference in the gain roll-off frequency correlates with the difference in lateral oscillatory mode frequency between the math model and flight. For the gain response, the sharp sink in gain near 0.2 rad/sec appears to correspond to the lateral oscillatory mode frequency. However the sharp rise in magnitude indicates that there is also a zero in this area. The phase response near 0.2 rad/sec appears to correlate to the lateral-directional oscillation frequency. The phase shift indicates that the lateral-directional oscillation is stable. However, when the poles are analyzed, the lateral-directional oscillation mode appears to be unstable. The phase response near 0.2 rad/sec again indicates that there is a pair of zeros in that frequency range. When the poles and zeros were analyzed it was determined

that there was in deed an unstable pair of zeros that were not quite cancelling out the unstable lateral-directional oscillation poles. This pole-zero pair shows up in the math model Bode since all other controls are held fixed. During the flight test frequency sweep, the pilot was actively or passively cancelling out off axis response therefore this does not exist in the flight data. If the math model pole-zero pair had cancelled better, the r/δ_{rud} response would look like a simple 1/(s±1) response with the gain plot not having a spike and the phase plot having a standard 0º to –90º or –180º to –90º phase shift.

$$\frac{r}{\delta_{rud}} \Rightarrow \frac{zeros}{poles} = \frac{(0)(-0.1204)(-1.236)(-0.7961)(0.147 \pm 0.462i)(0.0033 \pm 0.2136i)}{(0)(-0.1204)(-0.0823)(-1.2331)(-0.7961)(0.147 \pm 0.462i)(0.0315 \pm 0.2136i)}$$

$$\Rightarrow \frac{zeros}{poles} = \frac{(-1.236)(0.0033 \pm 0.2136i)}{(-0.0823)(-1.2331)(0.0315 \pm 0.2136i)}$$

For frequencies greater than 0.5 rad/sec the gain shows the 20 dB/decade roll off associated with a 1/s yaw rate command system. The math model does have a slight parallel offset in gain of about 5–7 dB which means that the math model is over predicting the yaw response by about a factor of two. The flight test tail ballast that is not modeled in the math model could be the culprit in that the ballast increases the inertia thereby reducing the control sensitivity of the aircraft. The phase offset has a great match from 0.5 to 3 rad/sec. The apparent oscillatory phase offset less than –90 deg is due to the low coherence at greater than 3 rad/s. At the low frequencies, the large phase discrepancy indicates that the math model over estimates the amount of yaw damping in the aircraft, which can be seen in the pedal step input time history.

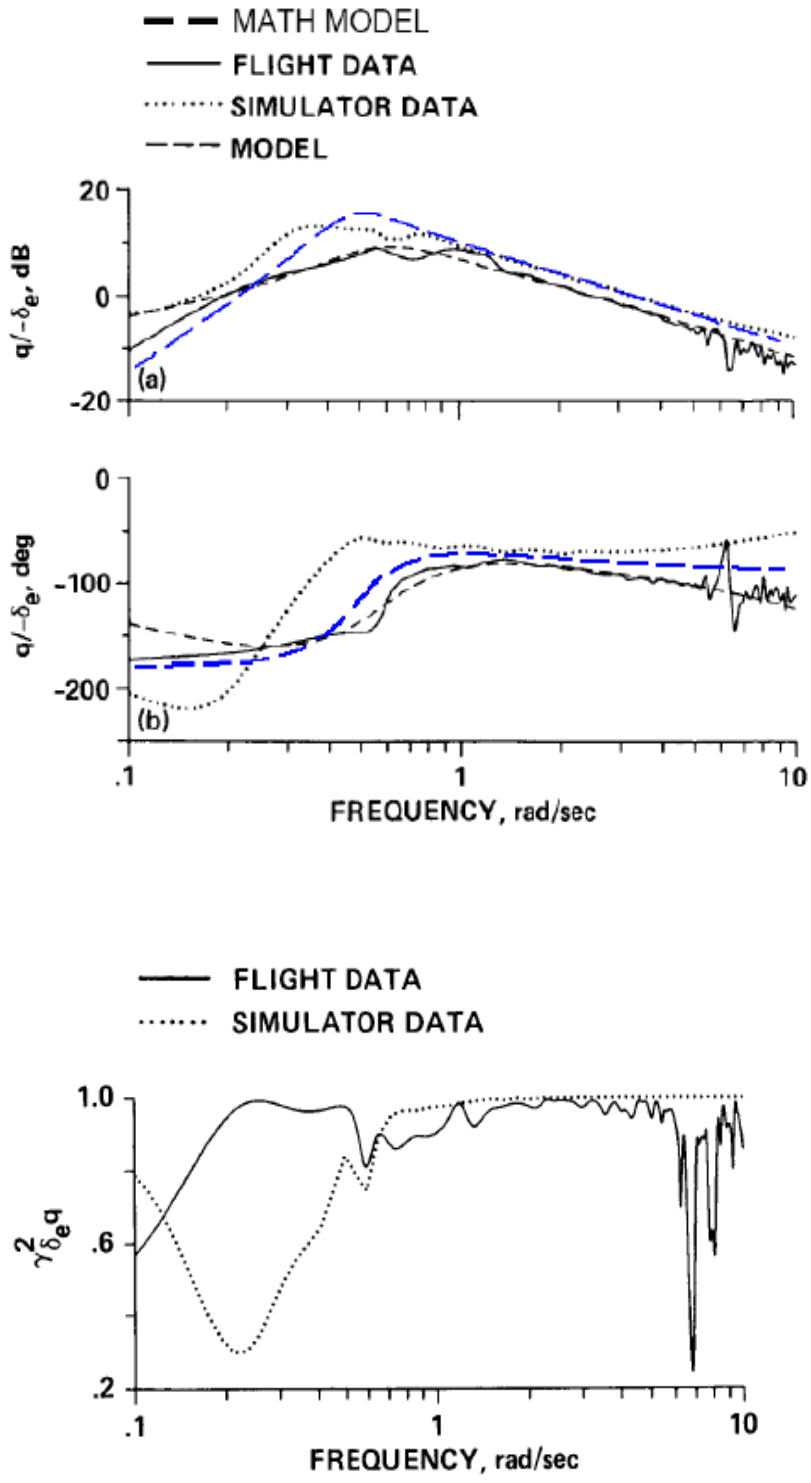

Figure 44: Helicopter Mode Hover q/δ_{elev} Bode Plot and Coherence Function

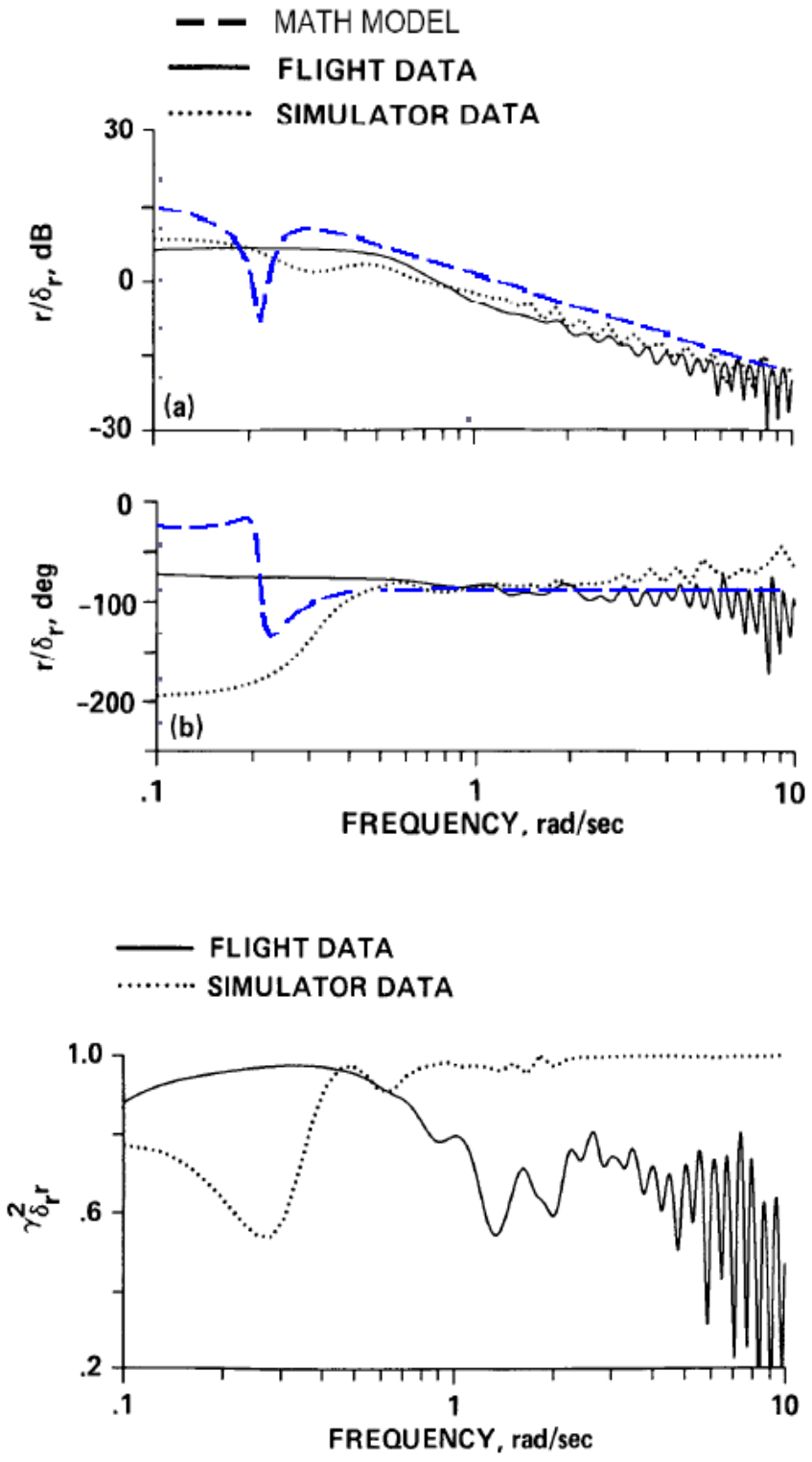

Figure 45: Helicopter Mode Hover r/δ_{rud} Bode Plot and Coherence Function

No flight data was available for the conversion mode conditions; however, Bode plots for one speed at each trim nacelle setting are described below. The mode data from the poles is also included.

The Bode plots for the math model 15º β_M conversion mode, 40 kts data is presented in Figures 46 – 48. Figure 46 is the q/δ_{elev} Bode plot. The large peak in the gain plot that is associated with the large phase increase occurs as the phugoid frequency and indicates that the phugoid is unstable. The minor inflection associated with the 45º phase crossing in the phase roll off from 0º to –90º is at the longitudinal short period frequency.
For the p/δ_{ail} plot in Figure 47, the first peak in the gain plot that is associated with the start of the phase roll off occurs at the lateral-directional oscillatory mode frequency. For the frequencies greater than 0.6 rad/sec, the gain has the characteristic 20 dB/decade roll off. The short period is located at the point where the phase offset is –45º on the phase decay from 0º to –90º.

Figure 48 is the r/δ_{rud} Bode plot. The peak in the gain plot occurs at the Dutch roll frequency and a phase offset of –45º. The short period mode appears to occur at the frequency where the phase offset reaches –90º.

Math Model 15º β_M Conversion Mode Longitudinal Roots (40 kts):

Eigenvalue	Damping	Frequency (rad/sec)
–0.6785 + 0.7835i	0.655	1.04
–0.6785 – 0.7835i	0.655	1.04
0.0022 + 0.2961i	–0.00754	0.296
0.0022 – 0.2961i	–0.00754	0.296

Math Model 15º β_M Conversion Mode Lateral Roots (40 kts):

Eigenvalue	Damping	Frequency (rad/sec)
0	–1.00	0
–1.5413	1.00	1.54
0.0683	–1.00	0.0683
–0.1215 + 0.5312i	0.223	0.545
–0.1215 – 0.5312i	0.223	0.545

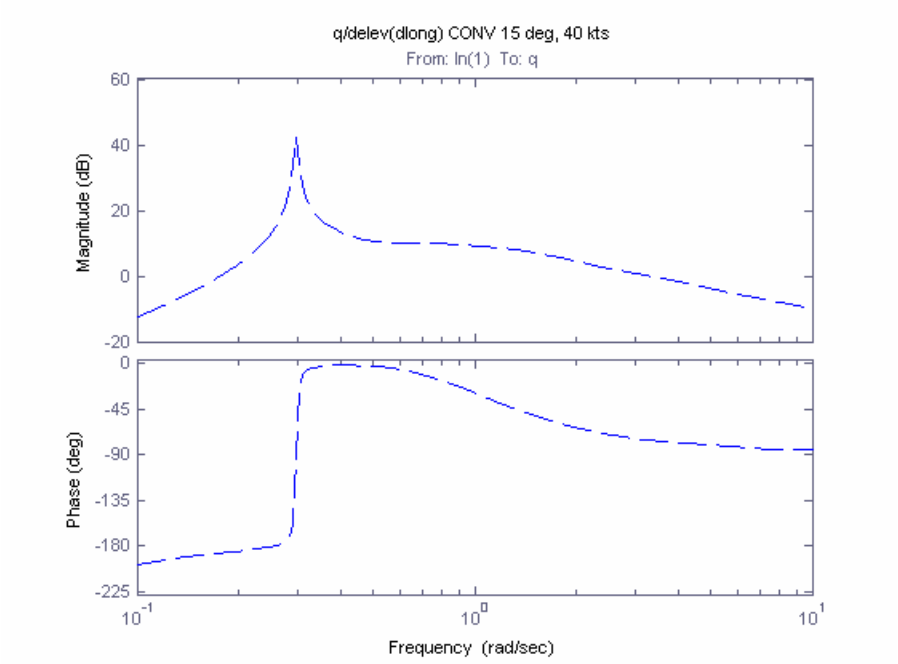

Figure 46: 15º β_M Conversion Mode, 40kts q/δ_{elev} Bode Plot

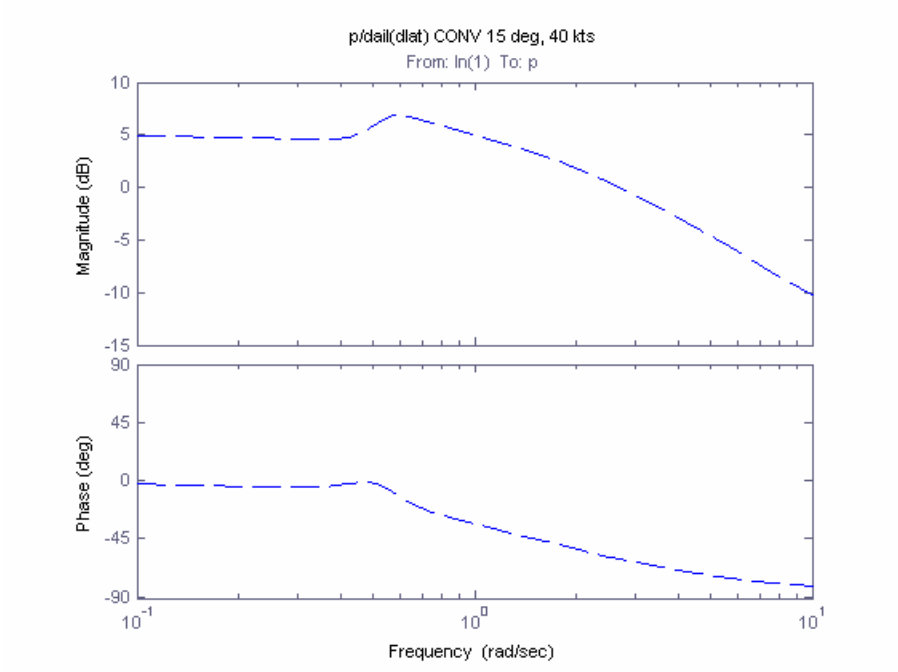

Figure 47: 15º β_M Conversion Mode, 40kts p/δ_{ail} Bode Plot

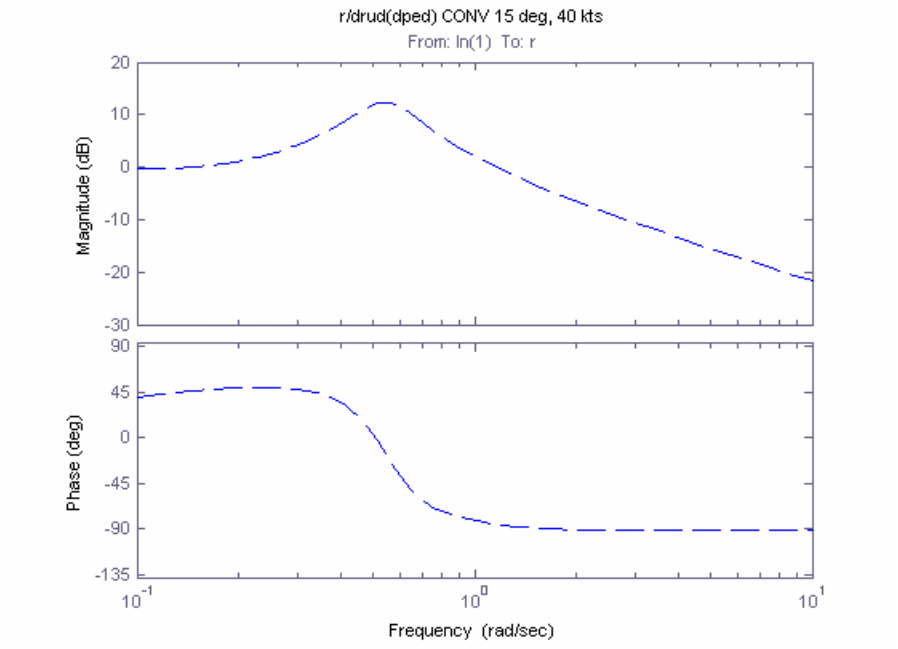

Figure 48: 15º β_M Conversion Mode, 40kts r/δ_{rud} Bode Plot

The Bode plots for the math model 30º β_M conversion mode, 80 kts data is presented in Figures 49 – 51. Figure 49 is the q/δ_{elev} Bode plot. The large peak in the gain plot at the lower frequency is associated with the phugoid mode. The phase offset associated with this mode is 45º. The second peak at the higher frequency is associated with the short period mode. The phase at this frequency is –45º phase crossing in the phase roll off from 0º to –90º. The phase plot also shows that both longitudinal modes are stable.

For the p/δ_{ail} plot in Figure 50, the peak in the gain plot that is associated with the increase in the phase roll off occurs at the lateral-directional oscillatory mode frequency. For the frequencies greater than approximately 2 rad/sec, the gain has the characteristic 20 dB/decade roll off. The short period is located at the point where the phase offset is –45º.

Figure 51 is the r/δ_{rud} Bode plot. The peak in the gain plot occurs at the Dutch roll frequency and a phase offset of –45º. The change in the phase plot shows that the Dutch roll mode is stable. The short period mode appears to occur at the frequency where the phase offset reaches –90º. Due to the shape of the low frequency area of the gain plot, there appears to be an additional mode that is below the pilot frequency range. This can be seen in the pole listing and is the long period mode that has a frequency of 0.0023 rad/sec.

Math Model 30º β_M Conversion Mode Longitudinal Roots (80 kts):

Eigenvalue	Damping	Frequency (rad/sec)
–0.950 + 1.7003i	0.488	1.95
–0.950 – 1.7003i	0.488	1.95
–0.0341 + 0.2002i	0.168	0.203
–0.0341 – 0.2002i	0.168	0.203

Math Model 30º β_M Conversion Mode Lateral Roots (80 kts):

Eigenvalue	Damping	Frequency (rad/sec)
0	–1.00	0
–1.8298	1.00	1.83
–0.1878 + 1.0443	0.177	1.06
–0.1878 – 1.0443	0.177	1.06
–0.0023	1.00	0.0023

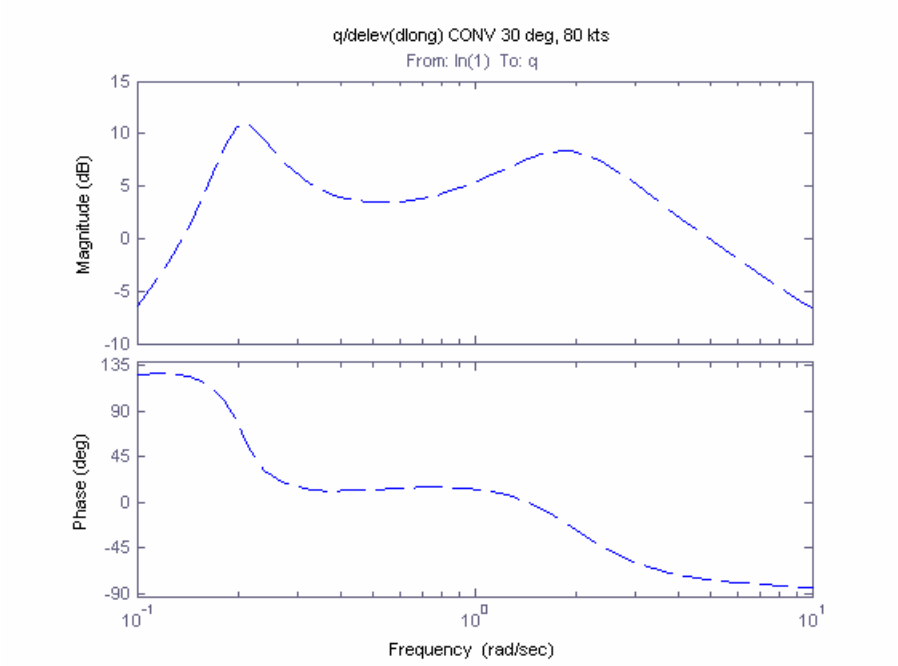

Figure 49: 30º β_M Conversion Mode, 80kts q/δ_{elev} Bode Plot

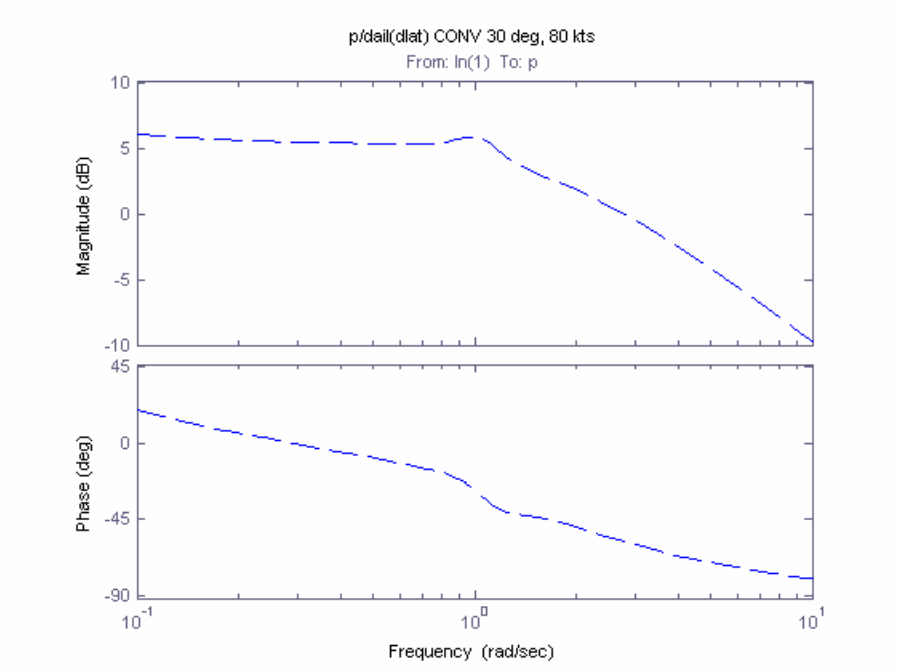

Figure 50: 30º β_M Conversion Mode, 80kts p/δ_{ail} Bode Plot

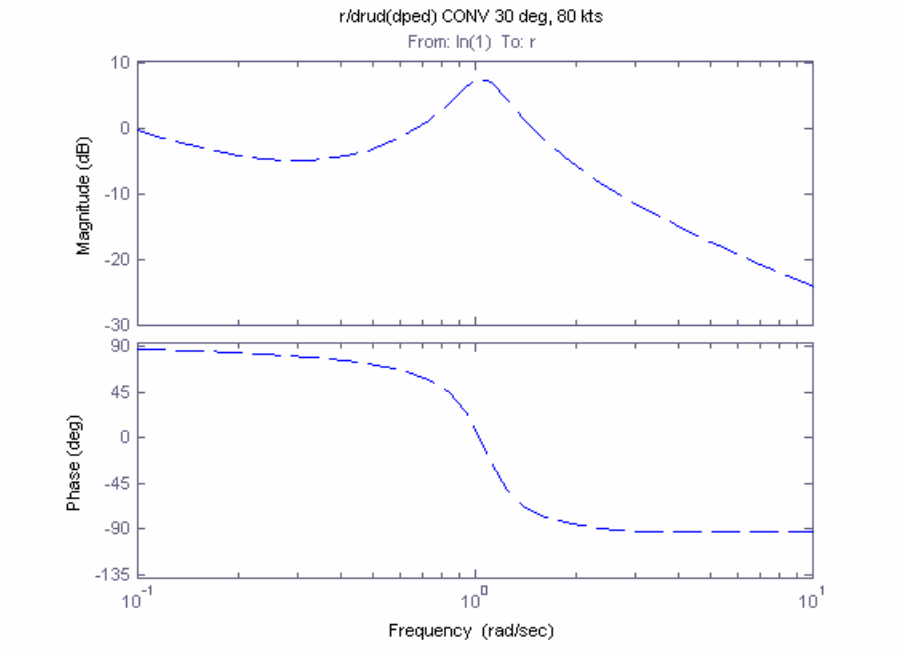

Figure 51: 30º β_M Conversion Mode, 80kts r/δ_{rud} Bode Plot

The Bode plots for the math model 60º β_M conversion mode, 100 kts data is presented in Figures 52 – 54. Figure 52 is the q/δ_{elev} Bode plot. The low frequency peak in the gain plot is associated with the phugoid mode. The phase offset associated with this mode is 45º. The second peak at the higher frequency is associated with the short period mode. The phase at this frequency is –45º phase crossing in the phase roll off from 0º to –90º. The phase plot also shows that both longitudinal modes are stable and oscillatory.

For the p/δ_{ail} plot in Figure 53, the peak in the gain plot that is associated with the increase in the phase roll off occurs at the lateral-directional oscillatory mode frequency. For the frequencies greater than approximately 1.5 rad/sec, the gain has the characteristic 20 dB/decade roll off. The short period is located at the point where the gain plot has a minor slope change and the phase offset slope also momentarily changes (approximately 1.5 rad/sec).

Figure 54 is the r/δ_{rud} Bode plot. The peak in the gain plot occurs between 1–2 rad/sec where both the Dutch roll mode and the short period mode reside. The change in phase associated with these modes is a phase roll off that asymptotically approaches –90º. The phase offset associated with the short period mode appears to be –45º. The change in the phase plot shows that the Dutch roll mode is stable. Due to the shape of the low frequency area of the gain plot, there appears to be an additional mode that is below the pilot frequency range. This can be seen in the pole listing and is the long period mode that has a frequency of 0.0618 rad/sec.

Math Model 60º β_M Conversion Mode Longitudinal Roots (100 kts):

Eigenvalue	Damping	Frequency (rad/sec)
–1.1004 + 2.1786i	0.451	2.44
–1.1004 – 2.1786i	0.451	2.44
–0.1079 + 0.2224i	0.437	0.247
–0.1079 – 0.2224i	0.437	0.247

Math Model 60º β_M Conversion Mode Lateral Roots (100 kts):

Eigenvalue	Damping	Frequency (rad/sec)
0	–1.00	0
–1.4851	1.00	1.49
–0.3702 + 1.1854i	0.298	1.24
–0.3702 – 1.1854i	0.298	1.24
–0.0618	1.00	0.0618

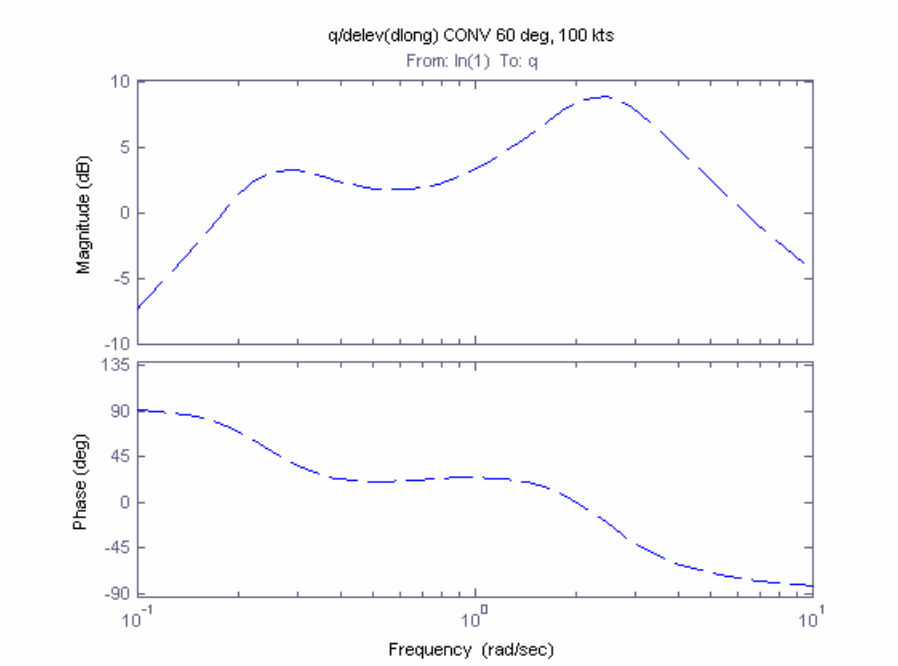

Figure 52: 60º β_M Conversion Mode, 100kts q/δ_{elev} Bode Plot

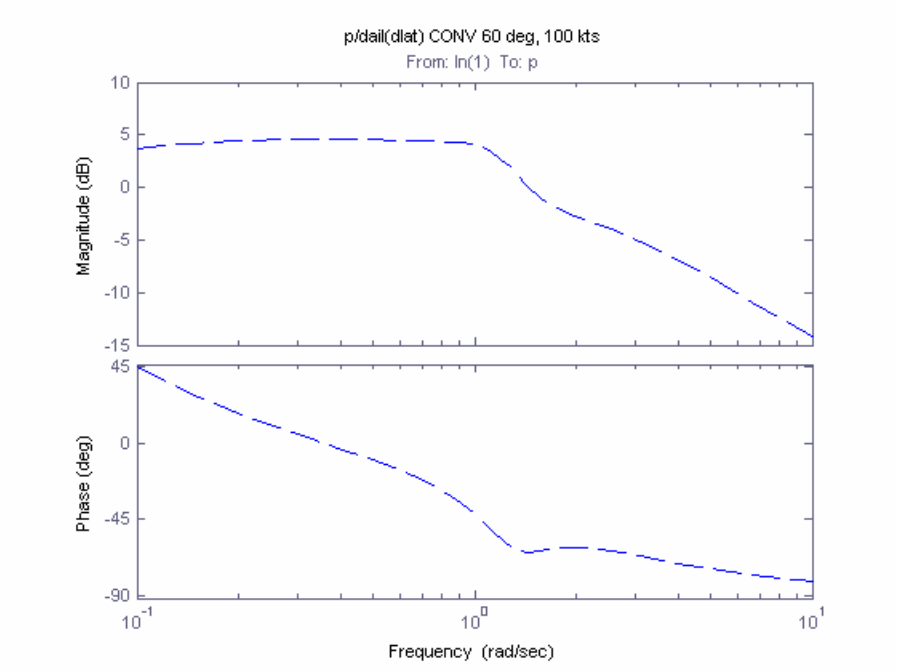

Figure 53: 60º β_M Conversion Mode, 100kts p/δ_{ail} Bode Plot

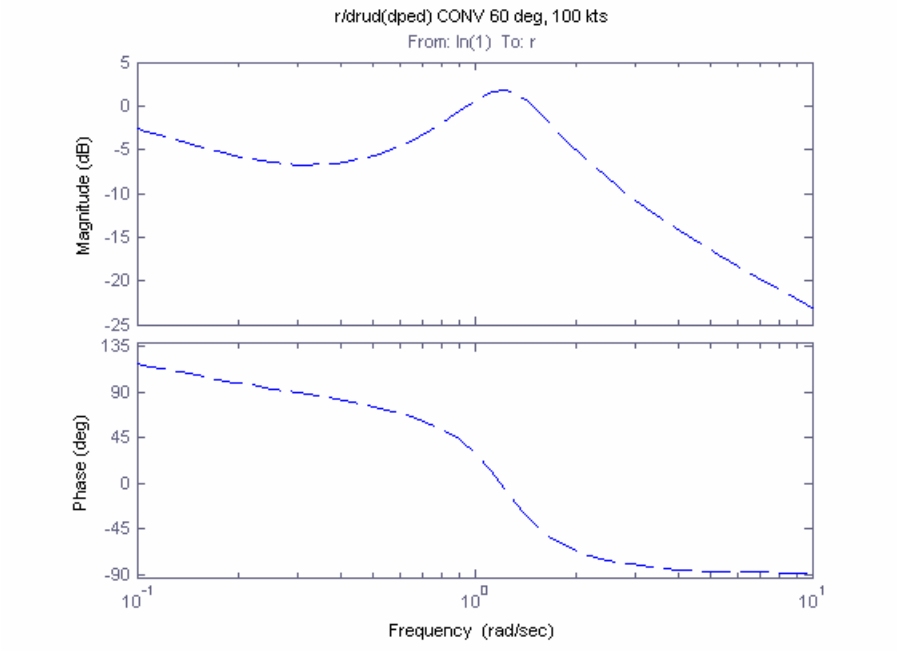

Figure 54: 60º β_M Conversion Mode, 100kts r/δ_{rud} Bode Plot

3.4 Specification Compliance

Using the above helicopter mode data, an attempt was made to determine the bandwidth and phase delay of the system in order to then apply the ADS-33 short term response criteria (Reference 27). Bode diagrams of $\delta\theta/\delta_{long}$ and $\delta\varphi/\delta_{lat}$ are shown in Figures 55 and 56. From these plots, it can be seen that both responses are unstable in helicopter mode. In order to accurately apply the ADS-33 criteria, a feed back loop or control system would need to be used in order to first make the system stable.

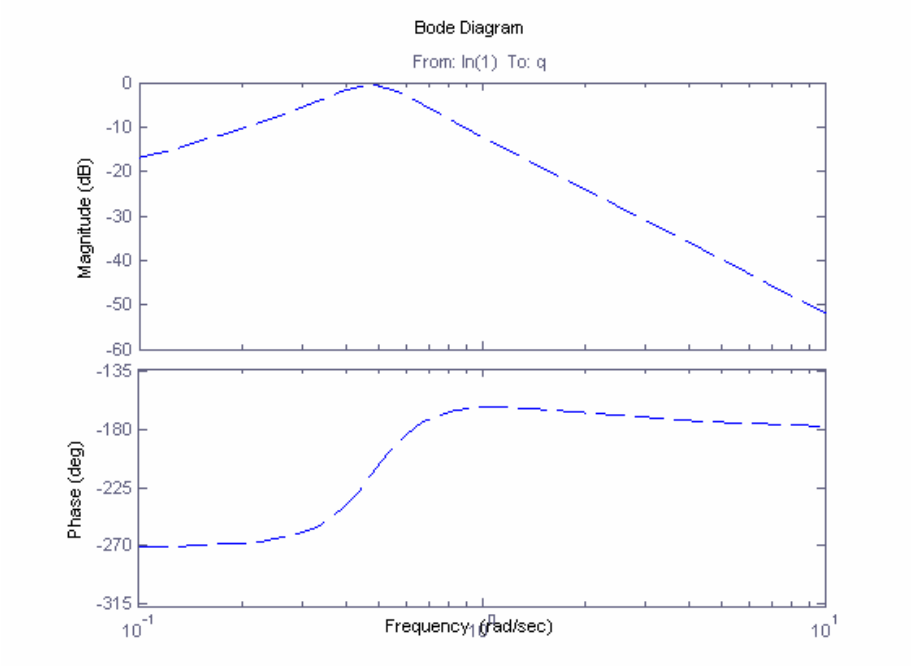

Figure 55: Helicopter Mode Hover $\delta\theta/\delta_{long}$ Bode Plot

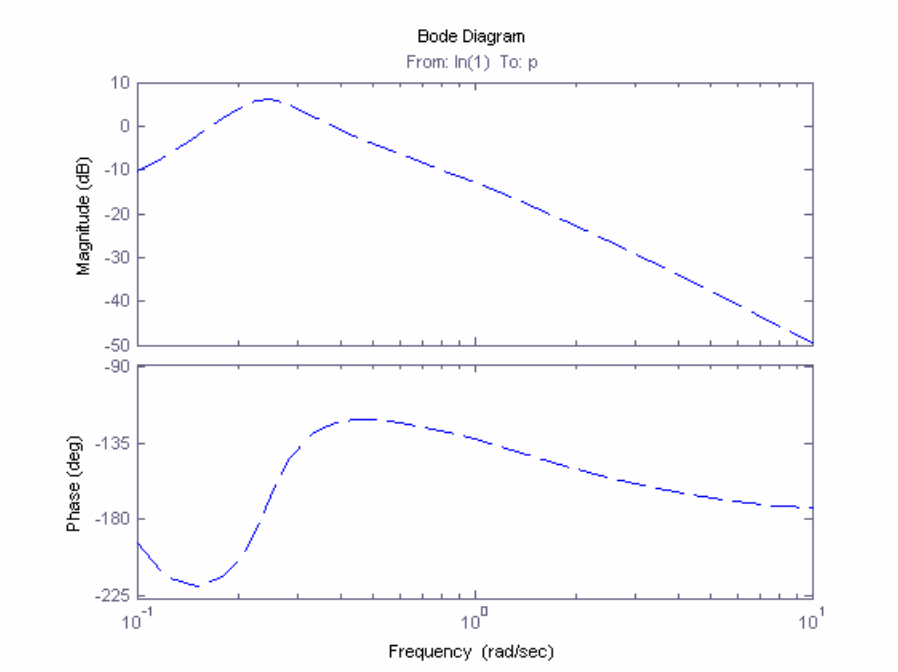

Figure 56: Helicopter Mode Hover $\delta\varphi/\delta_{lat}$ Bode Plot

In lieu of the ADS-33 bandwidth and phase delay criteria, the math model response was instead compared to ADS-33 mid-term response to control input criteria which set limits on the hover and low speed pitch and roll oscillatory mode pole locations. These criteria are shown in Figure 55 with the hover pole data also plotted. The open face symbols are math model data while the filled symbols are flight test data. Pitch oscillations are labeled by the ovals, roll oscillation data are the rectangles. As can be seen from Figure 57, the flight data for a SCAS OFF XV-15 is solid Level 3 in both pitch and roll, while the math model is predicting the aircraft is borderline Level 2/3 for pitch and Level 1/2 for roll. One item of note is that a frequency sweep was used to obtain the flight pole locations rather than a pulse. The criteria really only applies at all frequencies below the bandwidth frequency that was to have been obtained from the bandwidth/phase delay

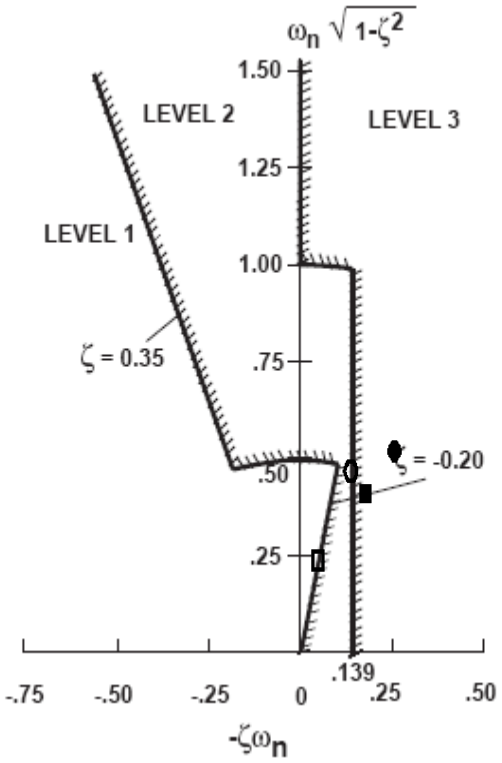

Figure 57: ADS-33 Limits on Pitch and Roll Oscillations for Hover

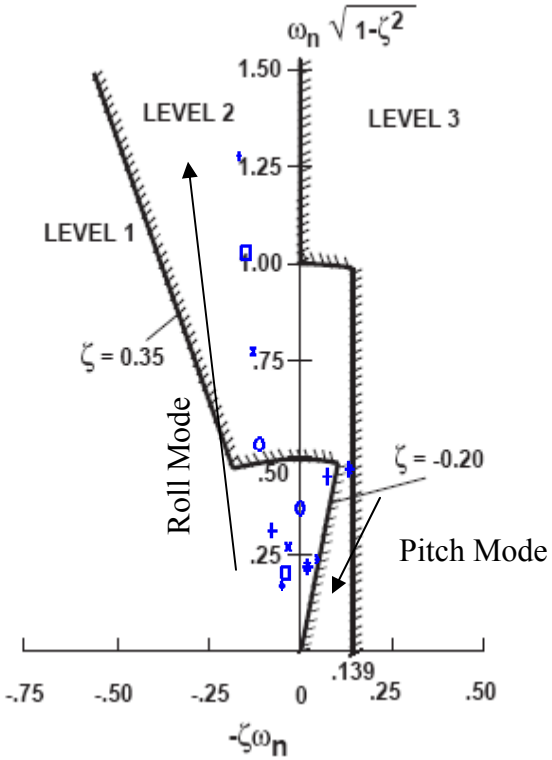

Figure 58: ADS-33 Limits on Pitch and Roll Oscillations for Low Speed Flight

short term response. Care must be taken in drawing conclusions from the data in that it is hard to extract data from a frequency sweep at those frequencies.

Figure 58 shows how the math model poles move with respect to the ADS-33 criteria as airspeed increases. The roll mode which started at Level 1/2 in a hover move into the Level 1 region as airspeed increases and then become Level 2 for larger speeds. The pitch mode, which started at the Level 2/3 boundary moves towards the Level 1 region as airspeed increases. For both Figures 57 and 58, the Level 1, 2, and 3 boundaries are shown for fully attended operations. For divided attention operations, the Level 1 boundary is defined by the extension of the $\zeta = .35$ line to the origin.

Figure 59 shows the math model data developed using the small perturbation technique against the ADS-33 criteria for lateral-directional oscillatory requirements following a yaw control doublet. The math model lateral-directional oscillation characteristics are Level 3.

Airplane mode flying qualities are governed by MIL-F-8785C (Reference 28). An attempt was made to apply the previous analyses to the specification to determine what level of handling qualities the XV-15 has in airplane mode, SCAS OFF. For the purposes of this analysis, the XV-15 was determined to be a Class II aircraft (medium weight, low-to-medium maneuverability airplane). Based on the data gathered previously, the XV-15 is a Level 1 aircraft based on the tests outline in Table 4. A true assessment would

require a much more rigorous set data and test specifically designed to extract the required information.

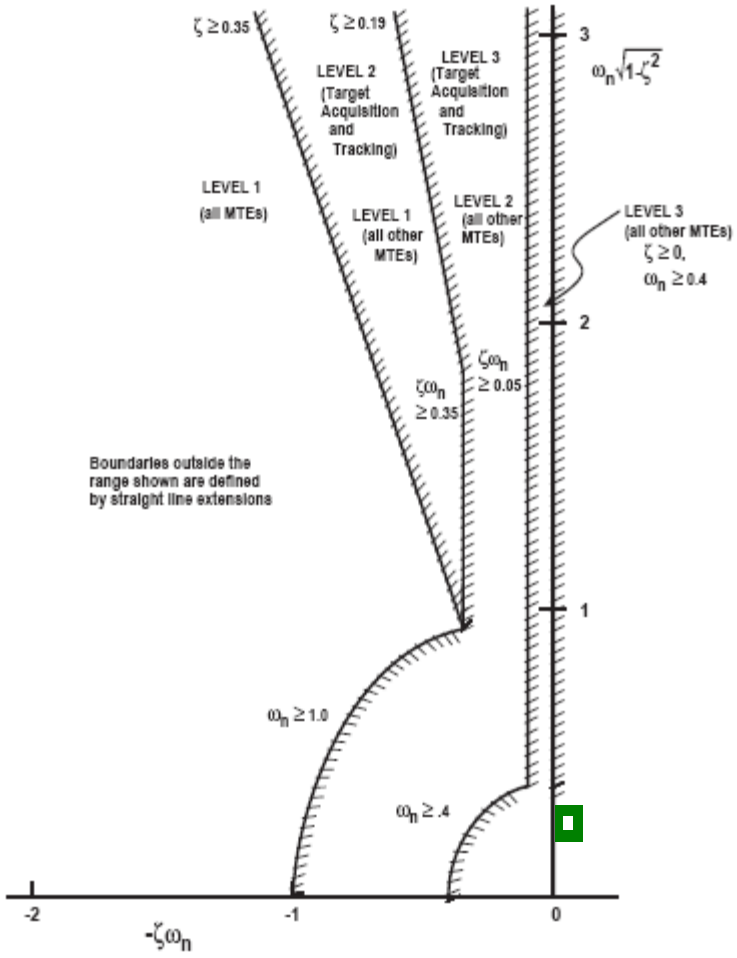

Figure 59: ADS-33 Lateral-Directional Oscillatory Requirements

Table 4: MIL-F-8785C Specification Assessment

Paragraph	Title	Flying Qualities Level (Flight, Math Model)	Rationale
3.2.1.2	Phugoid stability	Level 1	$\zeta > 0.04$
3.2.2.1.2	Short Period Damping	Level 1	$0.35 < \zeta < 1.3$
3.3.1.1	Lateral-Directional oscillations (Dutch roll)	Level 1	$\zeta > 0.19$ $\zeta\,\omega_n > 0.35$ $\omega_n > 0.4$

4. Conclusions

While tiltrotors have been in existence for many years, there exists little publicly released documentation on simple modeling of tiltrotor aircraft and handling qualities analysis using these models. Most of the research and published work related to tiltrotors stems from issues or problems encountered during aircraft development. The documentation that is available depicts extremely complex modes where the basic equations of motion are lost in the complexity of the system.

This thesis includes the development of the equations of motion for tiltrotor aircraft covering airplane mode, helicopter mode, and conversion mode flight. Subsequent analysis addresses the stability and control aspects of the XV-15 tiltrotor aircraft from the perspective of a trim and time history solution. A linearized state space model was also developed and analyzed using the state space matrices, Bode plots, and an eigenvalue analysis. The results were validated against generic tiltrotor simulation model results and compared to flight test where available.

Based on the previous results, the simple math model discussed in this report can be used to determine the equations of motion for all modes of tiltrotor flight (airplane mode, conversion mode, and helicopter mode). The trim solution reflects the actual aircraft trim solution well, especially with respect to trends. The fidelity of the elevator and longitudinal stick matches can be increased by including the rotor wake interactions on the wing and empennage. The low speed helicopter mode and high nacelle conversion

comparisons would be improved by including the rotor wake download on the wing. Use of an articulated rotor to approximate a gimbaled rotor appears to result in rotor Y-force errors.

For the time history solution, the implementation of the model resulted in time histories that showed the basic aircraft response to pilot control inputs; however, these time histories showed that there is a 'trim' residual pitch rate present in the helicopter trim time history which contaminates the helicopter mode results. Once the 'trim' pitch residual was removed, the math model appears to approximate flight fairly adequately. However, the removing some of the assumptions would greatly increase the utility of the model.

The linearized state space model that was developed and analyzed using the state space matrices, Bode plots, and an eigenvalue analysis was compared to the generic tiltrotor simulation model results and to flight test where available. The previously discussed math model limitations also manifested themselves in the linear analysis.

From the analysis of the state space matrices, the math model shows some sign issues with some of the non-primary derivatives. The main derivatives appeared to be approximated fairly well. From the pole analysis, the characteristic of the pole distribution between the math model, GTRS, and flight are similar.

The Bode analysis of the angular rates due to control inputs showed that the math model depicts the aircraft fairly well with respect to the gain (magnitude) and phase of the aircraft rate due to the control input. The differences in the pole locations were also depicted in the Bode plots. Overall, the comparison was favorable. Conversion mode Bode plots were also included.

The previously discussed results were compared to ADS-33 for helicopter mode and MIL-F-8785C for the airplane mode results to gain an understanding of how a SCAS OFF XV-15 compared to the specification flying qualities levels. For helicopter mode, the aircraft was Level 2 or Level 3 for roll and pitch response. As airspeed increased, the aircraft became more stable and moved into the Level 1 and Level 2 regimes. For the airplane specification criteria the aircraft is Level 1 SCAS OFF. Additional criteria and tests would need to be performed to characterize the entire XV-15 for specification compliance.

This project resulted in a fairly good basic tiltrotor model and was able to show some inherent tiltrotor characteristics. While the model works well for trims, further model refinements are needed to better correlate with flight test data and increase the fidelity of the dynamics extraction.

In addition, in order to make a true assessment of how well a simple model can approximate a tiltrotor, conversion mode flight data is required for comparison.

5. Future Work

While the model presented here is a good basic tiltrotor model, removing some of the assumptions will result in a higher fidelity model which will more accurately depict the tiltrotor characteristics. Removing some of the assumptions, however, will increase the model complexity and at some point the model will no longer be 'simple' in design. In addition, locating further flight data for comparison, especially in the conversion mode flight regime would greatly improve the validity of the comparisons.

Following is a list of suggested initial modifications to increase the model fidelity and model capability. Incorporation of the following set of improvements will increase model fidelity while retaining the 'simple' model approximation:

1. Include more refined downwash effects on the vertical tail and horizontal tail due to the wing wake. Include the rotor wake influences. This change will result in better correlation in the 20–50 kt range where there is wake impingement on the tail. The small angle assumption for angle of attack at the horizontal tail and the linear lift curve slope assumption for the horizontal tail are also negated.
2. Change blade twist to more accurately represent the blade shape. A better approximation would be a dual linear approximation or another higher order model, not the single linear approximation used for this analysis.
3. Include wing download model. Work regarding modeling of these effects can be found in Reference 29.
4. Incorporate dynamic inflow rather than assuming uniform inflow.

5. Remove the small angle approximation assumption for β and α. For heart of the envelope calculations, the small angle approximation is adequate, however, increased fidelity can be found by covering non-linear factors like stall and dynamics due to angular rates at the surfaces.
6. Use the quadratic lift coefficient method for determining angle of attack and sideslip rather than the currently used trigonometric functions. Rearward and sideward flight currently not modeled. The trigonometric functions for angle of attack and sideslip cause singularities in the model. The quadratic lift coefficient method can be used to mitigate this. "For this technique, forces for lifting surfaces are computed using quadratic coefficients multiplied by the squares of the velocity components so that negative velocities cannot cause singularities. No explicit computation of angle of attack or sideslip is needed..." (Reference 18)

The following improvements are more complex and start to violate the 'simple' model assumption:

1. Include nacelles as a separate configuration item. This will more provide more accurate aircraft forces and moments.
2. Include proprotor-fuselage interference. This change removes the assumption that the dynamic pressure at the fuselage is the same as the free-stream dynamic pressure. This change will also fix the fuselage download discrepancy that currently exists (especially in the hover and low speed helicopter mode cases and the higher nacelle angle conversion mode cases).
3. Include drag due to elevator deflection.

4. Include forward wing sweep.
5. Include drag due to aileron deflections.
6. Include proprotor on proprotor interference on the rotor calculations. (This is a more complex modification.)
7. Add pressure altitude dependencies in order to trim the aircraft at different altitudes and understand the altitude effects due to density.
8. Include δ_3 and β_p in rotor modeling.
9. Include ground effects.
10. Incorporate higher order flapping and lead-lag blade motions.
11. Implement a rotor governor and SCAS

Appendices

Appendix A: XV-15 Basic Aircraft Parameters

(All data extracted from Reference 7 unless otherwise noted)

Rotor				
Parameter Description	**Symbol**	**Value**	**Units**	**Model Variable name**
Radius	R	12.5	ft	R
Rotor Speed [VTOL, CONV]	Ω	589	RPM	Omega
Rotor Speed [APLN]	Ω	517	RPM	Omega
Chord	c	14	in	c
Number of blades	N_b	3	--	Nb
Twist	θ_{tw}	–41	deg	theta_tw
Twist at Hub	θ_{tw0}	40	deg	thetatw0
Hinge offset	e	0		e
Blade flapping Inertia	I_b	102.5	slug ft^2	Ib
Mast height	R_H	4.67	ft	RH
Nacelle pivot point fuselage station	x_h	25	ft	(in R_{Ni})
Nacelle pivot point height above waterline	z_h	8.3	ft	(in R_{Nk})
Buttline Nacelle pivot point position	y_h	16.1	ft	(in R_{Nj})
Rate of nacelle movement	$\dot{\beta}_M$	0	deg/s	INdot
Blade pre-cone angle	β_p	0**	deg	betaP
Flapping spring constant	K_β	225	ft-lb/deg	Kbeta

**Actual value of blade pre-cone angle for the XV-15 is 2.5 deg.

Fuselage				
Parameter Description	**Symbol**	**Value**	**Units**	**Model Variable name**
Flat plate drag	f	1.6	ft^2	f
Lift curve slope	a_{fuse}	0.286	/rad	a_fuse
Zero lift angle of attack	$\alpha_{0L,fuse}$	–8.0	deg	alpha_zeroLfuse
Zero AOA Moment coefficient	$C_{M0,f}$	–0.070	ft-lb	CM_of
Moment coefficient vs. AOA	$C_{M\alpha,f}$	1.145	/rad	CM_alphaF
Center of pressure height above waterline	z_f	7	ft	z_f
Center of pressure fuselage station	x_f	293	in	x_f
Buttline center of pressure position	y_f	0	ft	y_f

Wing				
Parameter Description	**Symbol**	**Value**	**Units**	**Model Variable name**
Wing area	A_{wing}	181	ft^2	A_wing
Span	b_{wing}	32.2	ft	b_w
Aspect ratio	AR	5.7	--	AR_wing
Center of pressure height above waterline	z_{wing}	8	ft	z_w
Center of pressure buttline position	y_{wing}	0	ft	y_w
Center of pressure fuselage station	x_{wing}	24.3	ft	x_w
Incidence angle	i_{wing}	0	deg	i_wing
Lift curve slope	a_{wing}	5.31	/rad	a_w
Zero-lift angle of attack	α_{0L}	–4.02	deg	alpha_zeroL
Change in C_L with flap deflection	$\delta C_{L.\delta flap}/\delta_{flap}$	0.34	/rad	dCL_flap_dflap
Profile drag coefficient	C_{d0}	0.017	--	CDO_wing
Wing chord	c_{wing}	5.25	ft	c_wing
Moment coefficient at zero lift	$CM_{0L,w}$	–0.02	--	CM_ow
Drag due to flap deflection	$\delta C_{D,\delta flap}/\delta_{flap}$	.30367	rad	dCDflap_dflap
Wing efficiency factor	E	0.9	--	OEF_wing
Sweep at quarter chord	$\lambda_{c/4}$	–6.5	deg	sweepc4
Taper ratio	λ	1	--	Taperratio_wing
Moment coefficient vs. angle of attack	$C_{M,\alpha,w}$	0	deg	CM_alpha_w

Vertical Tail				
Parameter Description	**Symbol**	**Value**	**Units**	**Model Variable name**
Area	A_{VT}	25.25	ft^2	A_VT
Span	b_{VT}	7.7	ft	b_VT
Aspect Ratio	AR_{VT}	2.33	--	AR_VT
Lift curve slope	a_{VT}	3.06	/rad	a_VT
Oswald's efficiency factor	e	1	--	OEF_VT
Profile drag coefficient	C_{d0}	0.0071	--	CD0_VT
Height above waterline	z_{VT}	9.6	ft	z_VT
fuselage station	x_{VT}	47.5	ft	x_VT
position right of buttline	y_{VT}	6.4	ft	y_VT
zero lift angle of attack	$\alpha_{0L,VT}$	0	rad	alpha_zeroL_VT
Change in lift coefficient due to rudder deflection	$\delta C_{L,VT}/\delta_{rud}$	1.15	/rad	dCL_rud_drud

Horizontal Tail				
Parameter Description	**Symbol**	**Value**	**Units**	**Model Variable name**
Area	A_{HT}	50.25	ft^2	A_HT
Span	b_{HT}	12.83	ft	b_HT
Chord	c_{HT}	3.916	ft	c_HT
Aspect Ratio	AR_{HT}	3.27	--	AR_HT
Incidence angle	i_{HT}	0	deg	i_HT
Lift curve slope	a_{HT}	4.03	/rad	a_HT
Zero lift angle of attack	$\alpha_{0L,HT}$	0	deg	alpha_zeroL_HT
Change in lift of the horizontal tail with elevator deflection	$\delta C_{L,H}/\delta_{elev}$	2.29	/rad	dCL_H_delev
Profile drag coefficient	C_{d0}	0.0088	--	CD0_HT
Moment at zero lift angle of attack	$M_{0,\,HT}$	0	ft-lb	M_zeroHT
Horizontal tail efficiency factor	e	0.8	--	OEF_HT
Fuselage station	x_{HT}	46.7	ft	x_HT
Position right of buttline	y_{HT}	0	ft	y_HT
Position above waterline	z_{HT}	8.6	ft	z_HT

Aircraft Input Parameters				
Parameter Description	**Symbol**	**Value**	**Units**	**Model Variable name**
Mast angle	β_M	--	deg	IN
Gross Weight	GW	--	lbs	GW
Velocity	V	--	kts	V
Longitudinal CG, helicopter referenced	CG	--	ft	x_cg
Lateral CG, helicopter referenced	LCG	--	ft	y_cg
Waterline CG, helicopter referenced	WCG	--	ft	z_cg
Turn rate	$\dot{\psi}$	--	rad/s	psidot
Flight Path Angle	γ	--	rad	Gamma
Aircraft Mass	m_{ac}	eqn	slug	m_ac
pressure at altitude	ρ	eqn	slug/ ft^3	rho
flap deflection angle	δ_{flap}	--	deg	dflap

Constants				
Parameter Description	**Symbol**	**Value**	**Units**	**Model Variable name**
Helicopter mode Roll Moment of Inertia	I_{xx0}	52795	slug ft^2	Ixx0
Helicopter mode Pitch Moment of Inertia	I_{yy0}	21360	slug ft^2	Iyy0
Helicopter mode Yaw Moment of Inertia	I_{zz0}	66335	slug ft^2	Izz0
Helicopter mode Product of Inertia	I_{xz0}	1234	slug ft^2	Ixz0
Roll Inertia Coefficient	$KI1$	20.5	slug ft^2/deg	KI1
Pitch Inertia Coefficient	$KI2$	11.24	slug ft^2/deg	KI2
Yaw Inertia Coefficient	$KI3$	9.26	slug ft^2/deg	KI3
Product of Inertia Coefficient	$KI4$	1.76	slug ft^2/deg	KI4
qstar	$\overset{*}{q}$	0	deg/rad	qstar
pstar	$\overset{*}{p}$	0	deg/rad	pstar
rstar	$\overset{*}{r}$	0	deg/rad	rstar
Gravitational acceleration	g	32.2	ft/s^2	g
Sea level density	ρ_{SL}	0.00238	slug/ ft^3	Rho
Longitudinal stick to elevator gearing ratio	$\delta_{elev}/\delta_{long}$	4.17	°/in	--
Lateral stick to aileron gearing ratio	$\delta_{ail}/\delta_{lat}$	3.93	°/in	--
Pedal to rudder gearing ratio	$\delta_{rud}/\delta_{ped}$	8	°/in	--

Horizontal Tail $C_{L,\alpha,}$

α (deg)	C_L	α (deg)	C_L	α (deg)	C_L	α (deg)	C_L
-180	0	-40	-1.05	8	0.568	50	1.09
-170	0.7	-36	-1.04	12	0.852	60	0.88
-160	0.6	-32	-1.03	12.2	0.8662	70	0.62
-150	0.84	-28	-1.01	13	0.923	80	0.34
-140	0.98	-24	-0.98	15	1	90	0
-130	0.99	-20	-0.93	16	0.98	100	-0.4
-120	0.86	-18.4	-0.92	16.8	0.94	110	-0.66
-110	0.66	-17.5	-0.93	18	0.89	120	-0.86
-100	0.4	-16.8	-0.99	20	0.88	130	-0.99
-90	0	-16	-1.12	24	0.935	140	-0.98
-80	-0.425	-15.6	-1.1	28	1	150	-0.84
-70	-0.72	-14.2	-1.0082	32	1.05	160	-0.6
-60	-0.9	-12.5	-0.8875	36	1.08	170	-0.7
-50	-1.002	-12	-0.852	40	1.1	180	0

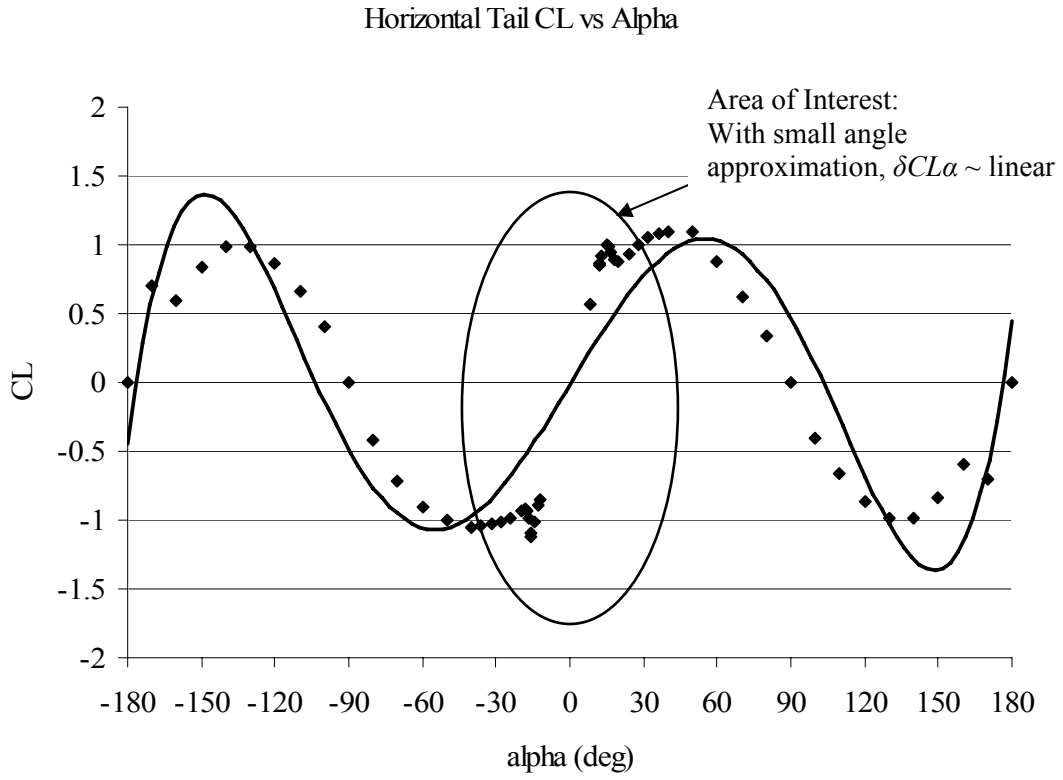

Linear Region of CLalpha,HT

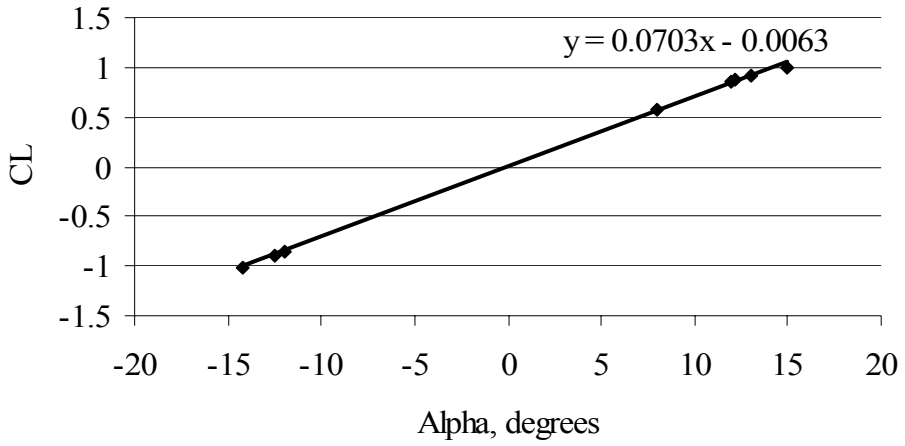

$C_{L,HT}$ = 0.0703 α -.0063 ~ 0. 0.0703 α

$C_{L,\alpha,\,HT}$ = 0.0703 /deg = 4.03 / rad

Horizontal Tail $C_{D,\alpha}$

α (deg)	C_D for Mach=0-0.2	C_D for Mach=0.4	C_D for Mach=0.5	C_D for Mach=0.6
-16	0.115	0.135	ND	ND
-12	0.068	0.068	0.088	ND
-8	0.035	0.035	0.035	0.045
-4	0.015	0.015	0.015	0.015
0	0.00875	0.00875	0.00875	0.00875
4	0.015	0.015	0.015	0.015
8	0.035	0.035	0.045	0.065
12	0.068	0.075	0.105	ND
16	0.115	0.145	ND	ND

ND = not defined

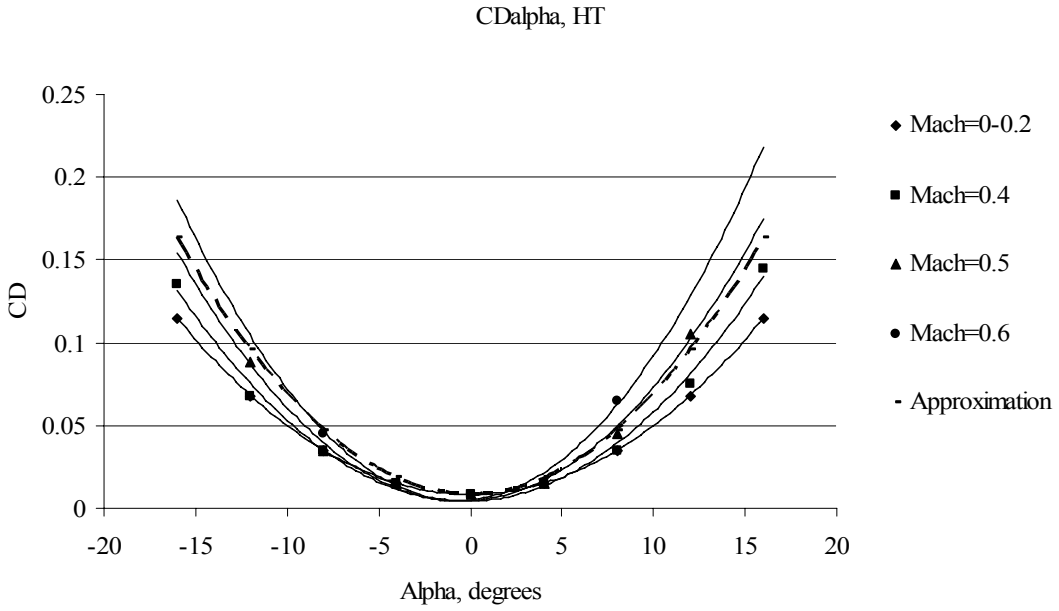

The dashed line in the above graph is the approximation used for $C_{D\alpha,\,HT}$ in the developed math model. The approximation is used so that C_D is no longer a function of Mach number. Values for the variables were found in Reference 9.

The equation of the approximation is:

$$C_{D,HT} = 0.0088 + 1.98\alpha^2$$

$C_{D,HT} = C_{D0,HT} + k_{HT} C_{L,HT}{}^2$ where

$$k_{HT} = \frac{1}{\pi OEF_{HT} AR_{HT}}$$

$$C_{L,HT} = C_{L,\alpha}\alpha$$

Therefore: $C_{D0,HT} = 0.0088$

$\delta C_{L\alpha} / \delta_{elev}$

α (deg)	C_L for δ_{elev}=0º	C_L for δ_{elev} =-10º	C_L for δ_{elev} =-15º	C_L for δ_{elev} =-20º	C_L for δ_{elev} =10º	C_L for δ_{elev} =15º	C_L for δ_{elev} =20º
-14.2	-1.0082	-1.4	-1.55	*	-0.61	-0.4	-0.27
-12.5	-0.8875	-1.31	-1.49	*	-0.48	-0.28	-0.15
-12	-0.852	-1.26025	-1.46438	-1.60318	-0.44375	-0.23963	-0.10082
8	0.568	0.15975	-0.04438	-0.18318	0.97625	1.18	1.31918
12	0.852	0.44375	0.239625	0.10082	1.25	1.42	1.5
12.2	0.8662	0.45795	0.253825	0.11502	1.27	1.43	*
13	0.923	0.51475	0.310625	0.17182	1.3	*	*
15	1	0.65	0.45	0.29	*	*	*

* = not linear

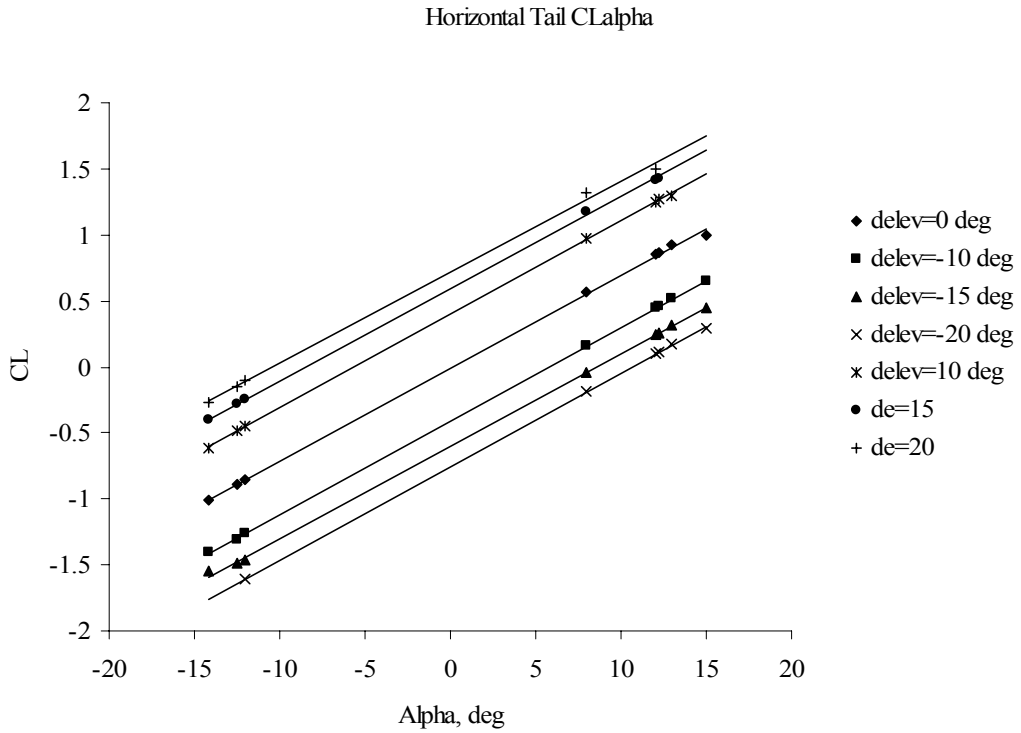

Degrees of elevator deflection	$C_{L\alpha}$	C_L at α =0º (y-intercept)	Change in y-intercept per º δ_{elev}
20	0.0689	0.7172	0.03586
15	0.0697	0.5939	0.03959
10	0.0706	0.4005	0.04005
0	0.0703	-0.0063	--
-10	0.0709	-0.4085	0.04085
-15	0.0699	-0.5996	0.03997
-20	0.0707	-0.7525	0.037625

Average $\delta C_{L,HT}/\delta_{elev}$ = 0.400 / deg
= 2.29 /rad

Vertical Tail $C_{L\alpha}$ and $\delta C_L/\delta_{rud}$

C_L for Mach = 0 to 0.2

α (deg)	δ_{rud}=0º	δ_{rud}=15º	δ_{rud}=20º	δ_{rud}=-15º	δ_{rud}=-20º
-16	-0.86	-0.555	-0.4616	-1.165	-1.2584
-12	-0.635	-0.33	-0.2366	-0.94	-1.0334
-8	-0.425	-0.12	-0.0266	-0.73	-0.8234
8	0.425	0.73	0.8234	0.12	0.0266
12	0.635	0.94	1.0334	0.33	0.2366
16	0.86	1.165	1.2584	0.555	0.4616

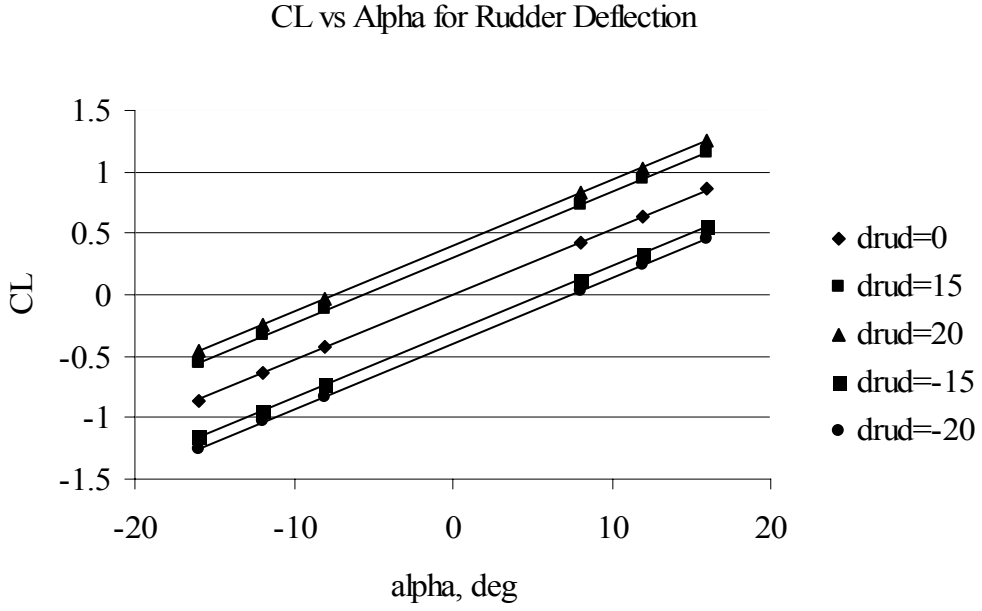

δ_{rud} (deg)	$C_{L\alpha}$ (/deg)	Intercept (C_L for 0º alpha)	dC_L/δ_{rud}
0	0.0534	0	--
15	0.0534	0.305	0.020333
20	0.0534	0.3984	0.01992
-15	0.0534	-0.305	0.020333
-20	0.0534	-0.3984	0.01992

$C_{L\alpha,VT}$ = 0.0534 /deg = 3.06 /radian

Average $\delta C_L/\delta_{rud}$ = 0.020127 /deg = 1.1532 / rad

Wing $C_{L\alpha}$

C_L for Mach 0 to 0.2 with β_M= 90º (APLN)				
α, deg	Flap Deflection, Deg			
	0	20	40	75
-16	-0.95	-0.57	-0.32	-0.048
-12	-0.67	-0.26	0	0.272
-8	-0.33	0.15	0.42	0.69
-4	-0.04	0.56	0.84	1.11
0	0.38	0.92	1.18	1.44
4	0.72	1.28	1.46	1.66
8	1.04	1.54	1.7	1.88
11	1.28	--	--	--
12	1.37	--	--	--

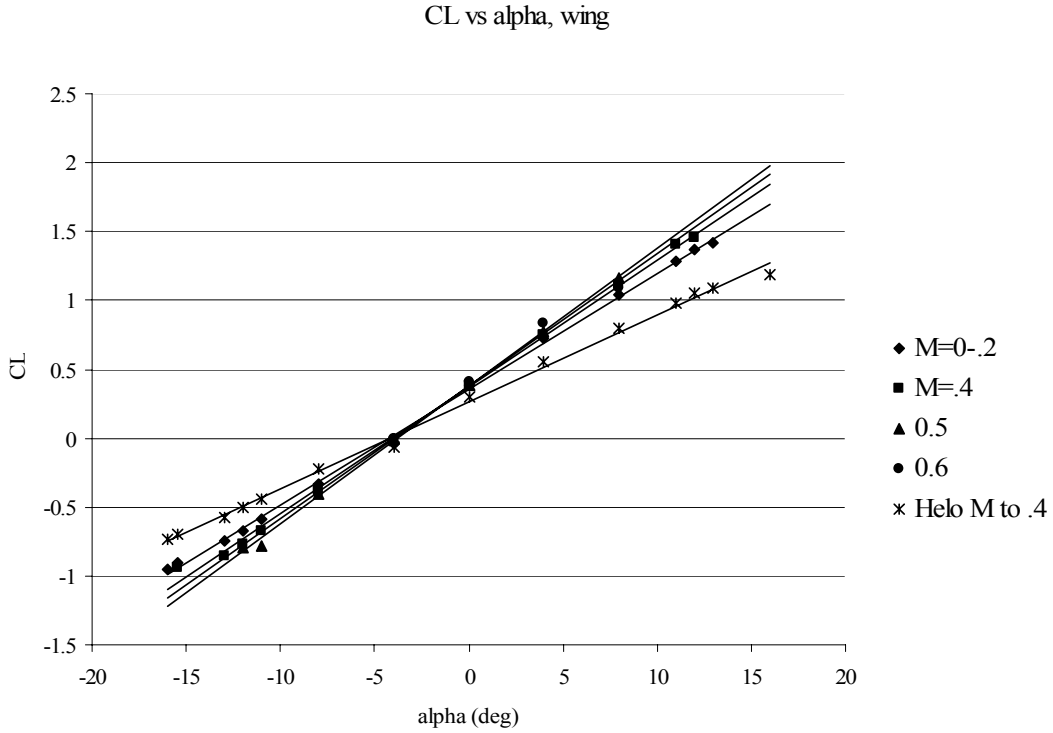

flap deflection (deg)	$C_{L\alpha}$ (slope)	intercept	Alpha for zero C_L (deg)
0/0	0.083	0.3546	-4.27229
0/12.5	0.096	0.382	-3.97917
40/25	0.0998	0.375	-3.75752
75/47	0.0919	0.3734	-4.06311

$C_{L\alpha,wing}$ = 0.0927/deg (average)
= 5.31 /rad

alpha0L = -4.02 deg (average)
= -.070 rad

$C_{D\alpha}$ Wing-Pylon

α, deg	C_D at Mach =0 - 0.2 Flap Deflection, δ_{flap} 0º	20º	40º	75º
-8	--	0.033	0.076	0.282
-4	0.017	0.044	0.106	0.33
0	0.0204	0.072	0.141	0.372
4	0.0418	0.109	0.186	0.424
8	0.072	0.157	0.243	0.492
12	0.118	0.227	0.322	0.58
16	0.171	0.29	0.404	0.667

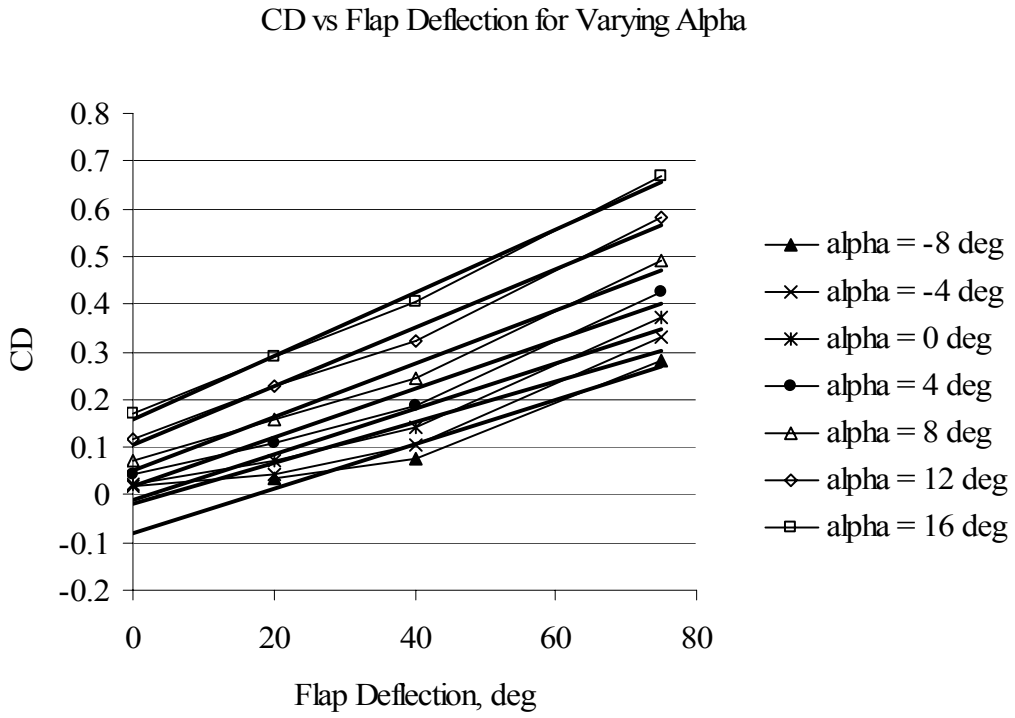

α (deg)	Change in C_D per degree flap deflection (slope)
-8	0.0066
-4	0.0061
0	0.0056
4	0.0051
8	0.0047
12	0.0043
16	0.0047

Change in C_D per degree flap deflection is essentially linear. Therefore:

dC_{Dflap}/δ_{flap} = 0.0053/deg (average)

=0.30367/rad

Fuselage Lift and Drag

α, deg	$Lift_\alpha$, lb
-16	-7.25
-12	-3.63
-8	-0.01
-4	3.61
0	7.23
4	10.85
8	14.47
12	18.09
16	21.71

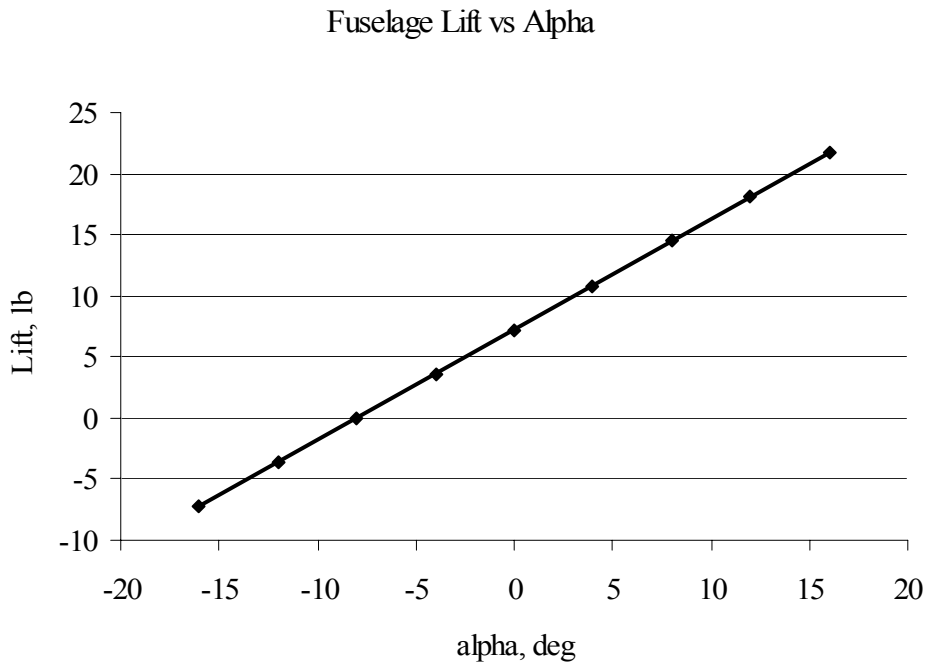

$L_\alpha = A_{fuse} * a_{fuse} * (\alpha_F - \alpha_{0F})$ where A_{fuse} = 181 ft^2 (see Appendix A)

From the data table, the zero lift alpha is -8º ($\alpha_{0L,fuse}$)

The equation for the above line is y=0.905x+7.23

Therefore, a_{fuse} = 0.905/181=0.005/deg = 0.286/rad

β_F, deg	Y_β	L_β

-20	29	150
-10	14.5	75
0	0	0
10	-14.5	-75
20	-29	-150

Y_β and L_β are linear. Therefore,

$Y_\beta = -1.45\ \beta_F$

$L_\beta = -7.5\ \beta_F$

Rotor Drag Coefficient and Lift Curve Slope:

As previously state, the rotor drag coefficient and lift curve slope were calculated as averages around the rotor disk. Per Reference 7:

$$a_{MR} = 4.95 + \frac{\mu(-8 + 30\mu)}{\left(1-(0.75M_{tip})^2 \sin\beta_M\right)^{1/2}}$$

$$cd = \min(0.11,\ .015 + \alpha_R*(.068 + \alpha_R*.81) + \max(0,.01*\alpha_R + .02*(.85 + \max(M_{tip},.35))))$$

where:

$$V_{tip} = \left(V^2 + (\Omega R)^2 + 2V\Omega\Omega\cos\beta_M\right)^{1/2}$$

$$M_{tip} = \frac{V_{tip}}{1116.45}$$

$$\alpha_R = \frac{7C_T}{\sigma a}$$

Appendix B: XV-15 Control System Development

(All data extracted from Reference 7 unless otherwise noted)

The pilot controls can be tied to the control surfaces as follows (units are radians/inch of control deflection with β_M in radians):

$\delta_{elev}=(\delta_{long}-\delta_{long,\ neutral})(\ \delta_{elev}/\delta_{long})$

$\delta_{ail}=-(\delta_{lat}-\delta_{lat,\ neutral})(\ \delta_{ail}/\delta_{lat})$

$\delta_{rud}=(\delta_{ped}-\delta_{ped,\ neutral})(\ \delta_{rud}/\delta_{ped})$

$\delta_{elev}/\delta_{long}$ = 4.17 deg/in

$\delta_{ail}/\delta_{lat}$ = 3.93 deg/in

$\delta_{rud}/\delta_{ped}$ = 8 deg/in

Per GTRS, the pilot controls can be tied to the rotor via the swashplate by:

$\theta_0=\delta\theta_0/\delta_{coll}\ \delta_{coll}+\theta_{0LL}\pm(\delta_{lat}-\delta_{lat,\ neutral})\ \delta\theta_0/\delta_{lat}+\theta_{rotor\ governor}$ + SCAS

$\theta_{1s}=-(\delta_{long}-\delta_{long,\ neutral})\ \delta\theta_{1s}/\delta_{long}\pm(\delta_{ped}-\delta_{ped,\ neutral})\ \delta\theta_{1s}/\delta_{ped}$ + 1.5º(1 - cosβ_M) + SCAS

$\theta_{1c}=0$ (Lateral cyclic is not used in the basic XV-15 control system)

For this analysis, the above equations were simplified via the removal of the SCAS and rotor governor which required using θ_0 as the trim variable rather than the δ_{coll}:

$\theta_{0,1}=\theta_0-(\delta_{lat}-\delta_{lat,\ neutral})\ \delta\theta_0/\delta_{lat}$

$\theta_{0,2}=\theta_0+(\delta_{lat}-\delta_{lat,\ neutral})\ \delta\theta_0/\delta_{lat}$

$\theta_{1s,1}=-(\delta_{long}-\delta_{long,\ neutral})\ \delta\theta_{1s}/\delta_{long}+(\delta_{ped}-\delta_{ped,\ neutral})\ \delta\theta_{1s}/\delta_{ped}-1.5\pi(1-\cos\beta_M)/180$

$\theta_{1s,2} = -(\delta_{long}-\delta_{long,\ neutral})\ \delta\theta_{1s}/\delta_{long} - (\delta_{ped}-\delta_{ped,\ neutral})\ \delta\theta_{1s}/\delta_{ped} - 1.5\pi(1-\cos\beta_M)/180$

$\theta_{1c1}=\theta_{1c2}=0$ (Lateral cyclic is not used in the basic XV-15 control system)

where:

$\delta_{long,\ neutral} = 4.8$ inches

$\delta_{lat,\ neutral} = 4.8$ inches

$\delta_{ped,\ neutral} = 2.5$ inches

The total control travel for the pilot cockpit control inceptors are

Controller	Total Control Travel (100%), in.
Longitudinal Stick	9.6
Lateral Stick	9.6
Pedal	5
Collective	10

The following ties pilot control to the control surfaces:

$\delta\theta_{1s}/\delta_{long} = -0.012\ \beta_M^2 - 0.0053\ \beta_M + 0.0374$ rad/in (β_M in rad)

$\delta\theta_0/\delta lat = -0.0027\ \beta_M^2 - 0.0014\ \beta_M + 0.0109$ rad/in

If $V < 60$ kts

$$\delta\theta_{1s}/\delta_{ped} = -0.0095\ \beta_M^2 - 0.0035\ \beta_M + 0.0283 \text{ rad/in}$$

If $V > 100$ kts

$$\delta\theta_{1s}/\delta_{ped} = -0.0023\ \beta_M^2 - 0.0009\ \beta_M + 0.0071 \text{ rad/in}$$

Else

$$\delta\theta_{1s}/\delta_{ped} = -0.006\ \beta_M^2 - 0.0026\ \beta_M + 0.0184 \text{ rad/in}$$

In order to remove the small residual in airplane mode due to the curve fitting,
If $\beta_M = 90^o$ (airplane mode)

$$\delta\theta_{1s}/\delta_{long}=0$$

$$\delta\theta_{1s}/\delta_{ped}=0$$

$\delta\theta_{1s}/\delta_{long}$

Mast angle	$\delta\theta_{1s}/\delta_{long}$
deg	deg/in
0	2.1
10	2.09
20	1.98
30	1.81
40	1.6
50	1.35
60	1.04
70	0.71
80	0.362
90	0

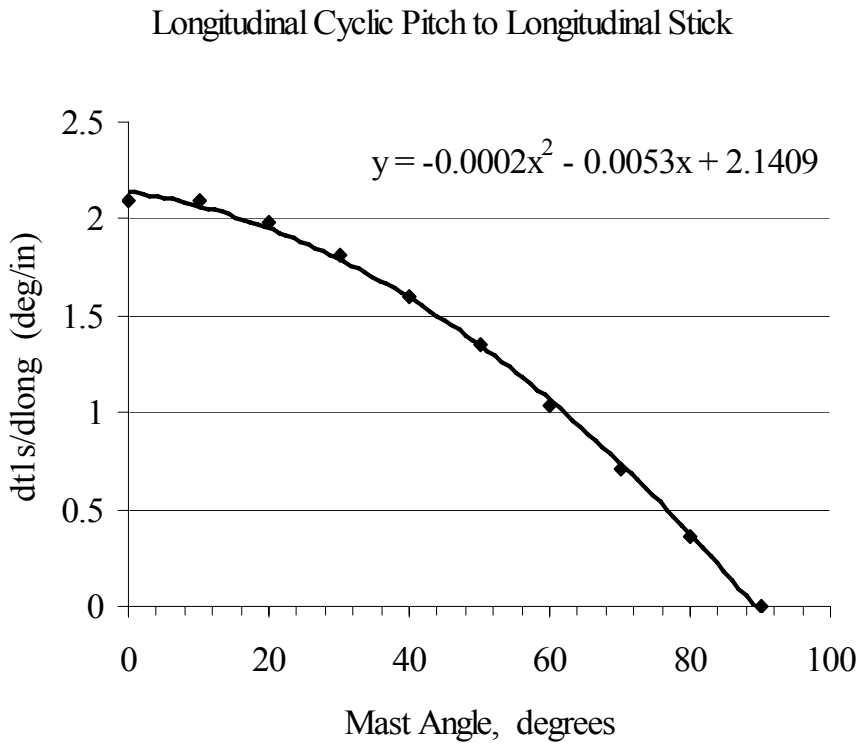

$\delta\theta_{1s}/\delta_{long} = -.0002\ \beta_M^2 - 0.0053\ \beta_M + 2.1409$ (deg/inch)

$\delta\theta_{1s}/\delta_{long} = -0.012\ \beta_M^2 - 0.0053\ \beta_M + 0.0374$ (rad/inch)

$\delta\theta_{1s}/\delta ped$

	0-60kts	80kts	>100kts
Mast angle	$\delta\theta_{1s}/\delta_{ped}$	$\delta\theta_{1s}/\delta_{ped}$	$\delta\theta_{1s}/\delta_{ped}$
deg	deg/in	deg/in	deg/in
0	1.6	1.04	0.4
10	1.58	1.025	0.394
20	1.51	0.975	0.375
30	1.39	0.9	0.345
40	1.225	0.795	0.305
50	1.035	0.67	0.257
60	0.803	0.52	0.2
70	0.55	0.325	0.137
80	0.28	0.18	0.069
90	0	0	0

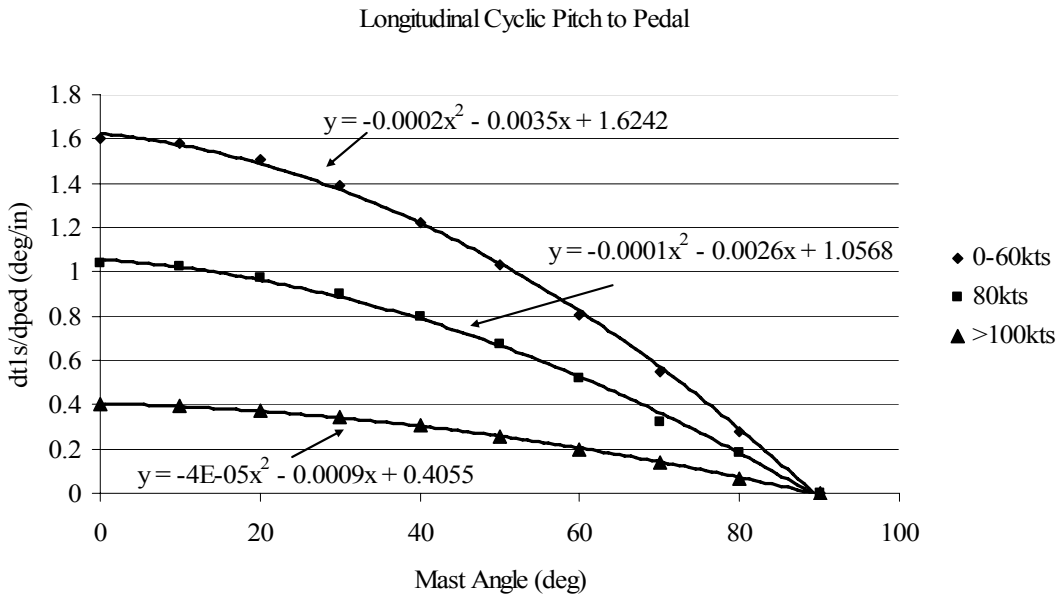

Converted to rad/inch:

If $V < 60$ kts: $\delta\theta_{1s}/\delta_{ped} = -0.0095\ \beta_M^2 - 0.0035\ \beta_M + 0.0283$

If $V > 100$ kts: $\delta\theta_{1s}/\delta_{ped} = -0.0023\ \beta_M^2 - 0.0009\ \beta_M + 0.0071$

Else: $\delta\theta_{1s}/\delta_{ped} = -0.006\ \beta_M^2 - 0.0026\ \beta_M + 0.0184$

$\delta\theta_0/\delta_{lat}$

Mast angle, β_M	$\delta\theta_0/\delta_{lat}$
deg	deg/in
0	0.625
10	0.606
20	0.575
30	0.541
40	0.5
50	0.438
60	0.365
70	0.293
80	0.209
90	0.121

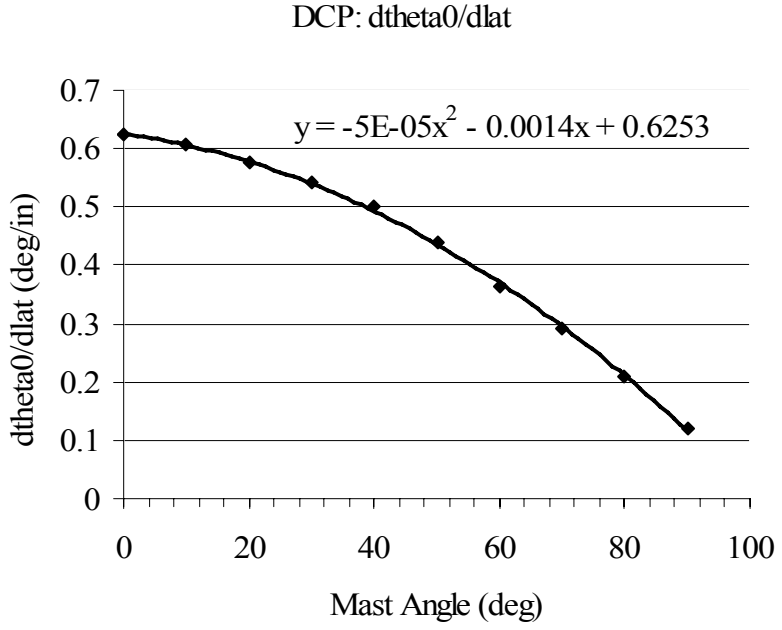

$\delta\theta_0/\delta_{lat}$=-5E-05 β_M^2 - 0.0014 β_M + 0.6253 (deg/in, β_M in degrees)

$\delta\theta_0/\delta_{lat}$= -0.0027 β_M^2 - 0.0014 β_M + 0.0109 (rad/in, β_M in radians)

Appendix C: Trim Results

The GTRS data shown here for comparison was gathered from Reference 6.

Helicopter Mode Input Parameters

Parameter	Units	Value
GW	lbs	13000
β_M	deg	0.00
Turn Rate	deg/s	0.00
Flight Path Angle	deg	0.00
x_{cg}	ft	25.10
y_{cg}	ft	0.00
z_{cg}	ft	6.80
Ω	rad/s	61.68
Ω	RPM	589
δ_{flap}	deg	40
I_{xx}	slug ft^2	52800
I_{yy}	slug ft^2	21360
I_{zz}	slug ft^2	66340
I_{xz}	slug ft^2	1234

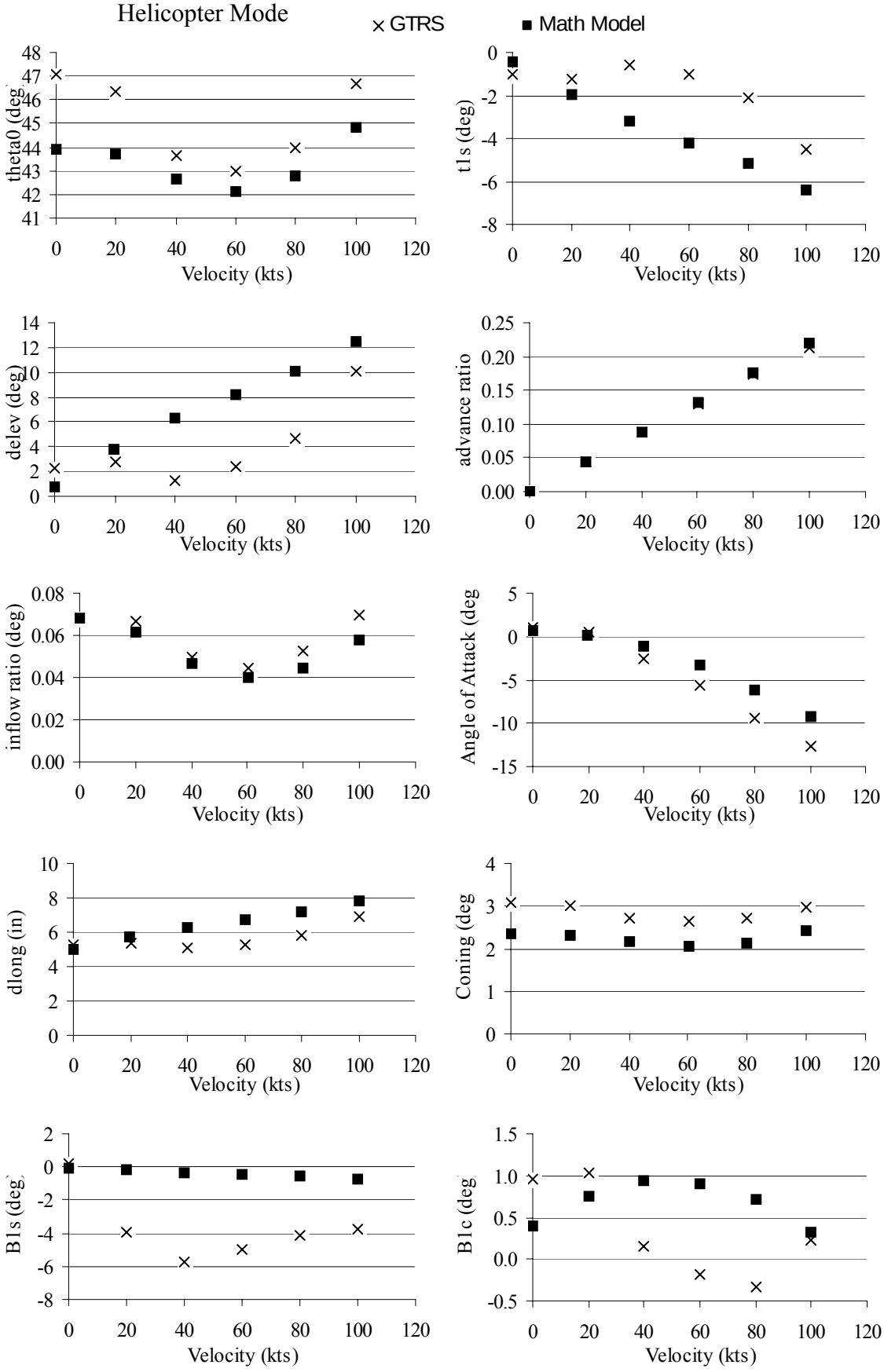
Helicopter Mode
× GTRS
■ Math Model
theta0 (deg)
t1s (deg)
delev (deg)
advance ratio
inflow ratio (deg)
Angle of Attack (deg
dlong (in)
Coning (deg
B1s (deg)
B1c (deg)
Velocity (kts)

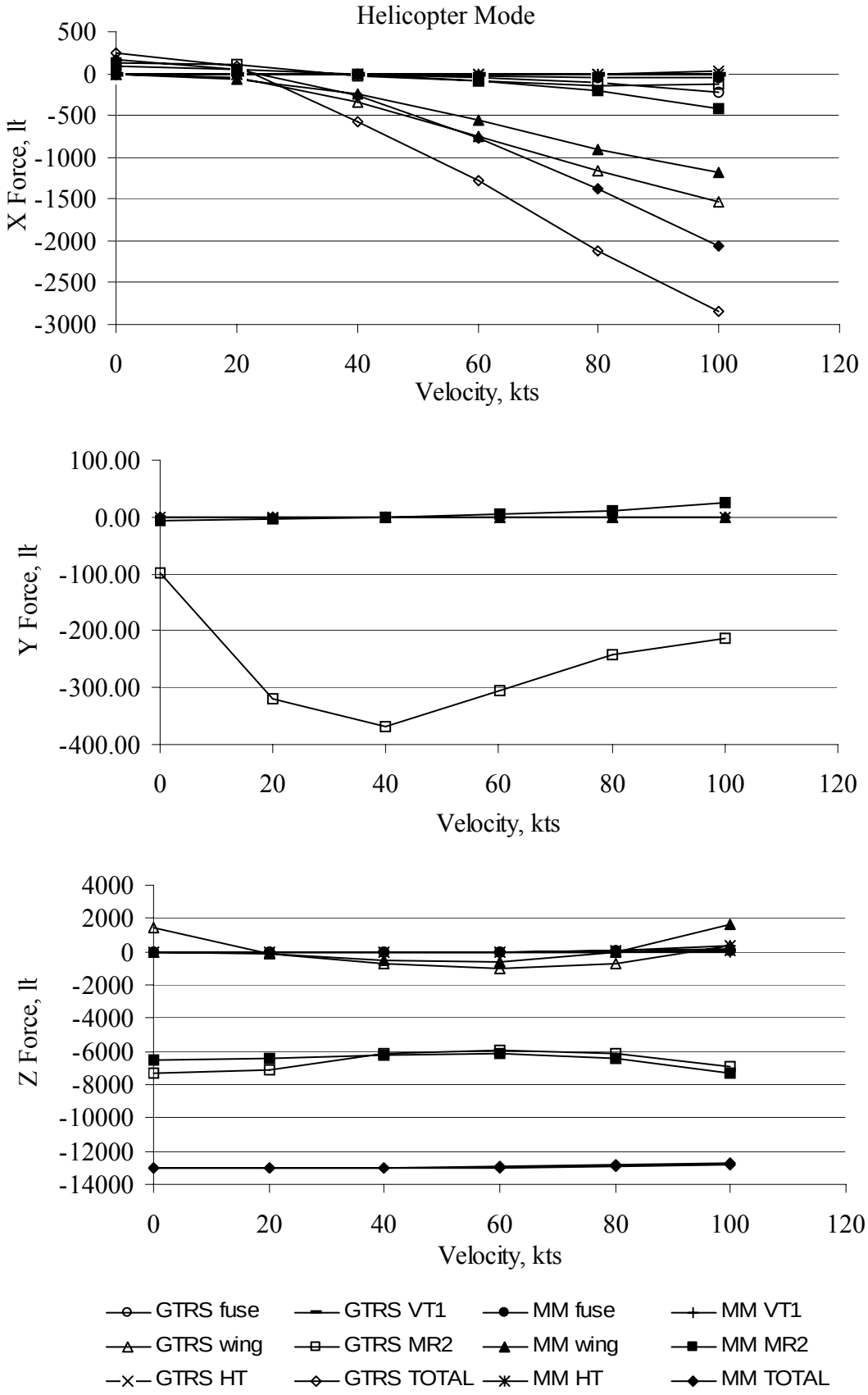
Helicopter Mode
X Force, lt
500
0
-500
-1000
-1500
-2000
-2500
-3000
0
20
40
60
80
100
120
Velocity, kts
Y Force, lt
100.00
0.00
-100.00
-200.00
-300.00
-400.00
0
20
40
60
80
100
120
Velocity, kts
Z Force, lt
4000
2000
0
-2000
-4000
-6000
-8000
-10000
-12000
-14000
0
20
40
60
80
100
120
Velocity, kts
GTRS fuse
GTRS VT1
MM fuse
MM VT1
GTRS wing
GTRS MR2
MM wing
MM MR2
GTRS HT
GTRS TOTAL
MM HT
MM TOTAL

Helicopter Mode

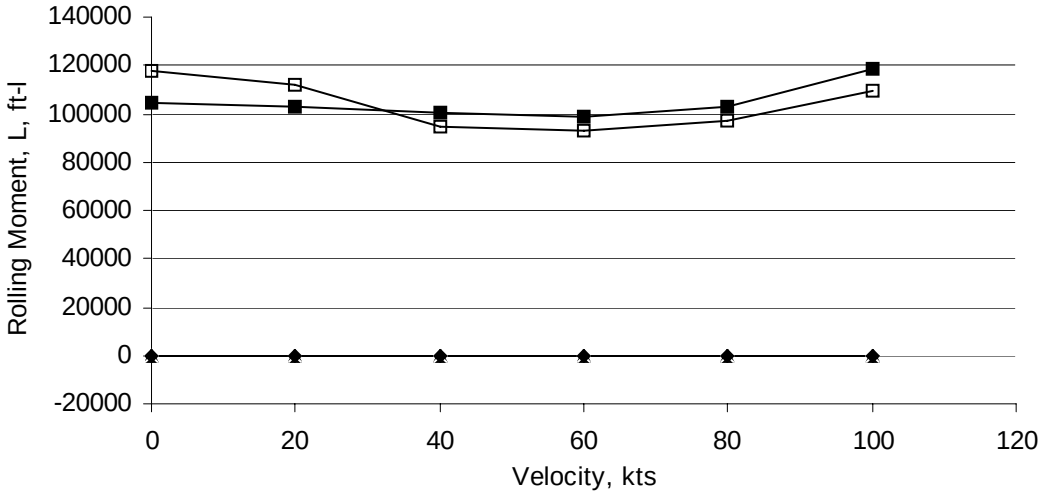

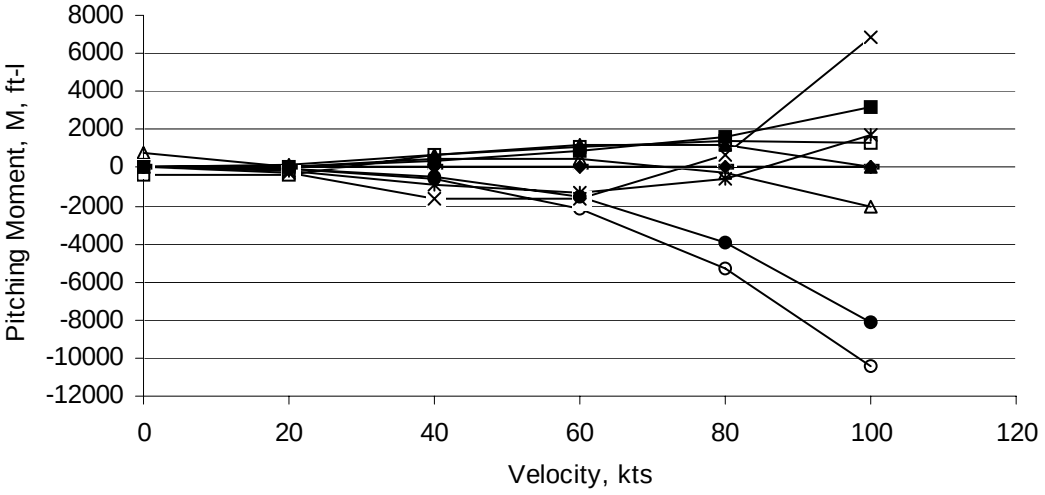

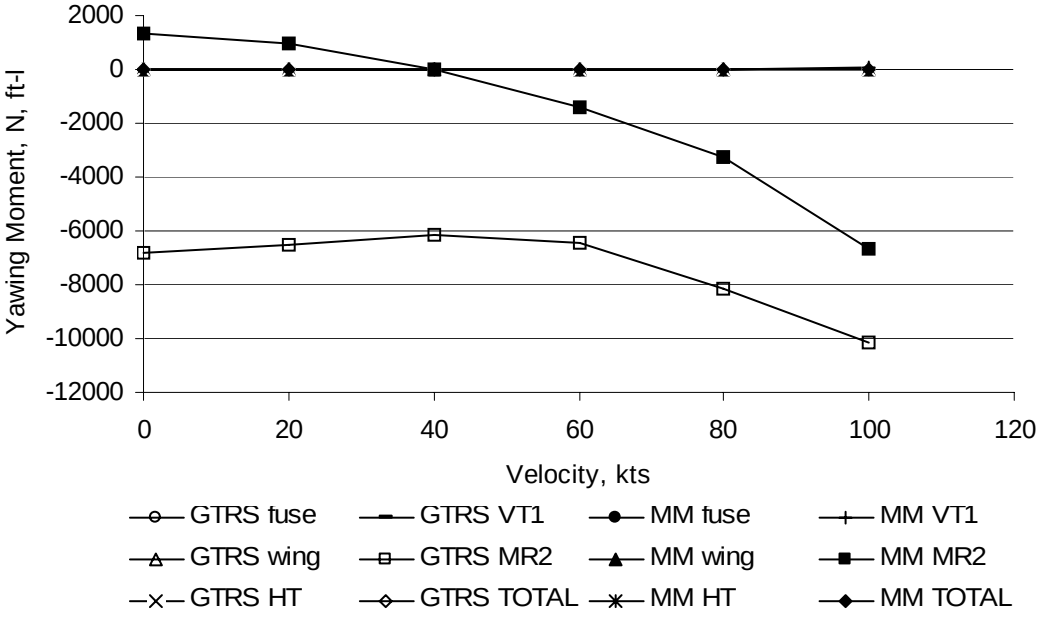

Table C-1: Helicopter Mode

Input Parameter	Units	GTRS	Math Model	GTRS	Math Model	GTRS	Math Model
V	ft/s	--	0.02	--	33.76	--	67.51
V	kts	0.01	0.01	20.00	20.00	40.00	40.00
φ	deg	0.00	0.00	0.00	0.00	0.00	0.00
θ	deg	1.11	0.73	0.41	0.22	-2.52	-1.18
α_F	deg	1.11	0.73	0.41	0.22	-2.52	-1.18
β_F	deg	0.00	0.00	0.00	0.00	0.00	0.00
λ_1	--	0.0682	0.0684	0.0670	0.0612	0.0498	0.0469
p	deg/s	0.00	0.00	0.00	0.00	0.00	0.00
q	deg/s	0.00	0.00	0.00	0.00	0.00	0.00
r	deg/s	0.00	0.00	0.00	0.00	0.00	0.00
pdot	deg/s/s	0.00	0.00	0.00	0.00	0.00	0.00
qdot	deg/s/s	-0.04	0.00	-0.01	0.00	0.00	0.00
rdot	deg/s/s	0.00	0.00	0.00	0.00	0.00	0.00
$\beta_{0,1}$	deg	3.09	2.34	3.02	2.30	2.71	2.16
$\beta_{1s,1}$	deg	0.21	-0.03	-3.96	-0.20	-5.74	-0.33
$\beta_{1c,1}$	deg	0.96	0.40	1.02	0.75	0.15	0.93
$\theta_{0,1}$	deg	47.09	43.92	46.38	43.72	43.67	42.66
$\theta_{1s,1}$	deg	-0.99	-0.41	-1.23	-1.97	-0.57	-3.23
$\theta_{1c,1}$	deg	0.00	0.00	0.00	0.00	0.00	0.00
δ_{rud}	deg	0.00	0.00	0.00	0.00	0.00	0.00
δ_{elev}	deg	2.23	0.79	2.77	3.84	1.27	6.29
δ_{ail}	deg	0.00	0.00	0.00	0.00	0.00	0.00
M	--	0.0000	0.0000	0.0438	0.0438	0.0875	0.0876
U	ft/s	0.01	0.02	33.76	33.76	67.45	67.50
V	ft/s	0.00	0.00	0.00	0.00	0.00	0.00
W	ft/s	0.00	0.00	0.24	0.13	-2.97	-1.39
Thrust_1	lb	7333.92	6499.47	7112.04	6413.13	6097.19	6218.68
C_{T1}	--	0.0106	0.0094	0.0103	0.0092	0.0088	0.0090
δ_{long}	In	5.27	4.99	5.38	5.72	5.07	6.31
δ_{lat}	In	4.80	4.80	4.80	4.80	4.80	4.80
δ_{ped}	In	2.50	2.50	2.50	2.50	2.50	2.50
λ_2	--	0.0682	0.0684	0.0670	0.0612	0.0498	0.0469
$\beta_{0,2}$	deg	3.09	2.34	3.02	2.30	2.71	2.16
$\beta_{1s,2}$	deg	0.21	-0.03	-3.96	-0.20	-5.74	-0.33
$\beta_{1c,2}$	deg	0.96	0.40	1.02	0.75	0.15	0.93
$\theta_{0,2}$	deg	47.09	3.92	46.38	3.72	43.67	2.66
θ_0	deg	47.09	3.92	46.38	3.72	43.67	2.66
Thrust_2	lb	7333.92	6499.47	7112.04	6413.13	6097.19	6218.68
C_{T2}	--	0.0106	0.0094	0.0103	0.0092	0.0088	0.0090

Table C-1: Helicopter Mode (cont.)

Input Parameter	Units	GTRS	Math Model	GTRS	Math Model	GTRS	Math Model
V	ft/s	--	101.27	--	135.02	--	168.78
V	kts	60.00	60.00	80.00	80.00	100.00	100.00
φ	deg	0.00	0.00	0.00	0.00	0.00	0.00
θ	deg	-5.69	-3.37	-9.35	-6.10	-12.61	-9.16
α_F	deg	-5.70	-3.37	-9.35	-6.10	-12.61	-9.16
β_F	deg	0.00	0.00	0.00	0.00	0.00	0.00
λ_1	--	0.0441	0.0398	0.0525	0.0441	0.0694	0.0581
p	deg/s	0.00	0.00	0.00	0.00	0.00	0.00
q	deg/s	0.00	0.00	0.00	0.00	0.00	0.00
r	deg/s	0.00	0.00	0.00	0.00	0.00	0.00
$pdot$	deg/s/s	0.00	0.00	0.00	0.00	0.00	0.00
$qdot$	deg/s/s	-0.04	0.00	-4.89	0.00	0.03	0.00
$rdot$	deg/s/s	0.00	0.00	0.00	0.00	0.00	0.00
$\beta_{0,1}$	deg	2.65	2.05	2.73	2.11	2.96	2.43
$\beta_{1s,1}$	deg	-4.96	-0.44	-4.10	-0.55	-3.78	-0.72
$\beta_{1c,1}$	deg	-0.18	0.90	-0.33	0.71	0.24	0.33
$\theta_{0,1}$	deg	42.96	42.14	43.99	42.81	46.68	44.86
$\theta_{1s,1}$	deg	-1.04	-4.18	-2.09	-5.15	-4.49	-6.40
$\theta_{1c,1}$	deg	0.00	0.00	0.00	0.00	0.00	0.00
δ_{rud}	deg	0.00	0.00	0.00	0.00	0.00	0.00
δ_{elev}	deg	2.34	8.14	4.71	10.03	10.13	12.45
δ_{ail}	deg	0.00	0.00	0.00	0.00	0.00	0.00
M	--	0.1307	0.1313	0.1728	0.1751	0.2136	0.2189
U	ft/s	100.80	101.09	133.20	134.26	164.70	166.63
V	ft/s	0.00	0.00	0.00	0.00	0.00	0.00
W	ft/s	-10.04	-5.96	-21.93	-14.34	-36.86	-26.86
Thrust_1	lb	5935.89	6120.84	6180.81	6392.96	6900.68	7315.05
C_{T1}	--	0.0086	0.0088	0.0089	0.0092	0.0100	0.0105
δ_{long}	In	5.29	6.75	5.80	7.21	6.94	7.79
δ_{lat}	In	4.80	4.80	4.80	4.80	4.80	4.80
δ_{ped}	In	2.50	2.50	2.50	2.50	2.50	2.50
λ_2	--	0.0441	0.0398	0.0525	0.0441	0.0694	0.0581
$\beta_{0,2}$	deg	2.65	2.05	2.73	2.11037	2.96	2.42693
$\beta_{1s,2}$	deg	-4.96	-0.44	-4.10	-0.54798	-3.78	-0.71929
$\beta_{1c,2}$	deg	-0.18	0.90	-0.33	0.71084	0.24	0.32646
$\theta_{0,2}$	deg	42.96	2.14	43.99	2.81147	46.68	4.85605
θ_0	deg	42.96	2.14	43.99	2.81147	46.68	4.85605
Thrust_2	lb	5935.89	6120.84	6180.81	6392.96	6900.68	7315.05
C_{T2}	--	0.0086	0.0088	0.0089	0.0092	0.0100	0.0105

Table C-1: Helicopter Mode (cont.)

0.01 kts

Math Model

	X force	*Y* force	*Z* force	Roll (*L*)	Pitch (*M*)	Yaw (*N*)
Fuselage	0.00	0.00	0.00	0.00	0.00	0.00
Wing	0.00	0.00	0.00	0.00	0.00	0.00
Horizontal Tail	0.00	0.00	0.00	0.00	0.00	0.00
Vertical Tail #1	0.00	0.00	0.00	0.00	0.00	0.00
Vertical Tail #2	0.00	0.00	0.00	0.00	0.00	0.00
Airframe	0.00	0.00	0.00	0.00	0.00	0.00
Left Rotor (*MR*2)	83.36	-5.23	-6499.47	104620.16	0.00	1341.62
Right Rotor (*MR*1)	83.36	5.23	-6499.47	-104620.16	0.00	-1341.62
Total Rotor	166.73	0.00	-12998.93	0.00	0.00	0.00
Total Aircraft (Body Axis)	166.73	0.00	-12998.93	0.00	0.00	0.00

GTRS

	X force	*Y* force	*Z* force	Roll (*L*)	Pitch (*M*)	Yaw (*N*)
Fuselage	0.00	0.00	0.00	0.00	0.00	0.00
Wing	0.00	0.00	1744.96	0.00	800.00	0.00
Horizontal Tail	0.00	0.00	0.00	0.00	0.00	0.00
Vertical Tail #1	0.00	0.00	0.00	0.00	0.00	0.00
Vertical Tail #2	0.00	0.00	0.00	0.00	0.00	0.00
Airframe	-0.02	0.00	1660.25	0.00	808.49	0.00
Left Rotor (*MR*2)	125.07	-98.84	-7333.31	117976.95	-412.06	-6817.25
Right Rotor (*MR*1)	125.07	98.84	-7333.31	-117975.95	-412.06	6817.25
Total Rotor	250.15	0.00	-14660.04	0.00	-824.76	0.00
Total Aircraft (Body Axis)	250.13	0.00	-12999.79	0.00	-16.28	0.00

Table C-1: Helicopter Mode (cont.)

20 kts

Math Model

	X force	*Y* force	*Z* force	Roll (*L*)	Pitch (*M*)	Yaw (*N*)
Fuselage	-2.13	0.00	-10.08	0.00	-77.62	0.00
Wing	-61.66	0.00	-154.95	0.00	197.69	0.00
Horizontal Tail	-0.79	0.00	-8.62	0.00	-184.79	0.00
Vertical Tail #1	-0.24	0.00	0.00	0.00	0.68	1.56
Vertical Tail #2	-0.24	0.00	0.00	0.00	0.68	-1.56
Airframe	-65.06	0.00	-173.65	0.00	-63.37	0.00
Left Rotor (*MR*2)	57.59	-4.06	-6413.13	103293.33	31.68	926.73
Right Rotor (*MR*1)	57.59	4.06	-6413.13	-103293.33	31.68	-926.73
Total Rotor	115.17	0.00	-12826.25	0.00	63.37	0.00
Total Aircraft (Body Axis)	50.11	0.00	-12999.90	0.00	0.00	0.00

GTRS

	X force	*Y* force	*Z* force	Roll (*L*)	Pitch (*M*)	Yaw (*N*)
Fuselage	-3.43	0.00	-10.32	0.00	-71.75	0.00
Wing	-39.83	0.00	1270.60	0.00	-5.81	0.00
Horizontal Tail	-1.53	0.00	-11.22	0.00	-239.17	0.00
Vertical Tail #1	-0.60	0.00	0.00	0.00	1.71	-3.86
Vertical Tail #2	-0.60	0.00	0.00	0.00	1.71	3.86
Airframe	-117.01	0.00	1201.03	0.00	630.20	0.00
Left Rotor (*MR*2)	109.84	-320.09	-7107.54	112017.00	-344.56	-6532.60
Right Rotor (*MR*1)	109.84	320.09	-7107.54	-112017.00	-344.56	6532.60
Total Rotor	210.27	0.00	-14200.67	0.00	-632.29	0.00
Total Aircraft (Body Axis)	93.27	0.00	-12999.64	0.00	-2.09	0.00

Table C-1: Helicopter Mode (cont.)

40 kts

Math Model

	X force	*Y* force	*Z* force	Roll (*L*)	Pitch (*M*)	Yaw (*N*)
Fuselage	-9.36	0.00	-33.25	0.00	-459.23	0.00
Wing	-250.14	0.00	-486.57	0.00	688.38	0.00
Horizontal Tail	-4.15	0.00	-40.07	0.00	-858.14	0.00
Vertical Tail #1	-0.97	0.00	0.00	0.00	2.72	6.22
Vertical Tail #2	-0.97	0.00	0.00	0.00	2.72	-6.22
Airframe	-265.60	0.00	-559.89	0.00	-623.55	0.00
Left Rotor (*MR*2)	-0.80	-0.91	-6218.68	100227.86	311.78	-12.97
Right Rotor (*MR*1)	-0.80	0.91	-6218.68	-100227.86	311.78	12.97
Total Rotor	-1.60	0.00	-12437.36	0.00	623.55	0.00
Total Aircraft (Body Axis)	-267.20	0.00	-12997.25	0.00	0.00	0.00

GTRS

	X force	*Y* force	*Z* force	Roll (*L*)	Pitch (*M*)	Yaw (*N*)
Fuselage	-15.85	0.00	-26.14	0.00	-598.52	0.00
Wing	-350.07	0.00	-719.31	0.00	451.96	0.00
Horizontal Tail	-3.86	0.00	-75.39	0.00	-1619.00	0.00
Vertical Tail #1	1.11	0.00	0.00	0.00	-3.16	7.15
Vertical Tail #2	1.11	0.00	0.00	0.00	-3.16	-7.15
Airframe	-465.06	0.00	0.00	0.00	-1621.14	0.00
Left Rotor (*MR*2)	-24.56	-367.07	-6091.71	94905.00	627.22	-6157.03
Right Rotor (*MR*1)	-24.56	367.07	-6091.71	-94905.00	627.22	6157.03
Total Rotor	-106.44	0.00	-12150.74	0.00	1606.38	0.00
Total Aircraft (Body Axis)	-571.50	0.00	-12987.87	0.00	-14.76	0.00

Table C-1: Helicopter Mode (cont.)

60 kts

Math Model

	X force	*Y* force	*Z* force	Roll (*L*)	Pitch (*M*)	Yaw (*N*)
Fuselage	-22.49	0.00	-49.77	0.00	-1558.81	0.00
Wing	-555.67	0.00	-624.88	0.00	1164.39	0.00
Horizontal Tail	-9.57	0.00	-61.14	0.00	-1303.43	0.00
Vertical Tail #1	-2.19	0.00	0.00	0.00	6.12	14.00
Vertical Tail #2	-2.19	0.00	0.00	0.00	6.12	-14.00
Airframe	-592.11	0.00	-735.78	0.00	-1685.62	0.00
Left Rotor (*MR*2)	-86.51	4.54	-6120.84	98720.99	842.81	-1392.33
Right Rotor (*MR*1)	-86.51	-4.54	-6120.84	-98720.99	842.81	1392.33
Total Rotor	-173.02	0.00	-12241.68	0.00	1685.62	0.00
Total Aircraft (Body Axis)	-765.13	0.00	-12977.46	0.00	0.00	0.00

GTRS

	X force	*Y* force	*Z* force	Roll (*L*)	Pitch (*M*)	Yaw (*N*)
Fuselage	-42.62	0.00	-21.25	0.00	-2107.49	0.00
Wing	-743.88	0.00	-1035.99	0.00	478.28	0.00
Horizontal Tail	-9.95	0.00	-78.06	0.00	-1665.80	0.00
Vertical Tail #1	-0.80	0.00	0.00	0.00	2.26	-5.12
Vertical Tail #2	-0.80	0.00	0.00	0.00	2.26	5.12
Airframe	-978.84	0.00	-1122.49	0.00	-3015.29	0.00
Left Rotor (*MR*2)	-82.60	-303.83	-5931.49	92882.39	1055.40	-6473.12
Right Rotor (*MR*1)	-82.59	303.83	-5931.49	-92882.39	1055.40	6473.12
Total Rotor	-309.80	0.00	-11814.09	0.00	3001.92	0.00
Total Aircraft (Body Axis)	-1288.64	0.00	-12936.58	0.00	-13.37	0.00

Table C-1: Helicopter Mode (cont.)

80 kts

Math Model

	X force	*Y* force	*Z* force	Roll (*L*)	Pitch (*M*)	Yaw (*N*)
Fuselage	-38.48	0.00	-33.42	0.00	-3929.17	0.00
Wing	-913.38	0.00	-79.91	0.00	1156.18	0.00
Horizontal Tail	-12.27	0.00	-27.23	0.00	-566.15	0.00
Vertical Tail #1	-3.89	0.00	0.00	0.00	10.87	24.89
Vertical Tail #2	-3.89	0.00	0.00	0.00	10.87	-24.89
Airframe	-971.90	0.00	-140.55	0.00	-3317.40	0.00
Left Rotor (*MR*2)	-204.35	12.01	-6392.96	103185.69	1658.70	-3288.84
Right Rotor (*MR*1)	-204.35	-12.01	-6392.96	-103185.69	1658.70	3288.84
Total Rotor	-408.70	0.00	-12785.93	0.00	3317.40	0.00
Total Aircraft (Body Axis)	-1380.61	0.00	-12926.48	0.00	0.00	0.00

GTRS

	X force	*Y* force	*Z* force	Roll (*L*)	Pitch (*M*)	Yaw (*N*)
Fuselage	-104.00	0.00	44.09	0.00	-5308.99	0.00
Wing	-1154.73	0.00	-676.32	0.00	-322.31	0.00
Horizontal Tail	-10.67	0.00	31.09	0.00	689.59	0.00
Vertical Tail #1	-2.33	0.00	0.00	0.00	6.61	-14.96
Vertical Tail #2	-2.33	0.00	0.00	0.00	6.61	14.96
Airframe	-1579.57	0.00	-550.50	0.00	-4466.39	0.00
Left Rotor (*MR*2)	-137.55	-243.07	-6177.51	97429.77	1442.41	-8137.28
Right Rotor (*MR*1)	-137.55	243.07	-6177.51	-97429.77	1442.41	8137.28
Total Rotor	-531.59	0.00	0.00	0.00	4466.21	0.00
Total Aircraft (Body Axis)	-2111.16	0.00	-12827.45	0.00	-0.18	0.00

Table C-1: Helicopter Mode (cont.)

100 kts

Math Model

	X force	*Y* force	*Z* force	Roll (*L*)	Pitch (*M*)	Yaw (*N*)
Fuselage	-47.91	0.00	43.60	0.00	-8173.22	0.00
Wing	-1175.54	0.00	1672.72	0.00	67.58	0.00
Horizontal Tail	-4.79	0.00	79.44	0.00	1724.60	0.00
Vertical Tail #1	-6.08	0.00	0.00	0.00	16.99	38.89
Vertical Tail #2	-6.08	0.00	0.00	0.00	16.99	-38.89
Airframe	-1240.39	0.00	1795.76	0.00	-6347.05	0.00
Left Rotor (*MR*2)	-414.15	24.48	-7315.05	118165.99	3173.52	-6665.37
Right Rotor (*MR*1)	-414.15	-24.48	-7315.05	-118165.99	3173.52	6665.37
Total Rotor	-828.30	0.00	-14630.11	0.00	6347.05	0.00
Total Aircraft (Body Axis)	-2068.69	0.00	-12834.35	0.00	0.00	0.00

GTRS

	X force	*Y* force	*Z* force	Roll (*L*)	Pitch (*M*)	Yaw (*N*)
Fuselage	-229.31	0.00	196.52	0.00	-10466.28	0.00
Wing	-1523.96	0.00	368.16	0.01	-2026.30	0.00
Horizontal Tail	26.08	0.00	320.06	0.00	6856.20	0.00
Vertical Tail #1	-4.26	0.00	0.00	0.00	12.07	-27.31
Vertical Tail #2	-4.26	0.00	0.00	0.00	12.07	27.31
Airframe	-2202.24	0.00	984.15	0.01	-4908.76	0.00
Left Rotor (*MR*2)	-123.95	-212.19	-6898.03	109339.56	1262.50	-10137.00
Right Rotor (*MR*1)	-123.95	212.19	-6898.03	-109339.56	1262.50	10137.00
Total Rotor	-636.43	0.00	-13669.72	0.00	4919.84	0.00
Total Aircraft (Body Axis)	-2838.67	0.00	-12685.57	0.01	11.08	0.00

Airplane Mode (517 RPM) Input Parameters

Parameter	Units	Values
GW	lbs	13000
β_M	deg	90
Turn Rate	deg/s	0
Flight Path Angle	deg	0
x_{cg}	ft	24.85
y_{cg}	ft	0.00
z_{cg}	ft	6.13
Ω	rad/s	54.14
Ω	RPM	517
δ_{flap}	deg	0
I_{xx}	slug ft^2	50950
I_{yy}	slug ft^2	20348
I_{zz}	slug ft^2	67168
I_{xz}	slug ft^2	1076

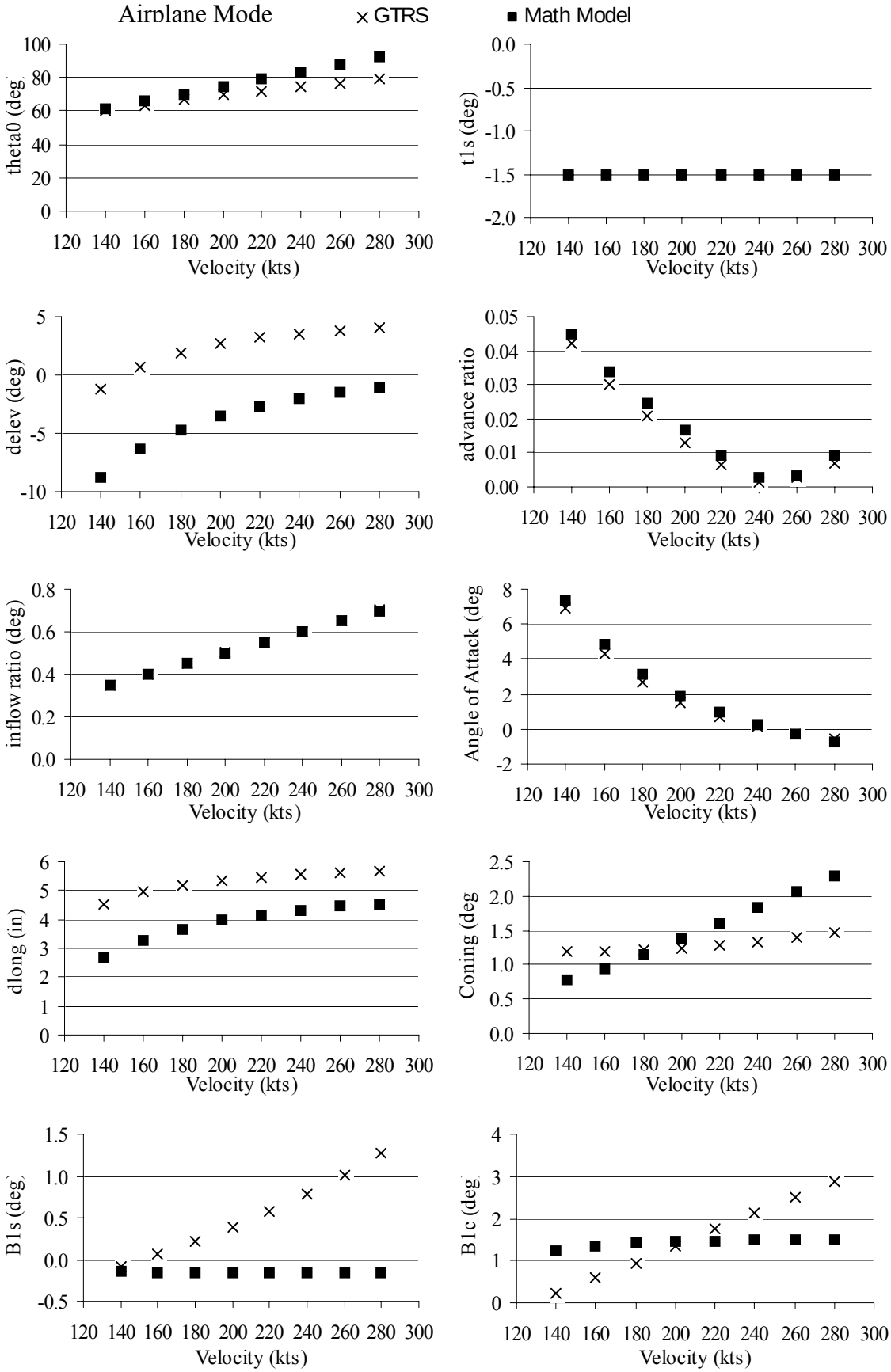
Airplane Mode
× GTRS
■ Math Model
theta0 (deg)
t1s (deg)
delev (deg)
advance ratio
inflow ratio (deg)
Angle of Attack (deg
dlong (in)
Coning (deg
B1s (deg)
B1c (deg)
Velocity (kts)

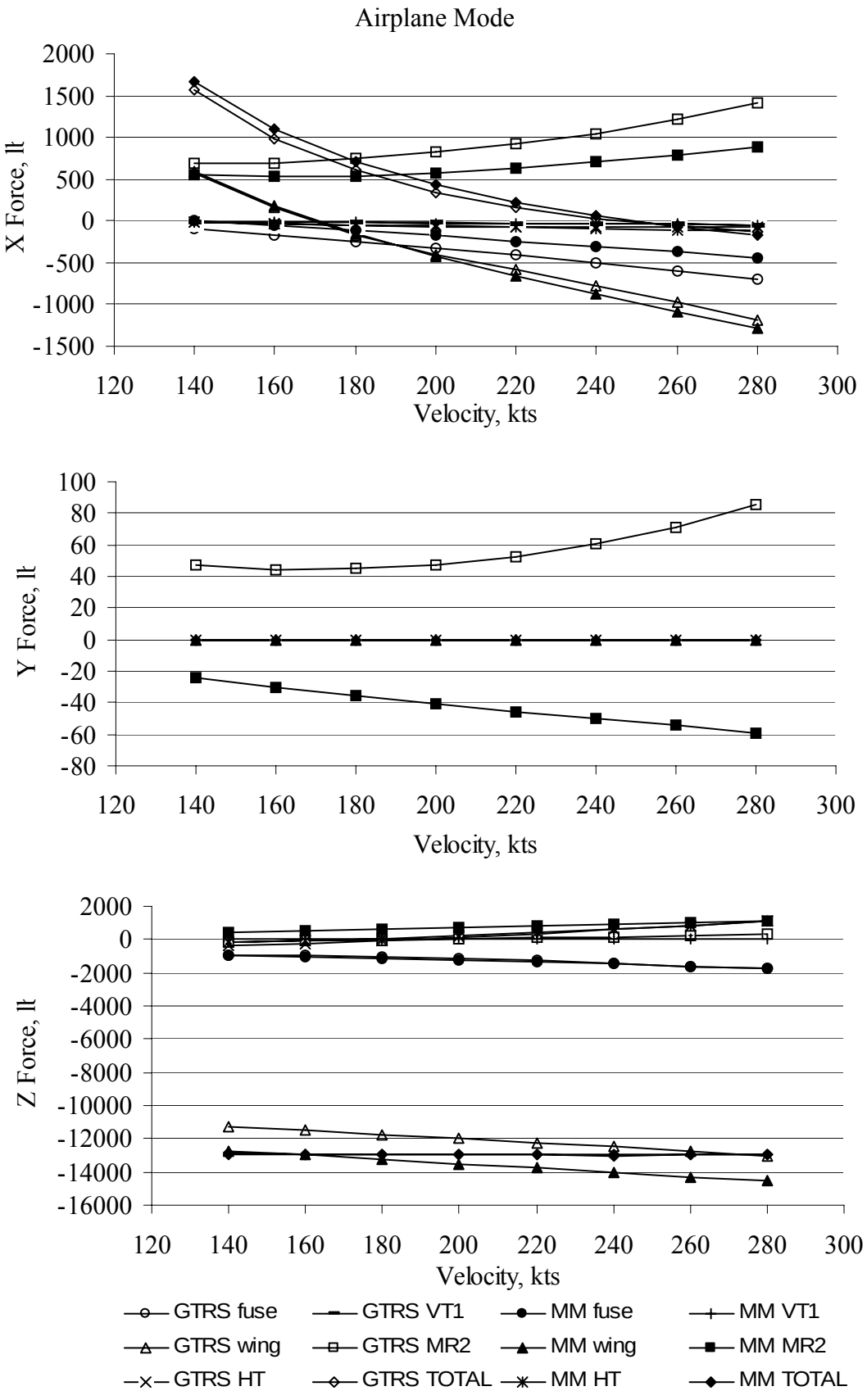
Airplane Mode
X Force, lt
2000
1500
1000
500
0
-500
-1000
-1500
120
140
160
180
200
220
240
260
280
300
Velocity, kts
Y Force, lt
100
80
60
40
20
0
-20
-40
-60
-80
120
140
160
180
200
220
240
260
280
300
Velocity, kts
Z Force, lt
2000
0
-2000
-4000
-6000
-8000
-10000
-12000
-14000
-16000
120
140
160
180
200
220
240
260
280
300
Velocity, kts
GTRS fuse
GTRS VT1
MM fuse
MM VT1
GTRS wing
GTRS MR2
MM wing
MM MR2
GTRS HT
GTRS TOTAL
MM HT
MM TOTAL

Airplane Mode

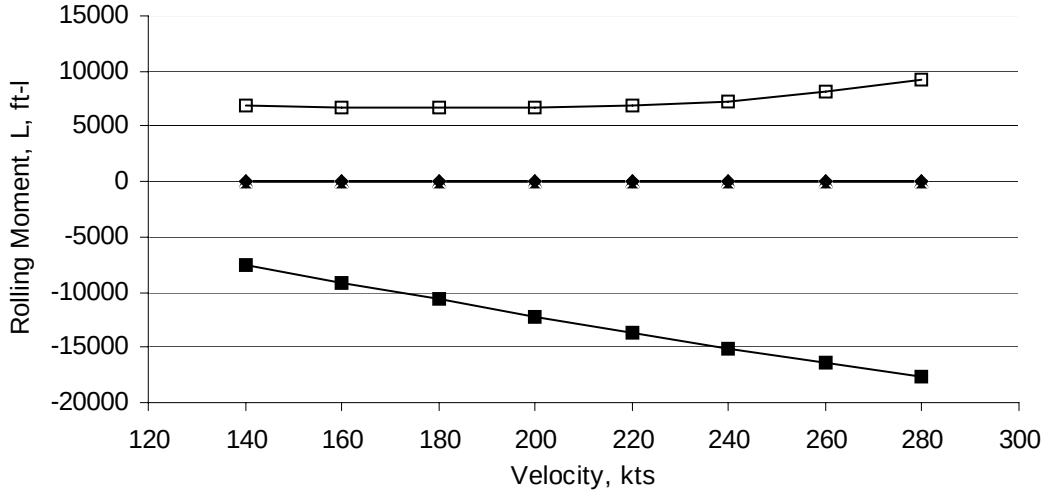

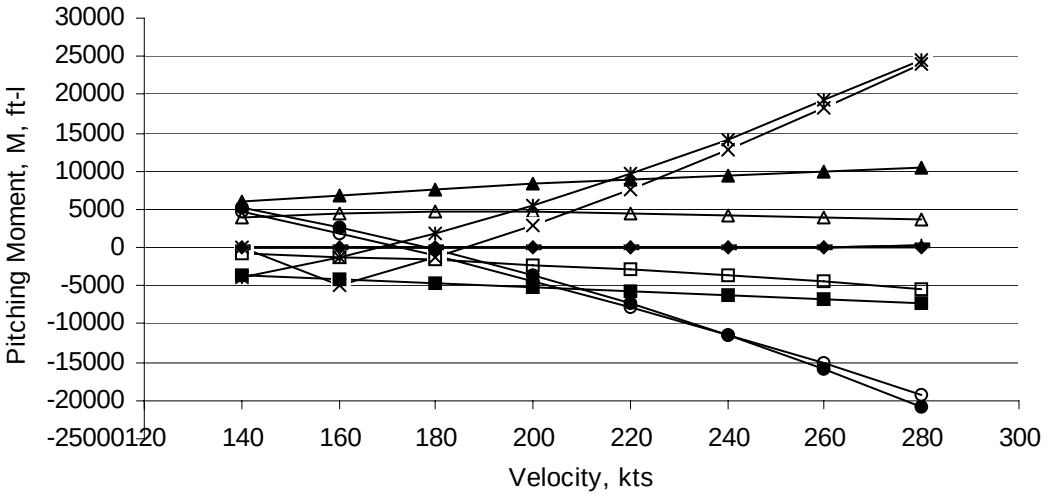

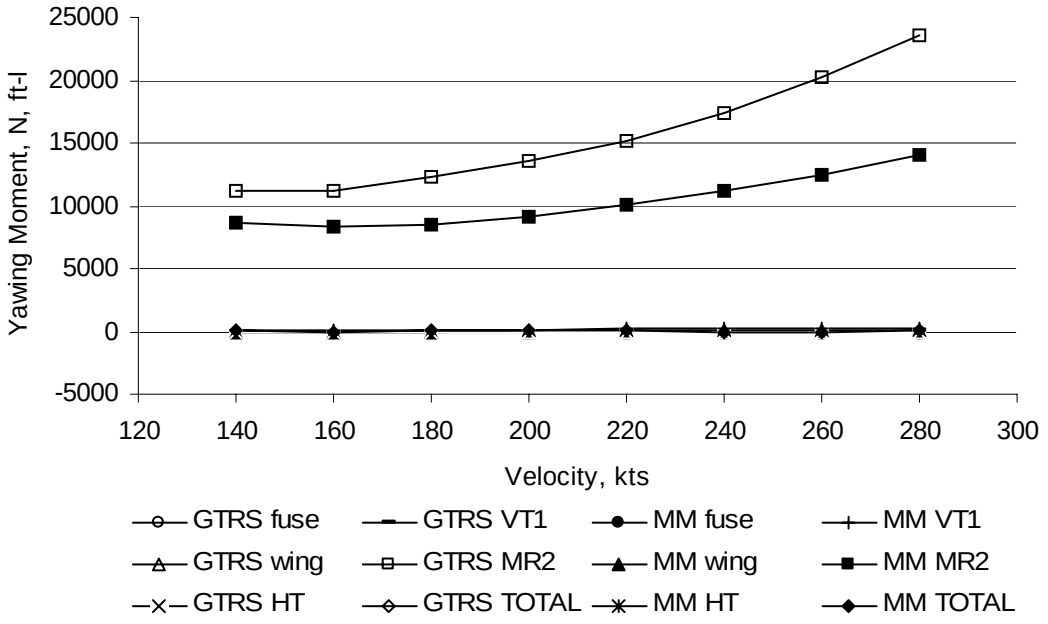

Table C-2: Airplane Mode, 517 RPM

Input Parameter	Units	GTRS	Math Model	GTRS	Math Model	GTRS	Math Model
V	ft/s	--	236.29	--	270.04	--	303.80
V	kts	140.00	140	160.00	160	180.00	180
φ	deg	0.00	0.00	0.00	0.00	0.00	0.00
θ	deg	6.94	7.37	4.33	4.88	2.67	3.16
α_F	deg	6.94	7.37	4.33	4.88	2.67	3.16
β_F	deg	0.00	0.00	0.00	0.00	0.00	0.00
λ_1	--	0.3484	0.3477	0.3995	0.3988	0.4500	0.4493
p	deg/s	0.00	0.00	0.00	0.00	0.00	0.00
q	deg/s	0.00	0.00	0.00	0.00	0.00	0.00
r	deg/s	0.00	0.00	0.00	0.00	0.00	0.00
pdot	deg/s/s	0.00	0.00	0.00	0.00	0.00	0.00
qdot	deg/s/s	0.00	0.00	0.00	0.00	0.00	0.00
rdot	deg/s/s	0.00	0.00	0.00	0.00	0.00	0.00
$\beta_{0,1}$	deg	1.19	0.78	1.19	0.95	1.21	1.15
$\beta_{1s,1}$	deg	-0.09	-0.15	0.07	-0.15	0.22	-0.16
$\beta_{1c,1}$	deg	0.22	1.24	0.58	1.34	0.95	1.41
$\theta_{0,1}$	deg	60.50	61.50	63.68	65.84	66.67	70.19
$\theta_{1s,1}$	deg	-1.50	-1.50	-1.50	-1.50	-1.50	-1.50
$\theta_{1c,1}$	deg	0.00	0.00	0.00	0.00	0.00	0.00
δ_{rud}	deg	0.00	0.00	0.00	0.00	0.00	0.00
δ_{elev}	deg	-1.24	-8.84	0.73	-6.36	1.89	-4.70
δ_{ail}	deg	0.00	0.00	0.00	0.00	0.00	0.00
M	--	0.0422	0.0449	0.0301	0.0340	0.0209	0.0248
U	ft/s	234.60	234.34	269.30	269.06	303.50	303.34
V	ft/s	0.00	0.00	0.00	0.00	0.00	0.01
W	ft/s	28.57	30.30	20.40	22.99	14.12	16.74
Thrust_1	lb	680.41	545.10	680.80	524.03	741.09	537.93
C_{T1}	--	0.0013	0.0010	0.0013	0.0010	0.0014	0.0010
δ_{long}	In	4.54	2.68	4.95	3.28	5.20	3.67
δ_{lat}	In	4.80	4.80	4.80	4.80	4.80	4.80
δ_{ped}	In	2.50	2.50	2.50	2.50	2.50	2.50
λ_2	--	0.3484	0.3477	0.3995	0.3988	0.4500	0.4493
$\beta_{0,2}$	deg	1.19	0.78	1.19	0.95	1.21	1.15
$\beta_{1s,2}$	deg	-0.09	-0.15	0.07	-0.15	0.22	-0.16
$\beta_{1c,2}$	deg	0.22	1.24	0.58	1.34	0.95	1.41
$\theta_{0,2}$	deg	60.50	21.50	63.68	25.84	66.67	30.19
θ_0	deg	60.50	21.50	63.68	25.84	66.67	30.19
Thrust_2	lb	680.41	545.10	680.80	524.03	741.09	537.93
C_{T2}	--	0.0013	0.0010	0.0013	0.0010	0.0014	0.0010

Table C-2: Airplane Mode, 517 RPM (cont.)

Input Parameter	Units	GTRS	Math Model	GTRS	Math Model	GTRS	Math Model
V	ft/s	--	337.56	--	371.31	--	405.07
V	kts	200.00	200	220.00	220	240.00	240
φ	deg	0.00	0.00	0.00	0.00	0.00	0.00
θ	deg	1.51	1.91	0.69	0.98	0.12	0.27
α_F	deg	1.51	1.91	0.69	0.98	0.12	0.27
β_F	deg	0.00	0.00	0.00	0.01	0.00	0.01
λ_1	--	0.5002	0.4996	0.5502	0.5497	0.6002	0.5996
p	deg/s	0.00	0.00	0.00	0.00	0.00	0.00
q	deg/s	0.00	0.00	0.00	0.00	0.00	0.00
r	deg/s	0.00	0.00	0.00	0.00	0.00	0.00
pdot	deg/s/s	0.00	0.00	0.00	0.00	0.00	0.00
qdot	deg/s/s	0.00	0.00	0.00	0.00	0.01	0.00
rdot	deg/s/s	0.00	0.00	0.00	0.00	0.00	0.00
$\beta_{0,1}$	deg	1.24	1.37	1.28	1.60	1.33	1.84
$\beta_{1s,1}$	deg	0.39	-0.16	0.58	-0.16	0.79	-0.16
$\beta_{1c,1}$	deg	1.34	1.45	1.74	1.47	2.13	1.48
$\theta_{0,1}$	deg	69.46	74.55	72.05	78.93	74.49	83.32
$\theta_{1s,1}$	deg	-1.50	-1.50	-1.50	-1.50	-1.50	-1.50
$\theta_{1c,1}$	deg	0.00	0.00	0.00	0.00	0.00	0.00
δ_{rud}	deg	0.00	0.00	0.00	-0.02	0.00	-0.02
δ_{elev}	deg	2.66	-3.52	3.20	-2.66	3.57	-2.01
δ_{ail}	deg	0.00	0.00	0.00	0.00	0.00	0.00
M	--	0.0131	0.0167	0.0066	0.0094	0.0013	0.0028
U	ft/s	337.40	337.37	371.30	371.26	405.10	405.06
V	ft/s	0.00	0.00	0.00	-0.05	0.00	-0.05
W	ft/s	8.90	11.27	4.45	6.37	0.87	1.90
Thrust_1	lb	821.18	576.41	916.24	633.57	1047.19	705.85
C_{T1}	--	0.0015	0.0011	0.0017	0.0012	0.0020	0.0013
δ_{long}	In	5.36	3.95	5.48	4.16	5.55	4.32
δ_{lat}	In	4.80	4.80	4.80	4.80	4.80	4.80
δ_{ped}	In	2.50	2.50	2.50	2.50	2.50	2.50
λ_2	--	0.5002	0.4996	0.5502	0.5497	0.6002	0.5996
$\beta_{0,2}$	deg	1.24	1.37	1.28	1.60	1.33	1.84
$\beta_{1s,2}$	deg	0.39	-0.16	0.58	-0.16	0.79	-0.16
$\beta_{1c,2}$	deg	1.34	1.45	1.74	1.47	2.13	1.48
$\theta_{0,2}$	deg	69.46	34.55	72.05	38.93	74.49	43.32
θ_0	deg	69.46	34.55	72.05	38.93	74.49	43.32
Thrust_2	lb	821.18	576.41	916.24	633.58	1047.19	705.86
C_{T2}	--	0.0015	0.0011	0.0017	0.0012	0.0020	0.0013

Table C-2: Airplane Mode, 517 RPM (cont.)

Input Parameter	Units	GTRS	Math Model	GTRS	Math Model
V	ft/s	--	438.82	--	472.58
V	kts	260.00	260	280.00	280
φ	deg	0.00	0.00	0.00	0.00
θ	deg	-0.27	-0.30	-0.57	-0.75
α_F	deg	-0.27	-0.30	-0.57	-0.75
β_F	deg	0.00	0.01	0.00	0.01
λ_1	--	0.6502	0.6496	0.7002	0.6994
p	deg/s	0.00	0.00	0.00	0.00
q	deg/s	0.00	0.00	0.00	0.00
r	deg/s	0.00	0.00	0.00	0.00
$pdot$	deg/s/s	0.00	0.00	0.00	0.00
$qdot$	deg/s/s	0.01	0.00	0.01	0.00
$rdot$	deg/s/s	0.00	0.00	0.00	0.00
$\beta_{0,1}$	deg	1.39	2.07	1.46	2.29
$\beta_{1s,1}$	deg	1.01	-0.16	1.26	-0.16
$\beta_{1c,1}$	deg	2.50	1.48	2.87	1.49
$\theta_{0,1}$	deg	76.78	87.73	78.91	92.17
$\theta_{1s,1}$	deg	-1.50	-1.50	-1.50	-1.50
$\theta_{1c,1}$	deg	0.00	0.00	0.00	0.00
δ_{rud}	deg	0.00	-0.02	0.00	-0.02
δ_{elev}	deg	3.81	-1.48	4.02	-1.04
δ_{ail}	deg	0.00	0.00	0.00	0.00
M	--	0.0030	0.0034	0.0070	0.0092
U	ft/s	438.80	438.82	472.60	472.54
V	ft/s	0.00	-0.05	0.00	-0.06
W	ft/s	-2.03	-2.28	-4.73	-6.21
Thrust_1	lb	1220.93	790.52	1411.35	886.22
C_{T1}	--	0.0023	0.0015	0.0026	0.0017
δ_{long}	In	5.60	4.45	5.65	4.55
δ_{lat}	In	4.80	4.80	4.80	4.80
δ_{ped}	In	2.50	2.50	2.50	2.50
λ_2	--	0.6502	0.6496	0.7002	0.6994
$\beta_{0,2}$	deg	1.39	2.07	1.46	2.29
$\beta_{1s,2}$	deg	1.01	-0.16	1.26	-0.16
$\beta_{1c,2}$	deg	2.50	1.48	2.87	1.49
$\theta_{0,2}$	deg	76.78	47.73	78.91	52.17
θ_0	deg	76.78	47.73	78.91	52.17
Thrust_2	lb	1220.93	790.52	1411.35	886.23
C_{T2}	--	0.0023	0.0015	0.0026	0.0017

Table C-2: Airplane Mode, 517 RPM (cont.)

140 kts

Math Model

	X force	*Y* force	*Z* force	Roll (*L*)	Pitch (*M*)	Yaw (*N*)
Fuselage	12.86	0.00	-928.48	0.00	5277.64	0.00
Wing	600.41	0.00	-12719.07	0.00	5906.02	0.00
Horizontal Tail	-12.69	0.00	-177.73	0.00	-3851.55	0.00
Vertical Tail #1	-11.91	0.00	0.00	0.00	41.30	76.23
Vertical Tail #2	-11.91	0.00	0.00	0.00	41.30	-76.23
Airframe	576.75	0.00	-13825.28	0.00	7414.71	0.00
Left Rotor (*MR*2)	545.10	-24.24	466.30	-7559.91	-3707.36	8715.67
Right Rotor (*MR*1)	545.10	24.24	466.30	7559.91	-3707.36	-8715.67
Total Rotor	1090.19	0.00	932.59	0.00	-7414.71	0.00
Total Aircraft (Body Axis)	1666.95	0.00	-12892.68	0.00	0.00	0.00

GTRS

	X force	*Y* force	*Z* force	Roll (*L*)	Pitch (*M*)	Yaw (*N*)
Fuselage	-100.26	0	-915.57	0	4827.38	0
Wing	573.88	0.00	-11291.42	0.00	4005.61	0.00
Horizontal Tail	-23.58	0	-359.39	0	146.32	0
Vertical Tail #1	-9.94	0	0.00	0	34.87	-63.762
Vertical Tail #2	-9.94	0	0.00	0	34.87	63.764
Airframe	343.68	0.00	-12574.47	0.00	1309.84	0.00
Left Rotor (*MR*2)	681.18	47.30	-156.94	6875.87	-839.41	11205.65
Right Rotor (*MR*1)	681.18	-47.30	-156.94	-6875.87	-839.41	-11205.65
Total Rotor	1227.93	0.00	-330.17	0.00	-1309.29	0.00
Total Aircraft (Body Axis)	1571.60	0	-12904.64	0	0.56	0.002

Table C-2: Airplane Mode, 517 RPM (cont.)

160 kts

Math Model

	X force	*Y* force	*Z* force	Roll (*L*)	Pitch (*M*)	Yaw (*N*)
Fuselage	-52.34	0.00	-1018.32	0.00	2716.52	0.00
Wing	176.24	0.00	-12993.73	0.00	6849.91	0.00
Horizontal Tail	-34.03	0.00	-67.98	0.00	-1401.14	0.00
Vertical Tail #1	-15.56	0.00	0.00	0.00	53.95	99.57
Vertical Tail #2	-15.56	0.00	0.00	0.00	53.95	-99.57
Airframe	58.75	0.00	-14080.02	0.00	8273.18	0.00
Left Rotor (*MR*2)	524.03	-30.10	563.61	-9139.42	-4136.59	8352.51
Right Rotor (*MR*1)	524.03	30.10	563.61	9139.42	-4136.59	-8352.51
Total Rotor	1048.07	0.00	1127.23	0.00	-8273.18	0.00
Total Aircraft (Body Axis)	1106.82	0.00	-12952.80	0.00	0.00	0.00

GTRS

	X force	*Y* force	*Z* force	Roll (*L*)	Pitch (*M*)	Yaw (*N*)
Fuselage	-172.57	0	-982.21	0	1946.89	0
Wing	155.58	0	-11523.17	0	4437.72	0
Horizontal Tail	-41.65	0.00	-228.12	0.00	-4874.12	0.00
Vertical Tail #1	-13.94	0.00	0.00	0.00	48.92	-89.46
Vertical Tail #2	-13.94	0.00	0.00	0.00	48.92	89.46
Airframe	-206.49	0	-12740.08	0	1871.40	0
Left Rotor (*MR*2)	681.50	44.491	-104.76	6618.969	-1157.33	11235.614
Right Rotor (*MR*1)	681.50	-44.49	-104.76	-6618.97	-1157.33	-11235.61
Total Rotor	1188.32	0.00	-22.69	0.00	-1870.59	0.00
Total Aircraft (Body Axis)	981.83	0.00	-12962.77	0.00	0.81	0.00

Table C-2: Airplane Mode, 517 RPM (cont.)

180 kts

Math Model

	X force	*Y* force	*Z* force	Roll (*L*)	Pitch (*M*)	Yaw (*N*)
Fuselage	-114.44	0.00	-1115.34	0.00	-233.96	0.00
Wing	-153.72	0.00	-13255.29	0.00	7610.62	0.00
Horizontal Tail	-51.89	0.00	73.03	0.00	1723.59	0.00
Vertical Tail #1	-19.69	0.00	0.00	0.01	68.27	125.97
Vertical Tail #2	-19.69	0.00	0.00	0.01	68.27	-126.06
Airframe	-359.43	0.00	-14297.60	0.02	9236.81	-0.10
Left Rotor (*MR*2)	537.94	-35.57	658.68	-10681.84	-4618.41	8552.82
Right Rotor (*MR*1)	537.93	35.58	658.68	10681.83	-4618.39	-8552.72
Total Rotor	1075.87	0.01	1317.36	-0.02	-9236.81	0.10
Total Aircraft (Body Axis)	716.44	0.02	-12980.24	0.00	0.00	0.00

GTRS

	X force	*Y* force	*Z* force	Roll (*L*)	Pitch (*M*)	Yaw (*N*)
Fuselage	-248.85	0.00	-1070.32	0.00	-1058.59	0.00
Wing	-168.37	0.00	-11741.56	0.00	4622.86	0.00
Horizontal Tail	-50.55	0.00	-65.03	0.00	-1294.71	0.00
Vertical Tail #1	-18.42	0.00	0.00	0.00	64.64	-118.21
Vertical Tail #2	-18.42	0.00	0.00	0.00	64.64	118.21
Airframe	-658.37	0.00	-12882.04	0.00	2736.51	0.00
Left Rotor (*MR*2)	741.77	44.67	-46.82	6611.14	-1634.03	12246.41
Right Rotor (*MR*1)	741.77	-44.67	-46.82	-6611.14	-1634.03	-12246.41
Total Rotor	1262.71	0.00	-103.88	0.00	-2735.69	0.00
Total Aircraft (Body Axis)	604.34	0	-12985.92	-0.001	0.82	0.004

Table C-2: Airplane Mode, 517 RPM (cont.)

200 kts

Math Model

	X force	*Y* force	*Z* force	Roll (*L*)	Pitch (*M*)	Yaw (*N*)
Fuselage	-176.29	0.00	-1220.96	0.00	-3564.49	0.00
Wing	-426.67	0.00	-13516.26	0.00	8264.54	0.00
Horizontal Tail	-67.30	0.00	239.93	0.00	5408.01	0.00
Vertical Tail #1	-24.31	0.00	0.00	0.00	84.29	155.55
Vertical Tail #2	-24.31	0.00	0.00	0.00	84.29	-155.60
Airframe	-718.88	0.00	-14497.29	0.01	10276.65	-0.05
Left Rotor (*MR*2)	576.42	-40.73	752.27	-12199.78	-5138.33	9149.43
Right Rotor (*MR*1)	576.41	40.72	752.27	12199.77	-5138.32	-9149.38
Total Rotor	1152.83	-0.01	1504.53	-0.01	-10276.65	0.05
Total Aircraft (Body Axis)	433.95	0.00	-12992.76	0.00	0.00	0.00

GTRS

	X force	*Y* force	*Z* force	Roll (*L*)	Pitch (*M*)	Yaw (*N*)
Fuselage	-328.14	0.00	-1173.23	0.00	-4323.86	0.00
Wing	-405.25	0	-11977.37	0	4592.67	0
Horizontal Tail	-58.66	0	126.89	0	2911.84	0
Vertical Tail #1	-23.41	0	0.00	0	82.13	-150.201
Vertical Tail #2	-23.41	0	0.00	0	82.13	150.201
Airframe	-1028.55	0	-13027.30	0	3761.93	0
Left Rotor (*MR*2)	821.87	47.20	19.50	6682.80	-2196.87	13592.08
Right Rotor (*MR*1)	821.87	-47.20	19.50	-6682.80	-2196.87	-13592.08
Total Rotor	1371.23	0	31.83	0	-3761.53	0
Total Aircraft (Body Axis)	342.68	0	-12995.46	-0.001	0.40	0

Table C-2: Airplane Mode, 517 RPM (cont.)

220 kts

Math Model

	X force	*Y* force	*Z* force	Roll (*L*)	Pitch (*M*)	Yaw (*N*)
Fuselage	-239.64	0.00	-1335.82	0.00	-7271.63	0.00
Wing	-664.67	0.00	-13781.39	0.00	8855.48	0.00
Horizontal Tail	-81.07	0.00	429.68	0.00	9587.56	0.00
Vertical Tail #1	-29.41	0.00	0.00	-0.01	101.99	188.34
Vertical Tail #2	-29.41	0.00	0.00	-0.01	101.99	-188.15
Airframe	-1044.20	-0.01	-14687.53	-0.03	11375.39	0.19
Left Rotor (*MR*2)	633.57	-45.59	844.72	-13698.73	-5687.67	10047.54
Right Rotor (*MR*1)	633.57	45.55	844.72	13698.76	-5687.72	-10047.73
Total Rotor	1267.13	-0.04	1689.44	0.03	-11375.39	-0.19
Total Aircraft (Body Axis)	222.94	-0.05	-12998.09	0.00	0.00	0.00

GTRS

	X force	*Y* force	*Z* force	Roll (*L*)	Pitch (*M*)	Yaw (*N*)
Fuselage	-410.73	0	-1291.61	0	-7838.43	0
Wing	-585.35	0	-12232.70	0	4404.57	0
Horizontal Tail	-66.17	0	343.32	0	7651.46	0
Vertical Tail #1	-28.90	0	0.00	0	101.39	-185.423
Vertical Tail #2	-28.90	0	0.00	0	101.39	185.423
Airframe	-1348.46	0	-13182.96	0	4922.76	0
Left Rotor (*MR*2)	916.99	52.21	93.99	6845.27	-2832.64	15196.37
Right Rotor (*MR*1)	916.99	-52.21	93.99	-6845.27	-2832.64	-15196.37
Total Rotor	1504.35	0	184.04	0	-4921.91	-0.001
Total Aircraft (Body Axis)	155.89	0	-12998.92	0	0.87	-0.001

Table C-2: Airplane Mode, 517 RPM (cont.)

240 kts

Math Model

	X force	*Y* force	*Z* force	Roll (*L*)	Pitch (*M*)	Yaw (*N*)
Fuselage	-305.55	0.00	-1460.20	0.00	-11354.23	0.00
Wing	-881.29	0.00	-14052.39	0.00	9409.76	0.00
Horizontal Tail	-93.79	0.00	640.44	0.00	14223.51	0.00
Vertical Tail #1	-35.00	0.00	0.00	-0.01	121.38	224.09
Vertical Tail #2	-35.00	0.00	0.00	-0.01	121.38	-223.96
Airframe	-1350.64	-0.01	-14872.15	-0.02	12521.80	0.13
Left Rotor (*MR*2)	705.85	-50.12	936.14	-15180.54	-6260.89	11190.45
Right Rotor (*MR*1)	705.85	50.10	936.15	15180.56	-6260.91	-11190.58
Total Rotor	1411.70	-0.02	1872.29	0.02	-12521.80	-0.13
Total Aircraft (Body Axis)	61.06	-0.02	-12999.86	0.00	0.00	0.00

GTRS

	X force	*Y* force	*Z* force	Roll (*L*)	Pitch (*M*)	Yaw (*N*)
Fuselage	-497.59	0	-1432.56	0	-11458.53	-0.003
Wing	-768.06	0	-12490.07	0	4158.49	0
Horizontal Tail	-71.81	0	575.93	0	12739.56	0
Vertical Tail #1	-34.86	0.00	0.00	0.00	122.31	-223.67
Vertical Tail #2	-34.86	0.00	0.00	0.00	122.31	223.67
Airframe	-1675.50	0.00	-13347.12	0.00	6274.69	0.00
Left Rotor (*MR*2)	1048.03	60.24	173.84	7330.26	-3568.48	17398.42
Right Rotor (*MR*1)	1048.03	-60.24	173.84	-7330.26	-3568.48	-17398.42
Total Rotor	1703.85	0	346.85	0	-6269.85	0
Total Aircraft (Body Axis)	25.35	0.00	-13000.27	0.00	4.84	0.00

Table C-2: Airplane Mode, 517 RPM (cont.)

260 kts

Math Model

	X force	*Y* force	*Z* force	Roll (*L*)	Pitch (*M*)	Yaw (*N*)
Fuselage	-374.92	0.00	-1592.80	0.00	-15841.59	0.00
Wing	-1085.68	0.00	-14304.09	0.00	9930.51	0.00
Horizontal Tail	-105.76	0.00	868.02	0.00	19224.97	0.00
Vertical Tail #1	-41.08	0.00	0.00	0.00	142.45	262.94
Vertical Tail #2	-41.08	0.00	0.00	0.00	142.45	-262.90
Airframe	-1648.51	0.00	-15028.88	-0.01	13598.79	0.03
Left Rotor (*MR*2)	790.52	-54.46	1014.52	-16451.89	-6799.39	12534.16
Right Rotor (*MR*1)	790.52	54.44	1014.53	16451.90	-6799.40	-12534.19
Total Rotor	1581.04	-0.02	2029.05	0.01	-13598.79	-0.03
Total Aircraft (Body Axis)	-67.47	-0.02	-12999.82	0.00	0.00	0.00

GTRS

	X force	*Y* force	*Z* force	Roll (*L*)	Pitch (*M*)	Yaw (*N*)
Fuselage	-596.90	0	-1597.07	0	-15157.05	-0.004
Wing	-977.98	0	-12751.50	0	3901.24	0
Horizontal Tail	-76.66	0	823.01	0	18141.44	0
Vertical Tail #1	-41.36	0.00	0.00	0.00	145.10	-265.36
Vertical Tail #2	-41.36	0.00	0.00	0.00	145.10	265.36
Airframe	-2043.62	0.00	-13524.50	0.00	7856.95	0.00
Left Rotor (*MR*2)	1221.91	71.53	261.32	8230.11	-4428.21	20311.72
Right Rotor (*MR*1)	1221.91	-71.53	261.32	-8230.11	-4428.21	-20311.72
Total Rotor	1983.54	0	524.77	0	-7852.84	0
Total Aircraft (Body Axis)	-60.08	0.00	-12999.73	0.00	4.10	0.00

Table C-2: Airplane Mode, 517 RPM (cont.)

280 kts

Math Model

	X force	*Y* force	*Z* force	Roll (*L*)	Pitch (*M*)	Yaw (*N*)
Fuselage	-448.06	0.00	-1734.30	0.00	-20721.00	0.00
Wing	-1282.69	0.00	-14547.67	0.00	10433.01	0.00
Horizontal Tail	-117.33	0.00	1113.32	0.00	24612.81	0.00
Vertical Tail #1	-47.64	0.00	0.00	0.00	165.21	304.95
Vertical Tail #2	-47.64	0.00	0.00	0.00	165.21	-304.90
Airframe	-1943.36	0.00	-15168.65	-0.01	14655.24	0.04
Left Rotor (*MR*2)	886.24	-59.16	1084.88	-17594.84	-7327.61	14054.69
Right Rotor (*MR*1)	886.22	59.10	1084.89	17594.85	-7327.63	-14054.73
Total Rotor	1772.46	-0.07	2169.77	0.01	-14655.24	-0.04
Total Aircraft (Body Axis)	-170.90	-0.07	-12998.88	0.00	0.00	0.00

GTRS

	X force	*Y* force	*Z* force	Roll (*L*)	Pitch (*M*)	Yaw (*N*)
Fuselage	-706.39	0	-1774.37	0	-19155.09	-0.004
Wing	-1184.38	0	-13052.07	0	3596.44	0
Horizontal Tail	-80.41	0	1094.32	0	24069.07	0
Vertical Tail #1	-48.40	0.00	0.00	0.00	169.83	-310.58
Vertical Tail #2	-48.40	0.00	0.00	0.00	169.83	310.58
Airframe	-2421.29	0.00	-13729.46	0.00	9628.13	0.00
Left Rotor (*MR*2)	1412.52	85.92	362.44	9306.03	-5388.19	23517.17
Right Rotor (*MR*1)	1412.52	-85.92	263.44	-9306.03	-5388.19	-23517.17
Total Rotor	2291.25	0.00	730.21	0.00	-9625.46	0.00
Total Aircraft (Body Axis)	-130.03	0.00	-12999.25	0.00	2.67	0.00

Conversion Mode 15º β_M Input Parameters

Parameter	Units	Values
GW	lbs	13000
β_M	deg	15
Turn Rate	deg/s	0.00
Flight Path Angle	deg	0.00
x_{cg}	ft	24.99
y_{cg}	ft	0.00
z_{cg}	ft	6.73
Ω	rad/s	61.68
Ω	RPM	589.00
δ_{flap}	deg	40.00
I_{xx}	slug ft^2	52487.50
I_{yy}	slug ft^2	21191.40
I_{zz}	slug ft^2	66473.90
I_{xz}	slug ft^2	1207.60

Conversion Mode 15°β_M

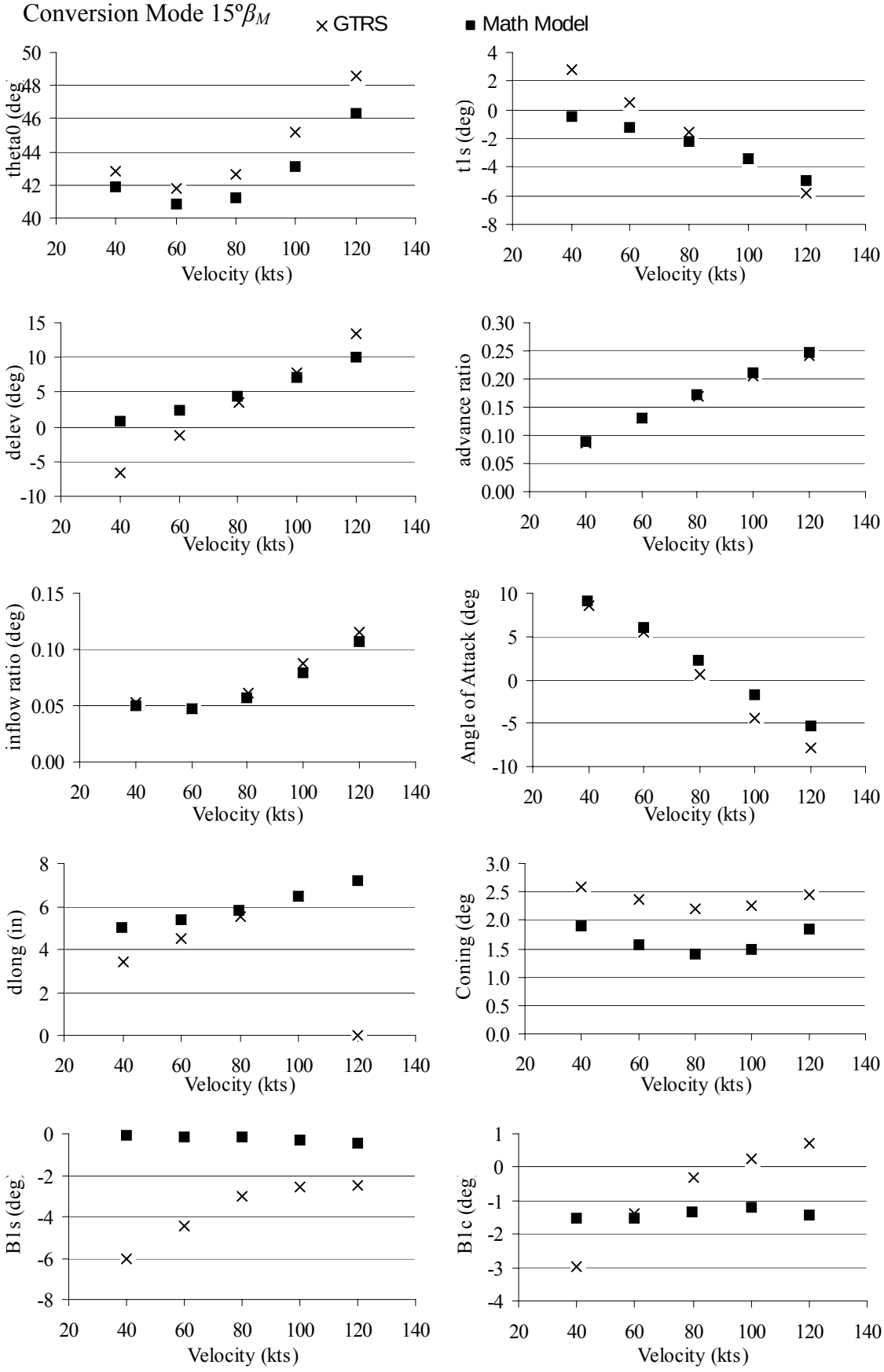

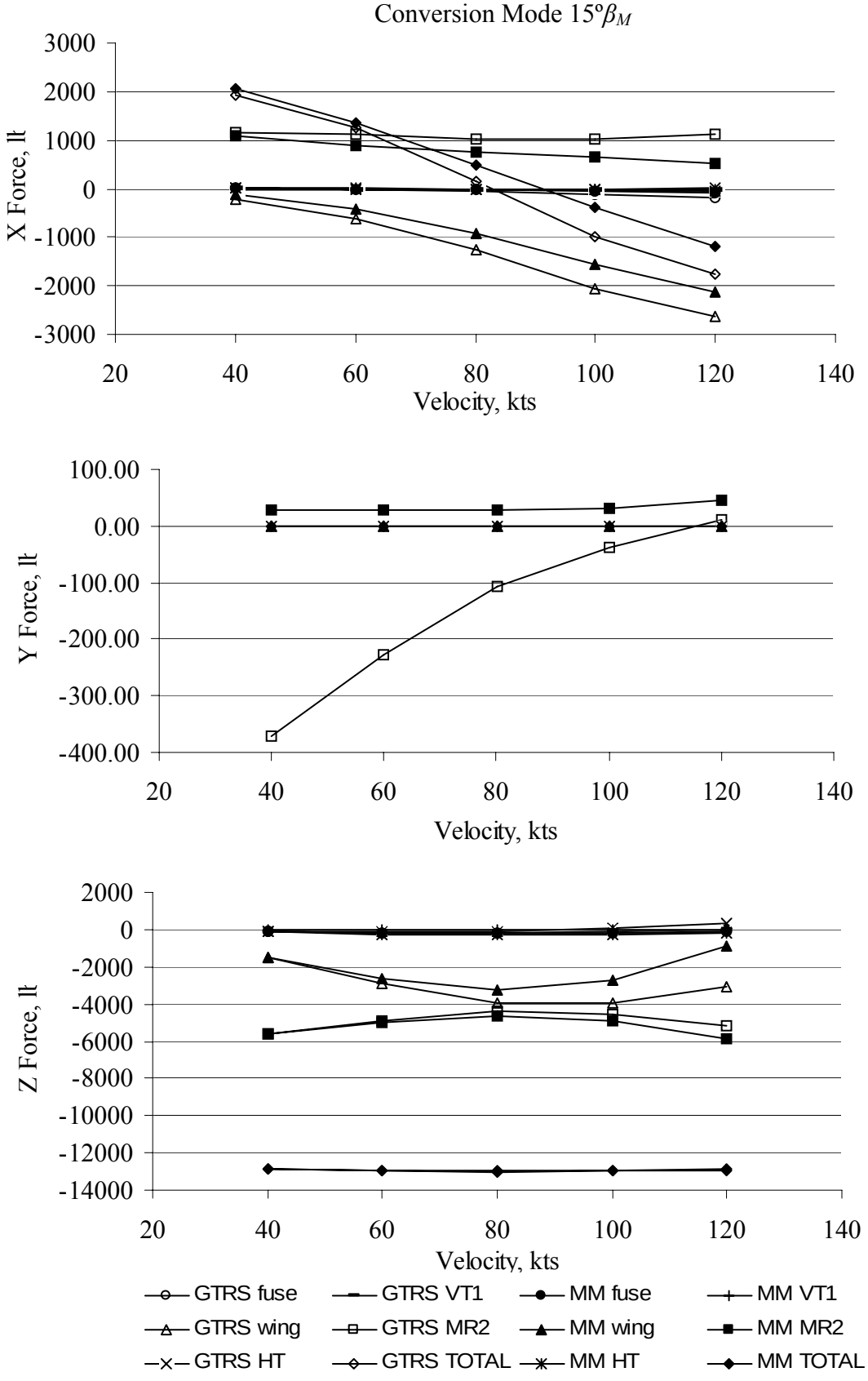
Conversion Mode 15°β_M
X Force, lt
3000
2000
1000
0
-1000
-2000
-3000
20
40
60
80
100
120
140
Velocity, kts
Y Force, lt
100.00
0.00
-100.00
-200.00
-300.00
-400.00
Velocity, kts
Z Force, lt
2000
0
-2000
-4000
-6000
-8000
-10000
-12000
-14000
Velocity, kts
GTRS fuse
GTRS VT1
MM fuse
MM VT1
GTRS wing
GTRS MR2
MM wing
MM MR2
GTRS HT
GTRS TOTAL
MM HT
MM TOTAL

Conversion Mode 15°β_M

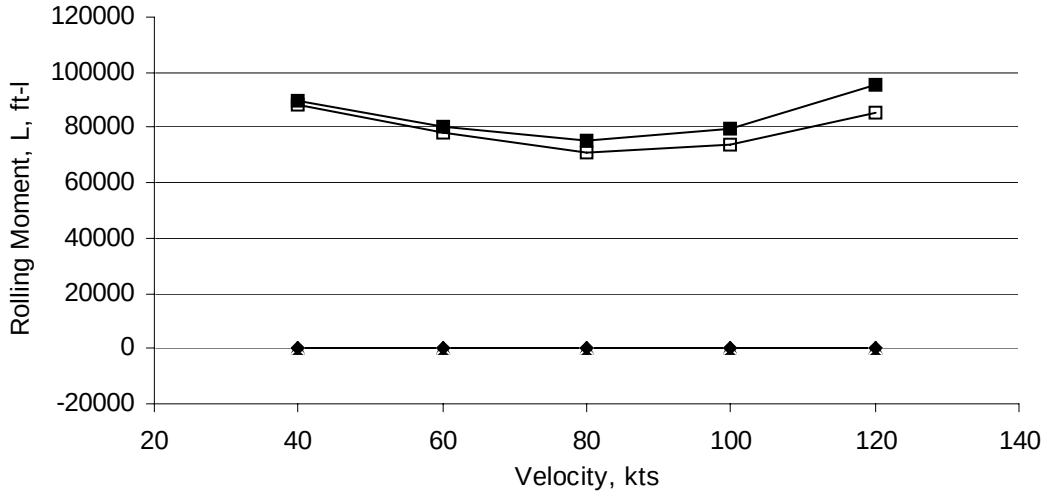

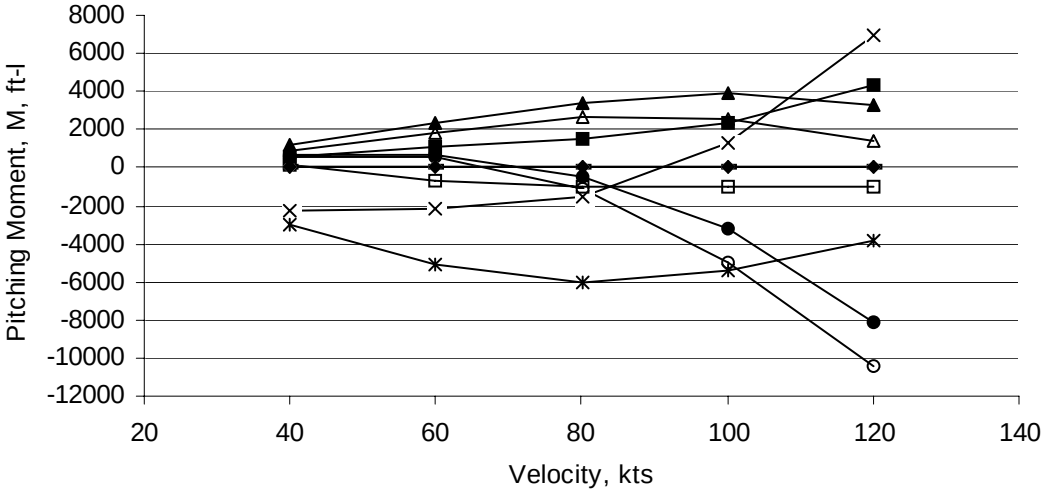

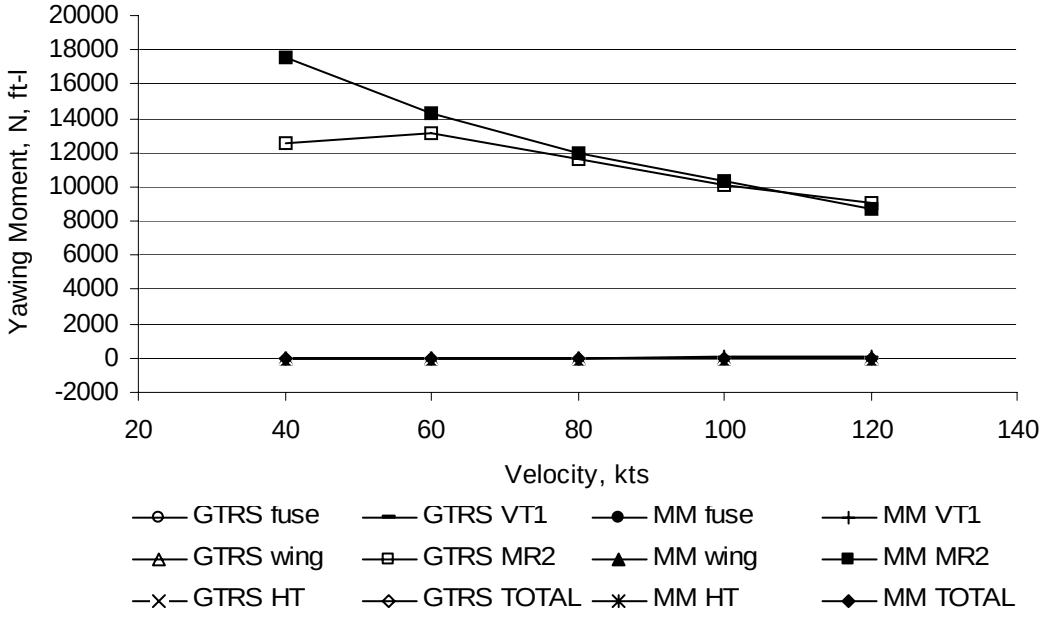

Table C-4: Conversion Mode, 15º β_M

Input Parameter	Units	GTRS	Math Model	GTRS	Math Model	GTRS	Math Model
V	ft/s	--	67.51	--	101.27		135.02
V	kts	40.00	40.00	60.00	60.00	80.00	80.00
φ	deg	0.00	0.00	0.00	0.00	0.00	0.00
θ	deg	8.57	9.10	5.58	5.95	0.66	2.17
α_F	deg	8.57	9.10	5.58	5.95	0.66	2.17
β_F	deg	0.00	0.00	0.00	0.00	0.00	0.00
λ_1	--	0.0525	0.0494	0.0478	0.0467	0.0611	0.0576
p	deg/s	0.00	0.00	0.00	0.00	0.00	0.00
q	deg/s	0.00	0.00	0.00	0.00	0.00	0.00
r	deg/s	0.00	0.00	0.00	0.00	0.00	0.00
pdot	deg/s/s	0.00	0.00	0.00	0.00	0.00	0.00
qdot	deg/s/s	0.01	0.00	0.00	0.00	0.00	0.00
rdot	deg/s/s	0.00	0.00	0.00	0.00	0.00	0.00
$\beta_{0,1}$	deg	2.58	1.91	2.36	1.57	2.21	1.40
$\beta_{1s,1}$	deg	-6.01	-0.09	-4.48	-0.13	-3.06	-0.19
$\beta_{1c,1}$	deg	-2.99	-1.53	-1.38	-1.52	-0.29	-1.33
$\theta_{0,1}$	deg	42.84	41.87	41.80	40.83	42.62	41.24
$\theta_{1s,1}$	deg	2.78	-0.49	0.47	-1.19	-1.56	-2.17
$\theta_{1c,1}$	deg	0.00	0.00	0.00	0.00	0.00	0.00
δ_{rud}	deg	0.00	0.00	0.00	0.00	0.00	0.00
δ_{elev}	deg	-6.60	0.92	-1.22	2.35	3.50	4.38
δ_{ail}	deg	0.00	0.00	0.00	0.00	0.00	0.00
M	--	0.0870	0.0882	0.1296	0.1304	0.1697	0.1709
U	ft/s	66.76	66.66	100.80	100.72	135.00	134.93
V	ft/s	0.00	0.00	0.00	0.00	0.00	0.00
W	ft/s	10.06	10.68	9.85	10.50	1.54	5.11
Thrust_1	lb	5706.89	5666.57	5012.95	5019.13	4520.48	4677.96
C_{T1}	--	0.0082	0.0082	0.0072	0.0072	0.0065	0.0067
δ_{long}	In	3.41	5.02	4.54	5.36	5.54	5.85
δ_{lat}	In	4.80	4.80	4.80	4.80	4.80	4.80
δ_{ped}	In	2.50	2.50	2.50	2.50	2.50	2.50
λ_2	--	0.0525	0.0494	0.0478	0.0467	0.0611	0.0576
$\beta_{0,2}$	deg	2.58	1.91	2.36	1.57	2.21	1.40
$\beta_{1s,2}$	deg	-6.01	-0.09	-4.48	-0.13	-3.06	-0.19
$\beta_{1c,2}$	deg	-2.99	-1.53	-1.38	-1.52	-0.29	-1.33
$\theta_{0,2}$	deg	42.84	1.87	41.80	0.83	42.62	1.24
θ_0	deg	42.84	1.87	41.80	0.83	42.62	1.24
Thrust_2	lb	5706.89	5666.57	5012.95	5019.13	4520.48	4677.96
C_{T2}	--	0.0082	0.0082	0.0072	0.0072	0.0065	0.0067

Table C-4: Conversion Mode, 15º β_M (cont.)

Input Parameter	Units	GTRS	Math Model	GTRS	Math Model
V	ft/s	--	168.78	--	202.53
V	kts	100.00	100.00	120.00	120.00
φ	deg	0.00	0.00	0.00	0.00
θ	deg	-4.39	-1.69	-7.78	-5.29
α_F	deg	-4.39	-1.69	-7.78	-5.29
β_F	deg	0.00	0.00	0.00	0.00
λ_1	--	0.0872	0.0786	0.1155	0.1067
p	deg/s	0.00	0.00	0.00	0.00
q	deg/s	0.00	0.00	0.00	0.00
r	deg/s	0.00	0.00	0.00	0.00
pdot	deg/s/s	0.00	0.00	0.00	0.00
qdot	deg/s/s	0.01	0.00	0.00	0.00
rdot	deg/s/s	0.00	0.00	0.00	0.00
$\beta_{0,1}$	deg	2.24	1.48	2.45	1.85
$\beta_{1s,1}$	deg	-2.58	-0.28	-2.52	-0.44
$\beta_{1c,1}$	deg	0.24	-1.21	0.74	-1.43
$\theta_{0,1}$	deg	45.14	43.13	48.59	46.29
$\theta_{1s,1}$	deg	-3.43	-3.45	-5.84	-4.95
$\theta_{1c,1}$	deg	0.00	0.00	0.00	0.00
δ_{rud}	deg	0.00	0.00	0.00	0.00
δ_{elev}	deg	7.87	7.02	13.48	10.13
δ_{ail}	deg	0.00	0.00	0.00	0.00
M	--	0.2065	0.2098	0.2422	0.2475
U	ft/s	168.30	168.70	200.70	201.67
V	ft/s	0.00	0.00	0.00	0.00
W	ft/s	-12.92	-4.97	-27.41	-18.66
Thrust_1	lb	4627.42	4904.32	5274.38	5829.65
C_{T1}	--	0.0067	0.0071	0.0076	0.0084
δ_{long}	In	6.46	6.48	0.00	7.23
δ_{lat}	In	4.80	4.80	8.03	4.80
δ_{ped}	In	2.50	2.50	4.80	2.50
λ_2	--	0.0872	0.0786	0.1155	0.1067
$\beta_{0,2}$	deg	2.24	1.48	2.45	1.85
$\beta_{1s,2}$	deg	-2.58	-0.28	-2.52	-0.44
$\beta_{1c,2}$	deg	0.24	-1.21	0.74	-1.43
$\theta_{0,2}$	deg	45.14	3.13	48.59	6.29
θ_0	deg	45.14	3.13	48.59	6.29
Thrust_2	lb	4627.42	4904.32	5274.38	5829.65
C_{T2}	--	0.0067	0.0071	0.0076	0.0084

Table C-4: Conversion Mode, 15º β_M (cont.)

40 kts

Math Model

	X force	*Y* force	*Z* force	Roll (*L*)	Pitch (*M*)	Yaw (*N*)
Fuselage	4.69	0.00	-84.12	0.00	624.66	0.00
Wing	-123.31	0.00	-1464.87	0.00	1164.51	0.00
Horizontal Tail	4.99	0.00	-136.39	0.00	-2970.68	0.00
Vertical Tail #1	-0.97	0.00	0.00	0.00	2.79	6.22
Vertical Tail #2	-0.97	0.00	0.00	0.00	2.79	-6.22
Airframe	-115.57	0.00	-1685.39	0.00	-1175.94	0.00
Left Rotor (*MR*2)	1086.10	28.55	-5575.45	89966.95	587.97	17528.03
Right Rotor (*MR*1)	1086.10	-28.55	-5575.45	-89966.95	587.97	-17528.03
Total Rotor	2172.20	0.00	-11150.90	0.00	1175.94	0.00
Total Aircraft (Body Axis)	2056.62	0.00	-12836.29	0.00	0.00	0.00

GTRS

	X force	*Y* force	*Z* force	Roll (*L*)	Pitch (*M*)	Yaw (*N*)
Fuselage	-6.63	0.00	-83.09	0.00	541.68	0.00
Wing	-225.88	0.00	-1462.84	0.00	881.30	0.00
Horizontal Tail	5.88	0.00	-105.73	0.00	-2302.90	0.00
Vertical Tail #1	0.77	0.00	0.00	0.00	-2.23	4.93
Vertical Tail #2	0.77	0.00	0.00	0.00	-2.23	-4.93
Airframe	-315.80	0.00	-1688.47	0.00	-739.69	0.00
Left Rotor (*MR*2)	1157.63	-370.02	-5592.20	88263.93	191.31	12558.47
Right Rotor (*MR*1)	1157.63	370.02	-5592.20	-88263.93	191.31	-12558.46
Total Rotor	2252.86	0.00	-11166.31	0.00	742.04	0.01
Total Aircraft (Body Axis)	1937.06	0.00	-12854.78	0.00	2.35	0.01

Table C-4: Conversion Mode, 15º β_M (cont.)

60 kts

Math Model

	X force	*Y* force	*Z* force	Roll (*L*)	Pitch (*M*)	Yaw (*N*)
Fuselage	-3.47	0.00	-155.01	0.00	655.28	0.00
Wing	-421.00	0.00	-2623.21	0.00	2338.91	0.00
Horizontal Tail	0.53	0.00	-235.26	0.00	-5108.87	0.00
Vertical Tail #1	-2.19	0.00	0.00	0.00	6.27	14.00
Vertical Tail #2	-2.19	0.00	0.00	0.00	6.27	-14.00
Airframe	-428.32	0.00	-3013.48	0.00	-2102.13	0.00
Left Rotor (*MR*2)	888.07	28.80	-4958.23	80045.39	1051.07	14343.86
Right Rotor (*MR*1)	888.07	-28.80	-4958.23	-80045.39	1051.07	-14343.86
Total Rotor	1776.14	0.00	-9916.46	0.00	2102.13	0.00
Total Aircraft (Body Axis)	1347.82	0.00	-12929.94	0.00	0.00	0.00

GTRS

	X force	*Y* force	*Z* force	Roll (*L*)	Pitch (*M*)	Yaw (*N*)
Fuselage	-21.80	0.00	-152.54	0.00	575.28	0.00
Wing	-609.34	0.00	-2901.06	0.00	1827.12	0.00
Horizontal Tail	-4.22	0.00	-98.50	0.00	-2127.47	0.00
Vertical Tail #1	-0.52	0.00	0.00	0.00	1.52	-3.36
Vertical Tail #2	-0.52	0.00	0.00	0.00	1.52	3.36
Airframe	-814.68	0.00	-3176.12	0.00	562.87	0.00
Left Rotor (*MR*2)	1114.05	-227.15	-4887.93	77819.48	-727.19	13108.65
Right Rotor (*MR*1)	1114.05	227.15	-4887.93	-77819.48	-727.19	-13108.65
Total Rotor	2079.37	0.00	-9762.15	0.00	-562.42	0.00
Total Aircraft (Body Axis)	1264.69	0.00	-12938.27	0.00	0.45	0.00

Table C-4: Conversion Mode, 15º β_M (cont.)

80 kts

Math Model

	X force	*Y* force	*Z* force	Roll (*L*)	Pitch (*M*)	Yaw (*N*)
Fuselage	-27.15	0.00	-200.46	0.00	-436.31	0.00
Wing	-938.25	0.00	-3221.53	0.00	3405.94	0.00
Horizontal Tail	-12.68	0.00	-278.63	0.00	-6025.89	0.00
Vertical Tail #1	-3.89	0.00	0.00	0.00	11.15	24.89
Vertical Tail #2	-3.89	0.00	0.00	0.00	11.15	-24.89
Airframe	-985.86	0.00	-3700.62	0.00	-3033.97	0.00
Left Rotor (*MR*2)	738.74	28.21	-4645.04	75017.95	1516.98	11943.85
Right Rotor (*MR*1)	738.74	-28.21	-4645.04	-75017.95	1516.98	-11943.85
Total Rotor	1477.47	0.00	-9290.08	0.00	3033.97	0.00
Total Aircraft (Body Axis)	491.61	0.00	-12990.70	0.00	0.00	0.00

GTRS

	X force	*Y* force	*Z* force	Roll (*L*)	Pitch (*M*)	Yaw (*N*)
Fuselage	-54.38	0.00	-170.13	0.00	-1059.48	0.00
Wing	-1271.90	0.00	-3966.06	0.00	2622.15	0.00
Horizontal Tail	-12.68	0.00	-72.51	0.00	-1548.51	0.00
Vertical Tail #1	-2.34	0.00	0.00	0.00	6.80	-15.00
Vertical Tail #2	-2.34	0.00	0.00	0.00	6.80	15.00
Airframe	-1650.81	0.00	-4214.12	0.01	519.08	0.00
Left Rotor (*MR*2)	1027.53	-106.64	-4403.37	71111.53	-1027.13	11649.07
Right Rotor (*MR*1)	1027.53	-106.64	-4403.36	-71111.42	-1027.13	-11649.06
Total Rotor	1799.54	0.00	-8785.22	0.11	-519.39	0.02
Total Aircraft (Body Axis)	148.73	0.00	-12999.34	0.12	-0.31	0.02

Table C-4: Conversion Mode, 15º β_M (cont.)

100 kts

Math Model

	X force	*Y* force	*Z* force	Roll (*L*)	Pitch (*M*)	Yaw (*N*)
Fuselage	-59.90	0.00	-191.70	0.00	-3229.52	0.00
Wing	-1564.67	0.00	-2738.77	0.00	3867.10	0.00
Horizontal Tail	-27.87	0.00	-252.80	0.00	-5436.64	0.00
Vertical Tail #1	-6.08	0.00	0.00	0.00	17.42	38.89
Vertical Tail #2	-6.08	0.00	0.00	0.00	17.42	-38.89
Airframe	-1664.60	0.00	-3183.26	0.00	-4764.22	0.00
Left Rotor (*MR*2)	641.07	31.77	-4905.55	79265.17	2382.11	10384.08
Right Rotor (*MR*1)	641.07	-31.77	-4905.55	-79265.17	2382.11	-10384.08
Total Rotor	1282.14	0.00	-9811.11	0.00	4764.22	0.00
Total Aircraft (Body Axis)	-382.46	0.00	-12994.37	0.00	0.00	0.00

GTRS

	X force	*Y* force	*Z* force	Roll (*L*)	Pitch (*M*)	Yaw (*N*)
Fuselage	-106.91	0.00	-102.36	0.00	-4990.42	0.00
Wing	-2050.60	0.00	-3966.88	-0.01	2561.77	0.00
Horizontal Tail	-11.03	0.00	60.88	0.00	1340.17	0.00
Vertical Tail #1	-4.90	0.00	0.00	0.00	14.26	-31.47
Vertical Tail #2	-4.90	0.00	0.00	0.00	14.26	31.47
Airframe	-2651.43	0.00	-3975.74	-0.01	-302.78	0.00
Left Rotor (*MR*2)	1014.40	-39.13	-4518.84	73871.19	-952.99	10137.56
Right Rotor (*MR*1)	1014.40	39.13	-4518.84	-73871.19	-952.99	-10137.56
Total Rotor	1656.17	0.00	-8985.86	0.00	307.94	0.00
Total Aircraft (Body Axis)	-995.26	0.00	-12961.59	-0.01	5.16	0.00

Table C-4: Conversion Mode, 15º β_M (cont.)

120 kts

Math Model

	X force	*Y* force	*Z* force	Roll (*L*)	Pitch (*M*)	Yaw (*N*)
Fuselage	-88.79	0.00	-111.94	0.00	-8079.41	0.00
Wing	-2120.18	0.00	-868.03	0.00	3283.05	0.00
Horizontal Tail	-38.10	0.00	-179.94	0.00	-3835.74	0.00
Vertical Tail #1	-8.75	0.00	0.00	0.00	25.09	56.01
Vertical Tail #2	-8.75	0.00	0.00	0.00	25.09	-56.01
Airframe	-2264.57	0.00	-1159.92	0.00	-8581.92	0.00
Left Rotor (*MR*2)	533.34	44.07	-5892.39	95279.85	4290.96	8678.32
Right Rotor (*MR*1)	533.34	-44.07	-5892.39	-95279.85	4290.96	-8678.32
Total Rotor	1066.69	0.00	-11784.77	0.00	8581.92	0.00
Total Aircraft (Body Axis)	-1197.89	0.00	-12944.69	0.00	0.00	0.00

GTRS

	X force	*Y* force	*Z* force	Roll (*L*)	Pitch (*M*)	Yaw (*N*)
Fuselage	-191.24	0.00	16.66	0.00	-10426.80	0.00
Wing	-2645.27	0.00	-3070.44	0.00	1390.49	0.00
Horizontal Tail	25.14	0.00	323.35	0.00	6963.26	0.00
Vertical Tail #1	-8.67	0.00	0.00	0.00	25.19	-55.60
Vertical Tail #2	-8.67	0.00	0.00	0.00	25.19	55.60
Airframe	-3500.22	0.00	-2652.98	0.00	-947.52	0.00
Left Rotor (*MR*2)	1122.90	11.43	-5160.56	85336.41	-1010.31	9086.83
Right Rotor (*MR*1)	1122.90	-11.43	-5160.56	-85336.41	-1010.31	-9086.83
Total Rotor	1741.25	0.00	-10227.39	0.00	0.00	0.00
Total Aircraft (Body Axis)	-1758.97	0.00	-12880.37	0.00	0.00	0.00

Conversion Mode 30º β_M Input Parameters

Parameter	Units	Values
GW	lbs	13000
β_M	deg	30
Turn Rate	deg/s	0.00
Flight Path Angle	deg	0.00
x_{cg}	ft	24.9
y_{cg}	ft	0.0
z_{cg}	ft	6.6
Ω	rad/s	61.68
Ω	RPM	589
δ_{flap}	deg	20.00
I_{xx}	slug ft^2	52180
I_{yy}	slug ft^2	21023
I_{zz}	slug ft^2	66613
I_{xz}	slug ft^2	1181

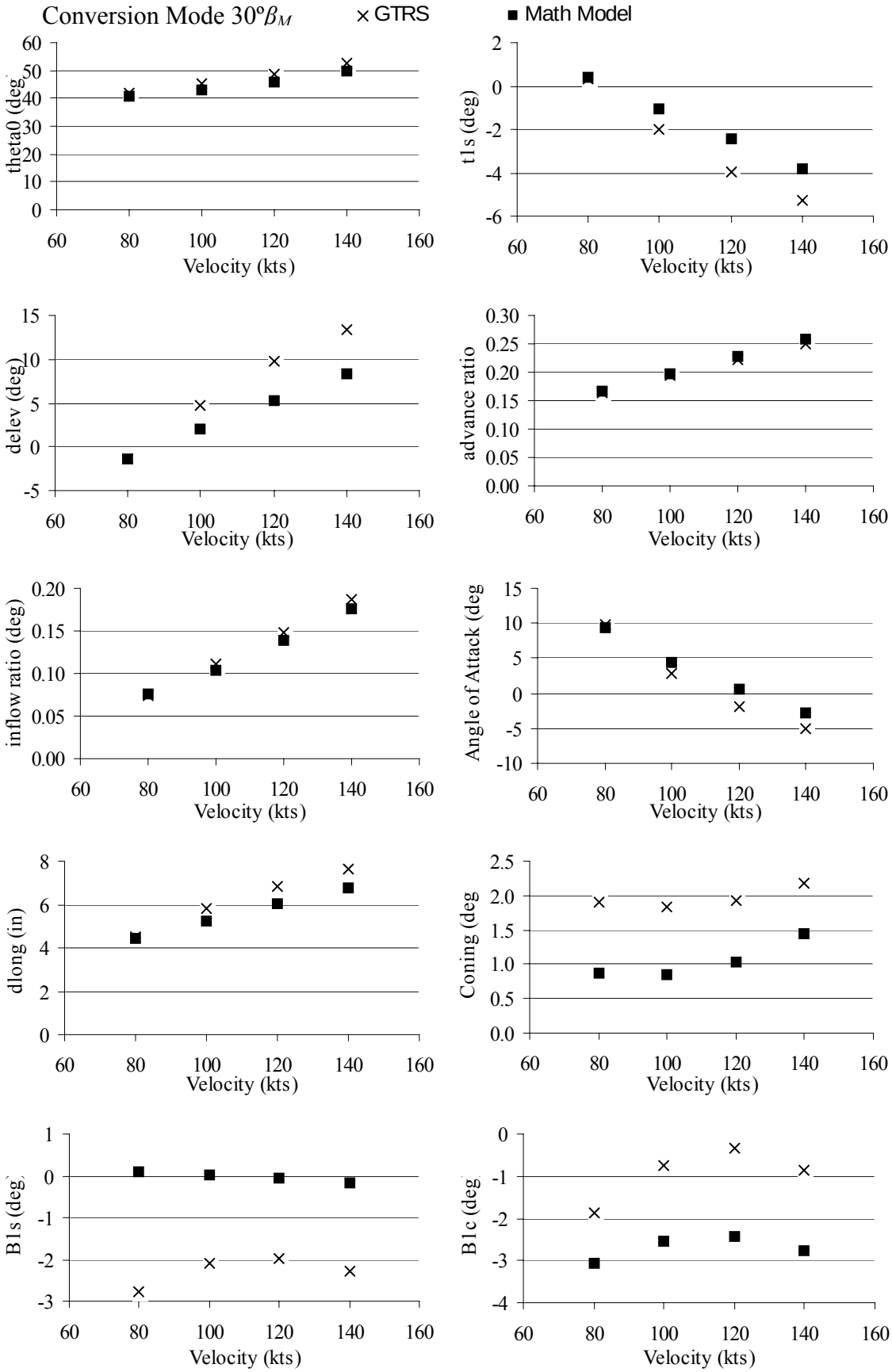
Conversion Mode 30°β_M
× GTRS
■ Math Model
theta0 (deg)
t1s (deg)
delev (deg)
advance ratio
inflow ratio (deg)
Angle of Attack (deg
dlong (in)
Coning (deg
B1s (deg)
B1c (deg)
Velocity (kts)

Conversion Mode 30°β_M

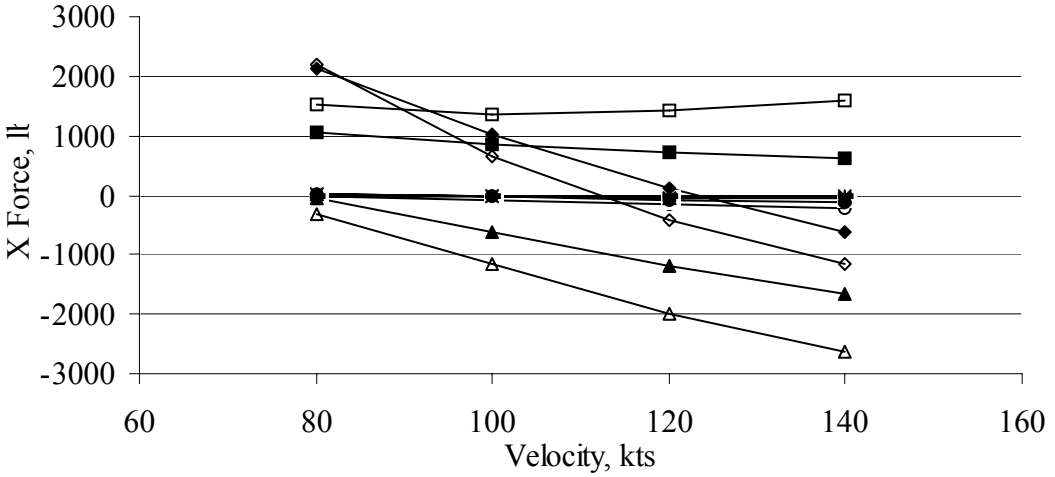

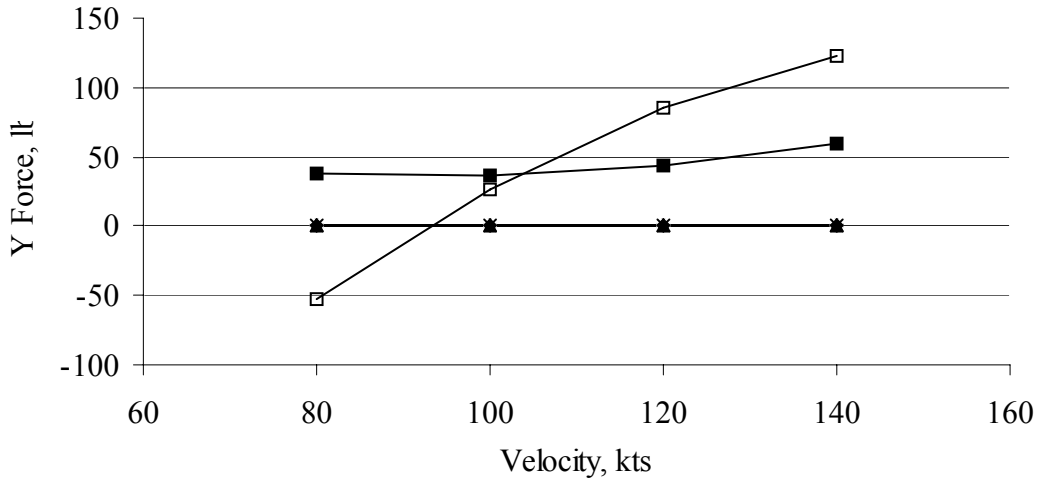

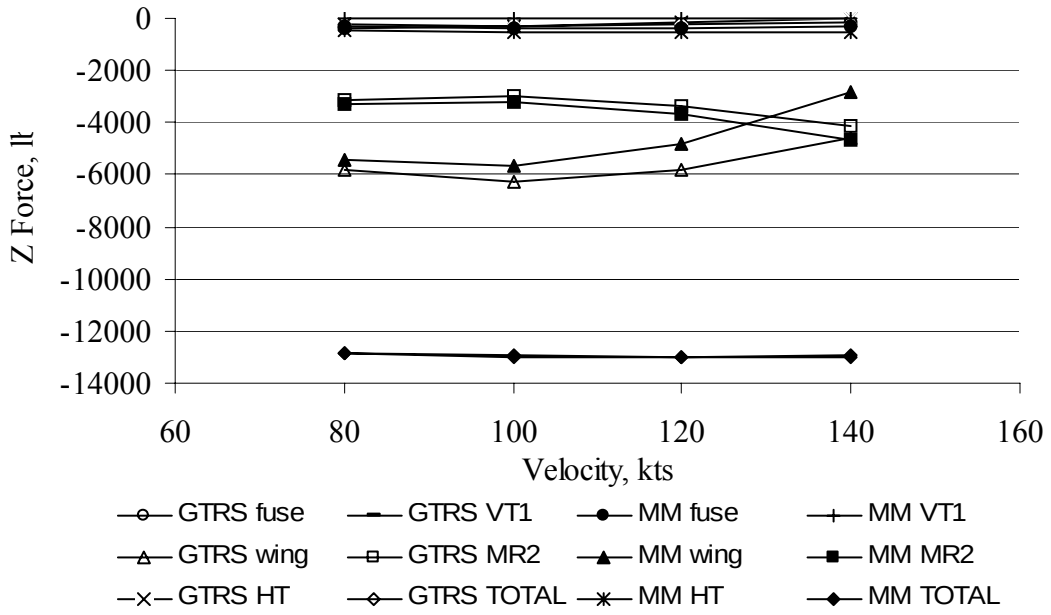

Conversion Mode 30°β_M

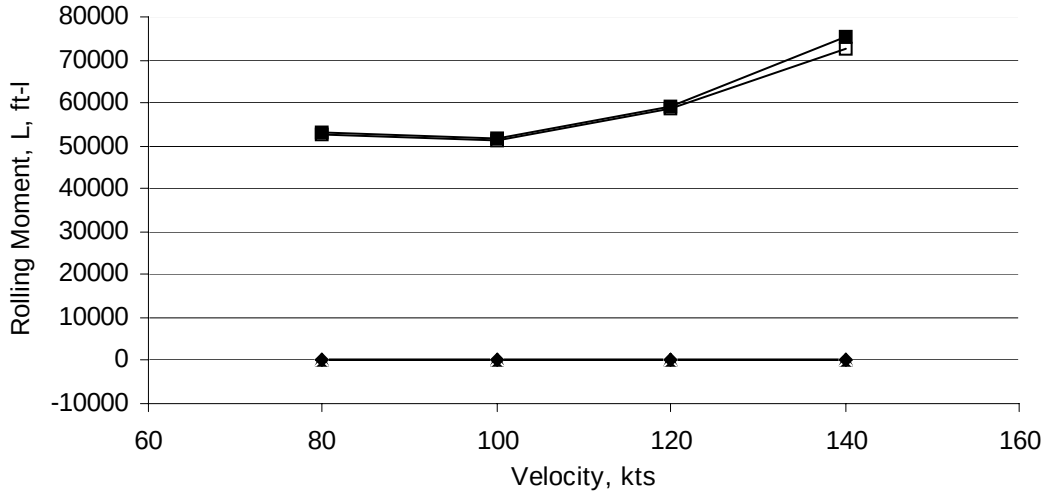

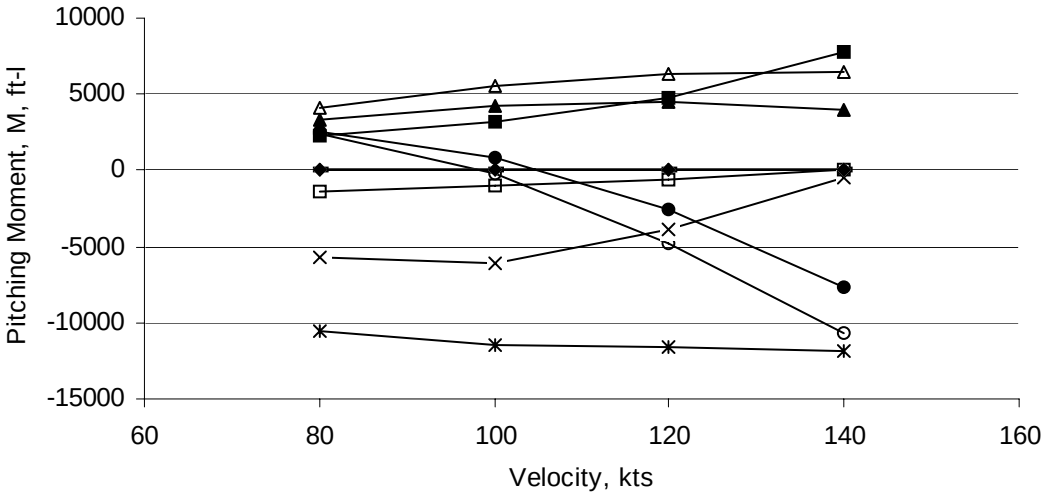

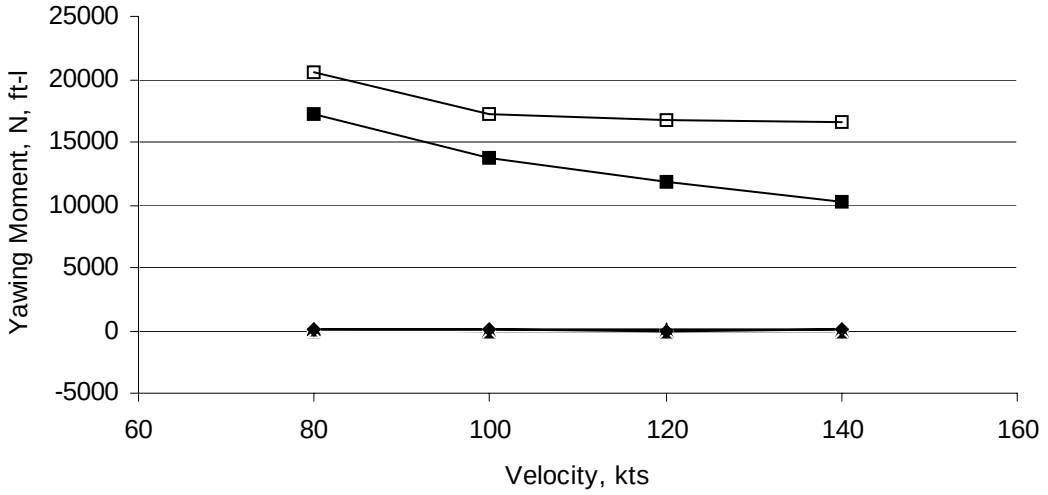

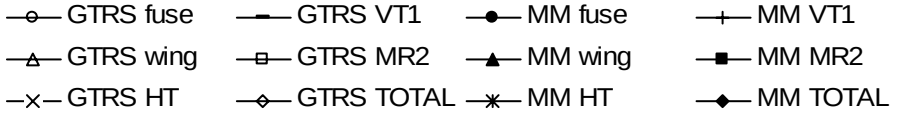

Table C-5: Conversion Mode, 30º β_M

Input Parameter	Units	GTRS	Math Model	GTRS	Math Model
V	ft/s	--	135.02	--	168.78
V	kts	80.00	80.00	100.00	100.00
φ	deg	0.00	0.00	0.00	0.00
θ	deg	9.72	9.39	2.85	4.52
α_F	deg	9.72	9.39	2.85	4.52
β_F	deg	0.00	0.00	0.00	0.00
λ_1	--	0.0745	0.0750	0.1103	0.1044
p	deg/s	0.00	0.00	0.00	0.00
q	deg/s	0.00	0.00	0.00	0.00
r	deg/s	0.00	0.00	0.00	0.00
pdot	deg/s/s	0.00	0.00	0.00	0.00
qdot	deg/s/s	-0.02	0.00	-0.03	0.00
rdot	deg/s/s	0.00	0.00	0.00	0.00
$\beta_{0,1}$	deg	1.89	0.88	1.83	0.84
$\beta_{1s,1}$	deg	-2.78	0.09	-2.10	0.02
$\beta_{1c,1}$	deg	-1.86	-3.06	-0.75	-2.54
$\theta_{0,1}$	deg	42.13	40.62	45.12	42.87
$\theta_{1s,1}$	deg	0.35	0.43	-2.00	-1.04
$\theta_{1c,1}$	deg	0.00	0.00	0.00	0.00
δ_{rud}	deg	0.00	0.00	0.00	0.00
δ_{elev}	deg	-1.45	-1.47	4.69	1.96
δ_{ail}	deg	0.00	0.00	0.00	0.00
M	--	0.1643	0.1660	0.1948	0.1982
U	ft/s	133.10	133.21	168.60	168.25
V	ft/s	0.00	0.00	0.00	0.00
W	ft/s	22.79	22.03	8.40	13.30
Thrust_1	lb	3512.68	3381.00	3296.78	3192.53
C_{T1}	--	0.0051	0.0049	0.0048	0.0046
δ_{long}	In	4.49	4.45	5.79	5.27
δ_{lat}	In	4.80	4.80	4.80	4.80
δ_{ped}	In	2.50	2.50	2.50	2.50
λ_2	--	0.0745	0.0750	0.1103	0.1044
$\beta_{0,2}$	deg	1.89	0.88	1.83	0.84
$\beta_{1s,2}$	deg	-2.78	0.09	-2.10	0.02
$\beta_{1c,2}$	deg	-1.86	-3.06	-0.75	-2.54
$\theta_{0,2}$	deg	42.13	0.62	45.12	2.87
θ_0	deg	42.13	0.62	45.12	2.87
Thrust_2	lb	3512.68	3381.00	3296.78	3192.53
C_{T2}	--	0.0051	0.0049	0.0048	0.0046

Table C-5: Conversion Mode, 30º β_M (cont.)

Input Parameter	Units	GTRS	Math Model	GTRS	Math Model
V	ft/s	--	202.53	--	236.29
V	kts	120.00	120.00	140.00	140.00
φ	deg	0.00	0.00	0.00	0.00
θ	deg	-1.92	0.55	-5.13	-2.70
α_F	deg	-1.92	0.55	-5.13	-2.70
β_F	deg	0.00	0.00	0.00	0.00
λ_1	--	0.1486	0.1386	0.1864	0.1756
p	deg/s	0.00	0.00	0.00	0.00
q	deg/s	0.00	0.00	0.00	0.00
r	deg/s	0.00	0.00	0.00	0.00
pdot	deg/s/s	0.00	0.00	0.00	0.00
qdot	deg/s/s	0.00	0.00	0.00	0.00
rdot	deg/s/s	0.00	0.00	0.00	0.00
$\beta_{0,1}$	deg	1.94	1.03	2.17	1.44
$\beta_{1s,1}$	deg	-1.99	-0.06	-2.30	-0.19
$\beta_{1c,1}$	deg	-0.35	-2.44	-0.86	-2.75
$\theta_{0,1}$	deg	48.72	46.07	52.40	49.93
$\theta_{1s,1}$	deg	-3.95	-2.44	-5.30	-3.79
$\theta_{1c,1}$	deg	0.00	0.00	0.00	0.00
δ_{rud}	deg	0.00	0.00	0.00	0.00
δ_{elev}	deg	9.81	5.20	13.35	8.33
δ_{ail}	deg	0.00	0.00	0.00	0.00
M	--	0.2230	0.2288	0.2507	0.2582
U	ft/s	202.40	202.52	235.30	236.03
V	ft/s	0.00	0.00	0.00	0.00
W	ft/s	-6.78	1.94	-21.13	-11.13
Thrust_1	lb	3655.53	3517.59	4389.78	4341.56
C_{T1}	--	0.0053	0.0051	0.0063	0.0063
δ_{long}	In	6.87	6.05	7.62	6.80
δ_{lat}	In	4.80	4.80	4.80	4.80
δ_{ped}	In	2.50	2.50	2.50	2.50
λ_2	--	0.1486	0.1386	0.1864	0.1756
$\beta_{0,2}$	deg	1.94	1.03	2.17	1.44
$\beta_{1s,2}$	deg	-1.99	-0.06	-2.30	-0.19
$\beta_{1c,2}$	deg	-0.35	-2.44	-0.86	-2.75
$\theta_{0,2}$	deg	48.72	6.07	52.40	9.93
θ_0	deg	48.72	6.07	52.40	9.93
Thrust_2	lb	3655.53	3517.59	4389.78	4341.56
C_{T2}	--	0.0053	0.0051	0.0063	0.0063

Table C-5: Conversion Mode, 30º β_M (cont.)

80 kts

Math Model

	X force	*Y* force	*Z* force	Roll (*L*)	Pitch (*M*)	Yaw (*N*)
Fuselage	21.39	0.00	-342.00	0.00	2590.47	0.00
Wing	-49.66	0.00	-5427.85	0.00	3315.37	0.00
Horizontal Tail	24.11	0.00	-479.53	0.00	-10501.88	0.00
Vertical Tail #1	-3.89	0.00	0.00	0.00	11.53	24.89
Vertical Tail #2	-3.89	0.00	0.00	0.00	11.53	-24.89
Airframe	-11.94	0.00	-6249.37	0.00	-4572.98	0.00
Left Rotor (*MR*2)	1066.70	38.62	-3288.18	53132.75	2286.49	17244.36
Right Rotor (*MR*1)	1066.70	-38.62	-3288.18	-53132.75	2286.49	-17244.36
Total Rotor	2133.40	0.00	-6576.36	0.00	4572.98	0.00
Total Aircraft (Body Axis)	2121.46	0.00	-12825.73	0.00	0.00	0.00

GTRS

	X force	*Y* force	*Z* force	Roll (*L*)	Pitch (*M*)	Yaw (*N*)
Fuselage	-24.44	0	-356.42	0	2386.50	0
Wing	-312.54	0	-5777.32	0	4086.71	0
Horizontal Tail	3.64	0	-260.16	0	-5670.25	0
Vertical Tail #1	-1.76	0	0.00	0	5.27	-11.261
Vertical Tail #2	-1.76	0	0.00	0	5.27	11.261
Airframe	-636.34	0	-6451.66	0	1315.82	0
Left Rotor (*MR*2)	1531.35	-52.275	-3171.41	52629.46	-1363.51	20498.03
Right Rotor (*MR*1)	1531.35	52.275	-3171.41	-52629.46	-1363.51	-20498.03
Total Rotor	2826.90	0	-6365.90	0	-1322.36	0
Total Aircraft (Body Axis)	2190.56	0	-12817.55	0	-6.53	0

Table C-5: Conversion Mode, 30º β_M (cont.)

100 kts

Math Model

	X force	*Y* force	*Z* force	Roll (*L*)	Pitch (*M*)	Yaw (*N*)
Fuselage	-23.85	0.00	-386.54	0.00	839.79	0.00
Wing	-626.60	0.00	-5651.49	0.00	4235.74	0.00
Horizontal Tail	-4.72	0.00	-525.53	0.00	-11448.11	0.00
Vertical Tail #1	-6.08	0.00	0.00	0.00	18.01	38.89
Vertical Tail #2	-6.08	0.00	0.00	0.00	18.01	-38.89
Airframe	-667.32	0.00	-6563.56	0.00	-6336.57	0.00
Left Rotor (*MR*2)	845.96	36.84	-3198.00	51690.88	3168.28	13698.01
Right Rotor (*MR*1)	845.96	-36.84	-3198.00	-51690.88	3168.28	-13698.01
Total Rotor	1691.91	0.00	-6396.00	0.00	6336.57	0.00
Total Aircraft (Body Axis)	1024.60	0.00	-12959.56	0.00	0.00	0.00

GTRS

	X force	*Y* force	*Z* force	Roll (*L*)	Pitch (*M*)	Yaw (*N*)
Fuselage	-75.83	0	-336.32	0	-227.72	-0.001
Wing	-1173.15	0	-6296.61	-0.004	5578.75	0
Horizontal Tail	-22.20	0	-279.70	0	-6045.34	0
Vertical Tail #1	-5.03	0	0.00	0	15.11	-32.271
Vertical Tail #2	-5.03	0	0.00	0	15.11	32.271
Airframe	-1751.88	0	-6941.11	-0.004	131.64	-0.001
Left Rotor (*MR*2)	1365.26	26.858	-3019.58	51246.89	-1012.92	17231.67
Right Rotor (*MR*1)	1365.26	-26.858	-3019.58	-51246.89	-1012.92	-17231.67
Total Rotor	2403.16	0	-6041.80	0	-141.42	0
Total Aircraft (Body Axis)	651.27	0	-12982.91	-0.004	-9.78	-0.001

Table C-5: Conversion Mode, 30º β_M (cont.)

120 kts

Math Model

	X force	*Y* force	*Z* force	Roll (*L*)	Pitch (*M*)	Yaw (*N*)
Fuselage	-74.49	0.00	-377.72	0.00	-2557.38	0.00
Wing	-1201.95	0.00	-4800.70	0.00	4511.07	0.00
Horizontal Tail	-34.42	0.00	-536.17	0.00	-11621.82	0.00
Vertical Tail #1	-8.75	0.00	0.00	0.00	25.93	56.01
Vertical Tail #2	-8.75	0.00	0.00	0.00	25.93	-56.01
Airframe	-1328.36	0.00	-5714.59	0.00	-9616.27	0.00
Left Rotor (*MR*2)	726.35	43.57	-3642.41	58909.93	4808.13	11802.19
Right Rotor (*MR*1)	726.35	-43.57	-3642.41	-58909.93	4808.13	-11802.19
Total Rotor	1452.70	0.00	-7284.82	0.00	9616.27	0.00
Total Aircraft (Body Axis)	124.34	0.00	-12999.41	0.00	0.00	0.00

GTRS

	X force	*Y* force	*Z* force	Roll (*L*)	Pitch (*M*)	Yaw (*N*)
Fuselage	-139.30	0	-263.38	0	-4840.10	-0.001
Wing	-1992.20	0	-5794.07	-0.003	6366.54	0
Horizontal Tail	-37.81	0	-179.56	0	-3835.17	0
Vertical Tail #1	-9.84	0	0.00	0	29.55	-63.106
Vertical Tail #2	-9.84	0	0.00	0	29.55	63.106
Airframe	-2864.95	0	-6220.00	-0.003	-1100.90	-0.001
Left Rotor (*MR*2)	1426.10	85.804	-3399.97	58705.50	-630.18	16711.91
Right Rotor (*MR*1)	1426.10	-85.804	-3399.97	-58705.50	-630.18	-16711.91
Total Rotor	2430.12	0	-6772.71	0	1100.98	0
Total Aircraft (Body Axis)	-434.83	0	-12992.71	-0.003	0.08	-0.001

Table C-5: Conversion Mode, 30º β_M (cont.)

140 kts

Math Model

	X force	*Y* force	*Z* force	Roll (*L*)	Pitch (*M*)	Yaw (*N*)
Fuselage	-121.18	0.00	-312.73	0.00	-7674.08	0.00
Wing	-1657.33	0.00	-2822.33	0.00	3948.18	0.00
Horizontal Tail	-63.31	0.00	-547.53	0.00	-11812.72	0.00
Vertical Tail #1	-11.91	0.00	0.00	0.00	35.30	76.23
Vertical Tail #2	-11.91	0.00	0.00	0.00	35.30	-76.23
Airframe	-1865.64	0.00	-3682.58	0.00	-15468.02	0.00
Left Rotor (*MR*2)	626.52	60.02	-4651.49	75286.13	7734.01	10252.49
Right Rotor (*MR*1)	626.52	-60.02	-4651.49	-75286.13	7734.01	-10252.49
Total Rotor	1253.03	0.00	-9302.97	0.00	15468.02	0.00
Total Aircraft (Body Axis)	-612.61	0.00	-12985.56	0.00	0.00	0.00

GTRS

	X force	*Y* force	*Z* force	Roll (*L*)	Pitch (*M*)	Yaw (*N*)
Fuselage	-222.81	0	-152.37	0	-10735.50	-0.001
Wing	-2641.74	0	-4599.63	0.007	64863442.00	0
Horizontal Tail	-33.03	0	-25.29	0	-486.12	0
Vertical Tail #1	-12.72	0	0.00	0	38.23	-81.64
Vertical Tail #2	-12.72	0	0.00	0	38.23	81.645
Airframe	-3833.68	0	-4711.01	0.006	-3106.78	0.004
Left Rotor (*MR*2)	1598.65	123.048	-4149.07	72663.18	112.94	16614.39
Right Rotor (*MR*1)	1598.65	-123.048	-4149.07	-72663.18	112.94	-16614.39
Total Rotor	2671.25	0	-8236.85	0	3107.88	0
Total Aircraft (Body Axis)	-1162.43	0	-12947.87	0.006	1.10	0.004

Conversion Mode 60º β_M Input Parameters

Parameter	Units	Values
GW	lbs	13000
β_M	deg	60
Turn Rate	deg/s	0.00
Flight Path Angle	deg	0.00
x_{cg}	ft	24.8
y_{cg}	ft	0.0
z_{cg}	ft	6.4
Ω	rad/s	61.68
Ω	RPM	589
δ_{flap}	deg	20.00
I_{xx}	slug ft^2	51565
I_{yy}	slug ft^2	20686
I_{zz}	slug ft^2	66891
I_{xz}	slug ft^2	1128

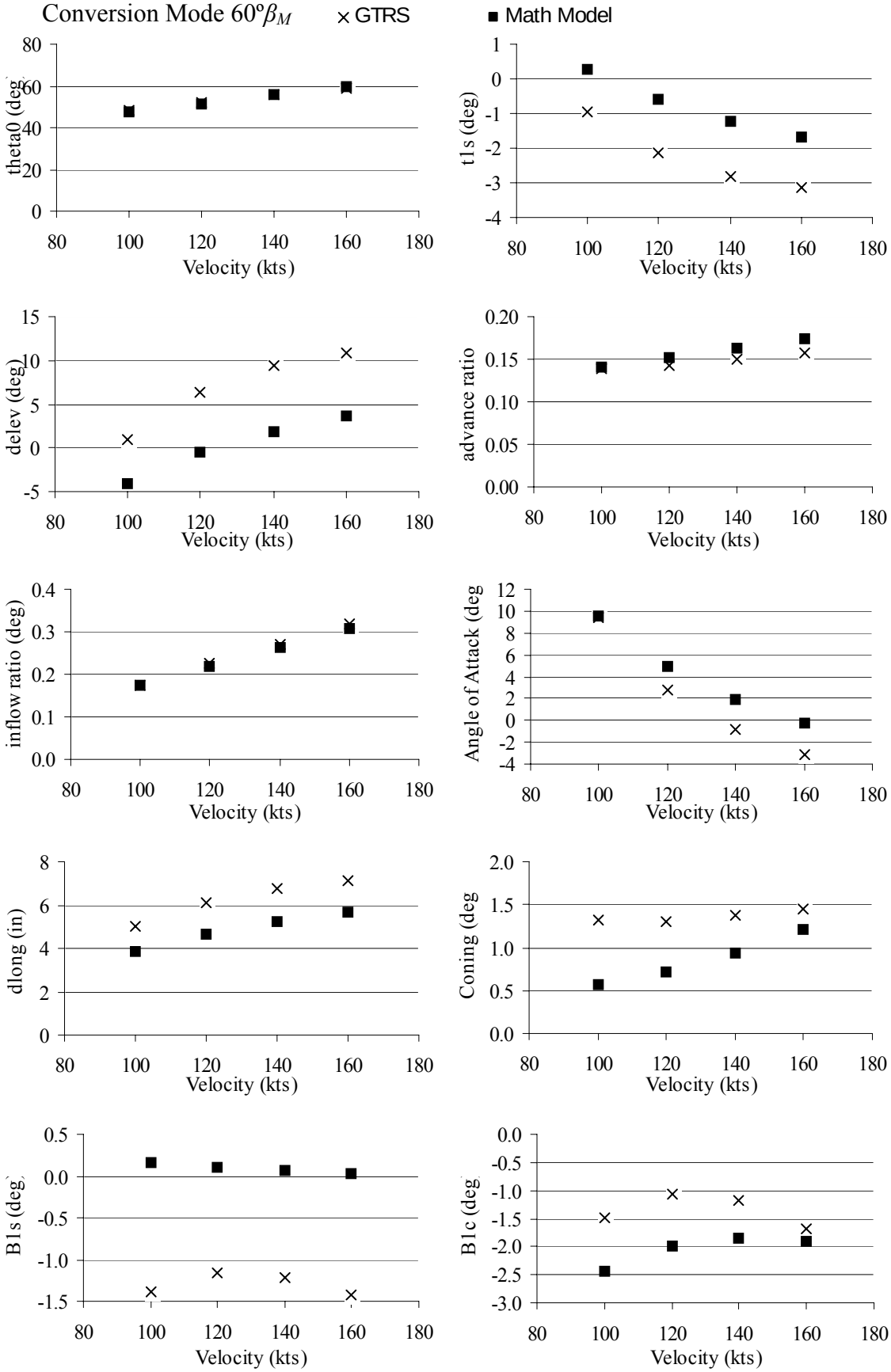
Conversion Mode 60ºβ_M
× GTRS
■ Math Model
theta0 (deg)
t1s (deg)
delev (deg)
advance ratio
inflow ratio (deg)
Angle of Attack (deg
dlong (in)
Coning (deg
B1s (deg)
B1c (deg)
Velocity (kts)

Conversion Mode 60°β_M

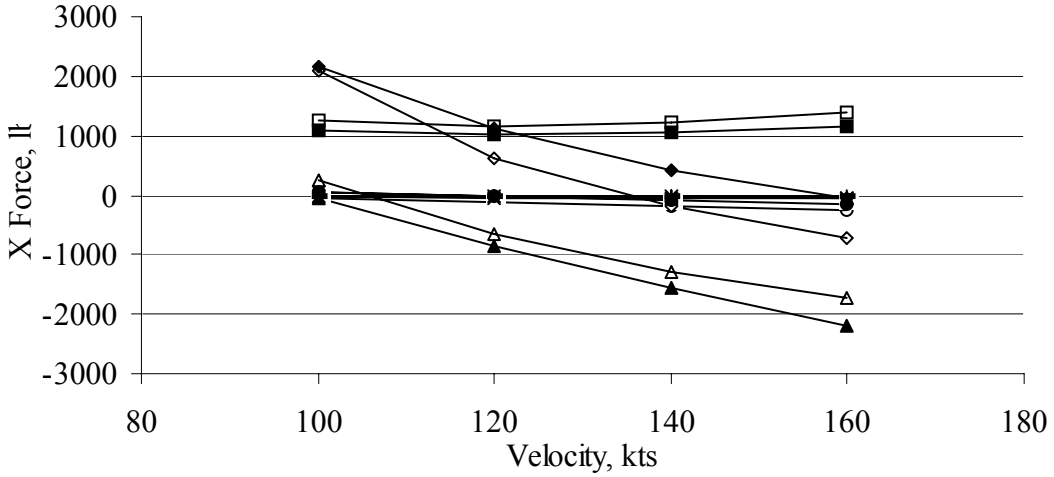

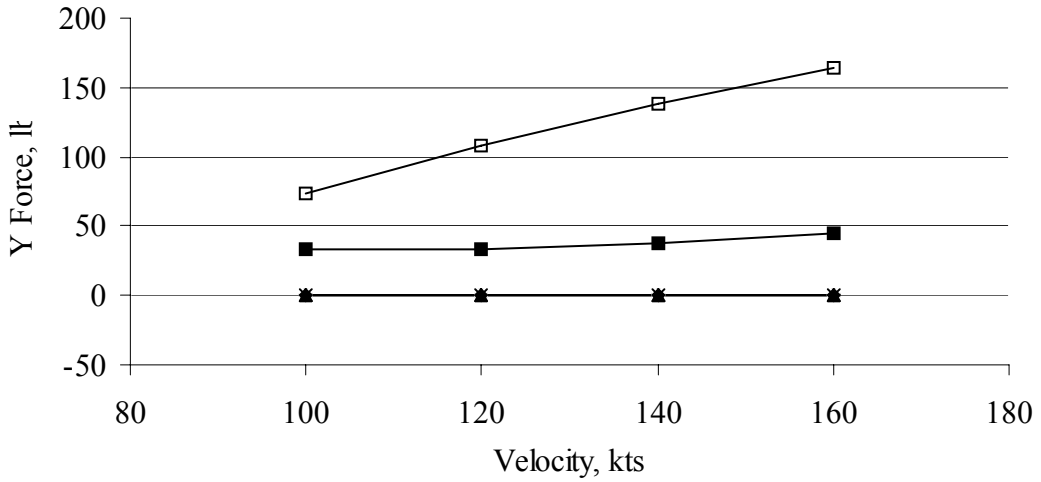

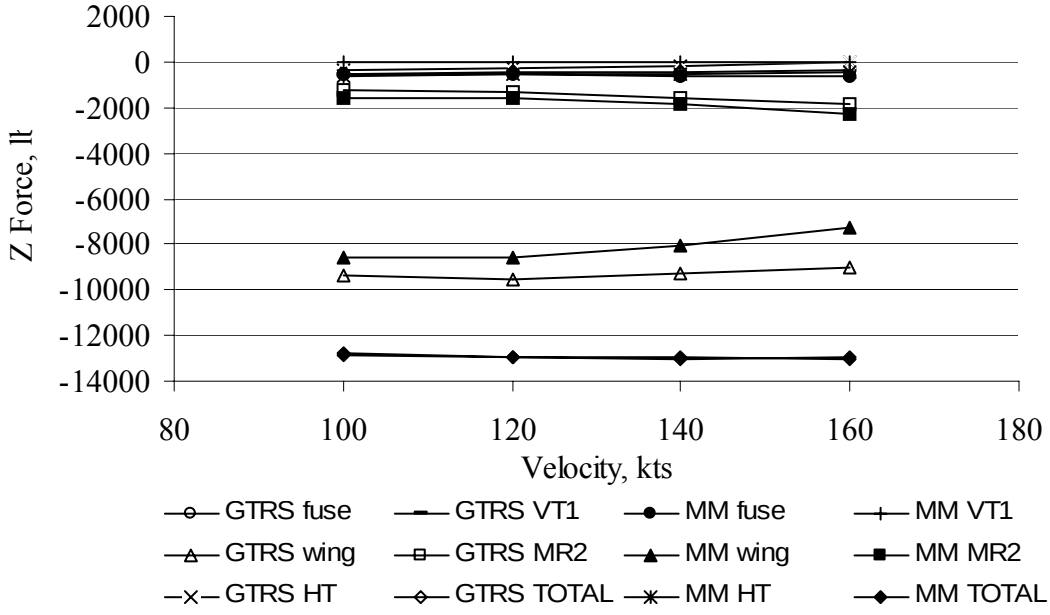

Conversion Mode 60ºβ_M

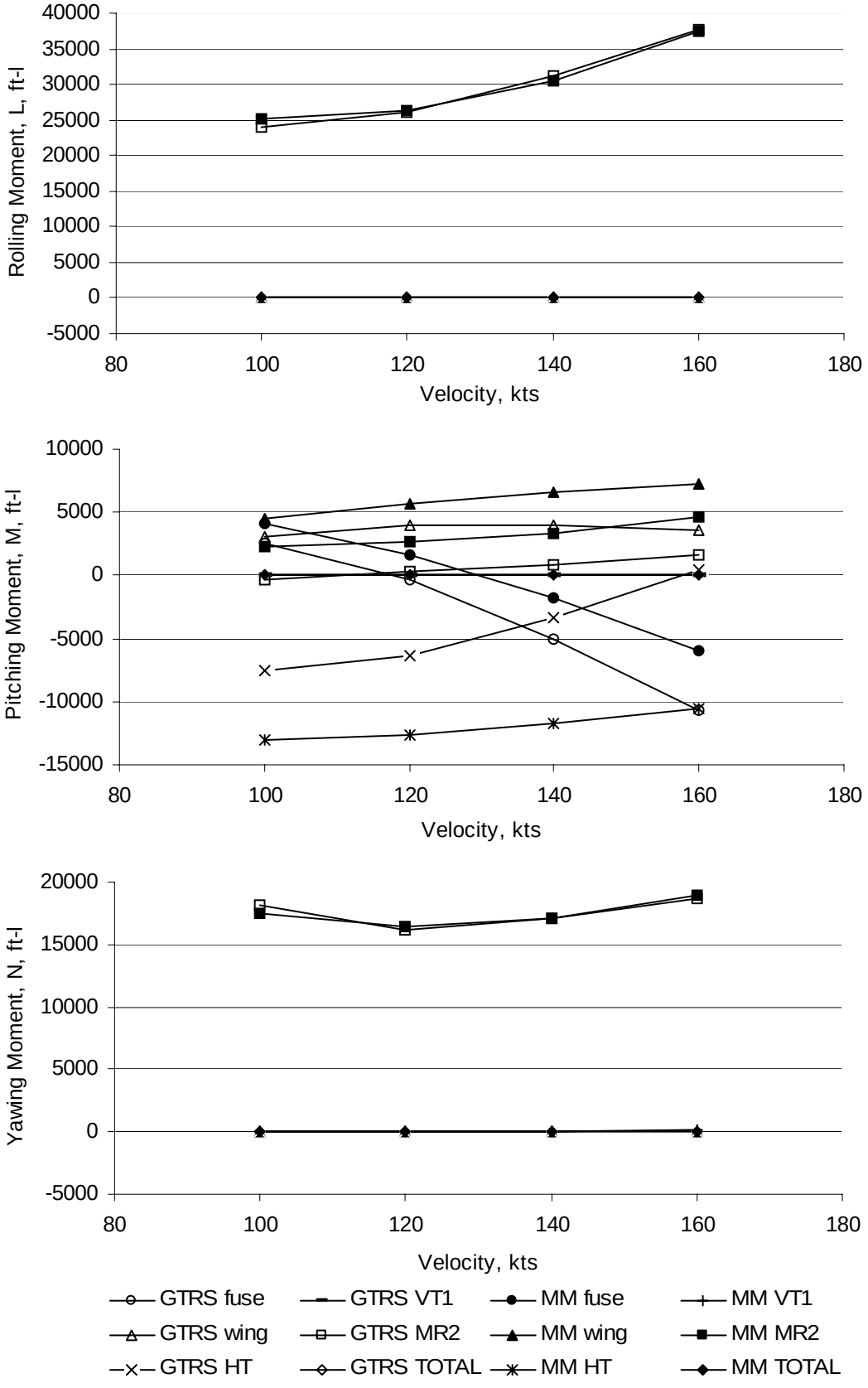

Table C-6: Conversion Mode, 60º β_M

Input Parameter	Units	GTRS	Math Model	GTRS	Math Model
V	ft/s	--	168.78	--	202.53
V	kts	100.00	100.00	120.00	120.00
φ	deg	0.00	0.00	0.00	0.00
θ	deg	9.341	9.57	2.807	5.00
α_F	deg	9.341	9.57	2.81	5.00
β_F	deg	0.00	0.00	0.00	0.00
λ_1	--	0.1749	0.1742	0.2253	0.2197
p	deg/s	0	0.00	0.00	0.00
q	deg/s	0	0.00	0	0.00
r	deg/s	0	0.00	0	0.00
pdot	deg/s/s	0.00	0.00	0.00	0.00
qdot	deg/s/s	0.00	0.00	0.00	0.00
rdot	deg/s/s	0.00	0.00	0.00	0.00
$\beta_{0,1}$	deg	1.33	0.57	1.31	0.71
$\beta_{1s,1}$	deg	-1.39	0.16	-1.16	0.10
$\beta_{1c,1}$	deg	-1.48	-2.44	-1.06	-1.98
$\theta_{0,1}$	deg	48.54	47.56	52.37	51.54
$\theta_{1s,1}$	deg	-0.94	0.28	-2.13	-0.61
$\theta_{1c,1}$	deg	0.00	0.00	0	0.00
δ_{rud}	deg	0.00	0.00	0	0.00
δ_{elev}	deg	0.89	-4.02	6.28	-0.54
δ_{ail}	deg	0.00	0.00	0	0.00
M	--	0.1388	0.1411	0.1423	0.1512
U	ft/s	166.50	166.43	202.3	201.76
V	ft/s	0.00	0.00	0.00	0.00
W	ft/s	27.40	28.07	9.919	17.66
Thrust_1	lb	1708.64	1708.14	1654.12	1690.07
C_{T1}	--	0.0025	0.0025	0.0024	0.0024
δ_{long}	In	4.99	3.84	6.13	4.67
δ_{lat}	In	4.80	4.80	4.80	4.80
δ_{ped}	In	2.50	2.50	2.50	2.50
λ_2	--	0.1749	0.1742	0.2253	0.2197
$\beta_{0,2}$	deg	1.33	0.57	1.31	0.71
$\beta_{1s,2}$	deg	-1.39	0.16	-1.16	0.10
$\beta_{1c,2}$	deg	-1.48	-2.44	-1.06	-1.98
$\theta_{0,2}$	deg	48.54	7.56	52.37	11.54
θ_0	deg	48.54	7.56	52.37	11.54
Thrust_2	lb	1708.64	1708.14	1654.12	1690.07
C_{T2}	--	0.0025	0.0025	0.0024	0.0024

Table C-6: Conversion Mode, 60º β_M (cont.)

Input Parameter	Units	GTRS	Math Model	GTRS	Math Model
V	ft/s	--	236.29	--	270.04
V	kts	140.00	140.00	160.00	160.00
φ	deg	0.00	0.00	0.00	0.00
θ	deg	-0.77	1.91	-3.14	-0.29
α_F	deg	-0.77	1.91	-3.14	-0.29
β_F	deg	0.00	0.00	0.00	0.00
λ_1	--	0.2718	0.2645	0.3169	0.3086
p	deg/s	0.00	0.00	0.00	0.00
q	deg/s	0.00	0.00	0.00	0.00
r	deg/s	0.00	0.00	0.00	0.00
pdot	deg/s/s	0.00	0.00	0.00	0.00
qdot	deg/s/s	0.00	0.00	0.00	0.00
rdot	deg/s/s	0.00	0.00	0.00	0.00
$\beta_{0,1}$	deg	1.37	0.93	1.46	1.22
$\beta_{1s,1}$	deg	-1.21	0.06	-1.42	0.04
$\beta_{1c,1}$	deg	-1.18	-1.84	-1.70	-1.92
$\theta_{0,1}$	deg	55.84	55.63	59.03	59.82
$\theta_{1s,1}$	deg	-2.81	-1.23	-3.14	-1.69
$\theta_{1c,1}$	deg	0.00	0.00	0.00	0.00
δ_{rud}	deg	0.00	0.00	0.00	0.00
δ_{elev}	deg	9.37	1.86	10.86	3.67
δ_{ail}	deg	0.00	0.00	0.00	0.00
M	--	0.1496	0.1621	0.1582	0.1736
U	ft/s	236.30	236.16	269.60	270.04
V	ft/s	0.00	0.00	0.00	0.00
W	ft/s	0.00	7.87	-14.80	-1.37
Thrust_1	lb	1847	1858.06	2127.38	2168.80
C_{T1}	--	0.0027	0.0027	0.0031	0.0031
δ_{long}	In	6.78	5.25	7.09	5.68
δ_{lat}	In	4.80	4.80	4.80	4.80
δ_{ped}	In	2.50	2.50	2.50	2.50
λ_2	--	0.2718	0.2645	0.3169	0.3086
$\beta_{0,2}$	deg	1.37	0.93	1.46	1.22
$\beta_{1s,2}$	deg	-1.21	0.06	-1.42	0.04
$\beta_{1c,2}$	deg	-1.18	-1.84	-1.70	-1.92
$\theta_{0,2}$	deg	55.84	15.63	59.03	19.82
θ_0	deg	55.84	15.63	59.03	19.82
Thrust_2	lb	1847	1858.06	2127.38	2168.80
C_{T2}	--	0.0027	0.0027	0.0031	0.0031

Table C-6: Conversion Mode, 60º β_M (cont.)

100 kts

Math Model

	X force	*Y* force	*Z* force	Roll (*L*)	Pitch (*M*)	Yaw (*N*)
Fuselage	36.03	0.00	-539.75	0.00	4118.37	0.00
Wing	-50.84	0.00	-8586.01	0.00	4439.21	0.00
Horizontal Tail	34.72	0.00	-592.08	0.00	-13038.89	0.00
Vertical Tail #1	-6.08	0.00	0.00	0.00	19.50	38.89
Vertical Tail #2	-6.08	0.00	0.00	0.00	19.50	-38.89
Airframe	7.76	0.00	-9717.84	0.00	-4442.31	0.00
Left Rotor (*MR*2)	1077.18	33.68	-1550.55	25080.43	2221.16	17426.71
Right Rotor (*MR*1)	1077.18	-33.68	-1550.55	-25080.43	2221.16	-17426.71
Total Rotor	2154.36	0.00	-3101.10	0.00	4442.31	0.00
Total Aircraft (Body Axis)	2162.12	0.00	-12818.94	0.00	0.00	0.00

GTRS

	X force	*Y* force	*Z* force	Roll (*L*)	Pitch (*M*)	Yaw (*N*)
Fuselage	-39.401	0	-544.594	0	2562.967	0
Wing	237.345	0	-9374.362	0.006	3115.676	0
Horizontal Tail	-9.714	0	-346.224	0	-7546.788	0
Vertical Tail #1	-4.348	0	0	0	14.133	-27.899
Vertical Tail #2	-4.348	0	0	0	14.133	27.905
Airframe	-257.938	0	-10345.079	0.005	-5.325	0.006
Left Rotor (*MR*2)	1264.86	74.253	-1229.298	24013.414	-389.49	18158.26
Right Rotor (*MR*1)	1264.86	-74.253	-1229.298	-24013.414	-389.49	-18158.26
Total Rotor	2368.035	0	-2482.559	0	4.703	0
Total Aircraft (Body Axis)	2110.10	0	-12827.638	0.005	-0.622	0.006

Table C-6: Conversion Mode, 60º β_M (cont.)

120 kts

Math Model

	X force	*Y* force	*Z* force	Roll (*L*)	Pitch (*M*)	Yaw (*N*)
Fuselage	-27.80	0.00	-578.07	0.00	1614.37	0.00
Wing	-844.88	0.00	-8542.72	0.00	5694.98	0.00
Horizontal Tail	-1.38	0.00	-577.09	0.00	-12630.87	0.00
Vertical Tail #1	-8.75	0.00	0.00	0.00	28.08	56.01
Vertical Tail #2	-8.75	0.00	0.00	0.00	28.08	-56.01
Airframe	-891.56	0.00	-9697.88	0.00	-5265.35	0.00
Left Rotor (*MR*2)	1012.58	33.33	-1626.30	26307.96	2632.68	16401.61
Right Rotor (*MR*1)	1012.58	-33.33	-1626.30	-26307.96	2632.68	-16401.61
Total Rotor	2025.17	0.00	-3252.60	0.00	5265.35	0.00
Total Aircraft (Body Axis)	1133.61	0.00	-12950.48	0.00	0.00	0.00

GTRS

	X force	*Y* force	*Z* force	Roll (*L*)	Pitch (*M*)	Yaw (*N*)
Fuselage	-109.528	0	-482.262	0	-386.488	0
Wing	-669.167	0	-9532.34	0	3944.824	0
Horizontal Tail	-37.828	0	-294.726	0	-6359.454	0
Vertical Tail #1	-9.653	0	-4.914	0	31.375	-61.938
Vertical Tail #2	-9.653	0	-4.914	0	31.375	61.942
Airframe	-1482.367	0	-10341.885	-0.001	-1488.538	0.004
Left Rotor (*MR*2)	1151.66	107.76	-1317.569	26156.285	336.735	16187.085
Right Rotor (*MR*1)	1151.66	-107.76	-1317.569	-26156.283	336.735	-16187.085
Total Rotor	2119.011	0	-2642.458	0.002	1489.777	0
Total Aircraft (Body Axis)	636.64	0	-12984.343	0.001	1.238	0.004

Table C-6: Conversion Mode, 60º β_M (cont.)

140 kts

Math Model

	X force	*Y* force	*Z* force	Roll (*L*)	Pitch (*M*)	Yaw (*N*)
Fuselage	-86.43	0.00	-598.02	0.00	-1778.72	0.00
Wing	-1543.65	0.00	-8090.82	0.00	6590.08	0.00
Horizontal Tail	-28.43	0.00	-535.59	0.00	-11662.51	0.00
Vertical Tail #1	-11.91	0.00	0.00	0.00	38.22	76.23
Vertical Tail #2	-11.91	0.00	0.00	0.00	38.22	-76.23
Airframe	-1682.33	0.00	-9224.42	0.00	-6774.70	0.00
Left Rotor (*MR*2)	1057.67	36.96	-1884.18	30481.52	3387.35	17152.27
Right Rotor (*MR*1)	1057.67	-36.96	-1884.18	-30481.52	3387.35	-17152.27
Total Rotor	2115.34	0.00	-3768.37	0.00	6774.70	0.00
Total Aircraft (Body Axis)	433.00	0.00	-12992.79	0.00	0.00	0.00

GTRS

	X force	*Y* force	*Z* force	Roll (*L*)	Pitch (*M*)	Yaw (*N*)
Fuselage	-178.774	0	-430.988	0	-5109.172	-0.001
Wing	-1295.226	0	-9315.258	0	3991.16	0
Horizontal Tail	-46.074	0	-160.634	0	-3410.256	0
Vertical Tail #1	-13.579	0	0	0	-12.939	-87.131
Vertical Tail #2	-13.579	0	0	0	-12.939	87.133
Airframe	-2432.085	0	-9892.166	0.003	-2715.082	0.001
Left Rotor (*MR*2)	1238.37	138.102	-1555.398	31170.746	897.303	17091.578
Right Rotor (*MR*1)	1238.37	-138.102	-1555.398	-31170.746	897.303	-17091.578
Total Rotor	2256.804	0	-3106.305	0	2717.845	0.001
Total Aircraft (Body Axis)	-175.28	0	-12998.471	0.003	2.763	0.002

Table C-6: Conversion Mode, 60º β_M (cont.)

160 kts

Math Model

	X force	*Y* force	*Z* force	Roll (*L*)	Pitch (*M*)	Yaw (*N*)
Fuselage	-141.92	0.00	-603.70	0.00	-6015.77	0.00
Wing	-2179.08	0.00	-7281.35	0.00	7201.78	0.00
Horizontal Tail	-49.21	0.00	-484.41	0.00	-10496.17	0.00
Vertical Tail #1	-15.56	0.00	0.00	0.00	49.93	99.57
Vertical Tail #2	-15.56	0.00	0.00	0.00	49.93	-99.57
Airframe	-2401.31	0.00	-8369.46	0.00	-9210.30	0.00
Left Rotor (*MR*2)	1167.64	44.50	-2315.19	37457.10	4605.15	18959.54
Right Rotor (*MR*1)	1167.64	-44.50	-2315.19	-37457.10	4605.15	-18959.53
Total Rotor	2335.27	0.00	-4630.37	0.00	9210.30	0.00
Total Aircraft (Body Axis)	-66.04	0.00	-12999.83	0.00	0.00	0.00

GTRS

	X force	*Y* force	*Z* force	Roll (*L*)	Pitch (*M*)	Yaw (*N*)
Fuselage	-258.695	0	-366.49	0	-10637	-0.001
Wing	-1726.646	0	-8983.6	0.005	3542.315	0
Horizontal Tail	-38.667	0	18.928	0	498.536	0
Vertical Tail #1	-17.114	0	0	0	55.624	-109.809
Vertical Tail #2	-17.114	0	0	0	55.624	109.815
Airframe	-3213.418	0	-9262.667	0.005	-4227.97	0.005
Left Rotor (*MR*2)	1382.26	164.533	-1866.861	37685.68	1581.305	18674.557
Right Rotor (*MR*1)	1382.26	-164.533	-1866.861	-37685.68	1581.305	-18674.557
Total Rotor	2500.778	0	-3717.738	0	4228.878	0
Total Aircraft (Body Axis)	-712.64	0	-12980.404	0.004	0.908	0.005

Appendix D: Linearized Model Eigenvalues

Airplane Mode, 517 RPM:

Column identifiers: 140, 160, 180, 200, 220, 240, 260, 280 kts

```
Columns 1 through 4

-1.3787 + 2.4324i  -1.5689 + 2.6211i  -1.7626 + 2.8017i        0
-1.3787 - 2.4324i  -1.5689 - 2.6211i  -1.7626 - 2.8017i  -0.9950 + 2.3457i
-0.1867 + 0.2368i  -0.1923 + 0.2178i  -0.9368 + 2.1196i  -0.9950 - 2.3457i
-0.1867 - 0.2368i  -0.1923 - 0.2178i  -0.9368 - 2.1196i  -1.9594 + 2.9700i
-0.8200 + 1.6530i  -0.8783 + 1.8884i  -0.1968 + 0.2024i  -1.9594 - 2.9700i
-0.8200 - 1.6530i  -0.8783 - 1.8884i  -0.1968 - 0.2024i  -1.0323
-0.7473            -0.8367            -0.9321            -0.0238
-0.0193            -0.0227            -0.0238            -0.2007 + 0.1898i
-0.0000             0.0000             0.0000            -0.2007 - 0.1898i

Columns 5 through 8

-2.1591 + 3.1222i  -2.3616 + 3.2546i  -2.5449 + 3.6090i        0
-2.1591 - 3.1222i  -2.3616 - 3.2546i  -2.5449 - 3.6090i  -1.2024 + 3.2100i
-1.0529 + 2.5662i  -1.1104 + 2.7808i  -1.1570 + 2.9950i  -1.2024 - 3.2100i
-1.0529 - 2.5662i  -1.1104 - 2.7808i  -1.1570 - 2.9950i  -2.7436 + 3.7843i
-0.2041 + 0.1798i  -0.2072 + 0.1720i  -0.2038 + 0.1541i  -2.7436 - 3.7843i
-0.2041 - 0.1798i  -0.2072 - 0.1720i  -0.2038 - 0.1541i  -1.3976
-1.1371            -1.2467            -1.3011            -0.0214
-0.0234            -0.0229            -0.0228            -0.2021 + 0.1475i
-0.0000             0.0000             0.0000            -0.2021 - 0.1475i
```

Helicopter Mode

Column identifiers: 0, 20, 40, 60, 80, 100, 120 kts

```
Columns 1 through 4

-0.7892            -0.7961             0.0864 + 0.4450i  -0.6766 + 0.4324i
 0.1483 + 0.4616i  -1.2331             0.0864 - 0.4450i  -0.6766 - 0.4324i
 0.1483 - 0.4616i   0.1470 + 0.4620i  -0.7686             0.0117 + 0.3618i
-1.1861             0.1470 - 0.4620i  -0.4001             0.0117 - 0.3618i
 0.0579 + 0.2321i   0.0315 + 0.2136i  -1.3545            -1.5447
 0.0579 - 0.2321i   0.0315 - 0.2136i  -0.0652 + 0.3041i  -0.1007 + 0.5292i
 0.0033            -0.1204            -0.0652 - 0.3041i  -0.1007 - 0.5292i
-0.1312            -0.0823             0.0554             0.0648
 0.0000            -0.0000             0.0000             0.0000

Columns 5 through 7

-0.8083 + 0.7271i        0                  0
-0.8083 - 0.7271i  -1.9878            -2.2489
-1.7629            -0.1372 + 1.0230i  -0.1591 + 1.2722i
-0.0187 + 0.2590i  -0.1372 - 1.0230i  -0.1591 - 1.2722i
-0.0187 - 0.2590i  -0.9666 + 0.9369i  -1.1462 + 1.0493i
-0.1168 + 0.7717i  -0.9666 - 0.9369i  -1.1462 - 1.0493i
-0.1168 - 0.7717i   0.0151             0.0066
 0.0328            -0.0298 + 0.1944i  -0.0398 + 0.1588i
 0.0000            -0.0298 - 0.1944i  -0.0398 - 0.1588i
```

Conversion Mode 15ºβ_M

Column identifiers: 40, 60, 80, 100, 120 kts

```
Columns 1 through 4

-0.6785 + 0.7835i  -0.8105 + 1.1161i        0                  0
-0.6785 - 0.7835i  -0.8105 - 1.1161i  -1.9357             -2.1698
 0.0022 + 0.2961i  -1.7354            -0.1593 + 1.0436i  -0.1826 + 1.3019i
 0.0022 - 0.2961i  -0.0173 + 0.2305i  -0.1593 - 1.0436i  -0.1826 - 1.3019i
-1.5413            -0.0173 - 0.2305i  -0.9567 + 1.3980i  -1.1253 + 1.6277i
-0.1215 + 0.5312i  -0.1384 + 0.7833i  -0.9567 - 1.3980i  -1.1253 - 1.6277i
-0.1215 - 0.5312i  -0.1384 - 0.7833i   0.0086             -0.0024
 0.0683             0.0306            -0.0296 + 0.1909i  -0.0406 + 0.1642i
 0.0000            -0.0000            -0.0296 - 0.1909i  -0.0406 - 0.1642i

Column 5

      0
-2.4584
-0.2060 + 1.5559i
-0.2060 - 1.5559i
-1.3185 + 1.7818i
-1.3185 - 1.7818i
-0.0066
-0.0526 + 0.1523i
-0.0526 - 0.1523i
```

Conversion Mode 30ºβ_M

Column identifiers: 80, 100, 120, 140 kts

0	0	0	0
-1.8298	-2.0255	-2.2662	-2.5645
-0.1878 + 1.0443i	-0.2162 + 1.3021i	-0.2461 + 1.5577i	-0.2742 + 1.8123i
-0.1878 - 1.0443i	-0.2162 - 1.3021i	-0.2461 - 1.5577i	-0.2742 - 1.8123i
-0.9500 + 1.7003i	-1.1124 + 1.9761i	-1.2985 + 2.2044i	-1.5077 + 2.3639i
-0.9500 - 1.7003i	-1.1124 - 1.9761i	-1.2985 - 2.2044i	-1.5077 - 2.3639i
-0.0023	-0.0153	-0.0192	-0.0185
-0.0341 + 0.2002i	-0.0469 + 0.1752i	-0.0585 + 0.1614i	-0.0700 + 0.1643i
-0.0341 - 0.2002i	-0.0469 - 0.1752i	-0.0585 - 0.1614i	-0.0700 - 0.1643i

Conversion Mode 60ºβ_M

Column identifiers: 100, 120, 140, 160 kts

0	0	-1.4839 + 2.6225i	0
-1.4851	-0.4239 + 1.4331i	-1.4839 - 2.6225i	-0.5058 + 1.9347i
-0.3702 + 1.1854i	-0.4239 - 1.4331i	-0.1273 + 0.1996i	-0.5058 - 1.9347i
-0.3702 - 1.1854i	-1.6135	-0.1273 - 0.1996i	-1.9859
-1.1004 + 2.1786i	-1.2856 + 2.4109i	-0.4691 + 1.6838i	-1.6944 + 2.8025i
-1.1004 - 2.1786i	-1.2856 - 2.4109i	-0.4691 - 1.6838i	-1.6944 - 2.8025i
-0.0618	-0.0605	-1.7805	-0.0478
-0.1079 + 0.2224i	-0.1192 + 0.2069i	-0.0546	-0.1331 + 0.1999i
-0.1079 - 0.2224i	-0.1192 - 0.2069i	0.0000	-0.1331 - 0.1999i

References

1. Kisor, Ron, Robert Blyth, Albert Brand, Tom MacDonald. V-22 Low-Speed/High Rate of Descent (HROD) Test Results. American Helicopter Society 60th Annual Forum. Baltimore, Maryland. 7-10 June 2004.

2. Brand, Albert, Ron Kisor, Robert Blyth, Dave Mason, and Chris Host. V-22 High Rate of Descent (HROD) Test Procedures and Long Record Analysis. American Helicopter Society 60th Annual Forum. Baltimore, Maryland. 7-10 June 2004.

3. Romander, Ethan, Mark Betzina, Mark Silva, Alan Wadcock, Gloria Yamauchi. Investigating Tiltrotor Formation Flight Via 1/48-Scale Wind Tunnel Experiment. American Helicopter Society 62nd Annual Forum. Phoenix, Arizona. 9-11 May 2006.

4. Strand, Trevor, Stephen Augustin, Robert J. Mayer, and Joshua M. Gorman. V-22 Osprey Heavy Gross Weight Short Take Off and Landing (STOL) Evaluation. 17th SFTE (EC) Symposium. Amsterdam, The Netherlands. 12-14 June 2006.

5. Klein, Gary D., Brad Roberts, Major Chris Seymour (USMC), MV-22 Handling Qualities Flight Test Summary. American Helicopter Society 56th Annual Forum. Virginia Beach, Virginia. 2-4 May 2000.

6. Ferguson, Samuel W. Development and Validation of a Simulation for a Generic Tilt-Proprotor Aircraft. NASA-CR-166537. Systems Technology, Inc. Mountain View, CA. April, 1989.

7. Ferguson, Samuel W. A Mathematical Model for Real Time Flight Simulation of a Generic Tilt-Proprotor Aircraft. NASA-CR-166536. Systems Technology, Inc. Mountain View, CA. October, 1983.

8. Harendra, P. B., M. J. Joglekar, T. M. Gaffey, and R. L. Marr. Final Report V/STOL Tilt Rotor Study – Volume V: A Mathematical Model for Real Time Flight Simulation of the Bell Model 301 Tilt Rotor Research Aircraft. NASA-CR-114614. Bell Helicopter Company. Fort Worth, TX. April 13, 1973.

9. Klein, Gary D. Linear Modeling of Tiltrotor Aircraft (In Helicopter and Airplane Modes) for Stability Analysis and Preliminary Design. Naval Post Graduate School, Monterey, CA. 1996.

10. RHILP Home. http://www.cert.fr/dcsd/TILT-ROTOR/RHILP/index_RHILP.html. 08 May 2007.

11. RHILP Piloted Simulation. http://www.cert.fr/dcsd/TILT-ROTOR/RHILP/piloted.html. 08 May 2007.

12. Meyer, Michael A. and Gareth D. Padfield. First Steps in the Development of Handling Qualities Criteria for a Civil Tiltrotor. American Helicopter Society 58th Annual Forum, Montreal, Canada. 11 June 2002.

13. Padfield, Gareth D. and Michael Meyer. Progress in Civil Tilt-Rotor Handling Qualities. University of Liverpool, Liverpool, UK.

14. Desopper, André, Olivier Heuzé, Vincent Routhieau, Sébastien Baehrel, German Roth, Wolfgang von Grünhagen, and Henk Haverdings. Study of the Low Speed Characteristics of a Tiltrotor. ONERA. Centre de Salon. Salon Air, France.

15. Maisel, Martin D., Demo J. Giulianetti and Daniel C. Dugan. The History of XV-15 Tiltrotor Research Aircraft: From Concept to Flight. NASA SP-2000-4517. National Aeronautics and Space Administration, Washington, DC. 2000.

16. Mass Properties: Metrics for various aircraft**.** Jon S. Berndt. 4/30/2005. JSBSim: The Open Source Flight Dynamics Model in C++. 22 June 2006. http://jsbsim.sourceforge.net/MassProps.html.

17. Padfield, Gareth D. Helicopter Flight Dynamics: The Theory and Application of Flying Qualities and Simulation Modeling. American Institute of Aeronautics and Astronautics, Inc., Herndon, VA. 1996.

18. Heffley, Robert K. and Marc A. Mnich. Minimum-Complexity Helicopter Simulation Math Model. NASA-CR-177476. Manudyne Systems Inc. Los Altos, CA. April, 1988.

19. Celi, Roberto. "ENAE 635 – Helicopter Stability and Control Class Notes". 2005.

20. Pamadi, Bandu N. Performance, Stability, Dynamics, and Control of Airplanes. American Institute of Aeronautics and Astronautics, Inc., Reston, VA. 1998.

21. Prouty, Raymond W. Helicopter Performance, Stability, and Control. Krieger Publishing Company. Malabar, FL. 1995.

22. Nixon, Mark W. Aeroelastic Response and Stability of Tiltrotors with Elastically-Coupled Composite Proprotor Blades. NASA-TM-108758. University of Maryland, College Park, MD. 1993.

23. Heffley, Robert K. A Compilation and Analysis of Helicopter Handling Qualities Data Volume 1: Data Compilation. NASA-CR-3144. Systems Technology, Inc. Mountain View, CA. August, 1979.

24. Tischler, Mark B. Frequency-Response Identification of XV-15 Tilt-Rotor Aircraft Dynamics. NASA-TM-89428. Moffett Field, CA. May 1987.

25. Tischler, Mark B, Joseph G.M. Leung, and Daniel C. Dugan. Identification and Verification of Frequency-Domain Models for XV-15 Tilt-Rotor Aircraft Dynamics. NASA-TM-86009.Moffett Field, CA. August, 1984.

26. Tischler, Mark B. and Jurgen Kaletka. Modeling XV-15 Tilt-Rotor Aircraft Dynamics by Frequency and Time-Domain Identification Techniques. NASA-TM-89404. Moffett Field, CA. December, 1986.

27. United States Army Aviation and Missile Command, Aviation Engineering Directorate. Aeronautical Design Standard Performance Specification Handling Qualities Requirements for Military Rotorcraft. ADS-33E-PRF. Redstone Arsenal, AL. 21 March 2000.

28. United States Navy. Military Specification Flying Qualities of Piloted Airplanes. MIL-F-8785C. 28 August 1996.

29. Heuzé, Olivier, Stéphanie Diaz, and André Desopper. Simplified Models for Tiltrotor Aerodynamic Phenomena in Hover and Low Speed Flight. CEAS Aerospace Aerodynamics Research Conference, Cambridge (UK), 10-13 June 2002.

30. Leishman, J. Gordon. Principles of Helicopter Aerodynamics. Cambridge University Press, New York, NY, 2000.

31. Raymer, Daniel P. Aircraft Design: A Conceptual Approach. American Institute of Aeronautics and Astronautics. Washington, DC. 1992.

32. Abbott, Ira H., Alvert E. von Doenhoff, and Louis S. Stivers, Jr. Summary of Airfoil Data. NACA Report 824. 1945.

33. Anderson, John D. Introduction to Flight. McGraw-Hill. New York, NY. 2000.

34. Dugan, Daniel C., Ronald G. Erhart, and Laurel G. Schroers. The XV-15 Tilt Rotor Research Aircraft. NASA-TM-81244. Moffett Field, CA. September, 1980.